
Effects of silicon and calcium availability on
the sustainability of carbon in Arctic
permafrost soils based on laboratory
experiments

DISSERTATION

zur Erlangung des akademischen Grades eines
Doktors der Naturwissenschaften (Dr. rer. nat.)
an der Fakultät für Biologie, Chemie und Geowissenschaften
der Universität Bayreuth

Vorgelegt von

M. Sc. Peter Klaus Stimmler
aus Würzburg

Bayreuth, 2024

Die vorliegende Arbeit wurde in der Zeit von 02/2019 bis 6/2023 in Bayreuth am Lehrstuhl für Agrarökologie unter Betreuung von Prof. Dr. Johanna Pausch angefertigt.

Vollständiger Abdruck der von der Fakultät für Biologie, Chemie und Geowissenschaften der Universität Bayreuth genehmigte Dissertation zur Erlangung des akademischen Grades eines Doktors der Naturwissenschaften (Dr. rer. nat.).

Art der Dissertation: Kumulative Dissertation

Dissertation eingereicht am: 18.12.2023

Zulassung durch die Promotionskommission: 20.12.2023

Wissenschaftliches Kolloquium: 13.05.2024

Amtierender Dekan: Prof. Dr. Cyrus Samimi

Prüfungsausschuss:

- Prof. Dr. Johanna Pausch (Gutachterin)
- Prof. Dr. Werner Borken (Gutachter)
- Prof. Dr. Martin Obst (Vorsitz)
- Prof. Dr. Jörg Schaller

Für Nemo

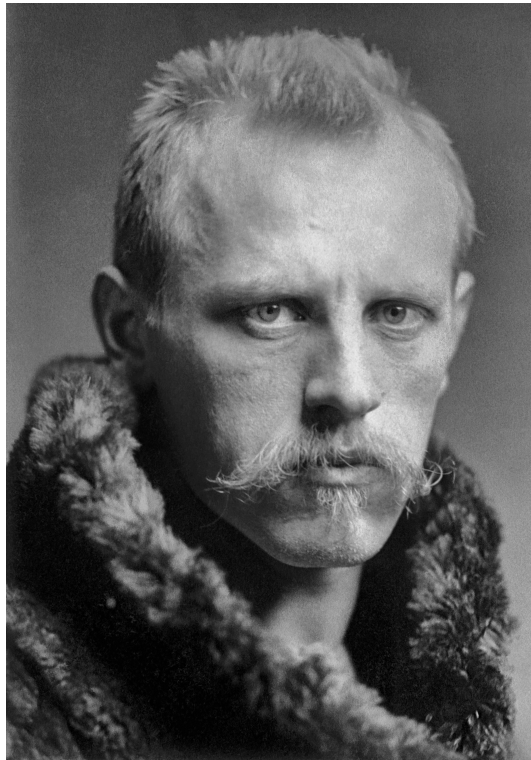


Figure 1: Fridtjof Nansen (1861-1930)
Norwegian polymath and Arctic researcher and Nobel Peace Prize laureate.
(www.wikipedia.org)

"Ich glaube, dass, wenn wir auf die sich in der Natur selbst vorfindenden Kräfte Acht geben und versuchen, mit denselben und nicht gegen sie zu arbeiten, wir den sichersten und leichtesten Weg zum Pole finden werden."

Contents

1	Introduction	1
1.1	Short overview	3
1.1.1	Abbreviations	3
1.1.2	Summary	5
1.1.3	Zusammenfassung	6
1.2	Theoretical background	7
1.2.1	Definitions of the Arctic	8
1.2.2	Arctic permafrost soils	9
1.2.3	The warming Arctic	12
1.2.4	Environmental factors affect GHG release	13
1.2.5	Plants affect GHG release	15
1.2.6	Microbes affect GHG release	17
1.2.7	Calcium sources and cycling in Arctic permafrost soils	19
1.2.8	Silicon sources and cycling in Arctic permafrost soils	23
2	Synopsis	29
2.1	The “Top - Down” research approach	31
2.2	Research questions	32
2.2.1	What are the available element concentration pools in the Arctic?	33
2.2.2	Does GHG release change with Si and Ca?	36
2.2.3	Does temperature affect Si and Ca effects on GHG release?	39
2.2.4	Does the microbial community structure change with Si and Ca?	42
2.2.5	Do Fe mineral phases interact with Si and Ca?	45

3	Manuscripts	49
3.1	Co-Payments	50
3.1.1	Study 1: Pan-Arctic soil element bio availability estimations	50
3.1.2	Study 2: The importance of calcium and amorphous silica for Arctic soil CO ₂ production	51
3.1.3	Study 3: Arctic soil CO ₂ release during freeze-thaw cycles modulated by silicon and calcium	51
3.1.4	Study 4: Arctic soil respiration and microbial community structure driven by silicon and calcium	52
3.1.5	Study 5: Silicon and calcium controls on iron and aluminum availability in Arctic soils	52
3.2	Manuscripts	53
3.2.1	Study 1: Pan-Arctic soil element bio availability estimations	55
3.2.2	Study 2: The importance of calcium and amorphous silica for Arctic soil CO ₂ production.	91
3.2.3	Study 3: Arctic soil CO ₂ release during freeze-thaw cycles modulated by silicon and calcium.	109
3.2.4	Study 4: Arctic soil respiration and microbial community structure driven by silicon and calcium	119
3.2.5	Study 5: Silicon and calcium controls on iron and aluminum availability in Arctic soils	145
4	Review and outlook	165
4.1	Conclusion	167
4.2	List of studies	168
4.3	List of references	170
4.4	List of figures	186
4.5	Danksagung	191
4.6	(Eidesstattliche) Versicherungen und Erklärungen	193

Chapter 1

Introduction

From Arctic ecosystems to mineral surfaces

1.1 Short overview

1.1.1 Abbreviations

Al aluminium

ASi amorphous silicon

bASi biogenic amorphous silicon

C carbon

C1 soil C1 from Chersky, NE-Siberia, Russia

C2 soil C2 from Chersky, NE-Siberia, Russia

C3 soil C3 from Chersky, NE-Siberia, Russia

Ca calcium

Ca1 soil Ca1 from Baffin Bay, Canada

CEC cation exchange capacity

CH₄ methane

CO₂ carbon dioxide

e⁻ electron

ESM earth system models

Fe iron

GC-FID gas chromatography / flame ionisation detector

GHG greenhouse gases

gram(+) gram-positive bacteria

gram(-) gram-negative bacteria

MAT moist acidic tundra

MCS microbial community structure

mMDS metric multi-dimensional scaling

MNT moist non-acidic tundra

N nitrogen

N₂O nitrous oxide

NEXAFS near-edge x-Ray absorbance fine structure

O₂ oxygen

OH⁻ hydroxide ion

OD optical density

P phosphorous

PO₄³⁻ phosphate

PTE potentially toxic element

qPCR quantitative poly chain reaction

rRNA ribosomal ribonucleic acid

SEM structural equation model

Si silicon

SiO₂ silicon dioxide

SOM soil organic matter

STXM scanning transmission X-ray microscopy

WSC water storage capacity

1.1.2 Summary

The Arctic warms twice as fast as the global average. Consequently, the permafrost thaws deeper and releases huge amounts of recently bound organic carbon (C) and further elements like amorphous silicon (ASi), silicon (Si), calcium (Ca), iron (Fe), aluminium (Al), and phosphorous (P). The elements Si and Ca as main components of mineral soil phases interact closely with the C-cycle and hold the potential to quicken the permafrost-C feedback. In Stimmler, Goeckede, Natali, et al. (2022) we show available concentrations of these six elements in different depths for 50% of the Arctic on-shore regions and discuss the potential of element release. For soils of five locations we observed an enhancing, positive effect of Si on carbon dioxide (CO₂) release, whereas Ca showed an inhibiting, negative effect on CO₂ release. In frozen soils, the positive Si effect prevails, whereas in thawed soils the negative Ca effect dominates (Schaller, Stimmler, et al. 2022). The microbial processes behind these effects are shown for two Greenlandic soils in Stimmler, Goeckede, Natali, et al. (2022). High CO₂ fluxes correlated positively with a gram(+) dominated microbial community structure (MCS). We hypothesized, Si promoted an increased availability of H₂O and P. Ca induced low CO₂ fluxes that were caused by a reduced microbial abundance and promotion of a MCS dominated by spore-forming, dormant gram(+) bacteria. This could be an adaption to increased salinity. At the mineral level we observed an increase in low crystallized ferrous phases with Si, leading to higher Fe availability (Stimmler, M. Obst, Stein, et al. 2023). The availability of toxic Al in presence of Si and Ca depended on the pH of the soil. These results show the complexity the biogeochemical processes of Si and Ca and how they and the associated global warming determine the C release from Arctic permafrost soils .

1.1.3 Zusammenfassung

Die Arktis erwärmt sich doppelt so schnell zum weltweiten Durchschnitt. In Folge dessen tauen die Permafrostböden tiefer auf und setzen große Mengen an bis dahin gebundenen organischen Kohlenstoffs (C) und weiteren Elementen wie amorphen Silicium (ASi), Silicium (Si), Calcium (Ca), Eisen (Fe), Aluminium (Al) und Phosphor (P) frei. Die Elemente Si und Ca als mineralische Hauptbestandteile des Bodens sind eng in den C-Zyklus eingebunden und haben das Potenzial die C-Freisetzung zu verstärken. In Stimmler, Goeckede, Elberling, et al. (2022) zeigen wir für ca. 50% der Landfläche der Arktis die verfügbaren Elementkonzentrationen dieser sechs Elemente in verschiedenen Tiefen und diskutieren das Potenzial der Mobilisierung in verschiedenen Regionen. Für Böden aus fünf Standorten konnten wir positive Effekte von Si und negative Effekte von Ca auf die CO₂-Freisetzung zeigen (Stimmler, Goeckede, Natali, et al. 2022). Im gefrorenen Boden überwog der positive Si-Effekt, im getauten Boden der negative Ca-Effekt (Schaller, Stimmler, et al. 2022). Die mikrobiologischen Prozesse hinter den Effekten werden in Stimmler, Priemé, et al. (2022) für zwei grönländische Böden gezeigt. Hohe CO₂-Flüsse korrelierten mit einer gram(-) dominierten Mikrobenstruktur, welche wahrscheinlich durch die Si bedingte Erhöhung der H₂O- und P-Verfügbarkeit gefördert wurden. Ca bedingte niedrige CO₂-Flüsse korrelierten mit verringerter Mikrobenanzahl und mehr sporenbildenden, physiologisch inaktiven gram(+) Bakterien, die für eine erhöhte Salinität sprechen. Auf mineralischer Ebene konnten wir in Stimmler, M. Obst, Stein, et al. (2023) erhöhte Anteile an Fe²⁺-Phasen in Gegenwart von Si zeigen, die mit einer Mobilisierung der Fe-Verfügbarkeit einherging. Die Verfügbarkeit von toxischem Al war pH-abhängig. Diese Ergebnisse zeigen, wie komplex die biogeochemischen Prozesse von Si und Ca sind und wie sehr sie über die Zukunft des C in arktischen Permafrostböden und somit über die globale Erwärmung bestimmen.

1.2 Theoretical background

1.2.1 – The definition of the Arctic

1.2.2 – Arctic permafrost soils

1.2.3 – The warming Arctic

1.2.4 – Environmental factors affect GHG release

1.2.5 – Plants affect GHG release

1.2.6 – Microbes affect GHG release

1.2.7 – Calcium sources and cycling in Arctic permafrost soils

1.2.8 – Silicon sources and cycling in Arctic permafrost soils

1.2.1 Definitions of the Arctic

The geographic definition of the Arctic describes the area northerly of the Arctic circle at $66^{\circ}34'N$. This area covers $17.62 \times 10^6 \text{ km}^2$ and is affected by polar day and night (Sale and P. Michelsen 2018). The climatic definition of the Arctic is the $10^{\circ}C$ July isotherm, which is in good agreement with the northern tree line in terrestrial Arctic systems (Köppen 1931). Using the climatic definition the Arctic covers an area of $24.6 \times 10^6 \text{ km}^2$ (Johnson 2022) (Fig. 1.1).

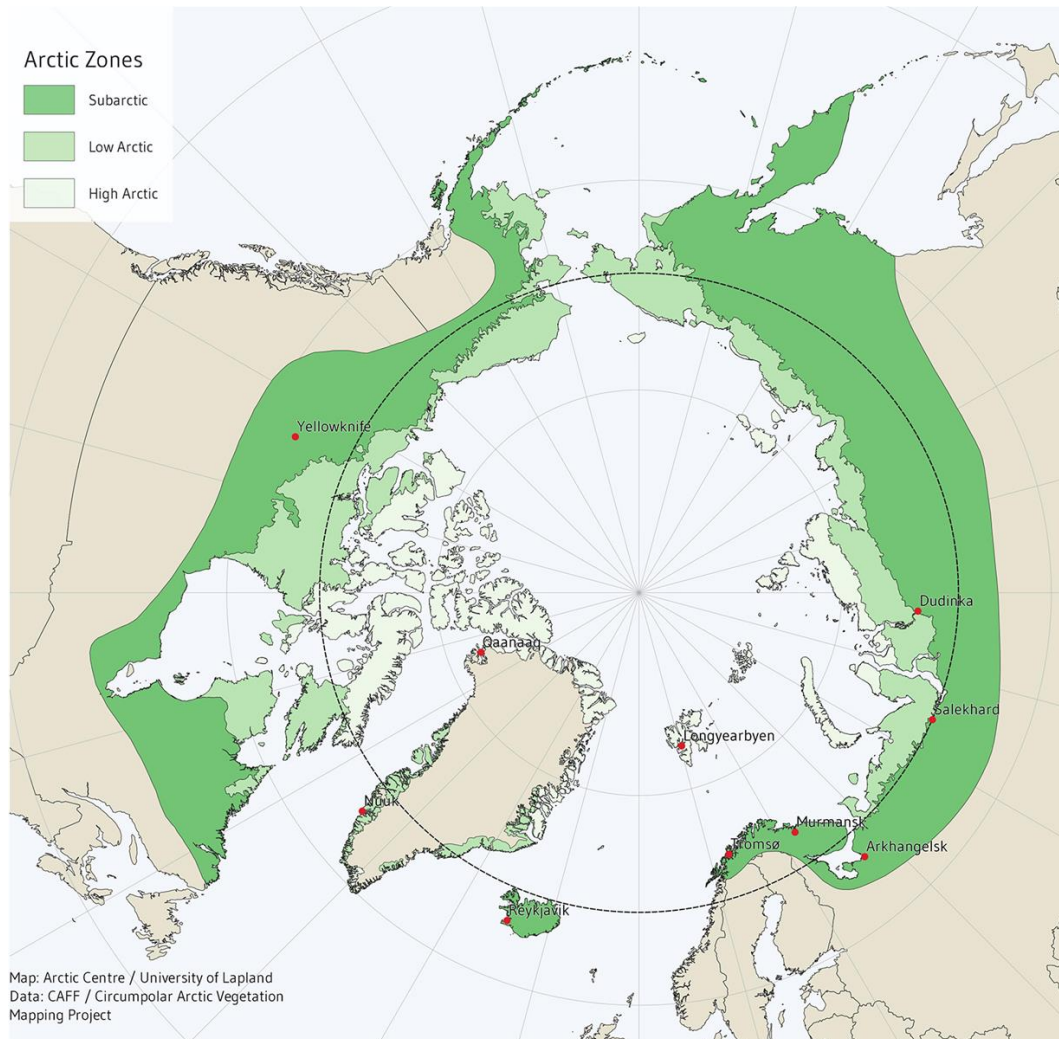


Figure 1.1: Map of the Arctic. The Arctic circle at $66^{\circ}34'N$ is shown in black. The outer border of the dark green area marks the $10^{\circ}C$ isotherm of the warmest month and mainly fits with the tree line. Map from Johnson (2022), based on the circumpolar arctic vegetation map from D. A. Walker et al. (2005)

The treeline defines the border between the boreal forest and tundra forest in the south, e.g. the taiga in Siberia and the tundra ecosystems in the north. Raynolds et al. (2019)

defines the land cover type northerly of the treeline in the circumpolar arctic vegetation map. An area of $7.02 \times 10^6 \text{ km}^2$ (46%) is covered by vegetation. This area is further distinguished by 47% shrub dominated tundra, 45% graminoid dominated tundra and 8% wetlands (Fig. 1.2) (Sale and P. Michelsen 2018).

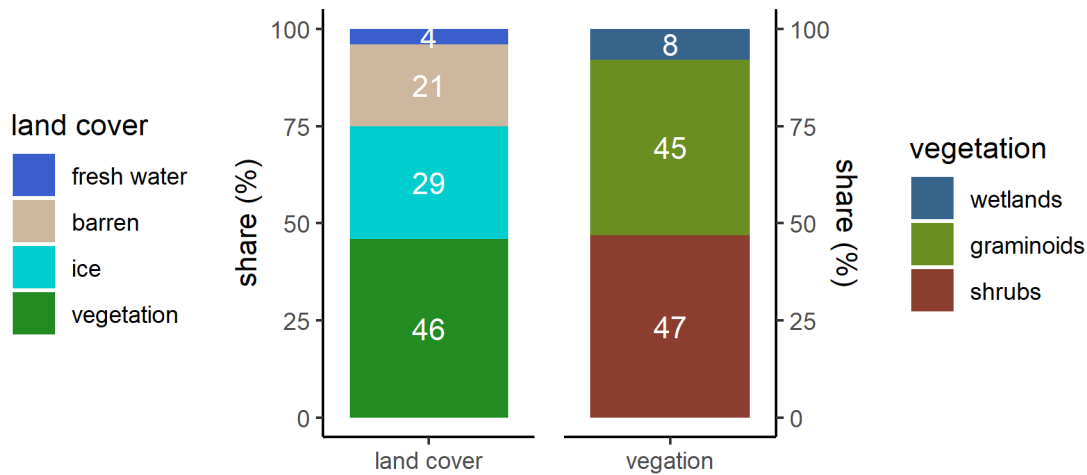


Figure 1.2: Characterization of Arctic landscape northerly the 10°C July isotherm. Left bar chart: Landcover type. Only the half of the area is covered by vegetation. One third of the Arctic is covered by ice, freshwater only covers 4%. Right bar chart: The vegetation types of the tundra ecosystems, from Reynolds et al. (2019)

Fresh water systems like lakes are common in the Arctic. Cold air temperatures reduce evaporation rates and permanently frozen ground below (permafrost) inhibits percolation. The largest share of fresh water is bound in the inland icesheet of Greenland ($1.7 \times 10^6 \text{ km}^2$) and in inland glaciers (Vasskog et al. 2015). Ice covers 29% of the area north of the treeline. Liquid fresh water covers only 4% of the Arctic (Fig. 1.2). Olefeldt, Hovemyr, et al. (2021) lists $0.12 \times 10^6 \text{ km}^2$ of large river systems and $1.4 \times 10^6 \text{ km}^2$ of lakes. When temperatures and precipitation rates are too low for vegetation to grow, barren ground forms. These polar deserts mainly occur in the outermost north regions (Sale and P. Michelsen 2018).

1.2.2 Arctic permafrost soils

In $21.6 \times 10^6 \text{ km}^2$ of the northern hemisphere (Obu et al. 2019) soil temperatures do not rise over 0°C for a minimum of two years and permafrost occurs (ASGR 1988) (Fig. 1.3). In regions where the ground was not covered by the ice shield during the last ice age the depth of the permafrost can reach more than 1,700 m (Alfred Wegener Institut 2023).

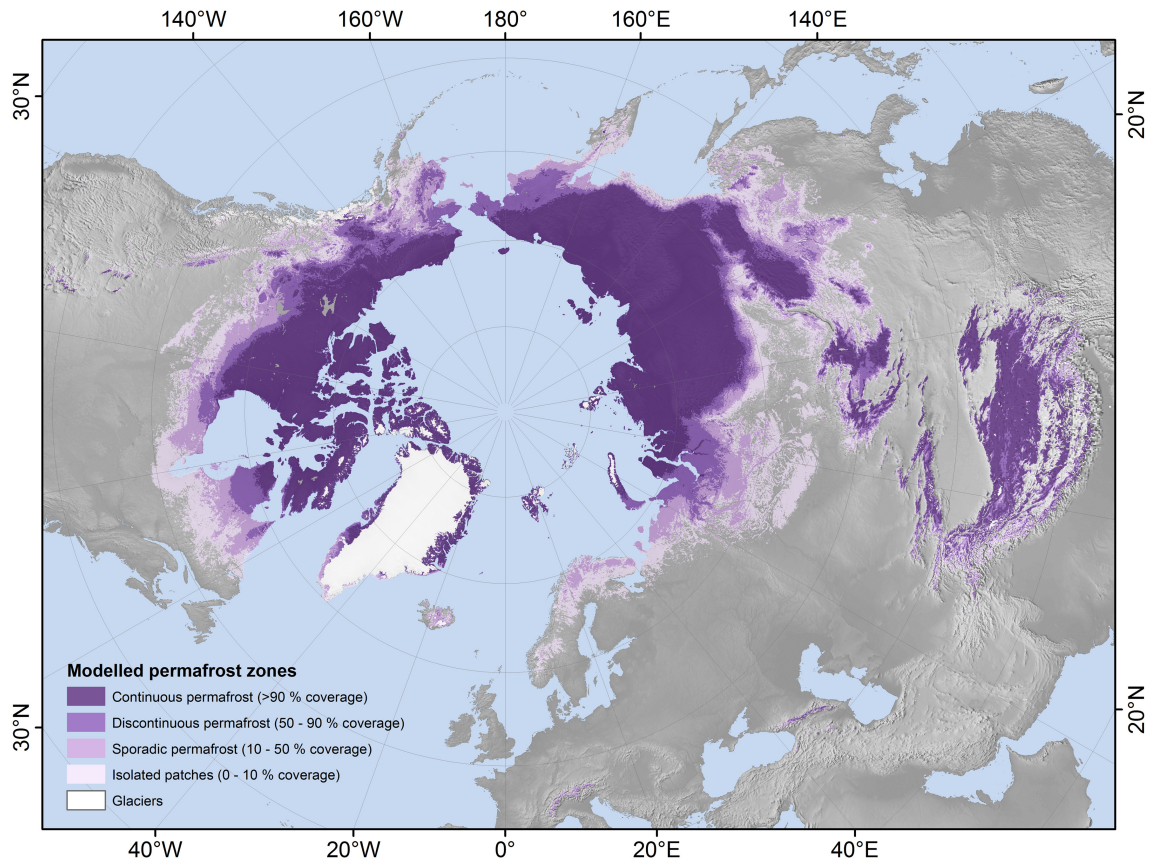


Figure 1.3: Northern hemisphere permafrost map as defined in Obu et al. (2019). In total 21.6×10^6 km² are affected by permafrost. Colors represent regions with continuous, discontinuous, sporadic and isolated permafrost soils.

In soils affected by permafrost, a typical vertical distribution of temperature and chemical composition forms. The first few centimeters, the organic layer, receive fresh organic material from vegetation and are rich in soil organic matter (SOM) (Höfle et al. 2013). Between the organic layer and the lower permafrost layer, the mineral SOM-poor mineral layer occurs. Below the mineral layer, the permafrost layer occurs (Fig. 1.4A). In summer temperature rises in the thermal active layer, that contains the organic and mineral layer. The maximal depth, where temperature exceeds 0°C and thawing occurs, defines the thermally active layer thickness. It can range from a few centimeters up to 20 m in some cases (Dobiński 2020). In autumn, the soil temperature sinks below 0°C and the freezing occurs. In contrast to thawing, the freezing process of the active layer starts from deeper permafrost layers below towards the top soil layer (Dobiński 2020) (Fig. 1.4B).

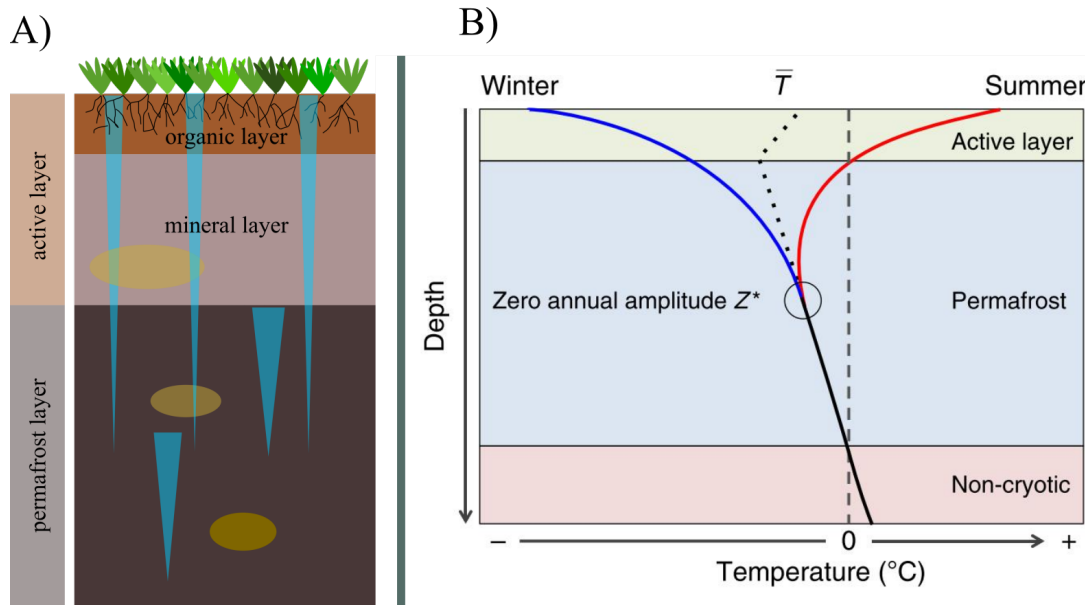


Figure 1.4: A) Schematic structure of permafrost soils. Below the vegetation cover the thermal active layer occurs, that is characterized by annual thawing and freezing. The active layer is divided into an upper SOM-rich organic layer (brown) and a lower SOM-poor mineral layer (grey). Below the thermal active layer, temperatures do not exceed 0°C and the ground stays frozen (permafrost layer; dark brown). The ice wedges (blue) cause cryoturbation and vertical mixing of soil material. In every layer organic rich peat lenses (yellow) can form. B) Principal structure of a permafrost affected soil with annual temperature regime. Dashed vertical line: Thaw temperature ($T=0^{\circ}\text{C}$). Green: active layer with annual freeze-thaw cycles ($T < 0^{\circ}\text{C} < T$). Blue: permafrost layer ($T < 0^{\circ}\text{C}$). Red: Below the permafrost layer non-cryotic layer occurs again ($T > 0^{\circ}\text{C}$). Blue line: The minimum ground temperature occurs during winter and the active layer freezes. Red line: Maximum ground temperature rises during summer and the active layer thaws again. The maximal depth, where temperature rises above 0°C defines the active layer thickness (circled). Black line: The mean temperature varies with seasonality (dotted line) but stays constant below the depth of zero annual amplitude (Z^*) (continuous). From Biskaborn et al. (2019).

Several seasonal parameters like air temperature, snow cover, and water content vary seasonally and affect the temperature regime and the active layer thickness (Luo et al. 2016). This annual freeze-thaw cycles cause physical sorting and vertical mixing of soil particles in mainly all permafrost affected regions (J. Bockheim and Tarnocai 1998). By cryoturbation SOM from the organic layer can be buried in deeper horizon (Bockheim 2007; Kaiser et al. 2007; Vandenberghe 2013). Bockheim (2007) attributed 55% of the SOM in the active layer to vertical transport by cryoturbation. In particular Yedoma soils are affected by cryoturbation. These ice-rich ($< 70\%$ ice content) soils developed mainly during the Pleistocene by fluvial deposition and contain large amounts of SOM (Schirrmeister et al. 2011).

When SOM is buried in deeper soil layers, several factors like low temperatures, anaerobic conditions (Kaiser et al. 2007), low microbial activity (Mishra et al. 2021), and association of SOM with mineral surfaces (Patzner, Kainz, et al. 2022) prevents the SOM from further decomposition (Ping et al. 2008). Since the Pleistocene (Abramov, Vishnivetskaya, and E. Rivkina 2021) these processes accumulated a pool of 1035 ± 150 Pg organic carbon in the Arctic in a depth of 0 – 3 m of the permafrost soils (Hugelius, J. Strauss, et al. 2014).

1.2.3 The warming Arctic

The Arctic is part of the cryosphere and characterized by permafrost soils, glaciers and ice sheets. The global cryosphere and is massively affected by climate change. The surface temperature in the Arctic has increased twice as fast as the global average in the last two decades (IPCC 2022), some studies reported nearly a four time faster warming in the last 43 years (Rantanen et al. 2022). At the same time, heavier heat and more extreme weather events occurred (Overland 2020). The consequences are severe changes in all Arctic ecosystems. Increased mean annual ground temperature (Smith et al. 2022) and changed precipitation rates cause a longer vegetation period (Box et al. 2019) and have already changed $\sim 40\%$ of the tundra vegetation state. Greening, browning (Wang and Friedl 2019; Berner et al. 2020) and wildfires (McCarty et al. 2021) are obviously changes in the vegetation cover.

In the soil the effects of the Arctic warming are severe too. Biskaborn et al. (2019) estimated the warming of the permafrost layer to $0.39 \pm 0.15^\circ\text{C}$ per decade in continuous permafrost (Fig. 1.5a). For cold permafrost, mainly in the high Arctic, Smith et al. (2022) observed a warming up to 1.0°C per decade.

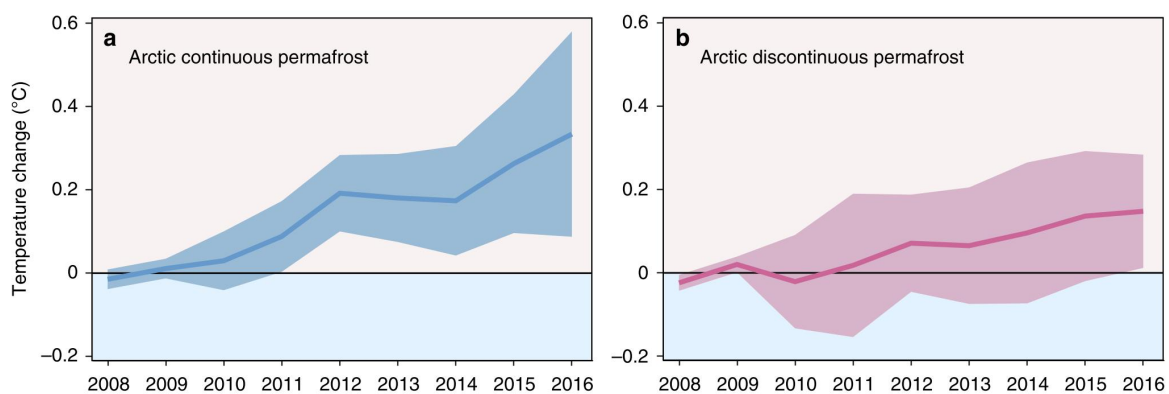


Figure 1.5: Change of mean temperature in pan-Arctic permafrost boreholes near the zero annual amplitude Z^* (see Fig. 1.4B), relative to the decade 2008 – 2009. a) Arctic continuous permafrost zone, b) Arctic discontinuous permafrost zone (see Fig.1.3). From Biskaborn et al. (2019).

The warming causes a decline of winter freezing days (Henry 2008) and increases cumulative degree-days of thawing, as shown by Abramov, Vishnivetskaya, and E. Rivkina (2021) for the eastern Arctic. Together, these two processes increase the active layer thickness (Luo et al. 2016). The increased number of winter freeze-thaw cycles (Henry 2008) and the increased cryoturbation processes could transport SOM to lower soil layers and prevent it from decomposition for thousands of years (Bockheim 2007).

However, warming can mobilize nutrients during rapid thawing processes, in particular when permafrost collapses (thermokarst) (Abbott et al. 2015). Permafrost soils contain huge amounts of labile organic carbon (C) (Mueller et al. 2015) and nitrogen (N). For peatland soils Hugelius, J. Strauss, et al. (2014) estimated 415 ± 150 Pg C and 10 ± 7 Pg N, nearly the half of it is affected by permafrost and vulnerable to Arctic warming. Yedoma soils are very vulnerable for thermokarst processes (Fuchs et al. 2018), Jens Strauss et al. (2013) estimated the C store in the first 3 m of the Yedoma soils to 181 ± 54 Pg.

1.2.4 Environmental factors affect GHG release

The SOM can become vulnerable to mineralization after thawing. When nutrients and water become available after thaw, microbial activity can increase. In consequence the microbial decomposition of SOM, greenhouse gases (GHG) are released to the atmosphere. The release of GHG from permafrost affected soils is a natural process and is predicted to accelerate in future with further warming of the Arctic (Miner et al. 2022). The GHG release varies with geography (Virkkala et al. 2021), seasonality (Sapronov 2021) and the effects of climate change differ within the Arctic (Virkkala et al. 2021). The hydrologic and thermal regimes affect GHG release from permafrost soils (Göckede, Kittler, et al. 2017; Merbold et al. 2009) and interactions with further abiotic and biotic factors complicate predictions of GHG release on a larger geographical scale (Fig. 1.6). The regional variability of precipitation rates for example can promote anaerobic conditions in areas with higher precipitation rates. Here, newly waterlogged soils often show more anaerobic conditions, and methane (CH_4) production rates will increase (Olefeldt, Turetsky, et al. 2013).

In regions with lower precipitation rates, increased air temperature and thermokarst of ice-rich permafrost could drain soils. This can potentially reduce CH_4 and CO_2 release dramatically (Göckede, Kittler, et al. 2017; Merbold et al. 2009) and stabilize the permafrost below (Göckede, Kwon, et al. 2019). When precipitation falls as snow in winter it acts as isolation, preventing heat to emit from the ground below and lead to higher soil temperatures (Yi et al. 2015).

There is a considerable rate of GHG production from frozen soils. Higher soil temperatures in future can increase microbial activity, promote SOM decomposition and increase GHG release (Capek et al. 2015).

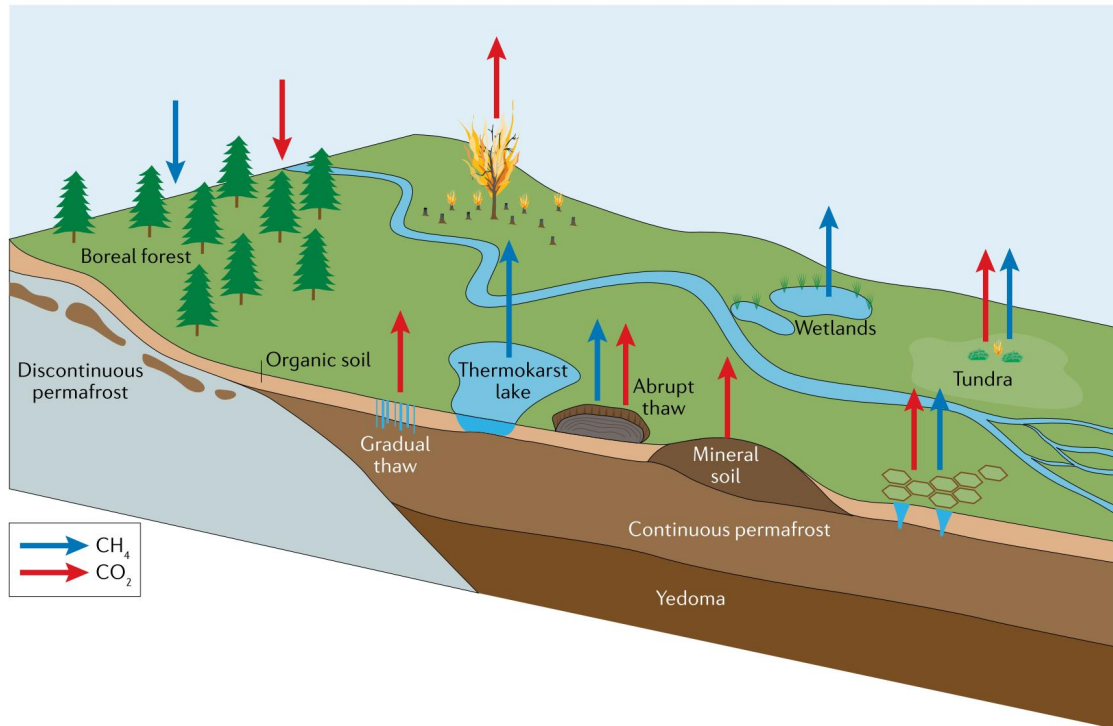


Figure 1.6: GHG flux dynamics in a permafrost affected landscape. CO₂ is released by microbial SOM decomposition, in particular in areas affected when warming causes gradual and abrupt thaw. Wildfires are already an important source for CO₂ emissions, and will become more frequent in the future. CO₂ is bound by photosynthesis and fixed in the soil. CH₄ emissions occur in ecosystems with anaerobic conditions like wetlands and peatlands. From Miner et al. (2022), adapted from Hassol (2005).

The GHG release can increase with lower temperatures too. Deep-freezing temperatures will decrease the share of vital microbes and the release of nutrients from dead organic matter can fertilize remaining microbes and promote SOM decomposition (Zhang et al. 2022). The release of GHG is not constant, but starts with a pulse directly after thawing (Kim et al. 2012). The release of CO₂ was estimated in Dutta et al. (2006) with 40 Pg C for Northeastern Siberia (within 40 years). Besides CO₂, the GHG CH₄ (Schuur, Abbott, et al. 2013) and nitrous oxide (N₂O) (Voigt et al. 2020) are critical for future warming as the sustained-flux global warming potential is 34.9 times (CH₄) and 250 times (N₂O) that of CO₂. Schuur, Abbott, et al. (2013) estimated the cumulative release of CH₄ by 2040 was 0.26–0.85 Pg CH₄-C by and 2.03–6.21 Pg CH₄-C by 2100. The importance of N₂O release for the N cycling in Arctic permafrost soils was discussed by Lacroix et al. (2022).

Further, soil properties can massively affect GHG release. Faucherre et al. (2018) could show from 241 samples from the pan-Arctic that the dry bulk density explains variations in GHG release the best. Zheng et al. (2022) highlights the importance of pH buffering capacity and cation exchange capacity (CEC) for SOM stability in acidic permafrost soils. At last salinity was shown to have a huge impact on the vulnerability of SOM (Yu et al. 2020).

The increased GHG release increases further warming of Arctic regions, causing deeper permafrost thaw and by this mobilization of new GHG sources. This process is called permafrost carbon feedback (Schuur, McGuire, et al. 2015) and there is evidence that the Arctic will change from a carbon sink to a carbon source in the future (Koven et al. 2011).

1.2.5 Plants affect GHG release

In Arctic soils, the decomposition of SOM by microbes is of great importance, as the release of GHG to the atmosphere speeds up the permafrost carbon feedback. The solid soil fraction consists of SOM, mainly dead microbial and phytic material, and weathered underlying bedrock (Weil and Brady 2017). Micro-climatic conditions and the variability of the underlying bedrock can cause small-scale vegetation patterns in the Arctic (Raynolds et al. 2019).

An example of small-scale vegetation variability caused by availability of calcium (Ca) was shown by D. Walker et al. (2001). He distinguished between a tussock tundra dominated by a plant association of *Sphagno-Eriophoretum vaginati* (Ca-poor moist acidic tundra (MAT)) (Fig. 1.7a) and mammoth step like Ca-rich moist non-acidic tundra (MNT), dominated by a plant association of *Dryado integrifoliae-Caricetum bigelowii* (Fig. 1.7b). The Arctic plant associations have adapted and shifted with changing climate conditions over the millennia (Andreev, PAVEL E. Tarasov, et al. 2003; Andreev, P. E. Tarasov, et al. 2016). Although recent warming has not changed 50% of the Arctic vegetation (Callaghan, Cazzolla G., and Phoenix 2022), shifts in plant diversity like greening and browning (Berner et al. 2020) are common. Warming or shading can change plant community and decrease CO₂ uptake (Dahl et al. 2017). Degradation of permafrost is already a main driver for changes in vegetation cover and has a big impact on GHG release (Jin et al. 2020).



Figure 1.7: The vegetation cover in the Arctic is diverse and can differ on small-scale (Raynolds et al. 2019). An example of different vegetation on small-scale area was shown by D. Walker et al. (2001). He differed between a (a) tussock tundra dominated by a plant association of *Sphagno-Eriophoretum vaginati* (MAT) and (b) a mammoth step like tundra dominated by the plant association *Dryado integrifoliae-Caricetum bigelowii* (calcium-rich MNT).

Plants adapt to deeper permafrost thaw caused by warming by deepening root growth to use nutrients released from these new thawed soil layers (Blume-Werry et al. 2019) (Fig. 1.8). When water availability increases sedges can become the dominant plants. Their roots can then connect CH_4 to the atmosphere (King, Reeburgh, and Regli 1998) and by this increase emissions. Thereby the CH_4 emission rates correlates positively with vegetation height (Fischer et al. 2010).

The interactions of plants with soils and the atmosphere are complex and can create positive or negative feedbacks with climate change. This makes future predictions of GHG very difficult, when vegetation is taken into account. When climate change promotes plant and fine root growth, a negative feedback can be expected, as CO_2 is permanently fixated in the soil. In particular the sedge *Eriophorum* can increase its root length growth up to four times and stores C in the soil, whereas shrubs seem not to change the root growth (Blume-Werry et al. 2019) (Fig. 1.8). The increased root biomass release larger amounts of root exudates, that can promote microbial decomposition of older SOM in the rhizosphere and can increase GHG release (priming effect) (Wild, Schneckner, et al. 2014; Wild, Monteux, et al. 2023).

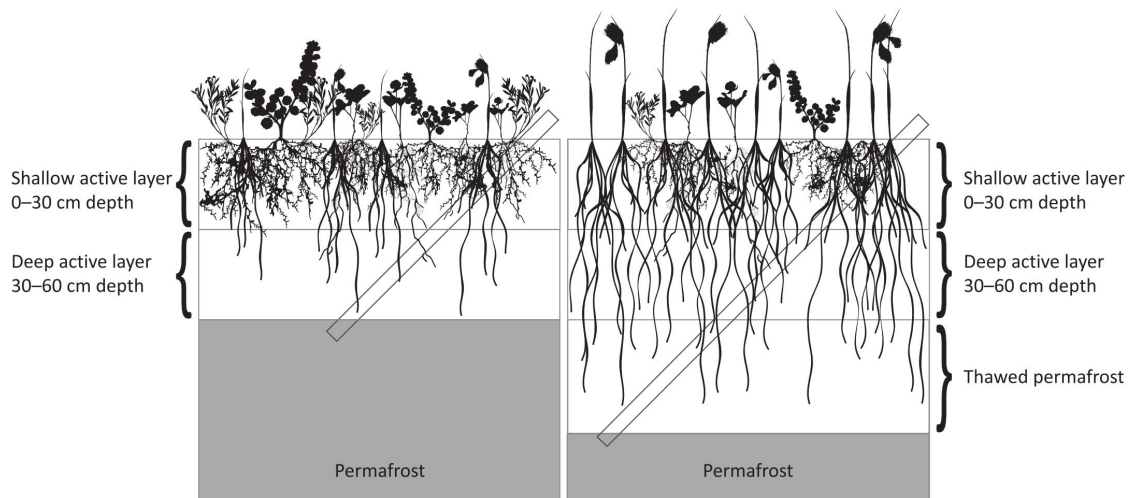


Figure 1.8: Experimental setup from Blume-Werry et al. (2019) in Abisko, Sweden. Left site: Control site without warming. Right site: Higher snow cover caused warming of the permafrost and deeper thawing of the active layer. The root growth of the graminoid *Eriophorum vaginatum* followed the thaw table to use fresh mobilized nutrients. This increased SOM fraction in the active layer. Dwarf shrubs (*Andromeda*, *Betula*, *Rubus*, *Vaccinium*) did not follow ongoing thaw and root length remained 30–40 cm.

1.2.6 Microbes affect GHG release

Plants and microbes interact and adapt together to a changed nutrient supply from thawed permafrost (Imai 2013). The MCS of Arctic soils was searched intensively in the last years, thanks to efficient next generation sequencing techniques (Margesin and Collins 2019). The MCS is just as diverse as in temperate soils: Common bacterial taxa found in Arctic soils rely on Acidobacteria, Actinobacteria (Barka et al. 2016), Bacteroidetes, Firmicutes, and Proteobacteria (Jansson and Taş 2014) (Fig. 1.9). In most soils, bacterial cells outnumber the fungi cells (Margesin and Collins 2019). Understanding the properties of the MCS is crucial for future predictions of GHG release as it strongly controls the C cycle in the Arctic (Monteux et al. 2020). Forecasting is difficult, as the adaptations of the MCS to changing environmental conditions relies on the nutrient availability of the soil (Biasi et al. 2005).

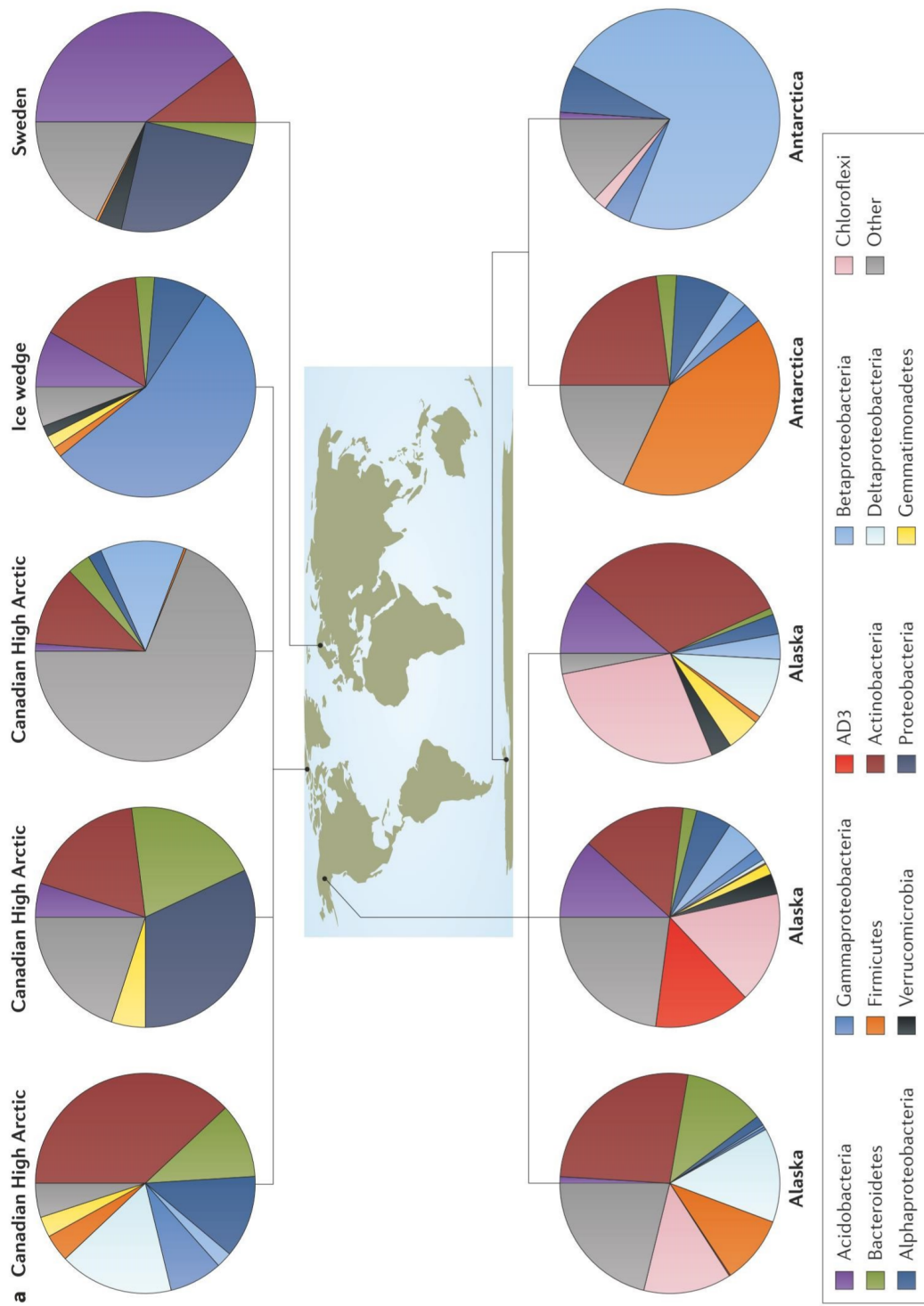


Figure 1.9: Microbial community structures based on 16s rRNA gene classifications from different locations in the Arctic (and Antarctica). From (Jansson and Taş 2014).

The thawing of permafrost not only increases the availability of nutrients and water, but also changes the community structure and activity of the microbes. Jansson and Hofmockel (2020) show a shift in MCS of the permafrost soil after thawing to a MCS that was equal to the active layer. Further, Coolen and Orsi (2015) could show with metagenomic data a shift in the expression of proteins related to different pathways. In frozen soils proteins related to pathways that are stress and surviving-relevant were expressed. After thawing proteins related to pathways for C and N cycling were up-regulated (Jansson and Hofmockel 2020). When microbes become more physiological active, they decompose more SOM and the GHG release can increase.

However, even under frozen conditions microbes are physiological active and release GHG (Sapronov 2021; Zhang et al. 2022). The bacteria and fungi of Arctic soils, also called Eutectophiles, have adapted to extreme and fast changing conditions of cold, drought, or salinity, and can be physiological active to temperatures of $< 20^{\circ}\text{C}$ (Deming 2002; E. M. Rivkina et al. 2000). Some fungal species of the taxa Mortierellomycota produce high concentrations of linoleic and arachidonic acid to prevent freezing of the cells (Hassan et al. 2016).

Bacteria differ in their cell wall structure and can handle stress caused by salinity or drought differently. The gram-positive bacteria (gram(+)) bacteria like Actinobacteria and Firmicutes, are characterized by an outer thick layer (30 – 100 nm) of peptidoglycan (Rohde 2019). Whereas gram-negative bacteria (gram(-)), only have two single layers of peptidoglycan. The gram(+) bacteria have a higher turgor pressure compared to gram(-) bacteria to reduce salt stress (Whatmore and Reed 1990) and can form physiological inactive dormant spores to survive under extreme environmental conditions (Barka et al. 2016), such as drought and high salinity. Salinity is common in Arctic soils and is often associated to high Ca availability (Jessen et al. 2014).

1.2.7 Calcium sources and cycling in Arctic permafrost soils

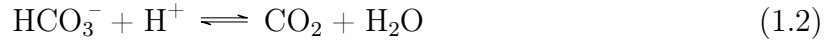
Calcium is a major element in Arctic permafrost soils. Monhonval, Mauclet, et al. (2021) estimated the total Ca pool in Yedoma soils to 123 Gt. Calcium is a macronutrient for all lifeforms and the biogeochemical Ca-cycle contains microbes, plants and soil minerals (Schaetzl and Thompson 2015). D. Walker et al. (2001) show that for northern Alaska the Ca availability defines the vegetation cover (see section 1.2.5 *Plants affect GHG release* and Fig. 1.7). The shrubs of the MNT enrich Ca in the plant material, e.g. in leaves (Villani et al. 2022). Elements that are cycled fast by plants like Ca and phosphorous (P) accumulate in the top-soil (Jobbágy and Jackson 2001). A shrub dominated vegetation will enrich Ca in the top soil layer (Mauclet et al. 2022). Drier conditions, such as warming and

permafrost degradation can shift the vegetation cover from a sedge to a shrub dominated plant community and cause enrichment of Ca in the topsoil in the Arctic (Mauclet et al. 2022).

Deeper active layer thaw and cryoturbation can mobilize Ca from the permafrost layer and transport it to near surface layers. Ice-rich Yedoma soils are massively affected by cryoturbation (Schirrmeister et al. 2011) and thermokarst processes are the main driver for Ca availabilities in the soil layers (Monhonval, J. Strauss, Hirst, et al. 2022).

The weathering of Ca containing minerals is a further important source for Ca and other elements (Schirrmeister et al. 2011). It is highly likely that element concentrations will change with mobilization of Ca containing minerals and free Ca from freshly permafrost in the future (Mauclet et al. 2022). The release of Ca to the soil depends on the lithology of the bedrock and the weathering rate. Depending on the concentration of Ca and the CEC of the silicate, it adsorbs exchangeable on the surface or it is strongly bound in the inner phases of the silicate (Bernard, Yan, and Lothenbach 2021). Gypsum (CaSO_4) has a high solubility in water and is an important Ca source in soils (Al-Barrak and Rowell 2006).

The main Ca mineral on earth is calcium carbonate (CaCO_3), which occurs in the crystal forms calcite and aragonite (CaCO_3) (Gavryushkin et al. 2021) in calcareous rocks of limestone and dolomite ($\text{CaMg}(\text{CO}_3)_2$) (Warren 2000). Carbonates are soluble in water and forms one hydroxide ion (OH^-), this explains the high pH value of calcareous soils (Eq. 1.1). The solubility of CaCO_3 and the availability of Ca strongly depend on the pH of the soil. The solubility increases with decreasing pH by formation of CO_2 (Eq. 1.2) (Dessert et al. 2003; Gal et al. 1996; Köhler, Hartmann, and Wolf-Gladrow 2010). The HCO_3^{-1} protonates to the unstable H_2CO_3 and immediately hydrolyses to H_2O and CO_2 (Eq.1.2). In soils with high pH, CO_2 precipitates with Ca and forms CaCO_3 , fixating CO_2 in the pool of soil inorganic carbon (Bughio et al. 2017; Zamanian, Pustovoytov, and Kuzyakov 2016) (Eq. 1.3). The CO_2 itself, like other acids, can dissolve carbonates (Eq. 1.3). The lysis of CaCO_3 as part of the soil inorganic carbon pool is predicted to be an important process of CO_2 emissions from calcareous soils (Sun, Meng, and Zhu 2023). This points out the importance of CaCO_3 for coupling the fast cycling soil organic carbon pool with the slow cycling soil inorganic carbon pool.



With phosphate (PO_4^{3-}) Ca forms apatite ($\text{Ca}_{10}(\text{PO}_4)_6(\text{OH},\text{F},\text{Cl})_2$) and limits the availability of PO_4^{3-} by calciumcarbonate/calciumphosphate co-precipitation (Otsuki and Wetzel 1972). The weathering of apatite from the bedrock and co-precipitated PO_4^{3-} aggregates are the most important inorganic source of fresh P in soils (Nezat et al. 2008). The calcium phosphate/carbonate co-precipitation is predicted to be a driving process causing the reduction of CO_2 release from Arctic permafrost soils with high available Ca concentrations (Schaller, Faucherre, et al. 2019).

In solution Ca^{2+} cations cause salinity. When the soil freezes, the Ca^{2+} cations are excluded from the crystal ice structure and enrich in the remaining water (Margesin and Collins 2019). This process lowers the freezing point of water and increases the share of liquid super-cooled water at soil temperatures below 0°C (Jessen et al. 2014). It covers soil particles as a few nm thick layer, promotes chemical altering of the soil components and enables microbial activity (Schaefer and Jafarov 2016), even in frozen permafrost soils.

When permafrost thaws, in particular when thermokarst occurs, Ca^{2+} is easily leached and enriched in the surface water systems (Colombo et al. 2018) where it can stabilize SOM and decrease GHG emissions (Monhonval, J. Strauss, Hirst, et al. 2022). Kosolov, Prokushkin, and Pokrovsky (2016) show a 4.5 times increase in the Ca^{2+} run-off from the Central Siberian Plateau during the time period 1955 – 2015 (Fig. 1.10). The river systems transport the Ca to the Arctic Ocean. Here it impacts ecosystem function (Mann et al. 2022) and the marine biodiversity, e.g. by supporting growth of coccolithophores (Daniels et al. 2018; Krause et al. 2018).

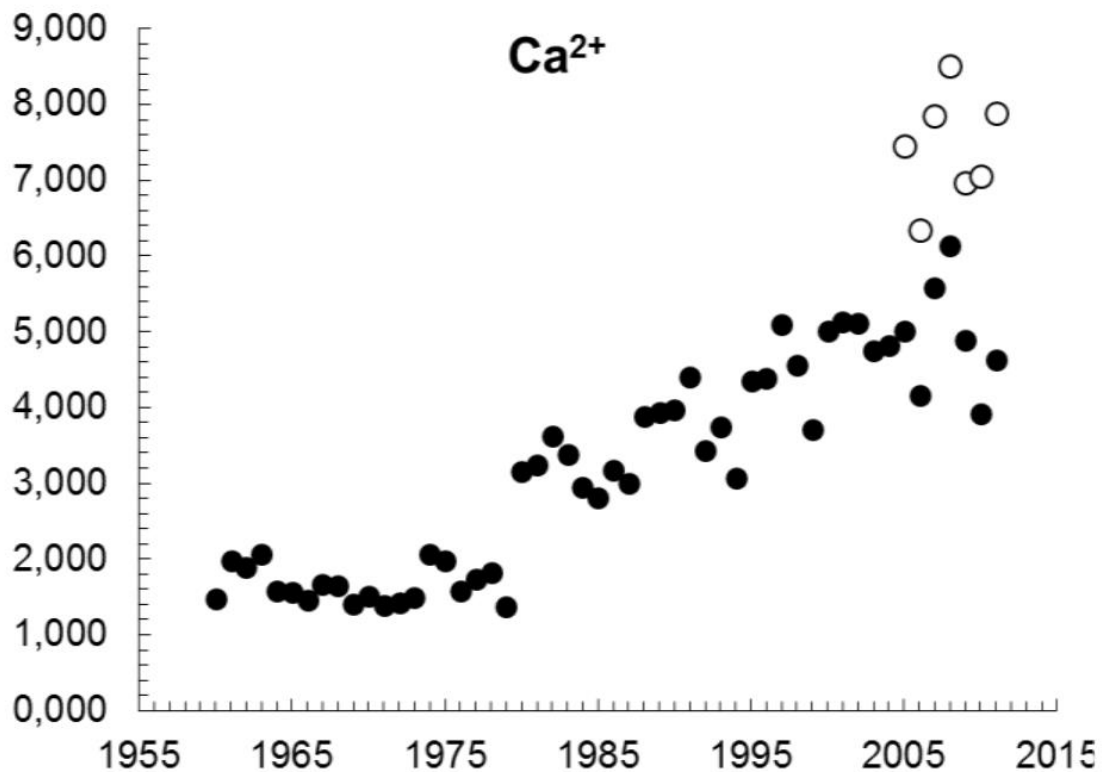


Figure 1.10: Fluxes of Ca_2^+ from the Nizhnyaya Tunguska river (Central Siberian Plateau) increased by 4.5 times in the time period 1955-2015. This increase is caused by I) an increase of water discharge and II) climate change induced permafrost degradation. From Kosolov, Prokushkin, and Pokrovsky (2016).

The Ca^{2+} cations can stabilize negatively charged SOM by cation bridging and prevent SOM from microbial decomposition (Rowley, Grand, and Verrecchia 2018). In consequence, Ca can decrease GHG emissions. Further, Ca^{2+} cations can act as bridges between SOM and the mineral surfaces of phyllosilicates (Barreto et al. 2021). With iron (Fe)-oxide minerals Ca^{2+} cations form stable Ca-Fe-SOM complexes (Rowley, Grand, and Verrecchia 2018; Beauvois et al. 2021). Sowers et al. (2020) used the scanning transmission X-ray microscopy (STXM) / near-edge x-Ray absorbance fine structure (NEXAFS) technique to show the association of C with Fe phases in the presence of Ca in Yedoma soils (Fig. 1.11 B,D,F,H).

In summary, these processes clarify, that Ca is a main driver for the availability of nutrients and the sustainability of SOM in Arctic ecosystems. Future warming may change the availability of Ca in the Arctic ecosystems. This may affect biogeochemical processes and impact the GHG release from Arctic permafrost soils.

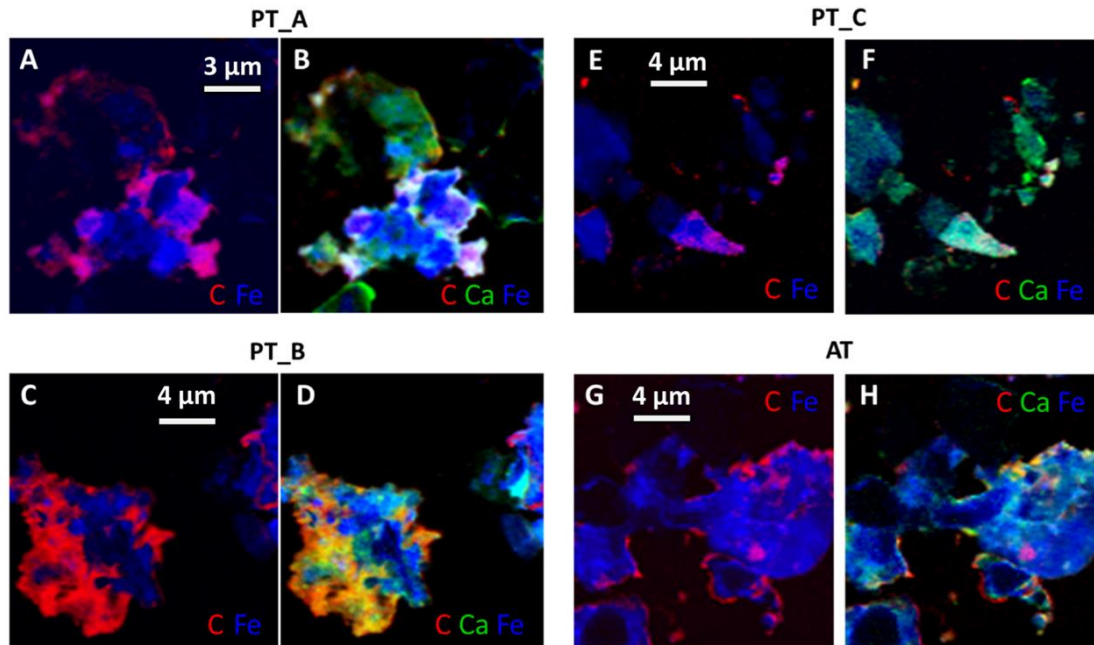


Figure 1.11: STXM/NEXAFS images of soil particles from four Yedoma soils (PT_A , PT_B , PT_C , AT). The red-blue (RB) and red-green-blue (RGB) composite images show element concentrations of C (red), Ca (green) and Fe (blue). Map areas containing high C concentrations are mainly associated with, indicate absorption of C on the surface of Fe mineral phases (A, E, C, G). The presence of Ca in the same areas are a strong hint for the importance of Ca in the formation of stable bridging Fe-Ca-SOM aggregates, shown by Beauvois et al. (2021). From Sowers et al. (2020)

1.2.8 Silicon sources and cycling in Arctic permafrost soils

The most second abundant element on earth is silicon (Si) (Turekian and Wedepohl 1961). It defines soil attributes, soil genesis, mineral formation as well as mobilization and fixation of nutrients. Monhonval, Mauclet, et al. (2021) estimated the minerogenic Si pool in Arctic Yedoma soils to 2,370 Gt of Si, mainly bound as Quartz (silicon dioxide (SiO_2)) and in silicates like Plagioclase, Illite, Kaolinite and Chlorite. From these minerals weathering processes leach silicic acid ($\text{Si}(\text{OH})_4$) from minerals to the soil (Schaller, Puppe, et al. 2021). This liquid phase of Si is biological available (Boehm 1980). The monomeric $\text{Si}(\text{OH})_4$ can condensate to dimers, trimers, tetramers etc. (polysilicic acid) and form non-crystalline amorphous silicon (ASi) (Singh, Stober, and Bucher 2002) (Fig. 1.12). The reactivity of $\text{Si}(\text{OH})_4$ and the rate of polymerization depends on the pH value. Alkaline conditions speed up polymerization, whereas acidic conditions inhibit ASi formation (Schaller, Puppe, et al. 2021).

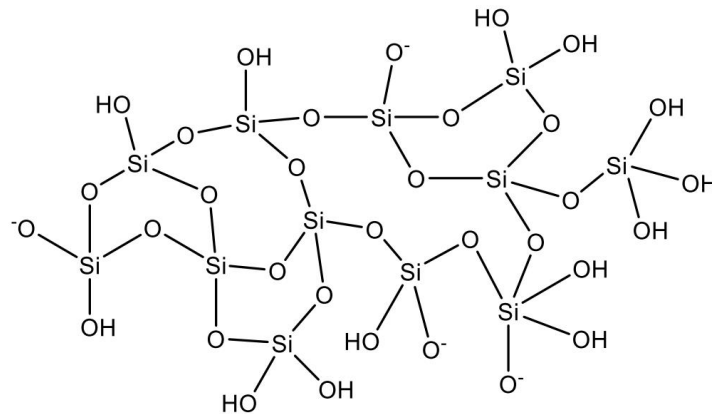


Figure 1.12: The $\text{Si}(\text{OH})_4$ can condensate to polysilicic acid and ASi. A typical crystalline structure that can be found in mineral silicates is missing. Note the different condensation states (number of OH^- groups of the single Si atoms: Primary $\text{OSi}(\text{OH})_3$, secondary $\text{O}_2\text{Si}(\text{OH})_2$, tertiary $\text{O}_3\text{Si}(\text{OH})$ and quaternary O_4Si). From Petkowski, Bains, and Seager (2020)

In contrast to crystalline Si phases like clay minerals, water can easily penetrate into the amorphous ASi phases. This results in a high water storage capacity (WSC) and increases water availability in the soil (Weil and Brady 2017; Schaller, Cramer, et al. 2020). When hydrated ASi gels forms around soil particles, it can slow the diffusion of water and substances like organic C (Schaller, Cramer, et al. 2020). When the supply of oxygen (O_2) as electron (e^-) acceptor is inhibited, other redox-sensitive substances like ferric minerals or organic substances are promoted as e^- -acceptors. Together, the reduced hydraulic conductivity and the increased WSC can promote anaerobic conditions in the soil.

Amorphous ASi easily hydrolyses to monomeric and polymeric $\text{Si}(\text{OH})_4$ and is an important source for Si in soils. This makes ASi to an important source of Si for the biosilification process in many lifeforms (Petkowski, Bains, and Seager 2020). Prokaryotic bacteria (Ikeda 2021) and eukaryotic plants, testate amoeba, diatoms and radiolarian use $\text{Si}(\text{OH})_4$ to synthesize hydrated biogenic amorphous silicon (bASi) ($\text{SiO}_2 \cdot \text{H}_2\text{O}$) (Bäuerlein, Epple, and Behrens 2007). The Si cycle is affected when plants and microbes adapt to changed environmental parameters like nutrient supply, temperature or precipitation rates. This makes clear, that the biogeochemical Si cycle will be affected directly and indirectly by Arctic climate change.

For many plants, Si is an important macronutrient (Liang et al. 2015). In particular sedges take up $\text{Si}(\text{OH})_4$ for biosilification and formation of intra- and extra-cellular phytoliths, that help to reduce biological and abiotic stressors (Katz et al. 2021). Opdekamp et al. (2012) points out the importance of tussocks (growth form of sedges) for accumu-

lation of Si, making wetlands important Si sources. A wetter and warmer future climate may promote sedge dominated wetlands and create water-filled collapse scars (Fig. 1.13). Alfredsson, Hugelius, et al. (2015) show an enrichment of bASi in the upper soil layers by litterfall of Si enriched sedge plant material and discusses the bASi accumulation in water-filled collapse scars by radiolarian and diatom growth. By now the warming and deeper active layer thickness thaw in peatlands are mobilizing Si and SOM, making it vulnerable for microbial decomposition (Alfredsson, Hugelius, et al. 2015). When future climate gets drier and warmer, shrubbification occurs. Shrubs don't accumulate high amounts of Si and it may be leached from the soil (Alfredsson, Clymans, et al. 2016) and thawing permafrost.

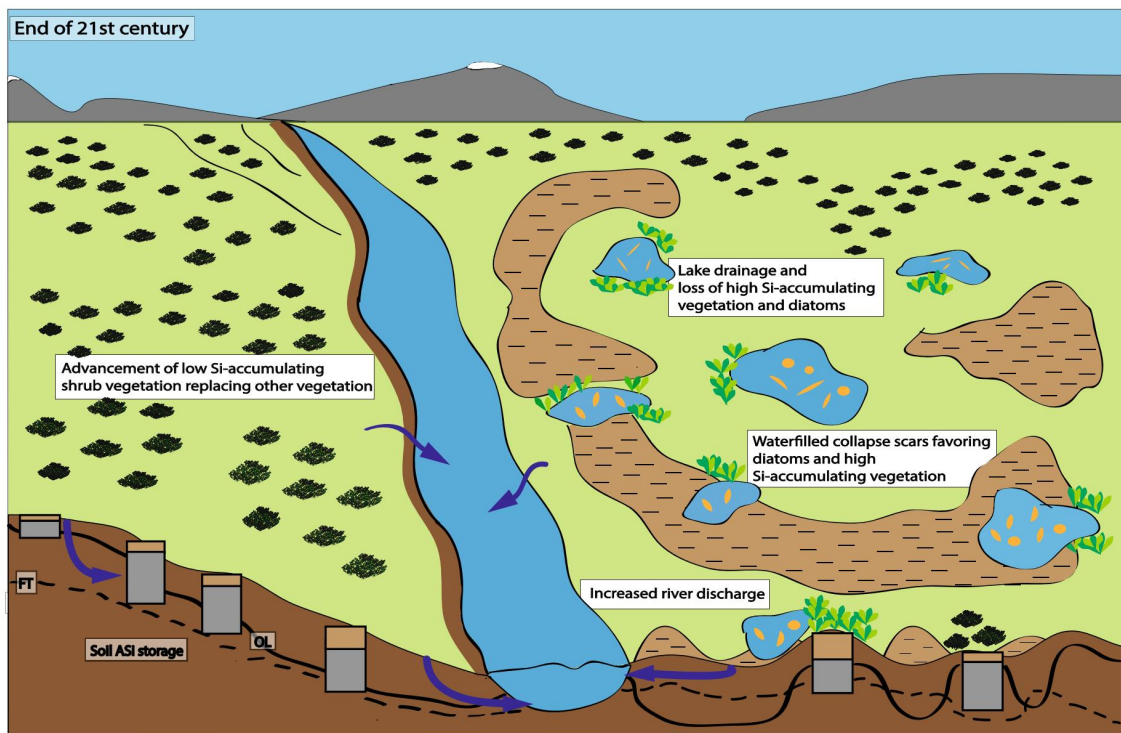


Figure 1.13: Schematic graph showing pools and transport processes of Si in Arctic tundra system. In a warmer future, two scenarios are expected: Drier climate leads to shrubbification and leaching of Si from the soil (left site). Wetter climate and thermokarst lead to sedge dominated vegetation that, together with diatoms, accumulate and fixate Si in the soil (right site). In both cases, there will be a run-off of Si to the river systems (blue arrows). Boxes represent Si pool in the organic layer (brown) and mineral layer (grey), dashed line represents active layer thickness, continuous line the organic layer depth. From Alfredsson, Hugelius, et al. (2015).

As discussed above, the Si cycle affect biotic processes and its availability will change with Arctic warming. Si, in particular $\text{Si}(\text{OH})_4$, affect the C cycling massively. Schaller, Faucherre, et al. (2019) show a positive effect of Si on the GHG release from two Greenlandic soils. The key to understanding these processes is estimated within the interactions of Si with mineral surfaces. Silicic acid interacts strongly with the surface of Fe minerals and a substitutes surface OH^- groups (Kanematsu, Waychunas, and Boily 2018). Schulz et al. (2022) show that Na_2SiO_3 treatment promotes a transformation of ferrihydrite to lepidocrocite. However, lepidocrocite was stabilized by Si and prevented from further transformation to magnetite or goethite (Fig. 1.14).

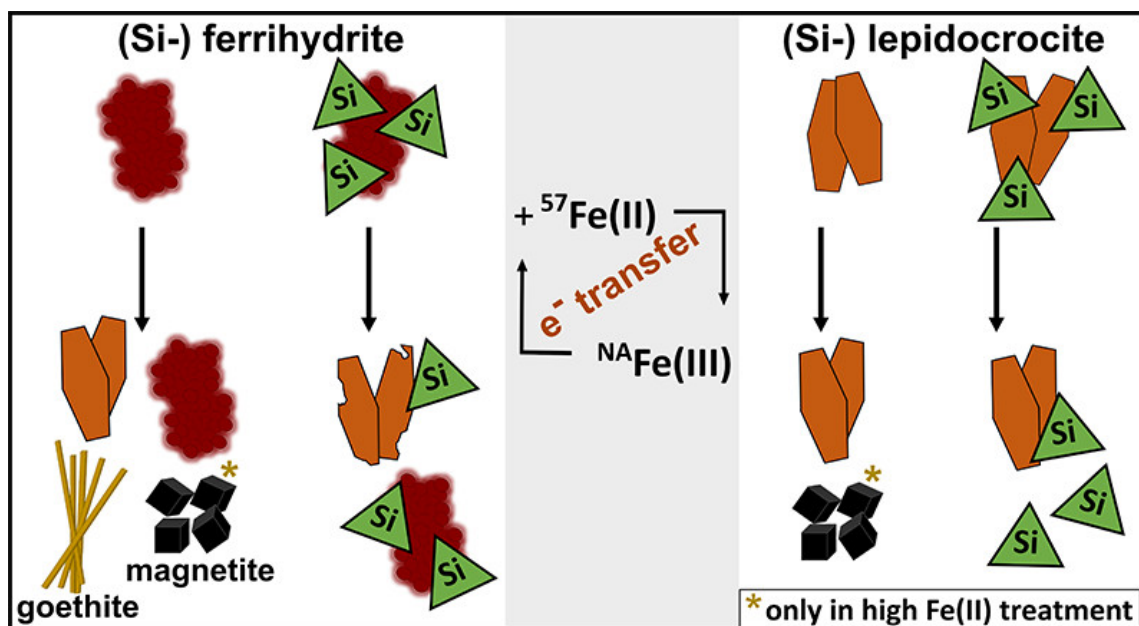


Figure 1.14: Silicate (Na_2SiO_3) substitutes OH^- groups on the surface of Fe minerals. Left side: The transformation of ferrihydrite \rightarrow lepidocrocite is promoted in the Si-treatment. Right side: The transformation of lepidocrocite \rightarrow goethite / magnetite is inhibited. From Schulz et al. (2022)

Further Si-Fe phases with high solubility are the aqueous complex $[\text{Fe}_{\text{aq}}\text{OSi}(\text{OH})_3]_{(\text{aq})}^{2+}$ (Perry and Keeling-Tucker 1998) and the amorphous phase hisingerite $[\text{Fe}_2^{3+}\text{Si}_2\text{O}_5(\text{OH})_4 \cdot 2\text{H}_2\text{O}]$ (Brigatti et al. 2011; Stamm, Zambardi, et al. 2019). Consequently, Si increases the availability of the macro nutrient Fe in the soil (Picard et al. 2016; Reithmaier et al. 2017). Simultaneously, further nutrients like P and SOM get substituted from the mineral binding sites and become vulnerable for microbial decomposition (Hömborg, Martin Obst, et al. 2020; Hömborg, Broder, et al. 2021; Schaller, Faucherre, et al. 2019).

Silicon interacts with the potentially toxic element (PTE) aluminium (Al). The formation of short-range order aluminosilicates from Al and Si in solution can decrease Al concentration in solution and by this Al availability at $\text{pH} < 5$ (Al^{3+}) and $\text{pH} > 7$ ($[\text{Al}(\text{OH})_4]^-$) (Wada and KUBO 1975; Schaller, Puppe, et al. 2021). Short-range order aluminosilicates can form from solid phases too. In this process, Si substitutes Al from solid $\text{Al}(\text{OH})_3$ phases at $\text{pH} 6 - 10$ and increases Al availability in the soil (Yokoyama et al. 2002). Short-range order aluminosilicates are secondary silicates, here $[\text{SiO}_4]$ tetrahedra, are replaced by $[\text{Al}(\text{O})_4]^-$ octahedra, creating extra negative charge in the crystal (Schaetzl and Thompson 2015). The resulting CEC is important for availability of elements like Fe in soils.

The transformation of soluble, amorphous and crystalline Si phases and the complex interactions with mineral surfaces point out the importance of the element Si in Arctic permafrost soils. In a warming Arctic, the availability of Si will change and will modify the biogeochemical processes that lead to the release of GHG.

Chapter 2

Synopsis

Using standard soil methods and cutting-edge research to unravel biogeochemical processes

2.1 The “Top - Down” research approach

This dissertation uses a “*Top – Down*” approach to search on the importance and role of Si and Ca in Arctic permafrost soils, as schematically presented in Fig. 2.1.

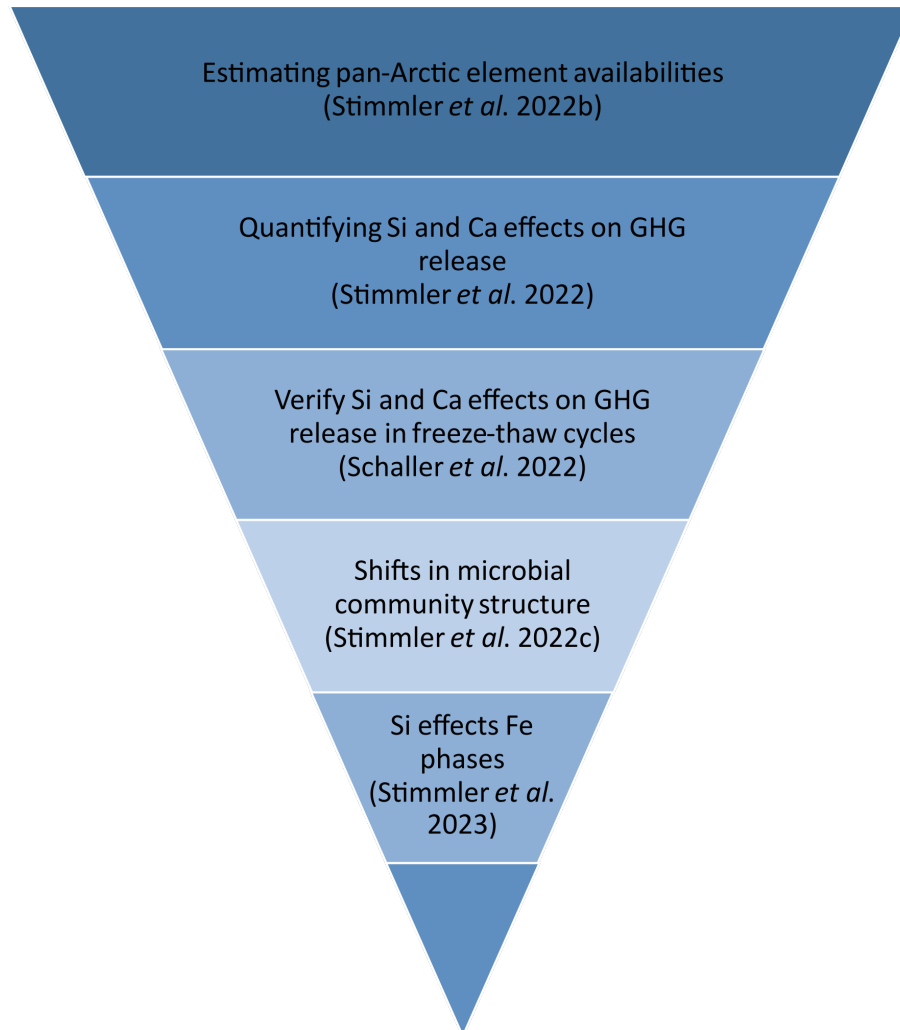


Figure 2.1: Schematic presentation of the “Top-Down” approach discussed in the dissertation. At the top, estimations are presented (Study 1: 2.2.1). In the middle, effects of Si and Ca are quantified (Study 2: 2.2.2 and Study 3: 2.2.3). At the bottom potentially underlying biological (Study 4: 2.2.4), and chemical processes are discussed (Study 5: 2.2.5).

2.2 Research questions

2.2.1 – What are the available element concentration pools in the Arctic?

2.2.2 – Does GHG release change with Si and Ca?

2.2.3 – Does temperature affect Si and Ca effects on GHG release?

2.2.4 – Does the microbial community structure change with Si and Ca?

2.2.5 – Do Fe mineral phases change with Si and Ca?

2.2.1 What are the available element concentration pools in the Arctic?

Thawing permafrost can release elements and alter element availabilities in the active layer (Patzner, Mueller, et al. 2020; Monhonval, J. Strauss, Mauclet, et al. 2021). Through run-off these elements can be transported to fresh water systems (Colombo et al. 2018; Kosolov, Prokushkin, and Pokrovsky 2016; Lamhonwah et al. 2017) and near shore systems of the Arctic Ocean. Here, they modify ecosystem functions (Goldman et al. 2013; Terhaar et al. 2021; Mann et al. 2022). In the soil, the release of elements and minerals can affect SOM stability. Release of SOM from mineral binding sites can increase microbial decomposition rates (Schaller, Faucherre, et al. 2019; Hömberg, Martin Obst, et al. 2020; Hömberg, Broder, et al. 2021), whereas the formation of mineral-SOM interactions can prevent SOM from microbial decomposition (Monhonval, J. Strauss, Hirst, et al. 2022). Modified availabilities of elements like Si, Ca, Fe and Al dramatically alter biogeochemical interactions in Arctic ecosystems. The estimation of Arctic element pools is crucial to understand C sustainability. The data on element availabilities help predict the permafrost carbon feedback and are crucial to predict future climate scenarios (Schuur, McGuire, et al. 2015; Treat et al. 2021; Virkkala et al. 2021).

The effect of the Arctic warming on the temperature regimes in Arctic ecosystems are complex and difficult to predict. It is likely that new pools of organic carbon and elements will be released from thawed permafrost and modify biogeochemical processes (Hugelius, Loisel, et al. 2020). In consequence, GHG release can increase and hold the potential to fasten global warming. Hence, reliable data on pools of organic carbon and element availabilities in the pan-Arctic are crucial for modelling carbon cycles and future climate scenarios. Most earth system models (ESM) do not take biogeochemical interactions into account and ignore the relevance of elements like Si or Ca. However, ESM approaches like QUINCY are capable of accounting for element availabilities (Lacroix et al. 2022; Thum et al. 2019). These models fill the gap of knowledge for element concentrations in the Arctic.

Alfredsson, Clymans, et al. (2016) used the circumpolar Arctic vegetation map (D. A. Walker et al. 2005) to estimate pools of ASi, based on the biogeochemical interactions of soil elements and plants (Jobbágy and Jackson 2001; D. Walker et al. 2001). Following the findings from Reimann et al. (2001) concerning the correlation of element concentrations and lithologies, we used 14 lithological classes from the high resolved Geological Map Of The Arctic (Harrison et al. 2011) to extrapolate local element availabilities on a pan-Arctic scale. This approach takes the parent material and lithology into account as drivers for element availability (Alloway 2013).

In Stimmler, Goeckede, Elberling, et al. (2022) we present one of the first datasets to close this data gap. We present pan-Arctic maps (At a scale of 1 : 5.000.000, Arctic regions northerly of latitude $60^{\circ}N$) of biologically available element concentrations, further referred to as available element concentrations. The maps represent the organic layer, the active layer, the uppermost permafrost layer and the average depth of 0 – 1 m. In total 574 soil samples from 25 locations in the pan-Arctic were extracted using the Mehlich III method (Sims 1989). These extracts represent the fraction of the elements Si, Ca, Fe, Al and P in the pore water and absorbed organic and inorganic particles, that are available for microbes and plant nutrition. For the solid fraction of biological available Si, an alkaline extraction of DeMaster (1981) was used.

Our data show that in regions like Iceland, where e.g. basalt and associated rock is dominant, ASi concentrations were highest ($6.7 \pm 1.2 \text{ mg ASi g}^{-1} \text{ DW}^{-1}$) (Fig. 2.2).

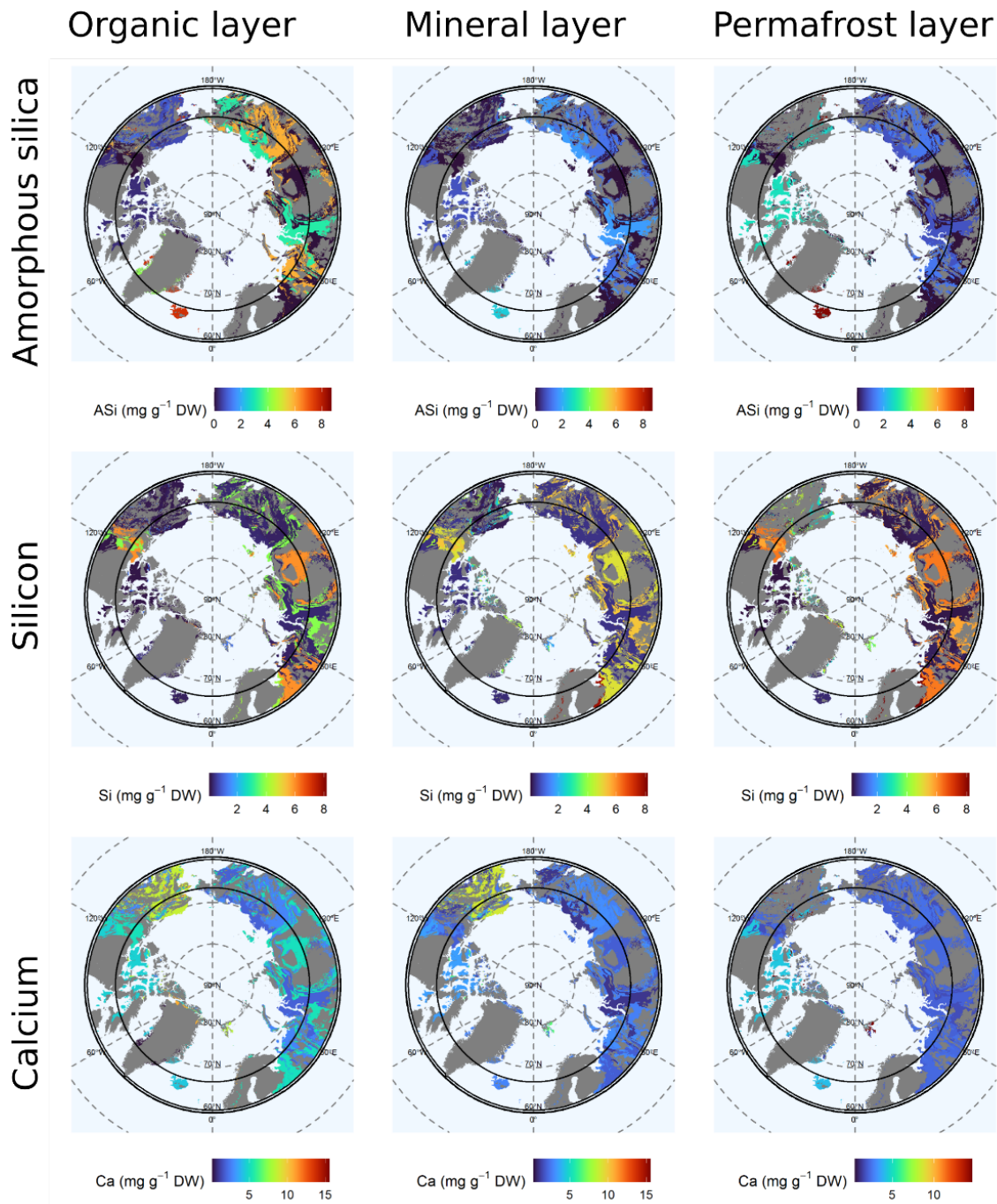


Figure 2.2: Solid fraction of ASi and available element concentrations Si and Ca in organic layer, mineral layer (as part of the active layer) and upper permafrost layer (maximal depth of 1 m) (left to right). Blue color represents low element concentrations, red color represent high element concentrations. From Stimmler, Goeckede, Elberling, et al. (2022).

In the Canadian Shield, ASi concentrations are higher in the permafrost layer (2.8 ± 2.5 mg ASi g^{-1} DW $^{-1}$), compared to the current active layer (1.2 ± 0.1 mg ASi g^{-1} DW $^{-1}$). A deeper thawing due to future warming will potentially increase ASi concentrations in the active layer in the Canadian Shield. In general, higher ASi concentrations were found in Siberia, compared to Canada and Alaska.

An increase of Ca with deeper thawing is expected in Alaska, here 10.4 ± 2.8 mg Ca g^{-1} DW $^{-1}$ were found in the permafrost layer compared to 2.9 ± 0.5 mg Ca g^{-1} DW $^{-1}$ in the active layer.

A wide range of element availabilities are found in Yedoma soils. These sediments formed mainly in Siberia from fluvial deposits during the Pleistocene and are rich in C and ice (Schirrmeister et al. 2011). Yedoma soils are very vulnerable to thermokarst and element release (Monhonval, Mauclet, et al. 2021; J. Strauss et al. 2017). In particular in these regions the maps of element availability presented in this study will help predict future changes in element release.

The maps give an overview on element availability distribution in the pan-Arctic regions and provide essential data for biogeochemical approaches in ESMs. Applying this data in ESMs will help to predict C cycling in Arctic permafrost soils and future climate scenarios.

2.2.2 Does GHG release change with Si and Ca?

The release of macro-nutrients and elements like Si and Ca from thawing permafrost, due to Arctic warming, change biogeochemical interactions. This points out the need for research on the effects of elements on GHG release. For this, in Stimmler, Goeckede, Natali, et al. (2022), I studied the effect of Si and Ca on GHG release on a local scale. I compared the GHG release of five soils: soil C1 from Chersky, NE-Siberia, Russia (C1), soil C2 from Chersky, NE-Siberia, Russia (C2), soil Ca1 from Baffin Bay, Canada (Ca1) and soils from the moist acidic tundra, Alaska (MAT) and moist non-acidic tundra, Alaska (MNT). Changing water availabilities are predicted (Göckede, Kittler, et al. 2017). These scenarios were simulated by incubation at 5°C under drained and waterlogged conditions.

Availabilities of Si and Ca in the active layer are predicted to change with increasing active layer thickness (D. Walker et al. 2001; Alfredsson, Hugelius, et al. 2015; Alfredsson, Clymans, et al. 2016; Stimmler, M. Obst, Stein, et al. 2023). To simulate altered levels of Si and Ca, soils were incubated with four expectable concentrations of Si (+0, +3, +6, +10 mg ASi g⁻¹ DW⁻¹, added as pyrogenic amorphous silicon) and Ca (+0, +5, +10, +15 mg Ca g⁻¹ DW⁻¹, added as CaCl₂). In total 20 treatments were incubated with n=4: 4 Si treatments × 4 Ca treatments + 4 controls. The GHG CO₂ and CH₄ were analyzed with gas chromatography / flame ionisation detector (GC-FID) from headspace after 4 d incubation in the closed vial. In order to analyze GHG release in a steady state the headspace was analyzed after intervals of 4, 8, 12 and 24 weeks of incubation (Henry 2008; Schaller, Faucherre, et al. 2019).

The effect of Si on the GHG release was complex: Under waterlogged conditions a strong positive effect of Si on CO₂ release was found with +6 mg ASi g⁻¹ DW⁻¹ in pH neutral mineral soils (MAT: 2695.8 ± 668.3 → 4417.8 ± 3228.9 μmol CO₂ kg⁻¹ DW⁻¹ d⁻¹; Fig. 2.3C) and with +10 mg ASi g⁻¹ DW⁻¹ in alkaline mineral soils (MNT: 499.6 ± 313.2 → 779.4 ± 346.5 μmol CO₂ kg⁻¹ DW⁻¹ d⁻¹) (Fig. 2.3B). However, in the organic soil under drained conditions +3 mg ASi g⁻¹ DW⁻¹ showed the largest positive effect on CO₂ release (Ca1: 1289.2 ± 246.2 → 2161.6 ± 618.3 μmol CO₂ kg⁻¹ DW⁻¹ d⁻¹) (Fig. 2.3D).

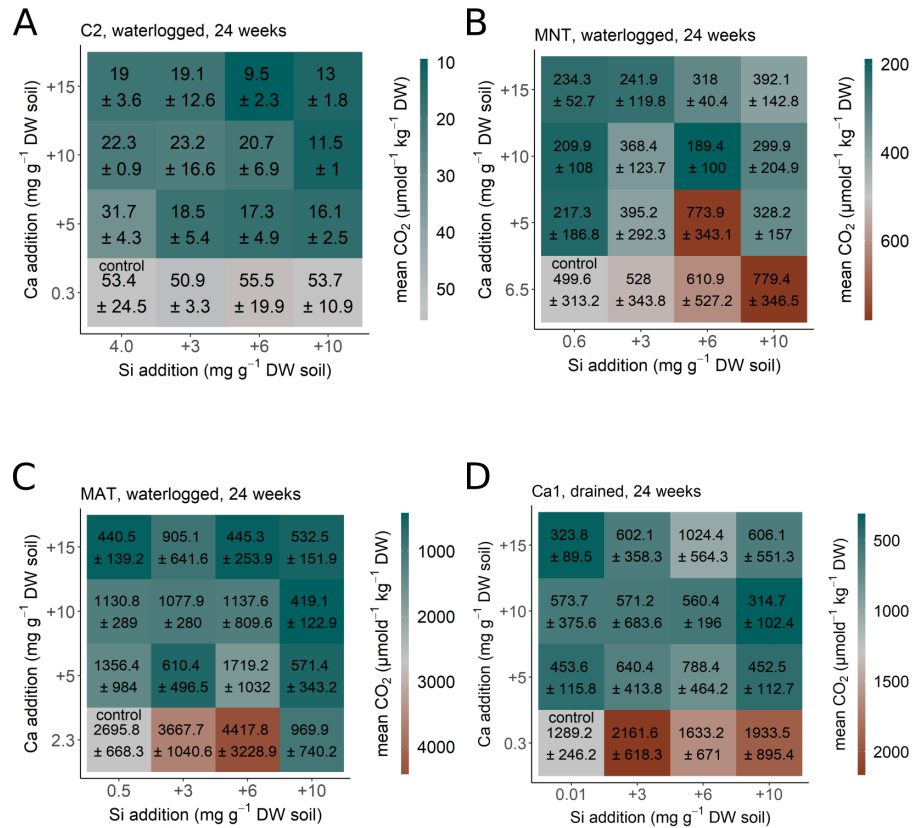


Figure 2.3: CO₂ production of the soils (A) C2, (B) MNT, and (C) MAT incubated under waterlogged conditions and (D) Ca1 incubated under drained conditions. Each square represents a treatment with n=5 of Ca (+0, +5, +10, +15 mg Ca g⁻¹ DW⁻¹) and Si (+0, +3, +6, +10 mg ASi g⁻¹ DW⁻¹). Data from the soil C1 are not shown. From Stimmler, Goeckede, Natali, et al. (2022).

The reason for the increased CO₂ production under increased Si concentrations could be the mobilization of P and SOM from mineral binding sites by substitution with polysilicic acid, making it vulnerable for microbial decomposition (Reithmaier et al. 2017; Schaller, Faucherre, et al. 2019; Hömberg, Martin Obst, et al. 2020; Hömberg, Broder, et al. 2021). Further, ASi is known to increase WSC and decrease hydraulic conductivity (Schaller, Cramer, et al. 2020; Schaller, Puppe, et al. 2021). The decreased diffusion rates of e⁻-acceptors like O₂ and organic carbon can promote anaerobic, reductive conditions (Schaller, Cramer, et al. 2020).

The negative effect of Ca on CO₂ release was cancelled out by Si only in the MNT soil. Assuming increased active layer thickness in the future, it is likely that cryoturbation will transport elements like Si and Ca from thawed permafrost layer to upper soil layers and will change element availability in the active layer. This will modify CO₂ release in differ-

ent ways: In soils from Siberia (C1, C2) Si and Ca concentrations are higher in the active layer, compared to the permafrost layer (Stimmler, M. Obst, Stein, et al. 2023). A deeper thaw could hence lead to reduction of both elements and by this increase CO₂ release. For soil from the MAT, D. Walker et al. (2001) showed higher Ca concentrations in the permafrost layer. Therefore, a deeper thaw would increase Ca level in the active layer and decrease CO₂ release. For the MNT soil, the CO₂ release is expected to decrease. We show general and site-specific effects of Si and Ca on CO₂ release. We conclude, that Si and Ca have major effects on the release of CO₂ from various soils. Yet, after this study, another major research gap remains concerning the temperature effect on GHG release in presence of Si and Ca, to simulate naturally occurring seasonal freeze-thaw cycles.

2.2.3 Does temperature affect Si and Ca effects on GHG release?

In Schaller, Stimmler, et al. (2022) we were able to show the positive effect of Si (+6 mg ASi g⁻¹ DW⁻¹) and negative effect of Ca (+5 mg Ca g⁻¹ DW⁻¹) again on CO₂ release for the soil C3 from Chersky, NE-Siberia, Russia (C3). These findings are in accordance with the results found by Stimmler, Goeckede, Natali, et al. (2022). An important addition in this second study about Si and Ca on CO₂ release was to take the effect of temperature into account.

The GHG release depends on seasonality, it is higher in thawed soil compared to frozen soil (Kim et al. 2012; Sapronov 2021; Zhang et al. 2022). The warming of the Arctic changes the temperature regime in the soil: The number of total annual freezing days is decreasing (Rantanen et al. 2022), whilst the number of annual freeze-thaw cycles (oscillation around 0°C) increases (Henry 2008). With every thawing fresh SOM may be mobilized from the active layer and becomes vulnerable for microbial decomposition. This causes a strong GHG pulse directly after thawing (Kim et al. 2012). Furthermore, nutrients like N (Larsen, Jasson, and A. Michelsen 2002) and other elements like Al and Fe (Loiko et al. 2017) can get mobilized.

We also assumed that the effect of Si and Ca on GHG release depends on seasonality, too. To analyze the effect of changing temperature on Si and Ca under laboratory conditions, we used an automated temperature and temporal high-resolution approach (PICARRO). Two complete freeze-thaw cycles (in total 65 days) were simulated as recommended by Henry (2008). To simulate field conditions we used the temperature profile occurring under field conditions at 50 – 60 cm depth (Göckede, Kittler, et al. 2017; Göckede, Kwon, et al. 2019) (Fig. 2.4).

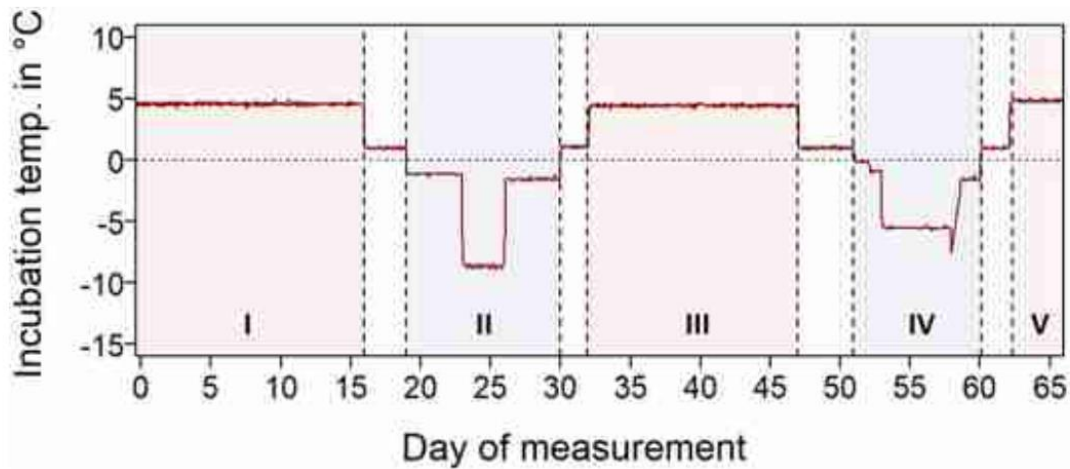


Figure 2.4: Air temperature regime representing two complete freeze-thaw cycles of the incubation experiment with the soil C3. Duration and value of temperature were extrapolated from field site data measured in 50 – 60 cm depth. From Schaller, Stimmler, et al. (2022).

As in our previous study by Stimmler, Goeckede, Natali, et al. (2022), we found a positive effect of Si (+28%) and negative effect of Ca (−40%) on CO₂ release over the whole incubation period, compared to the control soil without addition of Si and Ca. Addition of Si did not cancel out the Ca effect, in the Si+Ca treatment, as CO₂ release decreased only slightly less, in comparison to the pure Ca treatment (−29%). At this point, we cannot preclude that at certain Si:Ca ratios the effects of Si and Ca may cancel out.

The effect of Ca on CO₂ release was temperature dependent: under thawed conditions, the addition of a fixed dose of Ca reduced CO₂ release significantly (Fig. 2.5B), whilst CO₂ release remained constant for the frozen soil. The Si effect on CO₂ release was also temperature dependent. Here, soils treated with Si emitted significantly more CO₂, than the control soil under frozen conditions (Fig. 2.5C). The positive effect on CO₂ release decreased strongly during the incubation time (−82% CO₂ release from 1st to 3rd freezing period), compared to CO₂ release in the control soil (−24%). The decrease of GHG release of Arctic permafrost soils during repetitive thawing had been shown before in other studies (Kurganova, Teepe, and Lofffield 2007; Sapronov 2021). Our data suggests a fast response of labile C to an increasing number of freeze-thaw cycles in the future (Henry 2008). Rooney et al. (2022) suggested biogeochemical processes, soil properties, mineralogy, and element availabilities as further important factors controlling the stability of C in Arctic permafrost soils. Another significant factor revealed by our studies is Si: It has a positive effect on GHG release in Arctic soils (Schaller, Faucherre, et al. 2019; Stimmler, Goeckede, Natali, et al. 2022).

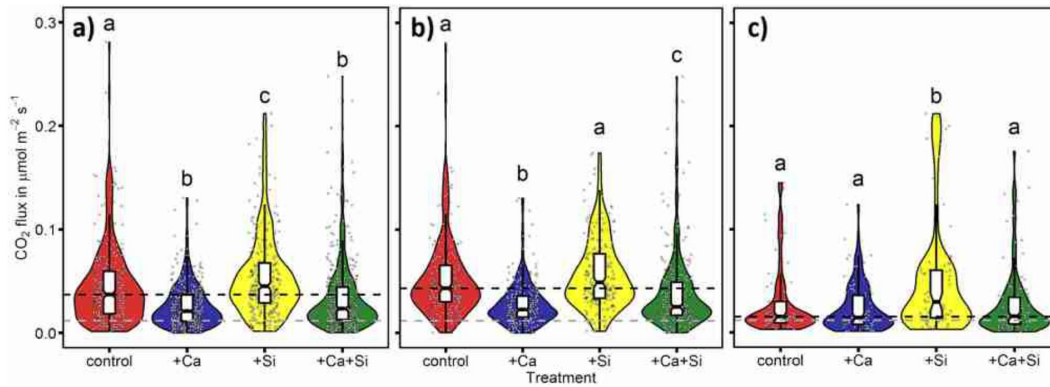


Figure 2.5: CO₂ fluxes from the soil C3 incubated with only water (control), +5 mg Ca g⁻¹ DW⁻¹ (+Ca), +6 mg Ca g⁻¹ DW⁻¹ (+Si), and same Ca and Si concentrations combined (+Ca + Si). a) during the entire incubation period of 65 days containing two complete freeze-thaw cycles, b) during the two periods with temperature > 1°C and c) during the three periods with temperature < 1°C. Letters indicate significant differences between the CO₂ fluxes between the treatments. From Schaller, Stimmler, et al. (2022).

In our recent study Schaller, Stimmler, et al. (2022), we point out the importance of Si on frozen soils. This indicates further effects of Si for GHG release in addition to Si being a source of ASi for Si(OH)₄ (Schaller, Puppe, et al. 2021), that can substitute P and SOM from mineral binding sites and make it more available for microbes (Hömborg, Martin Obst, et al. 2020; Schaller, Faucherre, et al. 2019).

The presence of Si can reduce the freezing point of water (Kahlenberg and Lincoln 1898; Kumar, M.lli, and P. 2019) and lead to thin layers of super cooled water covering soil particles (Schaefer and Jafarov 2016). Microbial activity below 0°C is limited rather by water availability than temperature (Margesin and Collins 2019), hence increased availability of liquid water at T < 0°C can increase the GHG release by enabling microbial activity. This super cooled water fraction can also be increased by increased Ca concentrations (Jessen et al. 2014). In contrast to Si addition, the increased film of super-cooled water caused by increased Ca did not increase CO₂ release, but decreased it. This in accordance with other studies that show that higher Ca concentration decreased GHG release (Whittinghill and Hobbie 2012; Schaller, Faucherre, et al. 2019; Stimmler, Goeckede, Natali, et al. 2022). Our results indicate that Si and Ca are the main drivers for water availability and salinity in the analyzed Arctic soils and by this affect the activity of microbial decomposers (Mavi et al. 2012).

2.2.4 Does the microbial community structure change with Si and Ca?

In Stimmler, Goeckede, Natali, et al. (2022) we show the effects of Ca and Si on GHG release from Arctic soils and that these effects are temperature-dependent (Schaller, Stimmler, et al. 2022). We hypothesized the liquid super-cooled water fraction and salinity as main drivers behind the effects of Si and Ca on GHG release. The super-cooled water on the surface of soil particles also changes conditions for microbial activity and would modify GHG release. Further, the thawing of permafrost affects microbes and their activity by:

1. Increased availability of liquid water induces elevated microbial activity (Margesin and Collins 2019).
2. The pool of microbial available SOM, nutrients and elements increases (Larsen, Jasson, and A. Michelsen 2002; Grogan et al. 2004; Loiko et al. 2017).
3. Increased availabilities of water and nutrients activates dormant states of microbes and causes changes in transcriptional profiles of microbes (Coolen and Orsi 2015). This promotes pathways for C and N cycling (Mackelprang et al. 2011).

In our next study Stimmler, Priemé, et al. (2022), we tested how the presence of Si and Ca affect MCS in Arctic soils. The MCS and microbial metabolisms strongly influence the cycling of C (Monteux et al. 2020). To analyze effects of Si and Ca on MCS, we sequenced prokaryotic 16s ribosomal ribonucleic acid (rRNA) gene *V3 – V4* regions and fungal 16s rRNA gene *ITS2* regions using Illumina® technique and quantitative polymerase chain reaction (qPCR). For this experiment, we sampled a salt-poor soil from Disko Island (pH~5.6) and a salt-rich soil from Peary Land (pH~8.4), two sampling locations in Greenland. Both soils were incubated with different levels of Si and Ca (Schaller, Faucherre, et al. 2019). The geology of the Greenlandic soils differs massively from many other Arctic soils, such as C1, C2, MAT, MNT and Ca1.

The location Peary Land is a polar desert characterized by low precipitation, low temperatures, and high salinity by salt input from the sea. This results in soils with high Ca concentrations ($15.6 \text{ mg Ca g}^{-1} \text{ DW}^{-1}$), high pH (~ 8.4), increased salt- and drought stress for microbes, and low vegetation cover. In contrast, Disko Island is characterized by high vegetation cover with underlying weathered basaltic rock. The soils contain comparatively high Si concentrations ($5.2 \text{ mg ASi g}^{-1} \text{ DW}^{-1}$) and have a lower pH (~ 5.6). We differentiate between direct and indirect effects of Si and Ca on GHG release, that were found by Schaller, Faucherre, et al. (2019). The results were summarized in a structural

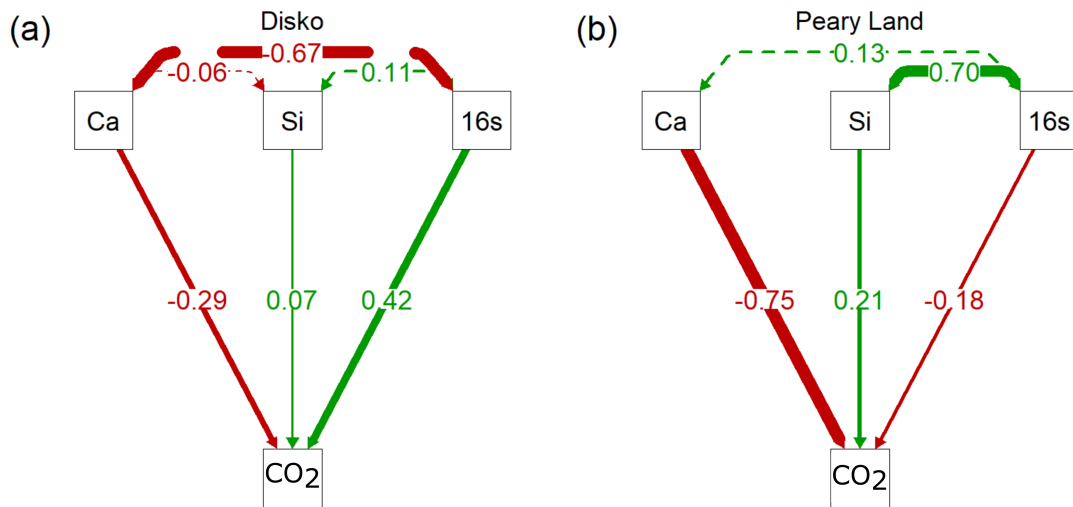


Figure 2.6: SEM of (a) salt-poor soil from Disko Island and (b) salt-rich soil from Peary Land. Boxes show the factors Ca concentration (Ca), Si concentration (Si), CO₂ release (CO₂) and bacterial abundance (16s). Green arrows represent positive effects, red arrows negative effect. Values given represent the strength of the effect. From Stimmler, Priémé, et al. (2022).

equation model (SEM). For the weakly acidic, salt-poor soil from Disko Island, the addition of Ca had an indirect effect on the GHG release. Calcium decreased the total number of bacteria and by this GHG release (Fig. 2.6A).

However, in alkaline, salt-rich soils from Peary Land, Ca had a direct negative effect on the CO₂ release (Fig. 2.6B). This could be explained by the calciumcarbonate/calciumphosphate-coprecipitation under alkaline conditions (Schaller, Faucherre, et al. 2019).

In addition to those effects, we show that gram(+) bacteria profited from the addition of Ca and led to a shift in the original MCS. In both soils Ca addition promoted the share of gram(+) bacteria. In the original salt-poor soils from Disko Island (1.7 mg Ca g⁻¹ DW⁻¹), the addition of Ca led to a shift from an originally gram(-) dominated MCS (Acidobacteria, Proteobacteria) to gram(+) dominated MCS (Actinobacteria, Firmicutes). In the salt-rich soils from Peary Land (15.6 mg Ca g⁻¹ DW⁻¹), the addition of Ca promoted the originally dominant gram(+) *Staphylococcus* (Firmicutes).

Our findings to MCS are in accordance with other studies on microbes in the Arctic. The gram(+) Firmicutes and Actinobacteria and the gram(-) Acidobacteria and Proteobacteria are important taxa in permafrost affected soils and were found all over the pan-Arctic (Jansson and Taş 2014) (Fig. 1.9). Many cold-adapted bacteria developed different strategies to survive under extreme conditions like cold, salinity, and drought: Modified extracellular polysaccharides (Qurashi 2011) and lower membrane viscosity (Denich et al.

2003), or cold shock proteins (Suetin et al. 2009), reduce freezing damages of the microbes and enable surviving at temperatures below 0°C . Bacteria of the genus *Staphylococcus* have increased intracellular potassium and glutamate levels (Whatmore and Reed 1990) to reduce osmotic stress under high salinity conditions. A common strategy, particularly in gram(+) taxa like Firmicutes, survive extreme conditions by the formation of physiologically inactive spores and other dormant states (Barka et al. 2016; Rosenberg et al. 2014).

The formation of physiological inactive spores could be a further explanation for reduced CO_2 release after Ca addition. In salt-poor soils from Disko Island, the relative share of potentially physiological inactive gram(+) Firmicutes and Actinobacteria increased after addition of Ca. Further, in soils from Peary Land, the absolute abundance of gram(+) dominated bacteria increased (data on qPCR). In both soils, the increase of potentially physiologically inactive gram(+) taxa could have led to decreasing CO_2 production rates. Interestingly, high concentrations of Si increased absolute abundance of the gram(+) bacterial taxa *Staphylococcus* in salt-rich soil from Peary Land, but without increasing CO_2 release. This is a hint for the presence of potentially dormant states of bacteria under high Si levels (Schaller, Böttger, et al. 2016; Song et al. 2021). However, in salt-poor soils from Disko Island addition of Si had no effect on absolute bacterial abundance. This indicates that Si can decrease Ca induced salt stress for halo-tolerant microbes, an effect that was already shown for plants (Coskun et al. 2016). In the lack of Ca induced salt stress, Si seems to promote the physiological activity of gram(-) bacteria, increasing rates of SOM decomposition and CO_2 release.

The shifts in the MCS and the microbial abundance depended on the original Ca and Si concentrations. In both soils, the microbial abundance was higher, compared to the fungal abundance. Fungal abundance decreased much less dramatically in the soil from Peary Land subjected to the Ca treatment, compared to the Ca treatment of the Disko Island soils. In soils from Disko Island, the fungal MCS was dominated by Ascomycota and Mortierellomycota at original conditions, but dominated by Basidiomycota at high Ca concentrations. Fungi require Ca and tolerate high Ca concentrations (Pitt and Ugalde 1984), especially Basidiomycota are known to be well adapted to cold and salinity stress (Hassan et al. 2016). Our findings point out at least two important processes in which Si and Ca can affect CO_2 release: Mobilization of nutrients and changes in microbial abundance and in the MCS.

The role of microbes for GHG release from Arctic soils cannot be underestimated. We show strong effects of Si and Ca on the microbial abundance and MCS. In the last study I analyzed the effects of Si and Ca on the mobilization of nutrients and SOM from in the mineral phases.

2.2.5 Do Fe mineral phases interact with Si and Ca?

After permafrost thaw, the availability of Si in the active layer is predicted to increase in certain regions of the Arctic (Stimmler, Goeckede, Elberling, et al. 2022). It was shown that $\text{Si}(\text{OH})_4$ can substitute SOM and P from mineral binding sites (Hömberg, Martin Obst, et al. 2020; Schaller, Faucherre, et al. 2019). Further, increased Si availabilities could mobilize macro-nutrients like Fe, as shown in temperate peatlands (Reithmaier et al. 2017) and PTE like aluminium. Nutrients and PTE can affect conditions for microbial activity and thus change the C cycling and GHG release from Arctic soils.

The effects of Si and Ca on Fe and Al in Arctic soils are poorly understood. To fill this knowledge gap, in Stimmler, M. Obst, Stein, et al. (2023), the effects of Si and Ca on the availability of the macronutrient Fe and cytotoxic Al were analyzed. Therefore, the element availabilities of Si and Ca on Fe and Al were analyzed in the four soils C2, MAT, MNT and Ca1 from Stimmler, Goeckede, Natali, et al. (2022).

The available element concentrations (Mehlich III extracts, see also Stimmler, M. Obst, Stein, et al. (2023)) of Si, Ca, Fe, and Al of the four soils were clustered in a metric multi-dimensional scaling (mMDS). The data suggests a high similarity of the weak acidic mineral soils C2 from NE-Siberia and MAT from Alaska. The mineral soil MNT from Alaska was clearly separated, likely due to the higher pH (~ 8.0). The SOM-rich soil Ca1 from Canada could also be separated clearly (data not shown).

In the next step, the results of the mMDS analysis were complemented by correlation analysis of the element availabilities in the four soils. In the mineral soils MAT and MNT from Alaska the availabilities of Si and Fe correlated significantly positively. One explanation could be, that ASi reduces the hydraulic conductivity around soil particles. This reduces diffusion rates of important e^- -acceptors like SOM and O_2 to the microbes on the particle surface and promotes the use ferric Fe(III) minerals as e^- -acceptors and increase the share of ferrous Fe(II) minerals (Fig. 2.8-2) (Schaller, Cramer, et al. 2020).

To test this hypothesis, we specified the Fe mineral phases of soils using the STXM-NEXAFS technique. This approach uses X-ray absorption and microscopy for spatially fine structured analysis to help identify, map, and specify chemical species (Hömberg, Martin Obst, et al. 2020; Schaller, Faucherre, et al. 2019; Schaller, Stimmler, et al. 2022). In the soil C2, the ratio of ferrous phases (vivianite-like) was significantly higher in the areas representing the bulk particle (high optical density (OD)), compared to areas of the particle surface (low OD) (Fig. 2.7). In the Si treatment the ferrous vivianite-like phases prevailed, whereas mainly ferric phases (ferrihydrite-like) were present in the control soil. This supports the hypothesis that ferric minerals act as e^- -acceptors, creating ferrous minerals. In the next step, these lower crystallized ferrous minerals get stabilized

by substitution of OH^- groups with $\text{Si}(\text{OH})_4$. The higher water solubility of low crystallized ferrous minerals, in consequence, increases the Fe availability.

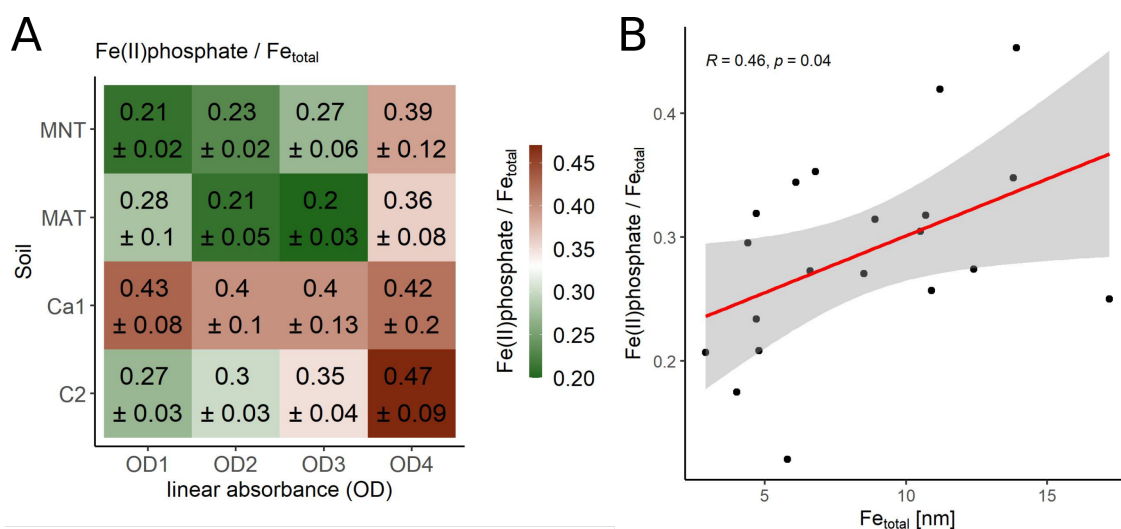


Figure 2.7: A) Ratio of ferrous vivianite-like phases (Fe(II)phosphate) to all Fe phases (Fe_{total}) for areas with specific ODs (Outer to inner particle: OD1→OD4). Layer thickness for single Fe phases were extracted from the species-specific curve fitting of spectra, including all treatments of Si. Rows represent the soils C1; Ca1; MAT and MNT. Given are the mean and standard deviation. B) Ratio of Fe(II)phosphate/ Fe_{total} of all soils and treatments in regression to Fe_{total} . Given is also the Pearson correlation at a confidence interval of 95%. From Stimmler, M. Obst, Stein, et al. (2023).

Another explanation for the positive effect of Si on the Fe availability could be the formation of short-range order ironsilicates (Stamm, Baldermann, et al. 2023), like hisingerite. Furthermore, $\text{Si}(\text{OH})_4$ can substitute OH^- -groups of existing Fe minerals surfaces (Kane-matsu, Waychunas, and Boily 2018) and prevent them from further crystallization and mineral transformation (Fig. 1.14 and Fig. 2.8-1) (Schulz et al. 2022). The high solubility of these low crystalline ferrous Fe silicates increase the pool of soluble Fe phases.

In contrast to the positive effect of Si on the Fe availability, the effect of Si on the availability of Al was pH dependent. In the weak alkaline soil MNT (pH= 8), the Al availability decreased significantly with Si addition. This could be explained by the formation of short-range order aluminosilicates under alkaline (pH> 7) conditions (Wada 1988) (Fig. 2.8-4). In the three more acidic soils (C2, MAT and Ca1), the addition of Si had a positive effect on the Si on Al availability. The underlying mechanism could be the substitution of Al with $\text{Si}(\text{OH})_4$ from solid $\text{Al}(\text{OH})_3$ phases (Yokoyama et al. 2002) (Fig. 2.8-3).

The addition of Ca increased the Fe availability in the soil C2), decreased the Fe availability in the soils Ca1 and MAT. There was no effect on Fe availability in the soil MNT.

The pH seemed to be the main driver for this Ca effect. Ionic Ca can increase the pH of soils and by this decrease the solubility of Fe minerals (H. Marschner and P. Marschner 2012). This would explain the decreased Fe availability in the neutral mineral soil (MAT) and organic soil (Ca1), as well as the absence of this effect in the alkaline soil (MNT).

The interaction of Ca with Fe phases is important for SOM stability, as the formation of Ca-Fe-SOM aggregates dramatically increases the sorption capacity of SOM and Fe (Beauvois et al. 2021) (Fig. 2.8-8). Increased Ca levels can stabilize these Ca-Fe-SOM aggregates and decrease availability of Fe. Further, Fe has a low availability when it is bound on mineral surfaces with high CEC. The positive effect of Ca on Fe can be explained by substitution from these mineral binding sites (Fig. 2.8-7).

The effect of Ca addition on the Al availability was negative in all soils. The soluble Al could be bound in the crystal structure of fresh formed solid $\text{Al}(\text{OH})_3$ phases at high pH (Kryzevicius et al. 2019). At low pH, an absorption in freshly formed Ca-SOM aggregates (cation bridging) is plausible (Fig. 2.8-5).

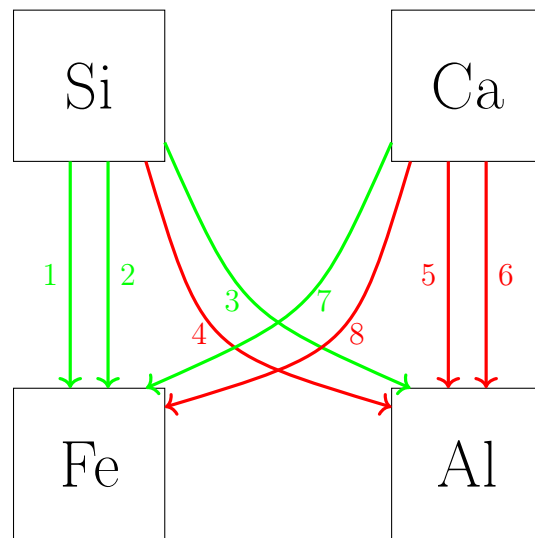


Figure 2.8: Processes changing availabilities of Fe and Al in the presence of Si and Ca. 1) Binding of Si on surface OH^- groups prevents Fe minerals from further transformation and mineralization 2) ASi increases waterholding capacity and decreases hydraulic conductivity (Schaller, Cramer, et al. 2020), promoting Fe minerals as e^- -acceptors. 3) Si releases Al from solid $\text{Al}(\text{OH})_3$ phases by substitution 4) High pH value promotes formation of short-range order aluminosilicates from free Al and Si 5) Immobilization of Ca by cation bridging (Ca-Al-SOM) 6) Ca increases pH and promotes $\text{Al}(\text{OH})_3$ precipitation 7) Ca releases Fe from mineral binding sites by substitution 8) cation-bridging (Ca-Fe-SOM). From Stimmler, M. Obst, Stein, et al. (2023).

Chapter 3

Manuscripts

Published research work

3.1 Co-Payments

3.1.1 Study 1: Pan-Arctic soil element bio availability estimations

Published 07.03.2023 in:

Earth Syst. Sci. Data, 15, 1059–1075, 2023

(<https://doi.org/10.5194/essd-15-1059-2023>)

Author	Contribution
Peter Stimmler	Experimental design, Soil extractions, statistics, Main author
Mathias Göckede	Sample collection, expert advice, proof-reading
Bo Elberling	Sample collection, expert advice, proof-reading
Susan Natali	Sample collection
Peter Kuhry	Sample collection, expert advice, proof-reading
Nia Perron	Sample collection
Fabrice Lacroix	Expert advice, proof reading
Oliver Sonnentag	Expert advice, proof-reading
Jens Strauss	Sample collection, mentoring, expert advice, proof-reading
Christina Minions	sample collection
Michael Sommer	Expert advice, proof-reading
Jörg Schaller	Experimental design, mentoring, proof-reading, writing

Table 3.1: Stimmler, Goeckede, Elberling, et al. (2022)

3.1.2 Study 2: The importance of calcium and amorphous silica for Arctic soil CO₂ production

Published 01.11.2022 in:

Front. Environ. Sci. 10:1019610.

(doi: 10.3389/fenvs.2022.1019610)

Author	Contribution
Peter Stimmler	Experimental implementation, statistics, writing
Mathias Göckede	Experimental design, soil collection, proof reading
Susan Natali	Soil collection, proof reading
Oliver Sonnentag	Experimental design, supervision, proof reading
Benjamin Gilfedder	Laboratory, practical mentoring
Nia Perron	Soil collection, proof reading
Jörg Schaller	Experimental design, mentoring, proof reading

Table 3.2: Stimmler, Goeckede, Natali, et al. (2022)

3.1.3 Study 3: Arctic soil CO₂ release during freeze-thaw cycles modulated by silicon and calcium

Published 20.04.2023 in:

Science of The Total Environment Volume 870, 161943

(<http://dx.doi.org/10.1016/j.scitotenv.2023.161943>)

Author	Contribution
Jörg Schaller	Experimental design, writing
Peter Stimmler	Sample preparation, expert advice
Jürgen Augustin	Experimental implementation, expert advice
Fabrice Lacroix	Proof-reading, expert advice
Mathias Hofmann	Statistics, expert advice

Table 3.3: Schaller, Stimmler, et al. (2022)

3.1.4 Study 4: Arctic soil respiration and microbial community structure driven by silicon and calcium

Published 10.09.2022 in:

Science of the Total Environment, Volume 838, Part 2, 161943

(<http://dx.doi.org/10.1016/j.scitotenv.2022.156152>)

Author	Contribution
Peter Stimmler	Statistics, Writing
Anders Priemé	Sample collection, experimental implementation, expert advice, statistics
Bo Elberling	Sample collection, experimental implementation, expert advice
Mathias Goeckede	Proof-reading, expert advice
Jörg Schaller	Experimental design, mentoring, Proof-reading

Table 3.4: Stimmler, Priemé, et al. (2022)

3.1.5 Study 5: Silicon and calcium controls on iron and aluminum availability in Arctic soils

Published 30.05.2023 in:

Chemosphere 335 (2023) 139087

(<https://doi.org/10.1016/j.chemosphere.2023.139087>)

Author	Contribution
Peter Stimmler	Statistics, writing
Martin Obst	Experimental implementation, expert advice, mentoring, proof-reading
Mathias Göckede	Proof-reading, expert advice
Kerstin Hockmann	Experimental implementation, expert advice, proof-reading
Jörg Schaller	Experimental design, mentoring, experimental implementation, writing

Table 3.5: Stimmler, M. Obst, Stein, et al. (2023)

3.2 Manuscripts

3.2.1– Study 1: Pan-Arctic soil element bio availability estimations (Stimmler et al. 2022b).

3.2.2– Study 2: The importance of calcium and amorphous silica for Arctic soil CO₂ production (Stimmler et al. 2022).

3.2.3– Study 3: Presence of silicon and calcium modulate permafrost soil CO₂ release during freeze-thaw cycles (Schaller et al. 2022).

3.2.4– Study 4: Arctic soil respiration and microbial community structure driven by silicon and calcium (Stimmler et al. 2022c).

3.2.5– Study 5: Silicon and calcium controls on iron and aluminum availability in Arctic soils (Stimmler et al. 2023).

3.2.1 Study 1: Pan-Arctic soil element bio availability estimations

Stimmler, Goeckede, Elberling, et al. (2022)

Published 07.03.2023 in:

Earth Syst. Sci. Data, 15, 1059–1075, 2023

(<https://doi.org/10.5194/essd-15-1059-2023>)



Pan-Arctic soil element bioavailability estimations

Peter Stimmler¹, Mathias Goeckede², Bo Elberling³, Susan Natali⁴, Peter Kuhry⁵, Nia Perron⁶,
Fabrice Lacroix², Gustaf Hugelius^{5,7}, Oliver Sonnentag⁶, Jens Strauss⁸, Christina Minions⁴,
Michael Sommer¹, and Jörg Schaller¹

¹Leibniz Centre for Agricultural Landscape Research (ZALF), Müncheberg, Germany

²Department of Biogeochemical Systems, Max Planck Institute for Biogeochemistry, Jena, Germany

³Center for Permafrost, Department of Geosciences and Natural Resource Management,
University of Copenhagen, Copenhagen, Denmark

⁴Woodwell Climate Research Center, Falmouth, USA

⁵Department of Physical Geography and Quaternary Geology, Stockholm University, Stockholm, Sweden

⁶Département de Géographie, Université de Montréal, Montréal, Canada

⁷Bolin Centre for Climate Research, Stockholm University, Stockholm, Sweden

⁸Permafrost Research Section, Alfred Wegener Institute, Helmholtz Centre for Polar
and Marine Research, Potsdam, Germany

Correspondence: Jörg Schaller (joerg.schaller@zalf.de)

Received: 7 April 2022 – Discussion started: 1 July 2022

Revised: 10 February 2023 – Accepted: 12 February 2023 – Published: 7 March 2023

Abstract. Arctic soils store large amounts of organic carbon and other elements, such as amorphous silicon, silicon, calcium, iron, aluminum, and phosphorous. Global warming is projected to be most pronounced in the Arctic, leading to thawing permafrost which, in turn, changes the soil element availability. To project how biogeochemical cycling in Arctic ecosystems will be affected by climate change, there is a need for data on element availability. Here, we analyzed the amorphous silicon (ASi) content as a solid fraction of the soils as well as Mehlich III extractions for the bioavailability of silicon (Si), calcium (Ca), iron (Fe), phosphorus (P), and aluminum (Al) from 574 soil samples from the circumpolar Arctic region. We show large differences in the ASi fraction and in Si, Ca, Fe, Al, and P availability among different lithologies and Arctic regions. We summarize these data in pan-Arctic maps of the ASi fraction and available Si, Ca, Fe, P, and Al concentrations, focusing on the top 100 cm of Arctic soil. Furthermore, we provide element availability values for the organic and mineral layers of the seasonally thawing active layer as well as for the uppermost permafrost layer. Our spatially explicit data on differences in the availability of elements between the different lithological classes and regions now and in the future will improve Arctic Earth system models for estimating current and future carbon and nutrient feedbacks under climate change (<https://doi.org/10.17617/3.8KGQUN>, Schaller and Goeckede, 2022).

1 Introduction

Temperatures in the northern high-latitude region have risen more than twice as fast as the global average within the last decades (IPCC, 2021). This warming leads to the thawing of perennially frozen ground known as permafrost (Brown and Romanovsky, 2008; Romanovsky et al., 2010). Frozen conditions prevent the microbial degradation of organic matter (OM) and also limit fluvial export of soil-bound nutrients to

the sea by runoff (Mann et al., 2022). Thawing of permafrost soils may, in turn, accelerate global warming by potentially releasing potent greenhouse gases (GHGs) such as carbon dioxide (CO₂) and methane (CH₄) through soil organic carbon mineralization (Schuur et al., 2015). The frozen ground of the Arctic boreal regions (hereafter called “Arctic” but also including subarctic regions) is the largest pool of soil organic carbon worldwide. Approximately 1014–1035 ± 194 Pg of organic carbon is stored within the upper 3 m of permafrost

region soils (Hugelius et al., 2014; Mishra et al., 2021). To full depth, approximately 1460–1600 Pg of organic carbon is stored in the permafrost region (Strauss, 2021), and approximately one-third of this is in ice-rich yedoma deposits, exceeding 3 m depth (Fuchs et al., 2018; Strauss et al., 2017b). The yedoma deposits formed in unglaciated areas of the Northern Hemisphere during the glacial period, when meltwater from glacial areas and eolian processes transported fine sediment to the unglaciated lowlands (Schuur et al., 2013; Strauss, 2021; Strauss et al., 2013). Yedoma deposits are characterized by high carbon and water contents. The water is mostly bound in massive ice in ice wedges as well as segregated ice and pore ice in sediment columns (Schirrmeister et al., 2011). Thus, yedoma soils are highly vulnerable to thawing because the loss of the high ice volume leads to surface subsidence and thermokarst processes, which can accelerate thaw and remobilize deep elemental stocks.

Low temperatures in Arctic systems slow down biological and chemical processes and preserve OM for millennia (Sher et al., 2005). Due to Arctic warming, these processes are accelerated by increased nutrient and OM mobilization from the permafrost (Salmon et al., 2016). Consequently, OM may become vulnerable to respiration (Hugelius et al., 2020; Strauss et al., 2017b). The temperature and near-surface water content in Arctic soils have changed rapidly in the last decades, and further changes are expected in the future (Box et al., 2019). An important effect of Arctic warming is a deepening of the seasonally thawed active layer and related thermokarst processes, which may lead to the mobilization of nutrients from permafrost soil layers (Abbott et al., 2015). Additionally, increased temperatures in Arctic regions may accelerate weathering, potentially enhancing nutrient availability in terrestrial Arctic ecosystems as well as export to freshwater systems and, finally, to the nearshore zone and sea (Goldman et al., 2013).

As the Arctic features a soil mineral composition that is different from many other global soils (Monhonval et al., 2021), the availability (for microbes and plants) of elements in Arctic soils may differ as well. Yedoma deposits, for example, are important pools of OM in the Arctic. Because yedoma deposits include materials transported from nearby mountains, the mineral compositions of these yedoma deposits depend on the original geology of the mountains (Schirrmeister et al., 2011). Furthermore, sediments of marine origin are often rich in available calcium (Ca), phosphorus (P), and silicic acid (Si), while magmatic rocks such as granite or basalt contain large amounts of Si, iron (Fe), aluminum (Al), and P. The complex mineral composition of fluvial and marine sediments is reflected in the element availability of the soils formed from these deposits. The availability of these elements in soils is the complex product of soil genesis, nutrient release, and plant cycling. The soil properties and the vegetation type interactions in terms of *Sphagnum-Eriophorum vaginatum* potentially lead to Si accumulation in the uppermost soil layer of the moist acidic tundra, whereas

interactions in terms of *Dryado integrifoliae-Caricetum* may lead to an accumulation of Ca in the uppermost soil layer in moist non-acidic tundra (Walker et al., 2001). Moreover, external inputs (e.g., by fluvial transport in yedoma regions) may alter soil genesis and element availability (Monhonval et al., 2021; Strauss et al., 2017a). These processes depend on physical and chemical conditions including temperature, water content, and pH. In this context, Si, Ca, Fe, Al, or P are bound in or on mineral phases and are released via enzymatic activity or weathering. Ongoing Arctic climate warming now threatens to disturb the pools that have equilibrated to conditions characteristic of the past millennia.

Nutrient availability (the easily available share of elements for potential uptake by plants within a short time span, e.g., days not months) is important to meet plants' requirements in terms of nutrition, as only optimal nutrition will result in high biomass production. The availability of elements, such as P, Fe, Ca, and Si, in soils is a known control with respect to soil OM respiration (Weil and Brady, 2017). A release of inorganic nutrients, such as P or Si, can lead to increased GHG production and potentially to further export of these elements to fresh and marine waters. In marine systems, P, Fe, Ca, and Si are well known to control carbon (C) fixation in terms of algae biomass productivity. In terrestrial systems, P availability is positively related to Si (Schaller et al., 2019) or its polymers, which mobilize from species such as amorphous silicon (ASi) (Stimmler et al., 2022). The mobilization of P by Si has been shown to occur due to competition for binding at Fe minerals (Schaller et al., 2019), which tend to strongly bind P under low-Si-availability conditions (Gérard, 2016). Contrary to Si, Ca binds P by calcium phosphate coprecipitation with calcium carbonate, at least under high-soil-pH conditions (Otsuki and Wetzell, 1972). Like P, OM also binds to Ca, Fe, and Al phases (Kaiser and Zech, 1997; Wiseman and Püttmann, 2006) but is mobilized from those phases by Si (Hömberg et al., 2020). If the Fe availability in soils is low, the binding of P may be related to Al minerals (Eriksson et al., 2015).

Despite the important role of soil elements in driving soil and ecosystem processes as well as the potential for rapid changes in the Arctic due to climate change, the spatial distribution of elemental stocks (beyond C and N) is not well understood. An ecologically based classification of soil Ca concentrations, which differentiated between a Ca-rich non-acidic tundra and a Ca-poor acidic tundra based on differences in vegetation types, was proposed by Walker et al. (2001) for the Alaskan Arctic region. This classification system was further used to estimate pan-Arctic soil OM stocks (Hugelius et al., 2014); this proved to be a useful approach, as vegetation is tightly connected to OM stocks (Quideau et al., 2001). Based on the work of Hugelius et al. (2014), Alfredsson et al. (2016) related vegetation cover to the ASi concentration to scale up Arctic ASi stocks. However, in contrast to OM stocks being clearly related to vegetation (Hugelius et al., 2014), vegetation might have an ef-

fect on mineral availability in soils (Villani et al., 2022). It is known that soils dominated by sedges may become enriched in available Si, whereas soils dominated by shrub vegetation may become enriched in available Ca (Mauclet et al., 2022). Climate-change-driven alterations in vegetation communities may also lead to changed element availabilities in Arctic soils. Moreover, other elements like P and Ca are intensively cycled by plants and, thus, the uppermost soil layer becomes enriched in the aforementioned elements (Jobbágy and Jackson, 2001). This points to the importance of biogeochemical interactions between vegetation and soil. However, this approach does not account for the inorganic element pool, which is initially dominated by the bedrock geology. Therefore, the extrapolation of circumpolar Arctic maps of element availability for P, Fe, Ca, Al, and Si based on vegetation distribution alone may be associated with high uncertainties. Much stronger drivers of element availability could be the parent material and lithology (Alloway, 2013).

In this study, we aim to map pan-Arctic soil element bioavailability (for microbes and plants) by applying a lithology-based extrapolation of plot-level sampling data on nutrient availability. We provide maps for the solid ASi fraction and the available Si, Ca, Fe, P, and Al concentrations, as these elements have direct effects on OM binding and GHG emissions from the circumpolar Arctic. In addition, these elements, once transported to marine systems, may affect primary production by diatoms and coccolithophores, as some of the nutrients are limiting for algae and, hence, limit CO₂ binding due to algae biomass production. A better understanding of element availability is crucial to reduce uncertainties and allow for the reliable modeling of future scenarios on how Arctic system may respond to global warming.

2 Material and methods

2.1 General approach

Based on the Geological Map of the Arctic (Harrison et al., 2011), we estimate the bioavailability and potential mobility of Si, Ca, Fe, Al, and P as well as the solid ASi fraction in Arctic soils. We analyzed soil samples from organic, mineral, and permafrost layers from pan-Arctic sampling campaigns. We used the biologically available element concentrations for mineral Si, Ca, Fe, Al, and P as well as the solid ASi fraction of certain lithologies to compile pan-Arctic maps covering $7.6 \times 10^6 \text{ km}^2$.

2.2 Sampling and storage

In total, we analyzed 574 Arctic soil samples from 25 locations taken over a period of 1 decade (Fig. 1). To ensure pan-Arctic coverage, we analyzed samples from Siberia (222 samples from 6 locations), North America (115 samples from 6 locations), Greenland (111 samples from 9 locations), northern Europe (13 samples from 1 location), and Svalbard

(103 samples from 3 locations) (Figs. 1, S1; Table S1). We analyzed samples from the thawed near-surface organic layer (252 soil samples, mainly 0–20 cm in depth), mineral layer (208 soil samples, mainly 20–50 cm depth), and permafrost layer (104 soil samples, mainly 50–100 cm depth). The sampling design accounted for the spatial variation at single locations (several samples were taken from $\sim 1 \text{ km}$ transects). Repeated sampling over months to decades was not possible. We split the annually thawed active layer into the upper organic layer and the mineral layer below based on the C content, except for soils where the organic layer corresponded to the active layer. The organic layer contained mainly organic matter (OM) in different mineralization states. The mineral soil layer has a variable OM content depending on which soil processes have affected this layer, and it reaches to the perennally frozen permafrost layer. We took samples using an auger or a spade and stored them frozen until analysis or as described in previous studies (Faucherre et al., 2018; Kuhry et al., 2020). Samples consisted of 5 to 50 g of frozen soil. Before analysis, the samples were freeze-dried for 48 h and ground. Freeze-drying inhibits the thermal degradation of the soil material and is standard for the Mehlich III extraction and alkaline extraction described below.

2.3 Extraction and analysis

2.3.1 Mehlich III extractions for available element concentrations

Available concentrations of Si, Ca, Fe, Al, and P were quantified using the Mehlich III method (Sims, 1989). Mehlich III extracts the silicic acid that is adsorbed to the soil particle surface as well as the free silicic acid. For Ca, Fe, Al, and P, the extract is defined as the *biologically available share of the analyzed elements*, in the script labeled as “available”. This fraction includes the element concentrations dissolved in the pore water and the fraction adsorbed to organic and inorganic soil particles. Microbes and plants are able to mobilize this adsorbed share of nutrients. We defined the Mehlich III extraction method to reflect these available element concentrations. Briefly, we extracted 0.5 to 5 g of freeze-dried soil using 10 mL of Mehlich III solution (0.015 M NH₄F, 0.001 M EDTA, 0.25 M NH₄NO₃, 0.00325 M HNO₃, and 0.2 M HAc) per gram of soil. The samples were shaken for 5 min at 200 rpm and centrifuged for 5 min at $10\,000 \times g$. Following this, the supernatant was filtered using a 0.2 μm cellulose acetate filter. The concentration of Si, Ca, Fe, Al, and P was measured by inductive coupled plasma optical emission spectroscopy (ICP-OES; Vista-PRO radial, Varian Medical Systems, Palo Alto, CA).

2.3.2 Alkaline extraction for the solid fraction of amorphous silicon

For the abstraction of the solid fraction of amorphous silicon (ASi), an alkaline extraction was used (DeMaster, 1981)

to extract ASi from 30 mg of freeze-dried soil using 40 mL of 0.1 M Na₂CO₃ solution at 85 °C for 5 h. After 1 h, 3 h, and 5 h, the suspension was mixed, and 10 mL of the supernatant was subsampled, filtered using a 0.2 µm cellulose acetate filter, and analyzed by ICP-OES. The ASi concentration was calculated using a linear regression of the ASi concentration in solution against time, and the intersection with the y axis was used as the available concentration, as per DeMaster (1981). The Mehlich III extract was used to determine the available concentrations of the elements, and the alkaline extraction was used to determine the pool of particulate ASi in the soil. To determine the dry weight (DW) of the samples, 0.5–2 g of frozen material was freeze-dried until it reached a constant weight.

2.4 Statistics

2.4.1 Statistics and graphics

Data were analyzed using RStudio software (R Core Team, 2022). We extracted the original data (lithology, location, and geometry) from GIS polygons (shapefiles from the different regions, including Greenland, Can_USA, Ice, and N_Europa_Russia) of the Geological Map of the Arctic containing the locations. We extracted 14 lithological classes in total. We matched the soil sampling locations for which we obtained element availability data (by extraction; see above) with the GIS polygons (geology) using the ArcView GIS 3.2 extensions “Spatial Analyst” command “analysis: tabulate Areas”. The sum of areas with the same map label was extracted using the map label “shape area”. We considered only terrestrial areas. For every location, we calculated the mean available element concentrations for ASi, Si, Ca, Fe, Al, and P with bootstrapping (boot = 1000) for the organic, mineral, and permafrost layers. We calculated quantiles, the mean, and the standard error using “summarise” from the “dplyr” R package. We clustered the available element concentration data for all locations by lithological class and calculated the mean and standard error for the organic, mineral, and permafrost layers. The number of samples for each lithological class is given in Fig. 1.

2.4.2 Element concentration maps

We used the Geological Map of the Arctic (1 : 5 000 000 scale, in the Arctic polar region, north of latitude 60° N) as the basis for our maps. We calculated the weighted numeric mean concentration for each element in the first 100 cm from the soil surface using Eq. (1). The mean mass fraction (w_m) of an element (X) is the sum of the products of the mass fractions in the organic layer (OL), mineral layer (ML), and permafrost layer (PL) and the thickness (d) of each layer in centimeters divided by 100 cm. We colored the represented

area based on the element concentration.

$$w_m(X) \left[\text{mg g}^{-1} \right] = \frac{(w_{\text{OL}}(X) \left[\text{mg g}^{-1} \right] \times d_{\text{OL}} \left[\text{m} \right] + w_{\text{ML}}(X) \left[\text{mg g}^{-1} \right] \times d_{\text{ML}} \left[\text{m} \right] + w_{\text{PL}}(X) \left[\text{mg g}^{-1} \right] \times d_{\text{PL}} \left[\text{cm} \right])}{100 \left[\text{cm} \right]} \quad (1)$$

3 Results

3.1 Geographical and lithological representation

Our sampling locations represent 13 of the 17 (76.5 %) original geographic domains (North Asia and North America, ice, and none assigned are missing) defined by the base map (Fig. S1; Tables 1, S2) of the Arctic. The single areas and shares for the maps of Canada and/or Alaska, Greenland, and northern Europe and/or Russia are given in Table S3. Our data represent 17 periods of the Geological Map of the Arctic. The ages range between 2.6 and 2500 Myr ago. The number of samples per age code are shown in Fig S2. Our data represent 14 lithological classes of the Geological Map of the Arctic (Table S4). These 14 lithological classes represent $7.63 \times 10^{12} \text{ m}^2$ of the $1.57 \times 10^{13} \text{ m}^2$ area (48.49 %) covered by the base map (including ice sheets). Sediments cover $1.03 \times 10^{13} \text{ m}^2$ of the Arctic. Our data represent sedimentary classes that incorporate $6.77 \times 10^{12} \text{ m}^2$ (65.9 %) of the Arctic sediment cover (Fig. S3). In total, $3.68 \times 10^{11} \text{ m}^2$ (49.9 %) of the $7.37 \times 10^{11} \text{ m}^2$ of yedoma deposits was represented (Fig. S4). The 14 lithological classes can be observed in the igneous type, comprising extrusive – mafic material (class 1, $n = 26$); the unclassified type, comprising metamorphic undivided material (class 2, $n = 21$); and the sedimentary type, comprising carbonate (class 3, $n = 24$; class 4, $n = 58$; class 5, $n = 64$), clastic – shallow marine (class 6, $n = 13$), clastic – deltaic and nearshore (class 7, $n = 68$), sedimentary – undivided (class 8, $n = 38$; class 9, $n = 39$), clastic – shallow marine (class 10, $n = 91$; class 11, $n = 60$), sedimentary and/or volcanic – undivided (class 12, $n = 21$), and slope and deep water (class 13, $n = 43$; class 14, $n = 8$) material.

3.2 Element availabilities across lithological classes at 0–1 m depth

The lithological classes differed substantially with respect to their element availabilities (Figs. 2, S5). The main findings were as follows:

- We found a large range of ASi concentrations in the Arctic, covering values from $0.03 \pm 0 \text{ mg g}^{-1} \text{ DW ASi}$ to $6.68 \pm 1.17 \text{ mg g}^{-1} \text{ DW ASi}$. The highest concentrations of ASi were found in basalt and associated rock (class 1: $6.68 \pm 1.17 \text{ mg g}^{-1} \text{ DW ASi}$), gneiss and associated rock (class 2: $4.11 \pm 1.24 \text{ mg g}^{-1} \text{ DW ASi}$), and sandstone and associated rock (class 9: $2.01 \pm 0.24 \text{ mg g}^{-1} \text{ DW ASi}$; class 10:

Table 1. The parameters used in this study, including the areal coverage of the geographical domain, the epochs, the represented area, the lithological class, the sediments, and the yedoma deposition, according to our data. The first column lists the original parameters given by the Geological Map of the Arctic (Harrison et al., 2011) as well as the yedoma deposits (Strauss et al., 2021). The “Represented” column gives absolute numbers with respect to the chronological or lithological classes extrapolated by this study. The represented area is the share of the entire area of the Arctic for each listed parameter according to the Geological Map of the Arctic used in this study.

Parameter	Represented	Explanation	Example
Geographic domain	13 (76.5%)	“Phanerozoic regions are based on major physiographic features of the Arctic” (Harrison et al., 2011)	Western Interior Alaska
Epochs	17 (2.6–2500 Myr ago)	“Standardization of map-unit attributes has been facilitated by the International Stratigraphic Chart (August 2009 version) published by the International Commission on Stratigraphy (ICS)” (Harrison et al., 2011)	Neogene (23.0–2.6 Ma)
Represented area	$7.63 \times 10^{12} \text{ m}^2$ (43.03%)	Area of the Geological Map of the Arctic (Harrison et al., 2011) co-located with element concentration data from this work (Figs. 3–8)	
Lithological class	14	Specification and examples of rock type	Lithological class 2: gneiss and migmatite; re-worked amphibolite and granulite facies rocks
Sediments	$6.77 \times 10^{12} \text{ m}^2$ (65.9%)	Areas with lithological classes of the sedimentary type	Lithological class 7: sandstone, siltstone, shale, and coal; plant fossils; metamorphic grade not identified
Yedoma deposition	$3.68 \times 10^{11} \text{ m}^2$ (49.9%)	Areas that contain yedoma deposits defined by Strauss et al. (2021)	

$2.06 \pm 0.01 \text{ mg g}^{-1} \text{ DW ASi}$). ASi concentrations were the lowest in limestone (class 3: $0.03 \pm 0 \text{ mg g}^{-1} \text{ DW ASi}$) (Fig. 2).

- Available Si concentrations were highest in limestone and associated rock, including shale (class 4: $5.65 \pm 0.78 \text{ mg g}^{-1} \text{ DW Si}$); quartz sandstone (class 6: $6.61 \pm 1.83 \text{ mg g}^{-1} \text{ DW Si}$); and sandstone (class 7: $5.46 \pm 0.66 \text{ mg g}^{-1} \text{ DW Si}$). Si concentrations were lowest in limestone and associated rock (class 3: $0.1 \pm 0.02 \text{ mg g}^{-1} \text{ DW Si}$) (Fig. 2). The differences in the available Si concentrations between the two classes of limestone are mainly driven by the presence of shale in one class that acts as source of silicic acid.
- The highest available Ca concentrations were observed in limestone (which consist of CaCO_3) and associated rock (class 3: $10.73 \pm 2.15 \text{ mg Ca g}^{-1} \text{ DW}$), sedimentary and/or volcanic rock (class 12: $8.77 \pm 0.12 \text{ mg Ca g}^{-1} \text{ DW}$), and sandstone and associated rock (class 8: $8.06 \pm 0.36 \text{ mg Ca g}^{-1} \text{ DW}$). Ca concentrations were lowest in gneiss (class 2: $0.05 \pm 0.02 \text{ mg Ca g}^{-1} \text{ DW}$) (Fig. 2). The data are consistent with the expectation that the highest Ca availability will be found in Ca-containing bedrock.
- Available Fe concentrations were highest in shale and associated rock (class 13: $2.93 \pm 0.45 \text{ mg g}^{-1} \text{ DW Fe}$), limestone (class 4: $2.28 \pm 0.32 \text{ mg g}^{-1} \text{ DW Fe}$), and quartz sandstone (class 6: $2.49 \pm 0.69 \text{ mg g}^{-1} \text{ DW Fe}$).

The lowest Fe concentrations were observed in lithological limestone and associated rock (class 3: $0.01 \pm 0.001 \text{ mg g}^{-1} \text{ DW Fe}$) (Fig. 2).

- The highest available Al concentrations were observed in quartz sandstone (class 6: $2.52 \pm 0.70 \text{ mg g}^{-1} \text{ DW Al}$), sandstone (class 7: $1.63 \pm 0.20 \text{ mg g}^{-1} \text{ DW Al}$), and shale and associated rock (class 13: $1.5 \pm 0.23 \text{ mg g}^{-1} \text{ DW Al}$). The lowest Al concentrations were observed in limestone and associated rock (class 3: $0.02 \pm 0 \text{ mg g}^{-1} \text{ DW Al}$) (Fig. 2).
- High available P concentrations were observed in limestone and associated rock (class 4: $0.31 \pm 0.04 \text{ mg g}^{-1} \text{ DW P}$), sandstone (class 7: $0.19 \pm 0.02 \text{ mg g}^{-1} \text{ DW P}$), and shale and associated rock (class 14: $0.15 \pm 0.05 \text{ mg g}^{-1} \text{ DW P}$). P concentrations were lowest in basalt and associated rock (class 1: $0.0116 \pm 0.002 \text{ mg g}^{-1} \text{ DW P}$) (Fig. 2).

3.3 Maps of the element concentrations at 1 m depth

3.3.1 Amorphous silicon in the top 1 m

We found the highest concentrations of ASi in the Arctic North Atlantic region (Fig. 3). Here, basalt and gneiss are dominant (lithological classes 1 and 2, respectively) and contained concentrations of 4.11 ± 1.24

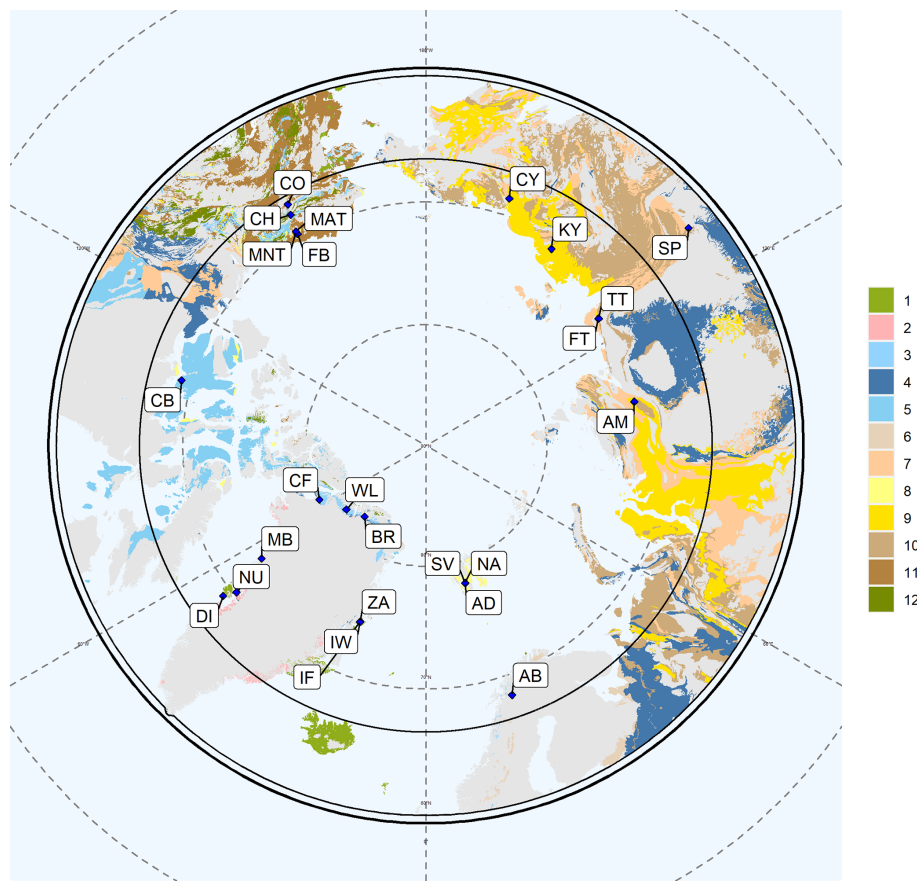


Figure 1. Map of the represented lithologies. The Arctic Circle (66.6° N) is included as a black circle. Each color represents a bedrock lithology. “1” denotes basalt, olivine basalt, tholeiite, alkali basalt, basanite, pillow basalt, and flood basalt ($n = 26$). “2” represents gneiss and migmatite; reworked amphibolite and granulite facies rocks ($n = 11$). “3” shows limestone, dolostone, shale, evaporites, and chalk; carbonate reefs or metamorphosed equivalent ($n = 24$). “4” denotes limestone, dolostone, shale, evaporites, and chalk; carbonate reefs; metamorphic grade not identified ($n = 58$). “5” represents limestone, dolostone, shale, evaporites and, chalk; carbonate reefs ($n = 64$). “6” shows quartz sandstone, siltstone, claystone, limestone, dolostone, conglomerate, and tillite ($n = 13$). “7” denotes sandstone, siltstone, shale, and coal; plant fossils; metamorphic grade not identified ($n = 68$). “8” represents sandstone, siltstone, shale, and limestone ($n = 38$). “9” shows sandstone, siltstone, shale, and limestone; metamorphic grade not identified ($n = 39$). “10” denotes sandstone, siltstone, and shale; marine fossils ($n = 91$). “11” represents sandstone, siltstone, and shale; marine fossils; metamorphic grade not identified ($n = 60$). “12” shows sedimentary and/or volcanic rock; undivided ($n = 21$). “13” denotes shale, chert, iron formation, greywacke, turbidite, argillaceous limestone, and matrix-supported conglomerate ($n = 43$). “14” represents shale, chert, iron formation, greywacke, turbidite, argillaceous limestone, and matrix-supported conglomerate or metamorphosed equivalent ($n = 8$). Gray color presents areas of the base map that are not represented by our element concentration data. The location abbreviations are as follows: CH – Alaska, Chandalar; CO – Alaska, Coldfoot; FB – Alaska, Franklin Bluffs, dry; MAT – Alaska, moist acidic tundra; MNT – Alaska, moist non-acidic tundra; CB – Canada, Cambridge Bay; BR – Greenland, Brønlund; CF – Greenland, Cass Fjord; DI – Greenland, Disko; MB – Greenland, Melville Bay; NU – Greenland, Nuussuaq; WL – Greenland, Warming Land; ZA – Greenland, Zackenberg; IW – Greenland, Zackenberg, infilling fan; AM – Russia, Ary-Mas; CY – Russia, Chersky; KY – Russia, Kytalyk; FT – Russia, Lena Delta, first terrace; TT – Russia, Lena Delta, third terrace; SP – Russia, Spasskaya; AB – Sweden, Abisko; AD – Svalbard, Adventdalen; NA – Svalbard, Adventalen; SV – Svalbard. This map is based on the Geological Map of the Arctic (Harrison et al., 2011).

to $6.68 \pm 1.17 \text{ mg ASi g}^{-1} \text{ DW}$. Other high concentrations of ASi were found for the Brooks Range (Alaska), Chukotka and the Arctic shelf (eastern Siberia), and the West Siberian Basin. These soils contained $2.01 \pm 0.24 \text{ mg ASi g}^{-1} \text{ DW}$ (lithological class 9). The Verkhoyansk–Kolyma region showed a lower concentration of $1.48 \pm 0.16 \text{ mg ASi g}^{-1} \text{ DW}$ (lithological

class 11). We found similar concentrations (class 5: $1.24 \pm 0.14 \text{ mg ASi g}^{-1} \text{ DW}$) for the Canadian Shield. We found low concentrations of $0.31 \pm 0.01 \text{ mg ASi g}^{-1} \text{ DW}$ (lithological class 12) in western Interior Alaska and western parts of the Brooks Range, Alaska, Chukotka, and the Arctic shelf. Increasing the active layer depth will potentially release higher ASi concentrations from permafrost soils

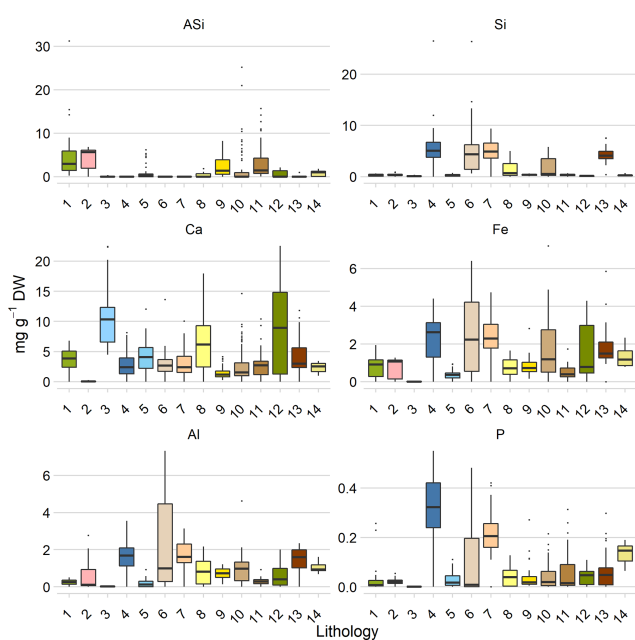


Figure 2. Element concentrations related to lithology. Lithology class 1 is igneous, class 2 is metamorphic, and the other classes are either sedimentary or sedimentary and mixed. Each color represents a bedrock lithology. “1” denotes basalt, olivine basalt, tholeiite, alkali basalt, basanite, pillow basalt, and flood basalt ($n = 26$). “2” represents gneiss and migmatite; reworked amphibolite and granulite facies rocks ($n = 11$). “3” shows limestone, dolostone, shale, evaporites, and chalk; carbonate reefs or metamorphosed equivalent ($n = 24$). “4” denotes limestone, dolostone, shale, evaporites, and chalk; carbonate reefs; metamorphic grade not identified ($n = 58$). “5” represents limestone, dolostone, shale, evaporites, and chalk; carbonate reefs ($n = 64$). “6” shows quartz sandstone, siltstone, claystone, limestone, dolostone, conglomerate, and tillite ($n = 13$). “7” denotes sandstone, siltstone, shale, and coal; plant fossils; metamorphic grade not identified ($n = 68$). “8” represents sandstone, siltstone, shale, and limestone ($n = 38$). “9” shows sandstone, siltstone, shale, and limestone; metamorphic grade not identified ($n = 39$). “10” denotes sandstone, siltstone, and shale; marine fossils ($n = 91$). “11” represents sandstone, siltstone, and shale; marine fossils; metamorphic grade not identified ($n = 60$). “12” shows sedimentary and/or volcanic rock; undivided ($n = 21$). “13” denotes shale, chert, iron formation, greywacke, turbidite, argillaceous limestone, and matrix-supported conglomerate ($n = 43$). “14” represents shale, chert, iron formation, greywacke, turbidite, argillaceous limestone, and matrix-supported conglomerate or metamorphosed equivalent ($n = 8$). All values are given as the mean and standard error. The distribution of the lithological classes is shown in Fig. 1, and the assignment to the geographic domain is given in Table S5.

(Fig. S6) in the Canadian Shield, as the concentration in the permafrost layer is $2.80 \pm 2.50 \text{ mg ASi g}^{-1} \text{ DW}$ (lithological class 5) compared with $1.24 \pm 0.14 \text{ mg ASi g}^{-1} \text{ DW}$ in the current active layer (Table S4). A further increase in the ASi concentration can be expected for the Arctic North Atlantic region due to permafrost thaw, as the concentration

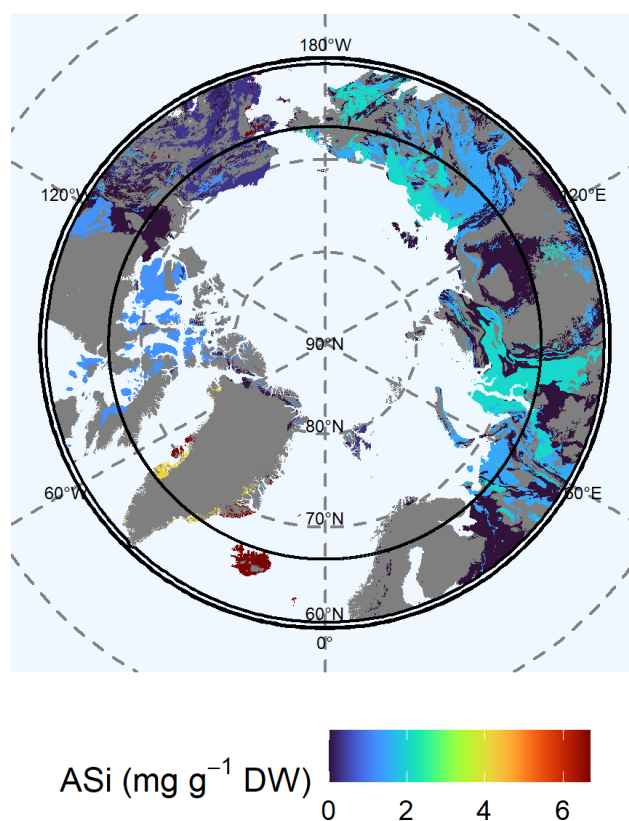


Figure 3. Map of the mean concentration of amorphous silicon (ASi) in the top 100 cm of soils. For each lithological class, the mean concentration is shown. Gray shaded areas are not represented by our data.

is $8.68 \pm 2.51 \text{ mg ASi g}^{-1} \text{ DW}$ in the permafrost layer compared with the $4.11 \pm 1.24 \text{ mg ASi g}^{-1} \text{ DW}$ of the current active layer (lithological class 1) (Fig. S6, Table S4). However, the permafrost layer in Siberia contains lower concentrations of ASi (class 9: $0.77 \pm 0.23 \text{ mg ASi g}^{-1} \text{ DW}$; class 11: $1.38 \pm 0.28 \text{ mg ASi g}^{-1} \text{ DW}$) compared with the current active layer, which has concentrations of $2.01 \pm 0.24 \text{ mg ASi g}^{-1} \text{ DW}$ (lithological class 9) and $1.48 \pm 0.16 \text{ mg ASi g}^{-1} \text{ DW}$ (lithological class 11), probably leading to lower overall ASi concentrations with proceeding thaw. The variability in the ASi data is high for lithological classes 1, 2, 9, and 11.

3.3.2 Silicon at 0–1 m depth

Available (Mehlich-III-extractable) Si (Fig. 4), extracted as silicic acid, showed a different distribution than the solid fraction of ASi (Fig. 3). High available Si concentrations were generally associated with sediments. The available Si extracted via Mehlich III extraction is water-soluble Si as well as Si bound to the surface of soil particles (Schaller et al., 2021). We found high concentrations ($5.65 \pm 0.78 \text{ mg Si g}^{-1} \text{ DW}$) for lithological class 4 in the

West Siberian Basin and the West Siberian Plain. Other regions with high available Si concentrations were the East European Plain, the Ural Mountains, and the Canadian Shield. Another lithological class with high available Si concentrations ($4.51 \pm 0.69 \text{ mg Si g}^{-1} \text{ DW}$) was class 13, located in the Inuitian region, North Greenland, and Alaska. In Alaska, lithological class 10, which has moderately high concentrations of available Si ($2.06 \pm 0.03 \text{ mg Si g}^{-1} \text{ DW}$), is also abundant. We found low concentrations of available Si (class 9: $0.36 \pm 0.05 \text{ mg Si g}^{-1} \text{ DW}$) for the Brooks Range, Chukotka, the Arctic shelf, the West Siberian Basin, and the West Siberian Plain. In addition, the Verkhoyansk–Kolyma region, the East European Plain, and the Ural Mountains were poor in available Si (class 11: $0.39 \pm 0.04 \text{ mg Si g}^{-1} \text{ DW}$). The lowest available concentrations (class 12: $0.15 \pm 0.01 \text{ mg Si g}^{-1} \text{ DW}$) were observed in western Interior Alaska. An increasing thawing depth may potentially increase the available Si concentrations in the western Verkhoyansk–Kolyma region to the East European Platform, as the concentration in the permafrost layer is $6.26 \pm 1.52 \text{ mg Si g}^{-1} \text{ DW}$ (lithological class 4) compared with the lower available Si concentration (class 4: $5.56 \pm 0.78 \text{ mg Si g}^{-1} \text{ DW}$) of the current active layer (Fig. S6, Table S4). The variability in the data of available Si is high for lithological classes 4, 6, and 7.

3.3.3 Calcium at 0–1 m depth

The highest available (Mehlich-III-extractable) Ca concentrations in soils were found in limestone and associated rock (class 3: $10.73 \pm 2.15 \text{ mg Ca g}^{-1} \text{ DW}$) in North Greenland, Alaska, and the Canadian Shield (class 5: $3.79 \pm 0.45 \text{ mg Ca g}^{-1} \text{ DW}$) (Fig. 5). In particular, limestone shows high solubility under the acidic conditions used in the Mehlich III extraction and, thus, presents high concentrations of available Ca. In addition, supracrustal rocks in Alaska contained very high available Ca concentrations (class 12: $8.77 \pm 0.12 \text{ mg Ca g}^{-1} \text{ DW}$). Mafic rocks in the Arctic North Atlantic region (class 1: $3.65 \pm 0.70 \text{ mg Ca g}^{-1} \text{ DW}$) contained moderate available Ca concentrations. We found moderate to low available Ca concentrations (class 11: $2.88 \pm 0.32 \text{ mg Ca g}^{-1} \text{ DW}$) for soils of the Verkhoyansk–Kolyma region, the East European Plain, and the Ural Mountains. Large regions of eastern and western Siberia and the Siberian Plain were poor in available Ca (class 9: $1.51 \pm 0.14 \text{ mg Ca g}^{-1} \text{ DW}$; class 4: $2.56 \pm 0.34 \text{ mg Ca g}^{-1} \text{ DW}$). The available Ca concentrations of the permafrost layer for Alaska (class 12: $10.42 \pm 2.08 \text{ mg Ca g}^{-1} \text{ DW}$) is higher than in the active layer ($2.93 \pm 0.45 \text{ mg Ca g}^{-1} \text{ DW}$) (Fig. S6). In the largest part of Siberia and the Canadian Shield, the available Ca concentrations are slightly lower in the permafrost layer (class 4: $2.15 \pm 0.96 \text{ mg Ca g}^{-1} \text{ DW}$; class 7: $1.59 \pm 0.32 \text{ mg Ca g}^{-1} \text{ DW}$) than in the active layer (class 4: $2.56 \pm 0.34 \text{ mg Ca g}^{-1} \text{ DW}$; class 7:

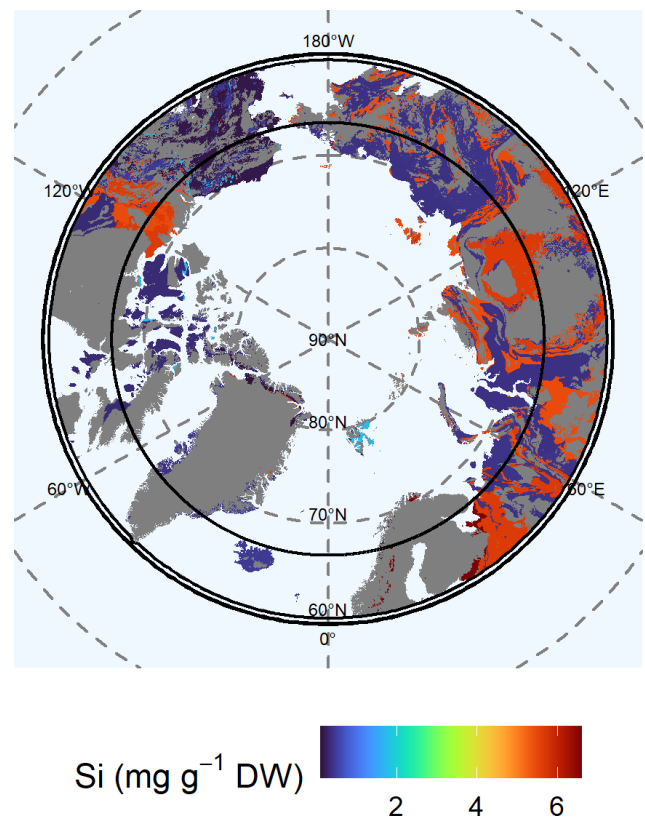


Figure 4. Map of the mean concentration of available (Mehlich-III-extractable) silicon (Si) for the uppermost 100 cm of soils. For each lithological class, the mean concentration is shown. Blue colors represent low concentrations of available Si, whereas red colors represent high concentrations. Gray shaded areas are not represented by our data.

$1.51 \pm 0.14 \text{ mg Ca g}^{-1} \text{ DW}$) (Fig. S6, Table S4). The variability in the data of available Ca is high for lithological classes 1, 3, 5, and 6.

3.3.4 Iron (Fe) at 0–1 m depth

Available (Mehlich-III-extractable) Fe concentrations were higher in the eastern Arctic than in the western Arctic (Fig. 6). We found the highest concentrations in northern Greenland (class 13: $2.93 \pm 0.45 \text{ mg Fe g}^{-1} \text{ DW}$). The soils of lithological class 4 in the West Siberian Basin and the Siberian and Canadian plains contained $2.28 \pm 0.32 \text{ mg Fe g}^{-1} \text{ DW}$. The Verkhoyansk–Kolyma region showed similar Fe concentrations (class 7: $2.21 \pm 0.27 \text{ mg Fe g}^{-1} \text{ DW}$). Moderate to high Fe concentration were found for igneous mafic rocks in Iceland and Greenland (class 1: $0.94 \pm 0.18 \text{ mg Fe g}^{-1} \text{ DW}$) and for supracrustal rocks in Alaska (class 12: $1.24 \pm 0.14 \text{ mg Fe g}^{-1} \text{ DW}$). The Chukotka region and western Siberia were relatively poor in Fe (class 9: $0.83 \pm 0.13 \text{ mg Fe g}^{-1} \text{ DW}$). Eastern Siberia and northern

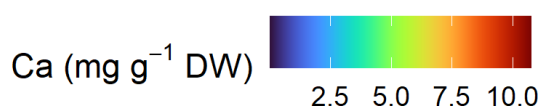
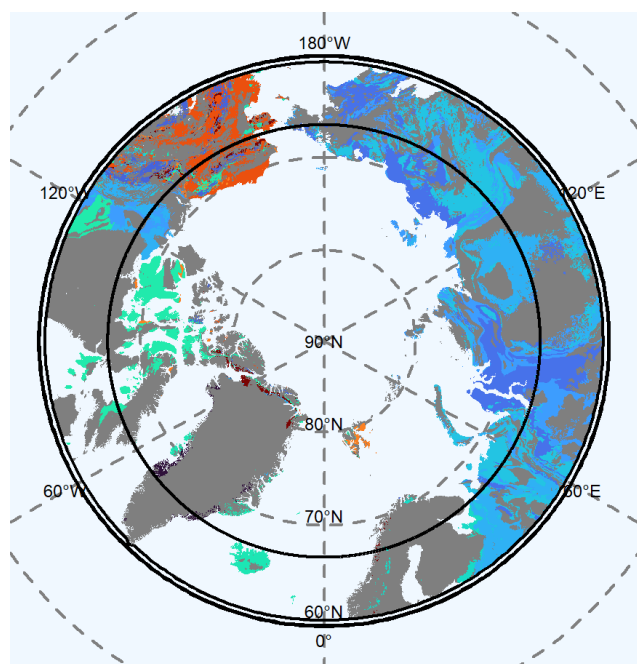


Figure 5. Map of the mean concentration of available (Mehlich-III-extractable) calcium (Ca) for the uppermost 100 cm of soils. For each lithological class, the mean concentration is shown. Blue colors represent low concentrations of Ca, whereas red colors represent high concentrations. Gray shaded areas are not represented by our data.

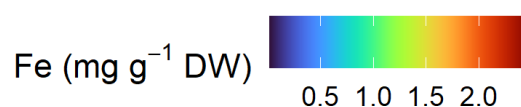
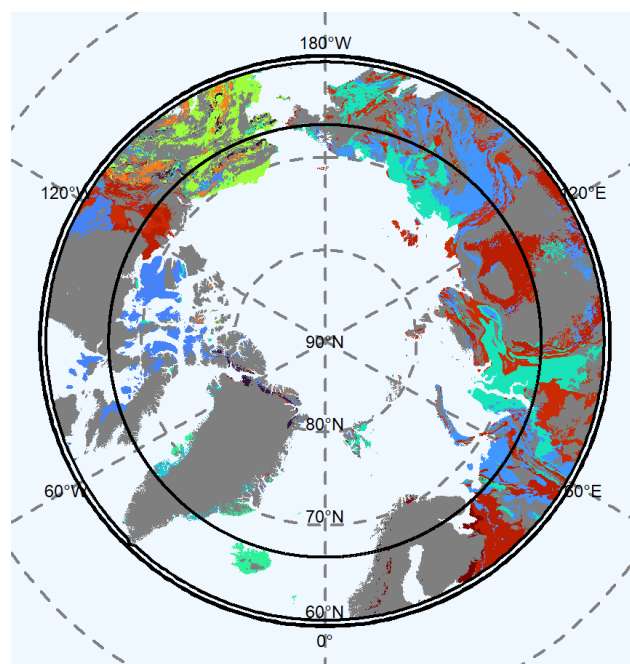


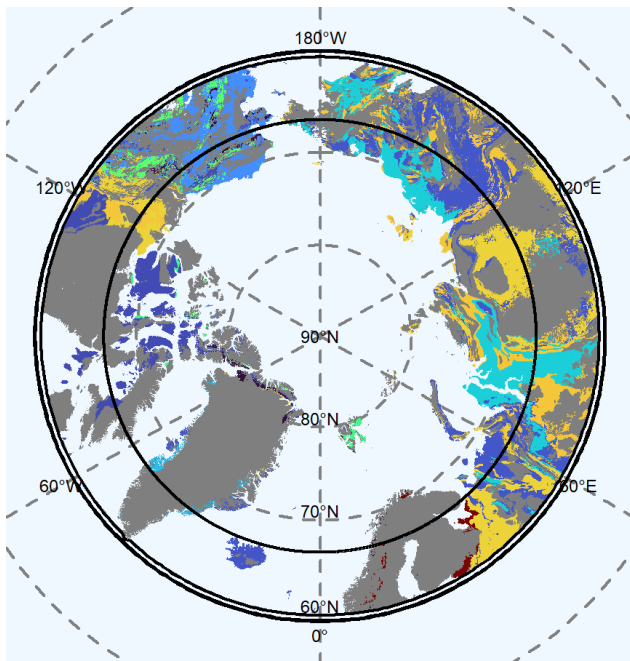
Figure 6. Map of the mean concentration of available (Mehlich-III-extractable) iron (Fe) for the uppermost 100 cm of soils. For each lithological class, the mean concentration is shown. Blue colors represent low concentrations of Fe, whereas red colors represent high concentrations. Gray shaded areas are not represented by our data.

Europe contained even lower Fe concentrations (class 11: $0.49 \pm 0.04 \text{ mg Fe g}^{-1} \text{ DW}$). Available Fe concentrations in the Canadian Shield were similarly low (class 12: $0.41 \pm 0.06 \text{ mg Fe g}^{-1} \text{ DW}$). We expect increasing Fe concentrations for the Canadian and Greenland shields due to predicted future thaw of the permafrost layer, as the Fe concentrations in the permafrost layer (class 5: $0.61 \pm 0.15 \text{ mg Fe g}^{-1} \text{ DW}$) and in parts of Alaska (class 14: $1.97 \pm 0.3 \text{ mg Fe g}^{-1} \text{ DW}$) are higher compared with the current active layer (class 5: $0.41 \pm 0.05 \text{ mg Fe g}^{-1} \text{ DW}$) and other parts of Alaska (class 14: $1.08 \pm 0.38 \text{ mg Fe g}^{-1} \text{ DW}$) (Fig. S7, Table S4). The variability in the data of available Fe is high for lithological classes 2 and 6.

3.3.5 Aluminum at 0–1 m depth

Northern Europe contained the highest concentrations of available (Mehlich-III-extractable) Al (class 6: $2.52 \pm 0.7 \text{ mg Al g}^{-1} \text{ DW}$) (Fig. 7). Relatively high concentrations of available Al were also distributed over Siberia and the Canadian Shield (class 7: $1.63 \pm 0.02 \text{ mg Al g}^{-1} \text{ DW}$;

class 4: $1.57 \pm 0.22 \text{ mg Al g}^{-1} \text{ DW}$). Parts of Alaska contained moderate available Al concentrations (class 10: $0.94 \pm 0.06 \text{ mg Al g}^{-1} \text{ DW}$; class 13: $1.5 \pm 0.23 \text{ mg Al g}^{-1} \text{ DW}$), whereas areas represented by supracrustal rocks were poor in available Al (class 12: $0.47 \pm 0.06 \text{ mg Al g}^{-1} \text{ DW}$). We found relatively low concentrations ($0.73 \pm 0.01 \text{ mg Al g}^{-1} \text{ DW}$) of available Al for Chukotka and for eastern and western Siberia in lithological class 9. The Verkhoyansk–Kolyma region and the East European Plain showed the lowest available Al concentrations (class 11: $0.26 \pm 0.02 \text{ mg Al g}^{-1} \text{ DW}$) as did the Canadian Shield (class 5: $0.21 \pm 0.03 \text{ mg Al g}^{-1} \text{ DW}$). An increasing thawing depth may increase the available Al concentration via the predicted thaw of the permafrost layer in northern Europe, as the Al concentration in the permafrost layer is $4.88 \pm 1.02 \text{ mg Al g}^{-1} \text{ DW}$ (lithological class 6) compared with the current active layer ($2.52 \pm 0.7 \text{ mg Al g}^{-1} \text{ DW}$; lithological class 6); moreover, across the Greenland and Canadian shields, the available Al concentration via the predicted thaw of the permafrost layer is $0.3 \pm 0.07 \text{ mg Al g}^{-1} \text{ DW}$ (lithological class 5) compared with the current active layer ($0.21 \pm 0.03 \text{ mg Al g}^{-1} \text{ DW}$;



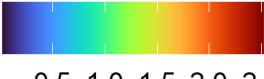
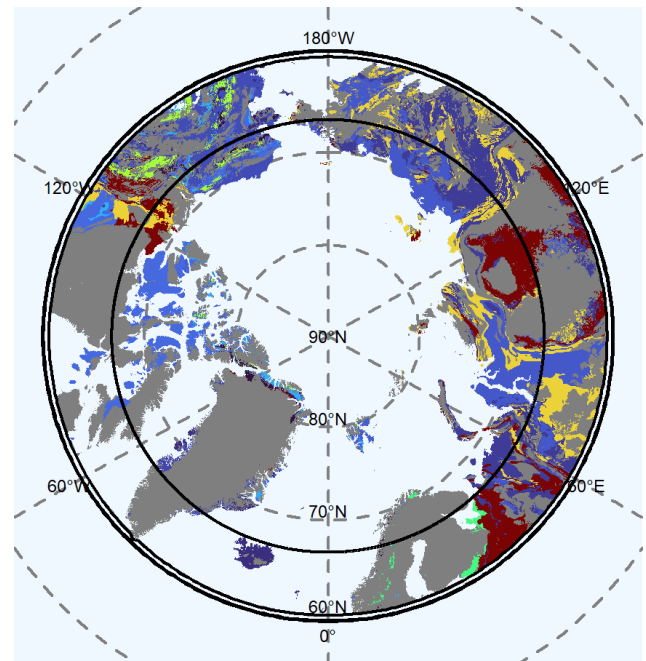
Al (mg g^{-1} DW)  0.5 1.0 1.5 2.0 2.5

Figure 7. Map of the mean concentration of available (Mehlich-III-extractable) aluminum (Al) for the uppermost 100 cm of soils. For each lithological class, the mean concentration is shown. Blue colors represent low concentrations of Al, whereas red colors represent high concentrations. Gray shaded areas are not represented by our data.



P (mg g^{-1} DW)  0.0 0.1 0.2 0.3

Figure 8. Map of the mean concentration of available (Mehlich-III-extractable) phosphorous (P) for the uppermost 100 cm of soils. For each lithological class, the mean concentration is shown. Blue colors represent low concentrations of P, whereas red colors represent high concentrations. Gray shaded areas are not represented by our data.

lithological class 5) (Fig. S7, Table S4). The variability in the data of available Al is high for lithological classes 2 and 6.

3.3.6 Phosphorous at 0–1 m depth

We found the highest available (Mehlich-III-extractable) P concentrations for the West Siberian Basin, the Canadian Shield, and the Siberian and East European plains (class 4: $0.306 \pm 0.042 \text{ mg P g}^{-1}$ DW) (Fig. 8). In the Chukotka region, the available P concentrations were $0.189 \pm 0.023 \text{ mg P g}^{-1}$ DW (lithological class 7). We found moderate available P concentrations for northern Europe (class 6: $0.123 \pm 0.034 \text{ mg P g}^{-1}$ DW) and Alaska (class 14: $0.153 \pm 0.054 \text{ mg P g}^{-1}$ DW). Wide areas of supracrustal rocks in Alaska were poor in available P (class 12: $0.024 \pm 0.004 \text{ mg P g}^{-1}$ DW). The Canadian Shield (class 5: $0.037 \pm 0.005 \text{ mg P g}^{-1}$ DW), the Verkhoyansk–Kolyma region, the East European Plain (class 11: $0.017 \pm 0.002 \text{ mg P g}^{-1}$ DW), and the Chukotka region (class 9: $0.030 \pm 0.003 \text{ mg P g}^{-1}$ DW) were also poor in P. Due to

permafrost thaw, we expect increasing available P concentrations for the Canadian Shield, as the available P concentration in the permafrost layer is $0.06 \pm 0.01 \text{ mg P g}^{-1}$ DW (lithological class 5) compared with the current active layer concentration of $0.04 \pm 0.005 \text{ mg P g}^{-1}$ DW (lithological class 5) (Fig. 7, Table S4). The variability in the data of available P is high for lithological classes 4, 6, and 7.

4 Discussion

4.1 Element availability in relation to lithology and geography

We found large differences in the availability of all of the analyzed elements among the different lithology classes in the Arctic. The igneous lithological type, for example, is dominated by alkaline and Ca-rich basaltic rocks from Alaska. Sedimentary rocks cover a wide range of pH values, as sediments of diverse origin can contribute to form a sedimentary rock (Schirrmeyer et al., 2011). In regions with fluvial deposition (e.g., in yedoma-affected areas), the soil-forming ma-

terial may differ from the underlying bedrock (Kokelj et al., 2017). Limestone sediments, for example, differ with respect to their available Fe and P contents, depending on whether their origin is biological (lithological class 4), physical, or chemical. Sandstone can also contain high available Fe concentrations, but it is mainly comprised of available Si (lithological classes 7 and 8) (Yurchenko et al., 2019). Previously, no map outlining the availability of Si, Ca, Fe, P, and Al in Arctic soils existed, and only a map of ASi stocks (but not concentrations) was available. Our maps show the element concentrations available for both plants and microbes. Furthermore, we show the potential changes in element availability due to a deepening of the active layer, element export by runoff from thawed soil, and thermokarst processes.

4.2 Relevance of element availability in a dynamic Arctic

Nutrient cycles and limitations have been identified as important for improving estimations of high-latitude ecosystem vegetation functional parameters, like gross primary production (GPP) (Chadburn et al., 2017). Therefore, the dataset presented in our study could serve as a basis to provide soil nutrient concentrations for biogeochemical models that are capable of considering nutrient limitations in permafrost ecosystems. Our maps cover nearly the half of the Arctic area. The distribution of ASi in Arctic regions was first estimated by Alfredsson et al. (2016), who presented maps of ASi stocks (not concentrations) related to vegetation cover (covering 30 soil profiles). Elements like Si and Ca are accumulated by plants, depending on the vegetation type (Jobbágy and Jackson, 2001; Mauclet et al., 2022). Therefore, the effect of the current vegetation on element availability in soils is associated with high uncertainties, as the vegetation involved in forming the soil ASi pool may be different from the current vegetation. Thus, more appropriate measures of element availability may be the parent material and lithology (Alloway, 2013). It has been shown that the geochemical element concentration in Arctic permafrost soil allows one to distinguish geologies (Reimann and Melezhik, 2001). Consequently, our lithology-based extrapolation of nutrient availability will help to reduce the current uncertainties in pan-Arctic soil element availability.

Due to deepening of the active layer, such as in the Canadian Shield and in the North Atlantic region, our data suggest higher ASi concentrations in the active layer in the future, as the ASi concentration in the permafrost layer is higher compared with the current active layer (Fig. S6). These higher ASi concentrations may increase P and OM availability (Reithmaier et al., 2017; Schaller et al., 2019) due to polysilicic acid competing for binding sites on the surface of minerals, subsequently mobilizing both P and OM (as ASi is a main source of polysilicic acid), and potentially increasing the leaching of both elements to the sea. It has also been shown that available Si leads to a release of P from minerals in Arctic soils and increases OM decomposition, thereby

increasing soil GHG release (Schaller et al., 2019, 2021). Available Ca can immobilize OM via cation bridging and, thus, preserve OM from microbial decomposition (Sowers et al., 2020). Available Ca is also relevant for mineral formation because it can bind CO₂ as Ca(HCO₃)₂ in soil with a pH higher than 7 (Dessert et al., 2003; Köhler et al., 2010). The concentration of soluble Ca in yedoma soils is mainly driven by thermokarst processes (Monhonval et al., 2022). In permafrost layers, the data presented in Fig. S6 show that Ca concentrations are lower than those in the current active layers at most locations, which is in accordance with other studies (Kokelj and Burn, 2005). Consequently, a future increase in temperatures may lead to a widespread decrease in the available Ca concentrations on average at 0–1 m depth, especially in yedoma regions. Iron minerals are important electron acceptors under anaerobic conditions, and available Fe is essential for microbial methane production (Colombo et al., 2018). After being released from rocks by weathering, Al forms amorphous aluminosilicates that crystallize slowly (Schaller et al., 2021). The Mehlich III extract contains all soluble forms of Al(OH)(H₂O) that are bioavailable for organisms, with Al being toxic (Rengel, 2004). Thawing permafrost may be a source of available Al, especially across Canada, the Greenland Shield, and northern Europe. Increasing P availability, as predicted for Greenland and the Canadian Shield (Fig. 7), may, for example, increase CO₂ release to the atmosphere by increasing the mineralization rates of OM (Street et al., 2018; Yang and Kane, 2021).

4.3 The importance of element interactions for nutrient availability

In permafrost layers, the mineralization of OM by microbial activity is negligible due to frozen conditions. As in temperate soils, the binding of OM in the mineral phases can prevent OM from mineralization (Dutta et al., 2006; Mueller et al., 2015). Mineral phases may bind parts of soil OM, thereby reducing the amount of OM available for microbial respiration. A large share of OM may be associated with iron and aluminum oxides/hydroxides. In particular, iron minerals may strongly bind OM, whereby a high stability of stored carbon is likely (Herndon et al., 2017). Thus, the binding between OM and the minerals is determined by the quantity of minerals that can bind OM (Wiseman and Püttmann, 2006). This would imply that a higher concentration of available Fe, Al, and Ca in Arctic soils due to permafrost thaw may lead to lower GHG emissions from Arctic soils due to the complexation of OM with those elements. Therefore, an increase in element availability and, in turn, the increased binding of OM could result in potentially lower GHG emissions in Alaska (due to a higher available Ca and available Fe concentration in the permafrost layer compared with current active layer), the Canadian Shield and Greenland (due to a higher available Fe and available Al concentration in the permafrost layer compared with the current active layer),

and northern Europe (due to a higher available Al concentration in the permafrost layer compared with the current active layer) (see Sect. 3). However, lower available Ca concentrations can be expected in large parts of Siberia and the Canadian Shield, as the concentrations in the permafrost layer are lower compared with the current active layer. Available Si, however, can potentially mobilize OM from these phases under slightly acidic to alkaline conditions and under oxic to anoxic conditions due to the binding competition of silicic acid with some functional groups of organic material (Hömborg et al., 2020), thereby potentially increasing GHG emissions. An increase in Si availability upon permafrost thaw can be expected in the western Verkhoyansk–Kolyma region to the East European Platform, as the concentration in the permafrost layer is higher compared with the current active layer (see Sect. 3). Available P competes with OM for binding sites on soil minerals (Schneider et al., 2010). Increasing P concentrations due to permafrost thaw can be expected for the Canadian Shield (Sect. 3). Based on the differences in element (Si, Fe, Al, Ca, and P) available concentrations, the stability of OM differs in Arctic regions depending on the dominant mineral composition, lithology, and element availability. Furthermore, the availability of nutrients (P in this case) is modified by the mineral composition. For example, P is often strongly bound to Fe mineral phases, reducing P availability (Gérard, 2016). Silicic acid, however, is able to mobilize P from strong bonds to Fe minerals by competing for binding sites under a wide range of conditions (Schaller et al., 2019). Unlike Si, Ca binds P via calcium phosphate precipitation under alkaline conditions (Cao and Harris, 2008) or via calcium carbonate/phosphate coprecipitation (Otsuki and Wetzel, 1972). Under low-Fe-availability conditions in soils, the binding of P may be related to Al minerals (Eriksson et al., 2015). A lack of available P also leads to a reduction in the physiological activity of microbes (Walker et al., 2001), thereby potentially reducing the microbial respiration of OM. Mobile Si, in the form of silicic acid and its polymers, may potentially limit the availability of ions like Fe, Al, or Ca by precipitating those elements in the amorphous or crystalline phases (Schaller et al., 2021). Hence, the mobilization of elements like Si, Ca, Fe, and Al strongly interferes with both P and OM availability and, thus, potentially with GHG emissions. To unravel the dominant processes upon permafrost thaw or the element mobilization that is dominant in terms of OM binding or mobilization, which affects GHG emissions, future studies are urgently needed.

4.4 Transport of elements to the Arctic Ocean

With the ongoing deepening of the active layer in Arctic soils, increased leaching of elements and nutrients may occur (Mann et al., 2022; Sanders et al., 2022), and this may substantially impact marine biodiversity and ecosystem function. We have shown, for several regions of the Arctic, that there will be regional differences in element mobilization

upon permafrost thaw. For example, the increased export of Fe and P, which are the main limiting nutrients for marine net primary production (NPP) (Zabel and Schulz, 2006), has already contributed to a 30 % increase in NPP in the Arctic Ocean between 1998 and 2009 (Arrigo and van Dijken, 2011). Increased available Fe concentrations at a soil depth of 0–1 m upon permafrost thaw can be expected for soils of the Canadian Shield, Greenland, and Alaska, whereas increased P mobilization may occur only in the Canadian Shield, according to the sites studied within these lithological classes. Si and Ca also have a crucial role in marine primary production. Moreover, both elements are components of the inorganic spheres of diatoms (Si) and coccolithophores (Ca), which fix CO₂ in the Arctic Ocean, an important global carbon sink (Krause et al., 2018). At the Arctic Canadian coast, Si inputs have led to an increase in diatoms from 2 % to 37 % (Terhaar et al., 2021). Diatoms and coccolithophores are the basis of the marine food chain; therefore, shifts in their populations may have widespread implications for the marine ecosystem (Daniels et al., 2018). Permafrost thaw is likely to accelerate inputs of available Si and Ca to Arctic waters. Increased Si availability in soils can be expected in the western Verkhoyansk–Kolyma region to the East European Platform, as the concentration in the permafrost layer is higher compared with the current active layer (see Sect. 3). Calcium mobilization may increase or decrease depending on the Arctic region. Increased Ca mobilization can be expected for Alaska, whereas a slight decrease in Ca mobilization may occur in large parts of Siberia and the Canadian Shield (see Sect. 3). Yedoma deposits readily leach soluble ions, including Si and Ca, as a result of thaw degradation (Strauss et al., 2017b). Alaskan soils store huge amounts of available Ca in the mineral layer (see above) that could be transported to the Beringia Sea with increasing soil degradation, thereby promoting the growth of coccolithophores. In Siberia, the Lena River could transport large amounts of available Si to the Laptev Sea, increasing the growth of diatoms. The same could happen on the East European Plain. In the same way, P concentrations in these regions of the Arctic Sea could also rise, as P concentrations in the permafrost layer of the Canadian Shield are higher compared with the current active layer (see Sect. 3). During transport to the ocean, the elements may be bound to soil particles, potentially inhibiting further transport, or may interact with other elements (see the previous paragraph), also potentially affecting further transport. In summary, in many areas of the Arctic with high available Si, Ca, and P storage, there could be increased inputs to Arctic waters, with permafrost thaw potentially increasing CO₂ fixation by marine primary production.

4.5 Limitations of data and statistics

Despite the sample number of our study being quite high and reflecting a broad range of pan-Arctic regions, this study still

has some limitations. The density of data points is not homogeneous over the whole area, and the sample number is low in some remote areas. To reduce potential uncertainties and variance in the presented data on available element concentrations, we carried out bootstrapping for the single layers within the lithological classes. Our data do not give total element pools, rather biologically available concentrations.

5 Data availability

The element availability data from all single locations, soil profiles, transects, and lithologies as well as bootstrap data for locations and lithologies can be downloaded via the Edmond open-access MPG repository: <https://doi.org/10.17617/3.8KGQUN> (Schaller and Goeckede, 2022). During review process, the data were made available from <https://edmond.mpdl.mpg.de/privateurl.xhtml?token=8cbb0bd8-790f-4719-8cd1-a3df4ff99477> (last access: 1 March 2023) to allow for corrections based on reviewer comments (Schaller and Goeckede, 2022). The repository contains a readme file (“Read me.docx”). In this file, all necessary information can be found, including all of the column descriptions need to use the data.

The element availability information from all single locations, soil profiles, transects, and lithologies is labeled (location_samples.txt) and contains the following parameters: the Geological Map of the Arctic; the individual ID of the polygon; the official name of the sampling site; the internal study name of the soil sample; the soil horizon; the coordinates of sampling sites; the concentration of alkaline-extractable amorphous silicon (ASi); the Mehlich-III-extractable Si, Ca, Fe, Al, and P; the thickness of the layer; the original depth from which soil was taken; the size of the polygon that contains the sampling site; the age code; the scientific name of the age during which the bedrock was formed; the scientific name of the eon during which the bedrock was formed; the scientific name of the era during which the bedrock was formed; the scientific name of the period during which the bedrock was formed; the maximal and minimal age of the bedrock; if lithogenesis was of the supracrustal, sedimentary, or igneous type; the most common rock types in the cluster group of the setting; the code of the metamorphic type; the code of the domain region; the name of the tectonic and geographic domain; and the name of the region within the geographic domain.

In the “location_bootstrap.txt” file, the bootstrapped means of concentration of alkaline extractable Si, Mehlich-III-extractable Si, Ca, Fe, Al, and P for the organic, mineral, and permafrost layers of the single locations are given in milligrams per gram dry weight (mg g^{-1} DW).

In the “lithology_bootstrap.txt” file, the element concentrations for the first 1 m, including the organic, mineral, and permafrost layers, are given as a bootstrapped mean and

the standard deviation for alkaline-extractable Si as well as Mehlich-III-extractable Si, Ca, Fe, Al, and P.

6 Conclusion

In this work, we identified large differences in the concentrations of available Si, Ca, Fe, Al, and P as well as the solid ASi fraction among different Arctic regions. With the future projected warming of the Arctic and the associated thaw of permafrost soils due to deepening of the active layer, the available concentration of the elements will change. Depending on the dominance or limitation of certain elements, biogeochemical processes such as OM mineralization may increase or decrease. Moreover, not only may microbial processes such as OM respiration be affected by changes in Si, Ca, Fe, P, and Al availability but processes such as primary production (CO_2 fixation by plants) in terrestrial systems might also be impacted. This could stabilize soil OM but may also trigger elevated biomass production by plants due to an increased nutrient supply. In addition, marine systems will receive higher loads of leached elements, which could increase algae biomass production due to increased nutrient transport to the sea. Our spatially explicit data product, including the differences in element availability among the different lithological classes and regions, will help improve models of Arctic biogeochemical cycles for estimating future carbon feedback under predicted climate change.

Supplement. The supplement related to this article is available online at: <https://doi.org/10.5194/essd-15-1059-2023-supplement>.

Author contributions. JSc And MG designed the study. MG, BE, SN, PK, NP, GH, OS, and CM sampled the soils. PS did the analysis and processed the data. PS and JSc wrote the first draft of the manuscript with input from MG and JSt. All co-authors commented on the manuscript and agreed upon the final version of the paper.

Competing interests. The contact author has declared that none of the authors has any competing interests.

Disclaimer. Publisher’s note: Copernicus Publications remains neutral with regard to jurisdictional claims in published maps and institutional affiliations.

Acknowledgements. We thank Lidia Völker (ZALF) for help with data extraction from the GIS polygons.

Financial support. The work was funded by the German Research Foundation (DFG; grant no. SCHA 1822/12-1 to Jörg Schaller). The work of Jens Strauss was embedded into the

“Changing Arctic Ocean” (CAO) program (CACOON project; grant no. 03F0806A, BMBF). This work was also supported by the National Science Foundation (NSF; grant no. NSF-1417700 to Susan Natali).

Review statement. This paper was edited by Attila Demény and reviewed by two anonymous referees.

References

- Abbott, B. W., Jones, J. B., Godsey, S. E., Larouche, J. R., and Bowden, W. B.: Patterns and persistence of hydrologic carbon and nutrient export from collapsing upland permafrost, *Biogeosciences*, 12, 3725–3740, <https://doi.org/10.5194/bg-12-3725-2015>, 2015.
- Alfredsson, H., Clymans, W., Hugelius, G., Kuhry, P., and Conley, D. J.: Estimated storage of amorphous silica in soils of the circum-Arctic tundra region, *Global Biogeochem. Cy.*, 30, 479–500, <https://doi.org/10.1002/2015GB005344>, 2016.
- Alloway, B. J.: Bioavailability of Elements in Soil, in: *Essentials of Medical Geology*, edited by: Selinus, O., Springer, Dordrecht, 351–373, https://doi.org/10.1007/978-94-007-4375-5_15, 2013.
- Arrigo, K. R. and van Dijken, G. L.: Secular trends in Arctic Ocean net primary production, *J. Geophys. Res.*, 116, C09011, <https://doi.org/10.1029/2011JC007151>, 2011.
- Box, J. E., Colgan, W. T., Christensen, T. R., Schmidt, N. M., Lund, M., Parmentier, F.-J. W., Brown, R., Bhatt, U. S., Euskirchen, E. S., Romanovsky, V. E., Walsh, J. E., Overland, J. E., Wang, M., Corell, R. W., Meier, W. N., Wouters, B., Mernild, S., Mård, J., Pawlak, J., and Olsen, M. S.: Key indicators of Arctic climate change: 1971–2017, *Environ. Res. Lett.*, 14, 45010, <https://doi.org/10.1088/1748-9326/aafc1b>, 2019.
- Brown, J. and Romanovsky, V. E.: Report from the International Permafrost Association: state of permafrost in the first decade of the 21st century, *Permafrost Periglac. Process.*, 19, 255–260, <https://doi.org/10.1002/ppp.618>, 2008.
- Cao, X. and Harris, W.: Carbonate and magnesium interactive effect on calcium phosphate precipitation, *Environ. Sci. Technol.*, 42, 436–442, <https://doi.org/10.1021/es0716709>, 2008.
- Chadburn, S. E., Krinner, G., Porada, P., Bartsch, A., Beer, C., Beletti Marchesini, L., Boike, J., Ekici, A., Elberling, B., Friberg, T., Hugelius, G., Johansson, M., Kuhry, P., Kutzbach, L., Langer, M., Lund, M., Parmentier, F.-J. W., Peng, S., Van Huissteden, K., Wang, T., Westermann, S., Zhu, D., and Burke, E. J.: Carbon stocks and fluxes in the high latitudes: using site-level data to evaluate Earth system models, *Biogeosciences*, 14, 5143–5169, <https://doi.org/10.5194/bg-14-5143-2017>, 2017.
- Colombo, N., Salerno, F., Gruber, S., Freppaz, M., Williams, M., Fratianni, S., and Giardino, M.: Review: Impacts of permafrost degradation on inorganic chemistry of surface fresh water, *Global Planet. Change*, 162, 69–83, <https://doi.org/10.1016/j.gloplacha.2017.11.017>, 2018.
- Daniels, C. J., Poulton, A. J., Balch, W. M., Marañón, E., Adey, T., Bowler, B. C., Cermeño, P., Charalampopoulou, A., Crawford, D. W., Drapeau, D., Feng, Y., Fernández, A., Fernández, E., Fragoso, G. M., González, N., Graziano, L. M., Heslop, R., Holligan, P. M., Hopkins, J., Huete-Ortega, M., Hutchins, D. A., Lam, P. J., Lipsen, M. S., López-Sandoval, D. C., Loucaides, S., Marchetti, A., Mayers, K. M. J., Rees, A. P., Sobrino, C., Tynan, E., and Tyrrell, T.: A global compilation of coccolithophore calcification rates, *Earth Syst. Sci. Data*, 10, 1859–1876, <https://doi.org/10.5194/essd-10-1859-2018>, 2018.
- DeMaster, D. J.: The supply and accumulation of silica in the marine environment, *Geochim. Cosmochim. Ac.*, 45, 1715–1732, 1981.
- Dessert, C., Dupré, B., Gaillardet, J., François, L. M., and Allègre, C. J.: Basalt weathering laws and the impact of basalt weathering on the global carbon cycle, *Chem. Geol.*, 202, 257–273, <https://doi.org/10.1016/j.chemgeo.2002.10.001>, 2003.
- Dutta, Schuur, E. A. G., Neff, and Zimov, S. A.: Potential carbon release from permafrost soils of Northeastern Siberia, *Glob. Change Biol.*, 12, 2336–2351, <https://doi.org/10.1111/j.1365-2486.2006.01259.x>, 2006.
- Eriksson, A. K., Gustafsson, J. P., and Hesterberg, D.: Phosphorus speciation of clay fractions from long-term fertility experiments in Sweden, *Geoderma*, 241–242, 68–74, <https://doi.org/10.1016/j.geoderma.2014.10.023>, 2015.
- Faucherre, S., Jørgensen, C. J., Blok, D., Weiss, N., Siewert, M. B., Bang-Andreasen, T., Hugelius, G., Kuhry, P., and Elberling, B.: Short and Long-Term Controls on Active Layer and Permafrost Carbon Turnover Across the Arctic, *J. Geophys. Res.-Biogeo.*, 123, 372–390, <https://doi.org/10.1002/2017JG004069>, 2018.
- Fuchs, M., Grosse, G., Strauss, J., Günther, F., Grigoriev, M., Maximov, G. M., and Hugelius, G.: Carbon and nitrogen pools in thermokarst-affected permafrost landscapes in Arctic Siberia, *Biogeosciences*, 15, 953–971, <https://doi.org/10.5194/bg-15-953-2018>, 2018.
- Gérard, F.: Clay minerals, iron/aluminum oxides, and their contribution to phosphate sorption in soils – A myth revisited, *Geoderma*, 262, 213–226, <https://doi.org/10.1016/j.geoderma.2015.08.036>, 2016.
- Goldman, C. R., Kumagai, M., Robarts, R. D., and Goldman, C. R. (Eds.): *Climatic Change and Global Warming of Inland Waters: Impacts and Mitigation for Ecosystems and Societies*, John Wiley & Sons Inc, Chichester, West Sussex, UK, ISBN 978-1-119-96866-5, 2013.
- Harrison, J. C., St-Onge, M. R., Petrov, O. V., Strelnikov, S. I., Lopatin, B. G., Wilson, F. H., Tella, S., Paul, D., Lynds, T., Shokalsky, S. P., Hults, C. K., Bergman, S., Jepsen, H. F., and Solli, A.: Geological map of the Arctic, Geological Survey of Canada, “A” Series Map 2159A, 9 sheets; 1 DVD, <https://doi.org/10.4095/287868>, 2011.
- Herndon, E., AlBashaireh, A., Singer, D., Roy Chowdhury, T., Gu, B., and Graham, D.: Influence of iron redox cycling on organo-mineral associations in Arctic tundra soil, *Geochim. Cosmochim. Ac.*, 207, 210–231, <https://doi.org/10.1016/j.gca.2017.02.034>, 2017.
- Hömberg, A., Obst, M., Knorr, K.-H., Kalbitz, K., and Schaller, J.: Increased silicon concentration in fen peat leads to a release of iron and phosphate and changes in the composition of dissolved organic matter, *Geoderma*, 374, 114422, <https://doi.org/10.1016/j.geoderma.2020.114422>, 2020.
- Hugelius, G., Strauss, J., Zubrzycki, S., Harden, J. W., Schuur, E. A. G., Ping, C.-L., Schirmer, L., Grosse, G., Michaelson, G. J., Koven, C. D., O’Donnell, J. A., Elberling, B., Mishra, U., Camill, P., Yu, Z., Palmtag, J., and Kuhry, P.: Estimated stocks of circumpolar permafrost carbon with quantified uncertainty

- ranges and identified data gaps, *Biogeosciences*, 11, 6573–6593, <https://doi.org/10.5194/bg-11-6573-2014>, 2014.
- Hugelius, G., Loisel, J., Chadburn, S., Jackson, R. B., Jones, M., MacDonald, G., Marushchak, M., Olefeldt, D., Packalen, M., Siewert, M. B., Treat, C., Turetsky, M., Voigt, C., and Yu, Z.: Large stocks of peatland carbon and nitrogen are vulnerable to permafrost thaw, *P. Natl. Acad. Sci. USA*, 117, 20438–20446, <https://doi.org/10.1073/pnas.1916387117>, 2020.
- IPCC: Climate Change 2021: The Physical Science Basis. Contribution of Working Group I to the Sixth Assessment Report of the Intergovernmental Panel on Climate Change, Climate Change, 236 pp., 2021.
- Jobbágy, E. and Jackson, R. B.: The distribution of soil nutrients with depth: Global patterns and the imprint of plants, *Biogeochemistry*, 53, 51–77, <https://doi.org/10.1023/A:1010760720215>, 2001.
- Kaiser, K. and Zech, W.: Competitive Sorption of Dissolved Organic Matter Fractions to Soils and Related Mineral Phases, *Soil Sci. Soc. Am. J.*, 61, 64–69, <https://doi.org/10.2136/sssaj1997.03615995006100010011x>, 1997.
- Köhler, P., Hartmann, J., and Wolf-Gladrow, D. A.: Geoengineering potential of artificially enhanced silicate weathering of olivine, *P. Natl. Acad. Sci. USA*, 107, 20228–20233, <https://doi.org/10.1073/pnas.1000545107>, 2010.
- Kokelj, S. V. and Burn, C. R.: Geochemistry of the active layer and near-surface permafrost, Mackenzie delta region, Northwest Territories, Canada, *Can. J. Earth Sci.*, 42, 37–48, <https://doi.org/10.1139/e04-089>, 2005.
- Kokelj, S. V., Lantz, T. C., Tunnicliffe, J., Segal, R., and Lacelle, D.: Climate-driven thaw of permafrost preserved glacial landscapes, northwestern Canada, *Geology*, 45, 371–374, <https://doi.org/10.1130/G38626.1>, 2017.
- Krause, J. W., Duarte, C. M., Marquez, I. A., Assmy, P., Fernández-Méndez, M., Wiedmann, I., Wassmann, P., Kristiansen, S., and Agustí, S.: Biogenic silica production and diatom dynamics in the Svalbard region during spring, *Biogeosciences*, 15, 6503–6517, <https://doi.org/10.5194/bg-15-6503-2018>, 2018.
- Kuhry, P., Bárta, J., Blok, D., Elberling, B., Faucherre, S., Hugelius, G., Jørgensen, C. J., Richter, A., Šantrůčková, H., and Weiss, N.: Lability classification of soil organic matter in the northern permafrost region, *Biogeosciences*, 17, 361–379, <https://doi.org/10.5194/bg-17-361-2020>, 2020.
- Mann, P. J., Strauss, J., Palmtag, J., Dowdy, K., Ogneva, O., Fuchs, M., Bedington, M., Torres, R., Polimene, L., Overduin, P., Mollenhauer, G., Grosse, G., Rachold, V., Sobczak, W. V., Spencer, R. G. M., and Juhls, B.: Degrading permafrost river catchments and their impact on Arctic Ocean nearshore processes, *AMBIO*, 51, 439–455, <https://doi.org/10.1007/s13280-021-01666-z>, 2022.
- Mauclet, E., Agnan, Y., Hirst, C., Monhonval, A., Pereira, B., Vandeuren, A., Villani, M., Ledman, J., Taylor, M., Jasinski, B. L., Schuur, E. A. G., and Opfergelt, S.: Changing sub-Arctic tundra vegetation upon permafrost degradation: impact on foliar mineral element cycling, *Biogeosciences*, 19, 2333–2351, <https://doi.org/10.5194/bg-19-2333-2022>, 2022.
- Mishra, U., Hugelius, G., Shelef, E., Yang, Y., Strauss, J., Lupachev, A., Harden, J. W., Jastrow, J. D., Ping, C.-L., Riley, W. J., Schuur, E. A. G., Matamala, R., Siewert, M., Nave, L. E., Koven, C. D., Fuchs, M., Palmtag, J., Kuhry, P., Treat, C. C., Zubrzycki, S., Hoffman, F. M., Elberling, B., Camill, P., Veremeeva, A., and Orr, A.: Spatial heterogeneity and environmental predictors of permafrost region soil organic carbon stocks, *Science Advances*, 7, eaaz5236, <https://doi.org/10.1126/sciadv.aaz5236>, 2021.
- Monhonval, A., Mauclet, E., Pereira, B., Vandeuren, A., Strauss, J., Grosse, G., Schirrmeister, L., Fuchs, M., Kuhry, P., and Opfergelt, S.: Mineral Element Stocks in the Yedoma Domain: A Novel Method Applied to Ice-Rich Permafrost Regions, *Front. Earth Sci.*, 9, 703304, <https://doi.org/10.3389/feart.2021.703304>, 2021.
- Monhonval, A., Strauss, J., Thomas, M., Hirst, C., Titeux, H., Louis, J., Gilliot, A., Du Bois d’Aische, E., Pereira, B., Vandeuren, A., Grosse, G., Schirrmeister, L., Jongejans, L. L., Ulrich, M., and Opfergelt, S.: Thermokarst processes increase the supply of stabilizing surfaces and elements (Fe, Mn, Al, and Ca) for mineral–organic carbon interactions, *Permafrost Periglac.*, 33, 452–469, <https://doi.org/10.1002/ppp.2162>, 2022.
- Mueller, C. W., Rethemeyer, J., Kao-Kniffin, J., Löppmann, S., Hinkel, K. M., and Bockheim, G. J.: Large amounts of labile organic carbon in permafrost soils of northern Alaska, *Glob. Change Biol.*, 21, 2804–2817, <https://doi.org/10.1111/gcb.12876>, 2015.
- Otsuki, A. and Wetzel, R.: Coprecipitation of phosphate with carbonates in a marl lake, *Limnol. Oceanogr.*, 17, 763–767, <https://doi.org/10.4319/lo.1972.17.5.0763>, 1972.
- Quideau, S. A., Chadwick, O. A., Trumbore, S. E., Johnson-Maynard, J. L., Graham, R. C., and Anderson, M. A.: Vegetation control on soil organic matter dynamics, *Org. Geochem.*, 32, 247–252, [https://doi.org/10.1016/S0146-6380\(00\)00171-6](https://doi.org/10.1016/S0146-6380(00)00171-6), 2001.
- R Core Team: R: A language and environment for statistical, R Foundation for Statistical Computing, Vienna, Austria, <http://www.r-project.org/index.html> (last access: 1 October 2022), 2020.
- Reimann, C. and Melezhik, V.: Metallogenic provinces, geochemical provinces and regional geology – what causes large-scale patterns in low density geochemical maps of the C-horizon of podzols in Arctic Europe?, *Appl. Geochem.*, 16, 963–983, 2001.
- Reithmaier, G.-M. S., Knorr, K.-H., Arnhold, S., Planer-Friedrich, B., and Schaller, J.: Enhanced silicon availability leads to increased methane production, nutrient and toxicant mobility in peatlands, *Scientific Reports*, 7, 8728, <https://doi.org/10.1038/s41598-017-09130-3>, 2017.
- Rengel, Z.: Aluminium cycling in the soil–plant–animal–human continuum, *Biometals*, 17, 669–689, <https://doi.org/10.1007/s10534-004-1201-4>, 2004.
- Romanovsky, V. E., Drozdov, D. S., Oberman, N. G., Malkova, G. V., Kholodov, A. L., Marchenko, S. S., Moskalenko, N. G., Sergeev, D. O., Ukraintseva, N. G., Abramov, A. A., Gilichinsky, D. A., and Vasiliev, A. A.: Thermal state of permafrost in Russia, *Permafrost Periglac.*, 21, 136–155, <https://doi.org/10.1002/ppp.683>, 2010.
- Salmon, V. G., Soucy, P., Mauritz, M., Celis, G., Natali, S. M., Mack, M. C., and Schuur, E. A. G.: Nitrogen availability increases in a tundra ecosystem during five years of experimental permafrost thaw, *Glob. Change Biol.*, 22, 1927–1941, <https://doi.org/10.1111/gcb.13204>, 2016.

- Sanders, T., Fiencke, C., Fuchs, M., Haugk, C., Juhls, B., Mollenhauer, G., Ogneva, O., Overduin, P., Palmtag, J., Povazhnyi, V., Strauss, J., Tuerena, R., Zell, N., and Dähnke, K.: Seasonal nitrogen fluxes of the Lena River Delta, *Ambio*, 51, 423–438, <https://doi.org/10.1007/s13280-021-01665-0>, 2022.
- Schaller, J. and Goeckede, M.: Pan-Arctic soil element availability estimations, 637, EDMOND open-access MPG repository [data set], <https://doi.org/10.17617/3.8KGQUN>, 2022.
- Schaller, J., Faucherre, S., Joss, H., Obst, M., Goeckede, M., Planer-Friedrich, B., Peiffer, S., Gilfedder, B., and Elberling, B.: Silicon increases the phosphorus availability of Arctic soils, *Scientific Reports*, 9, 449, <https://doi.org/10.1038/s41598-018-37104-6>, 2019.
- Schaller, J., Puppe, D., Kaczorek, D., Ellerbrock, R., and Sommer, M.: Silicon Cycling in Soils Revisited, *MDPI Plants*, 10, 295, <https://doi.org/10.3390/plants10020295>, 2021.
- Schirrmeister, L., Kunitsky, V., Grosse, G., Wetterich, S., Meyer, H., Schwamborn, G., Babiy, O., Derevyagin, A., and Siegert, C.: Sedimentary characteristics and origin of the Late Pleistocene Ice Complex on north-east Siberian Arctic coastal lowlands and islands – A review, *Quatern. Int.*, 241, 3–25, <https://doi.org/10.1016/j.quaint.2010.04.004>, 2011.
- Schneider, M., Scheel, T., Mikutta, R., van Hees, P., Kaiser, K., and Kalbitz, K.: Sorptive stabilization of organic matter by amorphous Al hydroxide, *Geochim. Cosmochim. Ac.*, 74, 1606–1619, <https://doi.org/10.1016/j.gca.2009.12.017>, 2010.
- Schuur, E. A. G., Abbott, B. W., Bowden, W. B., Brovkin, V., Camill, P., Canadell, J. G., Chanton, J. P., Chapin, F. S., Christensen, T. R., Ciais, P., Crosby, B. T., Czimczik, C. I., Grosse, G., Harden, J., Hayes, D. J., Hugelius, G., Jastrow, J. D., Jones, J. B., Kleinen, T., Koven, C. D., Krinner, G., Kuhry, P., Lawrence, D. M., McGuire, A. D., Natali, S. M., O'Donnell, J. A., Ping, C. L., Riley, W. J., Rinke, A., Romanovsky, V. E., Sannel, A. B. K., Schädel, C., Schaefer, K., Sky, J., Subin, Z. M., Tarnocai, C., Turetsky, M. R., Waldrop, M. P., Walter Anthony, K. M., Wickland, K. P., Wilson, C. J., and Zimov, S. A.: Expert assessment of vulnerability of permafrost carbon to climate change, *Climatic Change*, 119, 359–374, <https://doi.org/10.1007/s10584-013-0730-7>, 2013.
- Schuur, E. A. G., McGuire, A. D., Schädel, C., Grosse, G., Harden, J. W., Hayes, D. J., Hugelius, G., Koven, C. D., Kuhry, P., Lawrence, D. M., Natali, S. M., Olefeldt, D., Romanovsky, V. E., Schaefer, K., Turetsky, M. R., Treat, C. C., and Vonk, J. E.: Climate change and the permafrost carbon feedback, *Nature*, 520, 171–179, <https://doi.org/10.1038/nature14338>, 2015.
- Sher, A. V., Kuzmina, S. A., Kuznetsova, T. V., and Sulerzhitsky, L. D.: New insights into the Weichselian environment and climate of the East Siberian Arctic, derived from fossil insects, plants, and mammals, *Quaternary Sci. Rev.*, 24, 533–569, <https://doi.org/10.1016/j.quascirev.2004.09.007>, 2005.
- Sims, J. T.: Comparison of mehlich 1 and mehlich 3 extractants for P, K, Ca, Mg, Mn, Cu and Zn in atlantic coastal plain soils, *Commun. Soil Sci. Plan.*, 20, 1707–1726, <https://doi.org/10.1080/00103628909368178>, 1989.
- Sowers, T. D., Wani, R. P., Coward, E. K., Fischel, M. H. H., Betts, A. R., Douglas, T. A., Duckworth, O. W., and Sparks, D. L.: Spatially Resolved Organomineral Interactions across a Permafrost Chronosequence, *Environ. Sci. Technol.*, 54, 2951–2960, <https://doi.org/10.1021/acs.est.9b06558>, 2020.
- Stimmler, P., Priemé, A., Elberling, B., Goeckede, M., and Schaller, J.: Arctic soil respiration and microbial community structure driven by silicon and calcium, *Sci. Total Environ.*, 838, 156152, <https://doi.org/10.1016/j.scitotenv.2022.156152>, 2022.
- Strauss, J. (Ed.): Permafrost: Recarbonizing global soils – A technical manual of recommended management practices, Food and Agriculture Organization of the United Nations, Rome, <https://doi.org/10.4060/cb6378en>, 2021.
- Strauss, J., Schirrmeister, L., Grosse, G., Wetterich, S., Ulrich, M., Herzs Schuh, U., and Hubberten, H.-W.: The deep permafrost carbon pool of the Yedoma region in Siberia and Alaska, *Geophys. Res. Lett.*, 40, 6165–6170, <https://doi.org/10.1002/2013GL058088>, 2013.
- Strauss, J., Schirrmeister, L., Grosse, G., Fortier, D., Hugelius, G., Knoblauch, C., Romanovsky, V., Schädel, C., Schneider von Deimling, T., Schuur, E. A., Shmelev, D., Ulrich, M., and Veremeeva, A.: Deep Yedoma permafrost: A synthesis of depositional characteristics and carbon vulnerability, *Earth-Sci. Rev.*, 172, 75–86, <https://doi.org/10.1016/j.earscirev.2017.07.007>, 2017a.
- Strauss, J., Schirrmeister, L., Grosse, G., Fortier, D., Hugelius, G., Knoblauch, C., Romanovsky, V., Schädel, C., Schneider von Deimling, T., Schuur, E. A., Shmelev, D., Ulrich, M., and Veremeeva, A.: Deep Yedoma permafrost: A synthesis of depositional characteristics and carbon vulnerability, *Earth-Sci. Rev.*, 172, 75–86, <https://doi.org/10.1016/j.earscirev.2017.07.007>, 2017b.
- Strauss, J., Laboor, S., Schirrmeister, L., Fedorov, A. N., Fortier, D., Froese, D., Fuchs, M., Günther, F., Grigoriev, M., Harden, J., Hugelius, G., Jongejans, L. L., Kanevskiy, M., Kholodov, A., Kunitsky, V., Kraev, G., Lozhkin, A., Rivkina, E., Shur, Y., Siegert, C., Spektor, V., Streletskaya, I., Ulrich, M., Vartanyan, S., Veremeeva, A., Anthony, K. W., Wetterich, S., Zimov, N., and Grosse, G.: Circum-Arctic Map of the Yedoma Permafrost Domain, *Front. Earth Sci.*, 9, 758360, <https://doi.org/10.3389/feart.2021.758360>, 2021.
- Street, L. E., Mielke, N., and Woodin, S. J.: Phosphorus Availability Determines the Response of Tundra Ecosystem Carbon Stocks to Nitrogen Enrichment, *Ecosystems*, 21, 1155–1167, <https://doi.org/10.1007/s10021-017-0209-x>, 2018.
- Terhaar, J., Lauerwald, R., Regnier, P., Gruber, N., and Bopp, L.: Around one third of current Arctic Ocean primary production sustained by rivers and coastal erosion, *Nat. Commun.*, 12, 169, <https://doi.org/10.1038/s41467-020-20470-z>, 2021.
- Villani, M., Mauclet, E., Agnan, Y., Druel, A., Jasinski, B., Taylor, M., Schuur, E. A., and Opfergelt, S.: Mineral element recycling in topsoil following permafrost degradation and a vegetation shift in sub-Arctic tundra, *Geoderma*, 421, 115915, <https://doi.org/10.1016/j.geoderma.2022.115915>, 2022.
- Walker, D., Bockheim, J., Chapin III, F., Eugster, W., Nelson, F., and Ping, C.: Calcium-rich tundra, wildlife, and the “Mammoth Steppe”, *Quaternary Sci. Rev.*, 20, 149–163, [https://doi.org/10.1016/S0277-3791\(00\)00126-8](https://doi.org/10.1016/S0277-3791(00)00126-8), 2001.
- Weil, R. R. and Brady, N. C.: The nature and properties of soils, Fifteenth edition, global edition, Pearson, Harlow, England, London, New York, Boston, San Francisco, 1104 pp., ISBN 978-1-292-16224-9, 2017.
- Wiseman, C. and Pittmann, W.: Interactions between mineral phases in the preservation of soil organic matter, *Geoderma*, 134, 109–118, <https://doi.org/10.1016/j.geoderma.2005.09.001>, 2006.

- Yang, D. and Kane, D. L. (Eds.): Arctic Hydrology, Permafrost and Ecosystems, Springer eBook Collection, Springer International Publishing, Imprint Springer, Cham, 914 pp., ISBN 978-3030509286, 2021.
- Yurchenko, A. Y., Potapova, A. S., Bumagina, V. A., Vilesov, A. P., Chertina, K. N., Balushkina, N. S., Kalmykov, G. A., and Khotylev, O. V.: Morphological and Lithogenetic Classification of the Carbonate Rocks of the Abalak–Bazhenov Complex, Moscow Univ. Geol. Bull., 74, 372–379, <https://doi.org/10.3103/S0145875219040136>, 2019.
- Zabel, M. and Schulz, H. D. (Eds.): Marine Geochemistry, 2nd revised, updated and extended edition, SpringerLink Bücher, Springer Berlin Heidelberg, Berlin, Heidelberg, 574 pp., ISBN 3-540-32143-8, 2006.



Supplement of

Pan-Arctic soil element bioavailability estimations

Peter Stimmler et al.

Correspondence to: Jörg Schaller (joerg.schaller@zalf.de)

The copyright of individual parts of the supplement might differ from the article licence.

1

2 **1 Sampling locations and Domains**

3 Table S1: List of sampling locations, coordinates, and number of samples per location

Location	Coordinates	n (samples)	Depths organic/mineral/permafrost Layer (cm)
Alaska, Moist non-acidic tundra (MNT)	69.43303°N, 148.67435°W	10	11 / 48 / 41
Alaska, Moist acidic tundra (MAT)	69.42540°N, 148.69684°W	12	21 / 16 / 63
Alaska, Coldfoot (CO)	67.23727°N, 150.16176°W	9	30 / 33 / 37
Alaska, Chandalar (CH)	68.06904°N, 149.58072°W	8	10 / 35 / 55
Alaska, Franklin Bluff-Dry (FB)	69.67404°N, 148.72224°W	12	19 / 59 / 22
Canada, Cambridge Bay (CB)	69.23245°N, 104.1938°W	64	8-42 / 12-68 / 20-63
Russia, Chersky (CY)	68.61353°N, -161.35228°W	12	20 / 40 / 40
Russia, Kytalyk (KY)	70.83340°N, -147.45068°W	27	9-26 / 16-31 / 58-60
Russia, Ary-Masa (AM)	72.44968°N, -101.93294°W	34	6 / 63 / 32
Russia, Spasskaya (SP)	62.24558°N, -129.63319°W	26	6 / 94 / 0
Russia, Lena delta, first terrace (FT)	72.37942°N, -126.39018°W	55	16 / 22 / 62
Russia, Lena delta, third terrace (TT)	72.28748°N, -126.22118°W	68	9 / 29 / 92
Svalbard (SV)	78.19102°N, -15.85858°W	1	0 / 0 / 100

2

Svalbard, Adventalen (AD)	78,18347°N, -15.88292°W	78	6 / 14 / 80
Svalbard, Ny-Alesund (NA)	78.92427°N, -11.78364°W	24	7 / 63 / 30
Sweden, Abisko (AB)	68.35595°N, -19.04762°W	13	35 / 35 / 30
Greenland, Zackenberg (ZA)	74.46747°N, 20.55407°W	22	3 / 17 / 80
Greenland, Zackenberg, Ice Wedge (IW)	74.46485°N, 20.57802°W	1	3 / 17 / 80
Greenland, Zackenberg, Infilling FAN (IF)	74.46747°N, 20.55407°W	2	3 / 17 / 80
Greenland, Disko (DI)	69.26474°N, 53.46891°W	25	4-25 / 7-53 / 51-85
Greenland, Nussuaq (NU)	70.29722°N, 52.25667°W	12	100 / 0 / 0
Greenland, Melville Bay (MB)	73.55000°N, 55.51333°W	11	100 / 0 / 0
Greenland, Cass Fjord (CF)	80.09694°N, 63.15444°W	12	100 / 0 / 0
Greenland, Warming Land (WL)	81.53917°N, 51.29139°W	12	100 / 0 / 0
Greenland, Brønlund (BR)	82.22278°N, 40.80944°W	3	100 / 0 / 0

4

3

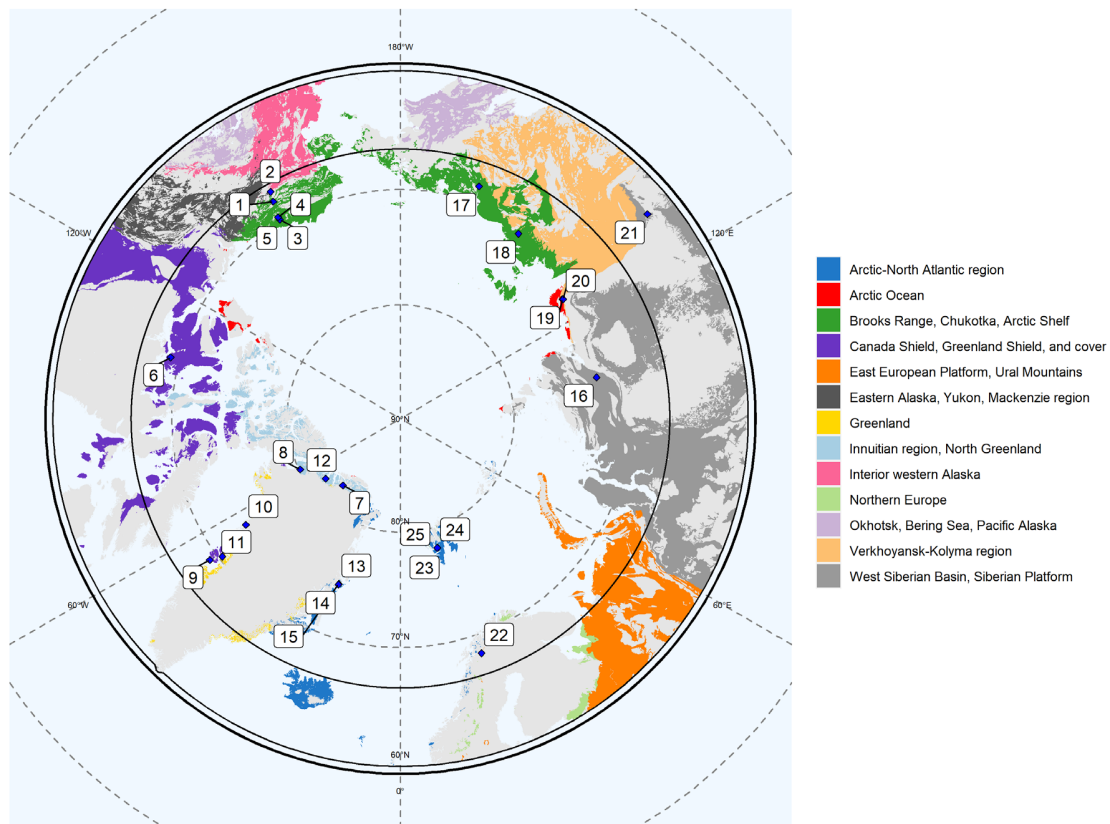


Fig. S1: Map with areas containing modelled element concentrations. The thirteen colors represent geographic domains of the original Geological Map of the Arctic, which are covered by modelled data. For allocation take care of the legend on the right side of the map. Numbers represent sampling locations: 1: Alaska, Chandalar; 2: Alaska Coldfoot; 3: Alaska, Franklin Bluff-Dry; 4: Alaska, MAT; 5: Alaska, MNT; 6: Canada; 7: Greenland, Brønlund; 8: Greenland, Cass Fjord; 9: Greenland, Disko; 10: Greenland, Melville Bay; 11: Greenland, Nussuaq; 12: Greenland, Warming Land; 13: Greenland, Zackenberg; 14: Greenland, Zackenberg, Ice Wedge; 15: Greenland, Zackenberg, Infilling FAN; 16: Russia, Ary-Mas; 17: Russia, Chersky; 18: Russia, Kytalyk; 19: Russia, Lena Delta, First terrace; 20: Russia, Lena Delta, Third terrace; 21: Russia, Spasskaya; 22: Sweden, Abisko; 23: Svalbard, Adventalen; 24: Svalbard, Ny-Alesund; 25: Svalbard, Svalbard

Table S2: Number of polygons with modelled element concentrations in the single domains.

Domain	n (Polygons)
Arctic-North Atlantic region	715
Arctic Ocean	90
Brooks Range, Chukotka, Arctic Shelf	835
Canada Shield, Greenland Shield, and cover	669
East European Platform, Ural Mountains	480
Eastern Alaska, Yukon, Mackenzie region	863
Greenland	604
Inuitian region, North Greenland	1502
Interior western Alaska	324
Northern Europe	92
Okhotsk, Bering Sea, Pacific Alaska	552
Verkhoyansk-Kolyma region	977
West Siberian Basin, Siberian Platform	923

Table S3: Original area of the three single maps of the Geological Map of the Arctic (“Canada, Alaska”, “Greenland” and “North Europe, Russia”) and area of extrapolated polygons in absolute and relative share.

Map	Area GMA (m ²)	Represented (m ²)	Share (%)
Canada, Alaska	5.42*10 ¹²	2.22*10 ¹²	40.93
Greenland, no icesheet	4.10*10 ¹¹	1.79*10 ¹¹	43.54
North Europe, Russia	1.02*10 ¹³	5.23*10 ¹²	51.45
Sum	1.77*10 ¹³	7.63*10 ¹²	43.03

From original 28,483 polygons of the geological map of the arctic 8,626 (30.3%) polygons could be extrapolated due to same lithology like the sampled polygons. In Canada and Alaska 3,912 polygons, in Greenland 1,278 polygon and in northern Europe and Russia 3,436 polygons were extrapolated.

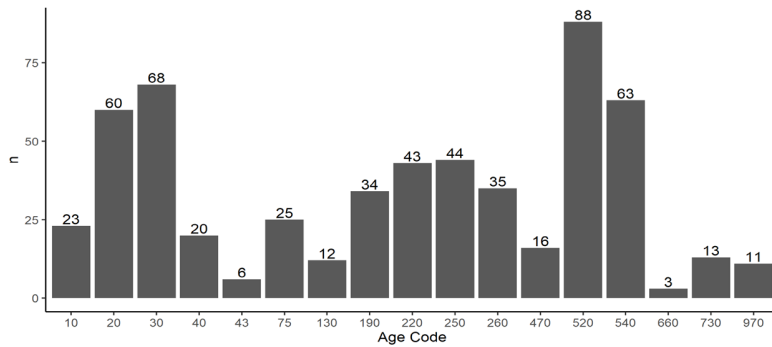


Fig S2: Number of samples per series epoch, represented by age code. 10: Paleogene and Neogene (65.5 - 2.6 Ma); 20: Neogene (23.0 - 2.6 Ma); 30: Pliocene to Holocene (5.3 - 0.0 Ma); 40: Pliocene (5.3 - 2.6 Ma); 43: Miocene (23.0 - 5.3 Ma); 75: Paleocene and Eocene (65.5 - 33.9 Ma); 130: Cretaceous and younger (145.5 - 0.0 Ma); 190: Late Cretaceous (99.6 - 65.5 Ma); 220: Early Cretaceous (145.5 - 99.6 Ma); 250: Late Jurassic and Early Cretaceous (161.2 - 99.6 Ma); 260: Jurassic and Cretaceous (199.6 - 65.5 Ma); 470: Carboniferous and Permian (359 - 251 Ma); 520: Cambrian to Devonian (542 - 359 Ma); 540: Late Devonian (385 - 359 Ma); 660: Neoproterozoic and Cambrian (1000 - 488 Ma); 730: Ediacaran (~635 - 542 Ma); Mesoarchean and Neoproterozoic (3200 - 2500 Ma).

Table S4: The 14 lithological classes with type, setting, and element concentration (mean and se in mg g⁻¹ DW) that were modelled.

Type	Setting	ID	Lithology	n (sam ples)	n (polygo ns)	ASi	Si	Ca	Fe	Al	P
Igneous: extrusive	Extrusive: mafic	1	Basalt, olivine basalt, tholeiite, alkali basalt, basanite, pillow basalt, flood basalt	26	455	6.68 ± 1.17	0.44 ± 0.08	3.65 ± 0.7	0.94 ± 0.18	0.25 ± 0.05	0.0116 ± 0.002
unclassified	Metamorphic: undivided	2	Gneiss, migmatite; reworked amphibolite and granulite facies rocks	11	604	4.11 ± 1.24	0.37 ± 0.11	0.05 ± 0.02	0.7 ± 0.21	0.65 ± 0.2	0.0217 ± 0.007
Sedimentary	Carbonate	3	Limestone, dolostone, shale, evaporites, chalk; carbonate reefs or metamorphosed equivalent	24	561	0.03 ± 0	0.1 ± 0.02	10.73 ± 2.15	0.01 ± 0	0.02 ± 0	0 ± 0
		4	Limestone, dolostone, shale, evaporites, chalk; carbonate reefs; metamorphic grade not identified	58	841	0 ± 0	5.65 ± 0.78	2.56 ± 0.34	2.28 ± 0.32	1.57 ± 0.22	0.3055 ± 0.042
		5	Limestone, dolostone, shale, evaporites, chalk; carbonate reefs	64	1174	1.24 ± 0.14	0.3 ± 0.03	3.79 ± 0.45	0.41 ± 0.05	0.21 ± 0.03	0.0372 ± 0.005
	Clastic: shallow marine	6	Quartz sandstone, siltstone, claystone, limestone, dolostone, conglomerate, tillite	13	92	0 ± 0	6.61 ± 1.83	3.34 ± 0.93	2.49 ± 0.69	2.52 ± 0.7	0.1226 ± 0.034
	Clastic: deltaic and nearshore	7	Sandstone, siltstone, shale, coal; plant fossils; metamorphic grade not identified	68	727	0 ± 0	5.46 ± 0.66	2.21 ± 0.27	2.21 ± 0.27	1.63 ± 0.2	0.1898 ± 0.023
	Sedimentary: undivided	8	Sandstone, siltstone, shale, limestone	38	308	0.28 ± 0	1.72 ± 0.07	8.06 ± 0.36	0.84 ± 0.09	1 ± 0.12	0.0311 ± 0.004
		9	Sandstone, siltstone, shale, limestone; metamorphic grade not identified	39	525	2.01 ± 0.24	0.36 ± 0.05	1.51 ± 0.14	0.83 ± 0.13	0.73 ± 0.1	0.0297 ± 0.003
	Clastic: shallow marine	10	Sandstone, siltstone, shale; marine fossils	91	707	2.06 ± 0.01	2.29 ± 0.03	2.04 ± 0.14	1.65 ± 0.1	0.94 ± 0.06	0.0377 ± 0.002
		11	Sandstone, siltstone, shale; marine fossils; metamorphic grade not identified	60	1362	1.48 ± 0.16	0.39 ± 0.04	2.88 ± 0.32	0.49 ± 0.04	0.26 ± 0.02	0.0171 ± 0.002

	Slope and deep water	13	Shale, chert, iron-formation, greywacke, turbidite, argillaceous limestone, matrix-supported conglomerate	43	0 ± 0	4.51 ± 0.69	1.8 ± 0.27	2.93 ± 0.45	1.5 ± 0.23	0.0701 ± 0.011	0 ± 0
		14	Shale, chert, iron-formation, greywacke, turbidite, argillaceous limestone, matrix-supported conglomerate or metamorphosed equivalent	8	0.11 ± 0.04	0.43 ± 0.15	1.27 ± 0.45	1.88 ± 0.66	1.08 ± 0.38	0.1528 ± 0.054	0.11 ± 0.04
Supracrustal rocks	Sedimentary and/or volcanic: undivided	12	Sedimentary and/or volcanic rock: undivided	21	0.31 ± 0	0.15 ± 0.01	8.77 ± 0.12	1.24 ± 0.14	0.47 ± 0.06	0.0242 ± 0.004	0.31 ± 0

Setting type: Sedimentary

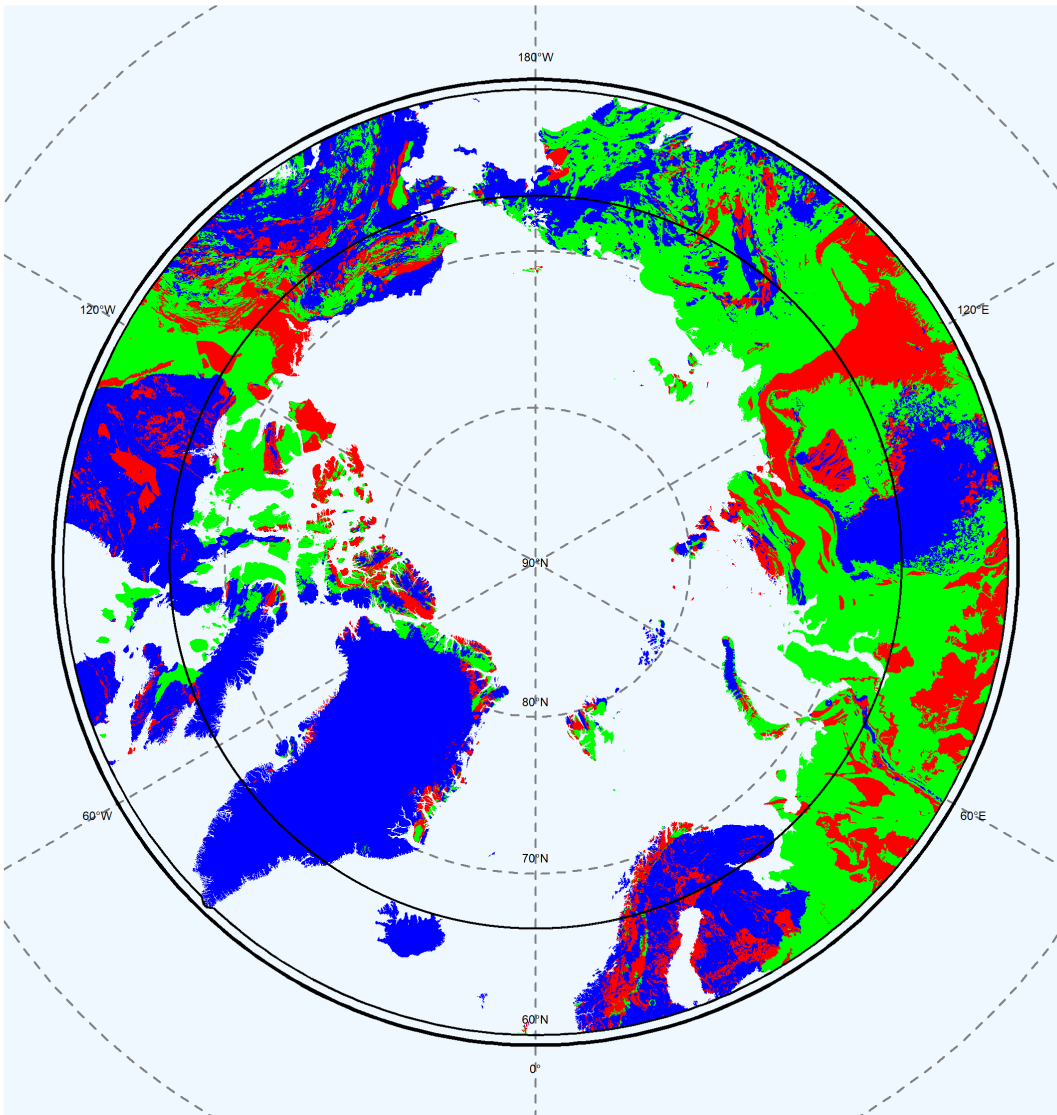


Fig. S3. Distribution of sediments in the arctic. Blue: Complete Geological Map of the Arctic. Red: Lithological classes of the setting type "Sedimentary". Green: Area represented by data for the lithological classes of the setting type "Sedimentary".

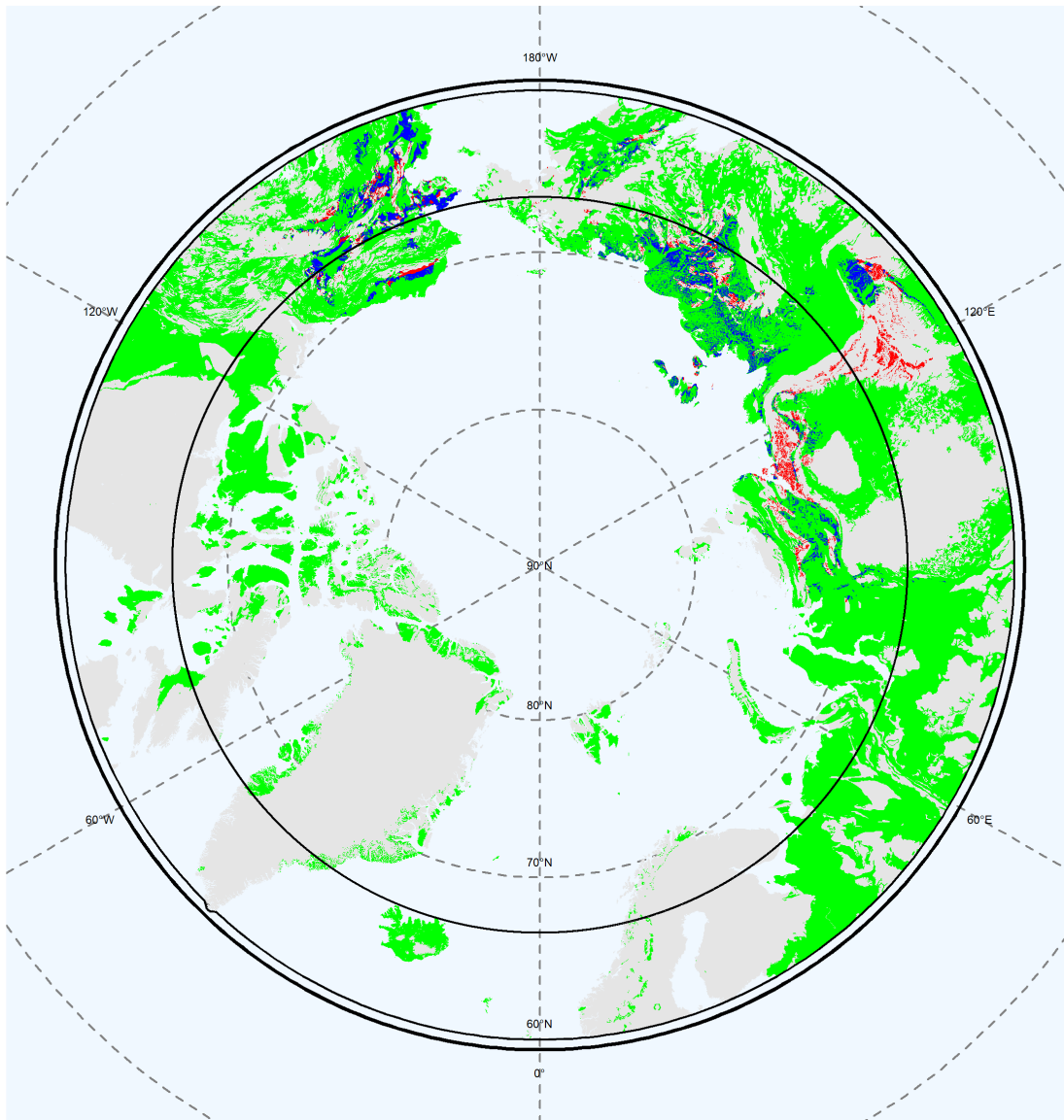


Fig. S4: Distribution of Yedoma soils in the Arctic. Grey: Complete Geological Map of the Arctic. Green: Area represented by data. Blue: Yedoma soils represented by data. Red: Yedoma soils not represented by data. White: Yedoma soils not represented by original Geological map of the Arctic.

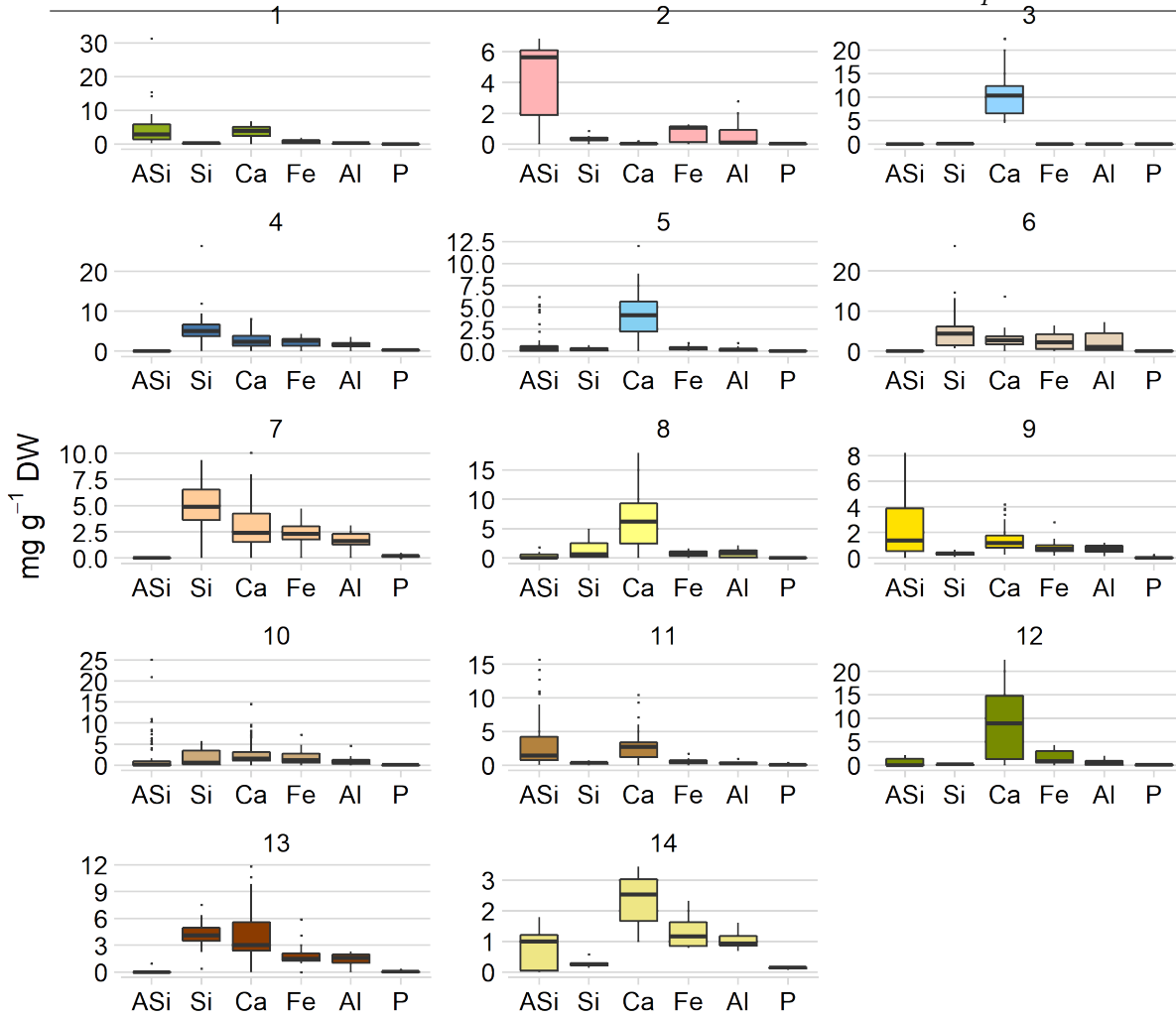


Fig S5: Element concentration in single lithological classes. 1: Basalt, olivine basalt, tholeiite, alkali basalt, basanite, pillow basalt, flood basalt (n=26); 2: Gneiss, migmatite; reworked amphibolite and granulite facies rocks (n=11); 3: Limestone, dolostone, shale, evaporites, chalk; carbonate reefs or metamorphosed equivalent (n=24); 4: Limestone, dolostone, shale, evaporites, chalk; carbonate reefs; metamorphic grade not identified (n=58); 5: Limestone, dolostone, shale, evaporites, chalk; carbonate reefs (n=64); 6: Quartz sandstone, siltstone, claystone, limestone, dolostone, conglomerate, tillite (n=13); 7: Sandstone, siltstone, shale, coal; plant fossils; metamorphic grade not identified (n=68); 8: Sandstone, siltstone, shale, limestone (n=38); 9: Sandstone, siltstone, shale, limestone; metamorphic grade not identified (n=39); 10: Sandstone, siltstone, shale; marine fossils (n=91); 11: Sandstone, siltstone, shale; marine fossils; metamorphic grade not identified (n=60); 12: Sedimentary and/or volcanic rock: undivided (n=21); 13: Shale, chert, iron-formation, greywacke, turbidite, argillaceous limestone, matrix-supported conglomerate (n=43); 14: Shale, chert, iron-formation, greywacke, turbidite, argillaceous limestone, matrix-supported conglomerate or metamorphosed equivalent (n=8).

Table S5: Number of polygons (n) per lithological class per geographic domain.

	Lith.ID	Lithological class	Geographic domain	n
1	1	Basalt, olivine basalt, tholeiite, alkali basalt, basanite, pillow basalt, flood basalt	Arctic-North Atlantic region	311
2	1	Basalt, olivine basalt, tholeiite, alkali basalt, basanite, pillow basalt, flood basalt	Brooks Range, Chukotka, Arctic Shelf	12
3	1	Basalt, olivine basalt, tholeiite, alkali basalt, basanite, pillow basalt, flood basalt	Canada Shield, Greenland Shield, and cover	45
4	1	Basalt, olivine basalt, tholeiite, alkali basalt, basanite, pillow basalt, flood basalt	Eastern Alaska, Yukon, Mackenzie region	27
5	1	Basalt, olivine basalt, tholeiite, alkali basalt, basanite, pillow basalt, flood basalt	Interior western Alaska	41
6	1	Basalt, olivine basalt, tholeiite, alkali basalt, basanite, pillow basalt, flood basalt	Okhotsk, Bering Sea, Pacific Alaska	19
7	2	Gneiss, migmatite; reworked amphibolite and granulite facies rocks	Greenland	604
8	3	Limestone, dolostone, shale, evaporites, chalk; carbonate reefs or metamorphosed equivalent	Arctic-North Atlantic region	77
9	3	Limestone, dolostone, shale, evaporites, chalk; carbonate reefs or metamorphosed equivalent	Brooks Range, Chukotka, Arctic Shelf	97
10	3	Limestone, dolostone, shale, evaporites, chalk; carbonate reefs or metamorphosed equivalent	Canada Shield, Greenland Shield, and cover	11
11	3	Limestone, dolostone, shale, evaporites, chalk; carbonate reefs or metamorphosed equivalent	East European Platform, Ural Mountains	4
12	3	Limestone, dolostone, shale, evaporites, chalk; carbonate reefs or metamorphosed equivalent	Eastern Alaska, Yukon, Mackenzie region	52
13	3	Limestone, dolostone, shale, evaporites, chalk; carbonate reefs or metamorphosed equivalent	Innuitian region, North Greenland	228
14	3	Limestone, dolostone, shale, evaporites, chalk; carbonate reefs or metamorphosed equivalent	Interior western Alaska	48
15	3	Limestone, dolostone, shale, evaporites, chalk; carbonate reefs or metamorphosed equivalent	Okhotsk, Bering Sea, Pacific Alaska	44
16	4	Limestone, dolostone, shale, evaporites, chalk; carbonate reefs; metamorphic grade not identified	Arctic-North Atlantic region	21
17	4	Limestone, dolostone, shale, evaporites, chalk; carbonate reefs; metamorphic grade not identified	Brooks Range, Chukotka, Arctic Shelf	75
18	4	Limestone, dolostone, shale, evaporites, chalk; carbonate reefs; metamorphic grade not identified	Canada Shield, Greenland Shield, and cover	38
19	4	Limestone, dolostone, shale, evaporites, chalk; carbonate reefs; metamorphic grade not identified	East European Platform, Ural Mountains	195
20	4	Limestone, dolostone, shale, evaporites, chalk; carbonate reefs; metamorphic grade not identified	Eastern Alaska, Yukon, Mackenzie region	163
21	4	Limestone, dolostone, shale, evaporites, chalk; carbonate reefs; metamorphic grade not identified	Innuitian region, North Greenland	41
22	4	Limestone, dolostone, shale, evaporites, chalk; carbonate reefs; metamorphic grade not identified	Interior western Alaska	4
23	4	Limestone, dolostone, shale, evaporites, chalk; carbonate reefs; metamorphic grade not identified	Okhotsk, Bering Sea, Pacific Alaska	1
24	4	Limestone, dolostone, shale, evaporites, chalk; carbonate reefs; metamorphic grade not identified	Verkhoyansk-Kolyma region	20

	Lith.ID	Lithological class	Geographic domain	n
25	4	Limestone, dolostone, shale, evaporites, chalk; carbonate reefs; metamorphic grade not identified	West Siberian Basin, Siberian Platform	283
26	5	Limestone, dolostone, shale, evaporites, chalk; carbonate reefs	Arctic-North Atlantic region	41
27	5	Limestone, dolostone, shale, evaporites, chalk; carbonate reefs	Arctic Ocean	2
28	5	Limestone, dolostone, shale, evaporites, chalk; carbonate reefs	Brooks Range, Chukotka, Arctic Shelf	45
29	5	Limestone, dolostone, shale, evaporites, chalk; carbonate reefs	Canada Shield, Greenland Shield, and cover	470
30	5	Limestone, dolostone, shale, evaporites, chalk; carbonate reefs	East European Platform, Ural Mountains	1
31	5	Limestone, dolostone, shale, evaporites, chalk; carbonate reefs	Eastern Alaska, Yukon, Mackenzie region	44
32	5	Limestone, dolostone, shale, evaporites, chalk; carbonate reefs	Inuitian region, North Greenland	568
33	5	Limestone, dolostone, shale, evaporites, chalk; carbonate reefs	Okhotsk, Bering Sea, Pacific Alaska	3
34	6	Quartz sandstone, siltstone, claystone, limestone, dolostone, conglomerate, tillite	Northern Europe	92
35	7	Sandstone, siltstone, shale, coal; plant fossils; metamorphic grade not identified	Arctic-North Atlantic region	27
36	7	Sandstone, siltstone, shale, coal; plant fossils; metamorphic grade not identified	Arctic Ocean	39
37	7	Sandstone, siltstone, shale, coal; plant fossils; metamorphic grade not identified	Brooks Range, Chukotka, Arctic Shelf	90
38	7	Sandstone, siltstone, shale, coal; plant fossils; metamorphic grade not identified	Canada Shield, Greenland Shield, and cover	54
39	7	Sandstone, siltstone, shale, coal; plant fossils; metamorphic grade not identified	East European Platform, Ural Mountains	32
40	7	Sandstone, siltstone, shale, coal; plant fossils; metamorphic grade not identified	Eastern Alaska, Yukon, Mackenzie region	3
41	7	Sandstone, siltstone, shale, coal; plant fossils; metamorphic grade not identified	Okhotsk, Bering Sea, Pacific Alaska	65
42	7	Sandstone, siltstone, shale, coal; plant fossils; metamorphic grade not identified	Verkhoyansk-Kolyma region	200
43	7	Sandstone, siltstone, shale, coal; plant fossils; metamorphic grade not identified	West Siberian Basin, Siberian Platform	217
44	8	Sandstone, siltstone, shale, limestone	Arctic-North Atlantic region	64
45	8	Sandstone, siltstone, shale, limestone	Brooks Range, Chukotka, Arctic Shelf	59
46	8	Sandstone, siltstone, shale, limestone	Canada Shield, Greenland Shield, and cover	12

47	8	Sandstone, siltstone, shale, limestone	Eastern Alaska, Yukon, Mackenzie region	114
----	---	--	---	-----

	Lith.ID	Lithological class	Geographic domain	n
48	8	Sandstone, siltstone, shale, limestone	Innuitian region, North Greenland	14
49	8	Sandstone, siltstone, shale, limestone	Interior western Alaska	10
50	8	Sandstone, siltstone, shale, limestone	Okhotsk, Bering Sea, Pacific Alaska	35
51	9	Sandstone, siltstone, shale, limestone; metamorphic grade not identified	Arctic-North Atlantic region	1
52	9	Sandstone, siltstone, shale, limestone; metamorphic grade not identified	Arctic Ocean	2
53	9	Sandstone, siltstone, shale, limestone; metamorphic grade not identified	Brooks Range, Chukotka, Arctic Shelf	85
54	9	Sandstone, siltstone, shale, limestone; metamorphic grade not identified	East European Platform, Ural Mountains	25
55	9	Sandstone, siltstone, shale, limestone; metamorphic grade not identified	Eastern Alaska, Yukon, Mackenzie region	45
56	9	Sandstone, siltstone, shale, limestone; metamorphic grade not identified	Interior western Alaska	5
57	9	Sandstone, siltstone, shale, limestone; metamorphic grade not identified	Okhotsk, Bering Sea, Pacific Alaska	150
58	9	Sandstone, siltstone, shale, limestone; metamorphic grade not identified	Verkhoyansk-Kolyma region	33
59	9	Sandstone, siltstone, shale, limestone; metamorphic grade not identified	West Siberian Basin, Siberian Platform	179
60	10	Sandstone, siltstone, shale; marine fossils	Arctic-North Atlantic region	108
61	10	Sandstone, siltstone, shale; marine fossils	Arctic Ocean	28
62	10	Sandstone, siltstone, shale; marine fossils	Brooks Range, Chukotka, Arctic Shelf	92
63	10	Sandstone, siltstone, shale; marine fossils	Canada Shield, Greenland Shield, and cover	15
64	10	Sandstone, siltstone, shale; marine fossils	East European Platform, Ural Mountains	21
65	10	Sandstone, siltstone, shale; marine fossils	Eastern Alaska, Yukon, Mackenzie region	69
66	10	Sandstone, siltstone, shale; marine fossils	Innuitian region, North Greenland	300
67	10	Sandstone, siltstone, shale; marine fossils	Interior western Alaska	63
68	10	Sandstone, siltstone, shale; marine fossils	Okhotsk, Bering Sea, Pacific Alaska	11
69	11	Sandstone, siltstone, shale; marine fossils; metamorphic grade not identified	Arctic-North Atlantic region	6
70	11	Sandstone, siltstone, shale; marine fossils; metamorphic grade not identified	Arctic Ocean	4
71	11	Sandstone, siltstone, shale; marine fossils; metamorphic grade not identified	Brooks Range, Chukotka, Arctic Shelf	88
72	11	Sandstone, siltstone, shale; marine fossils; metamorphic grade not identified	Canada Shield, Greenland Shield, and cover	19

	Lith.ID	Lithological class	Geographic domain	n
73	11	Sandstone, siltstone, shale; marine fossils; metamorphic grade not identified	East European Platform, Ural Mountains	199
74	11	Sandstone, siltstone, shale; marine fossils; metamorphic grade not identified	Eastern Alaska, Yukon, Mackenzie region	35
75	11	Sandstone, siltstone, shale; marine fossils; metamorphic grade not identified	Okhotsk, Bering Sea, Pacific Alaska	43
76	11	Sandstone, siltstone, shale; marine fossils; metamorphic grade not identified	Verkhoyansk-Kolyma region	724
77	11	Sandstone, siltstone, shale; marine fossils; metamorphic grade not identified	West Siberian Basin, Siberian Platform	244
78	12	Sedimentary and/or volcanic rock: undivided	Arctic-North Atlantic region	10
79	12	Sedimentary and/or volcanic rock: undivided	Arctic Ocean	5
80	12	Sedimentary and/or volcanic rock: undivided	Brooks Range, Chukotka, Arctic Shelf	67
81	12	Sedimentary and/or volcanic rock: undivided	Eastern Alaska, Yukon, Mackenzie region	110
82	12	Sedimentary and/or volcanic rock: undivided	Inuitian region, North Greenland	43
83	12	Sedimentary and/or volcanic rock: undivided	Interior western Alaska	53
84	12	Sedimentary and/or volcanic rock: undivided	Okhotsk, Bering Sea, Pacific Alaska	50
85	13	Shale, chert, iron-formation, greywacke, turbidite, argillaceous limestone, matrix-supported conglomerate	Arctic-North Atlantic region	47
86	13	Shale, chert, iron-formation, greywacke, turbidite, argillaceous limestone, matrix-supported conglomerate	Arctic Ocean	10
87	13	Shale, chert, iron-formation, greywacke, turbidite, argillaceous limestone, matrix-supported conglomerate	Brooks Range, Chukotka, Arctic Shelf	72
88	13	Shale, chert, iron-formation, greywacke, turbidite, argillaceous limestone, matrix-supported conglomerate	Canada Shield, Greenland Shield, and cover	5
89	13	Shale, chert, iron-formation, greywacke, turbidite, argillaceous limestone, matrix-supported conglomerate	East European Platform, Ural Mountains	3
90	13	Shale, chert, iron-formation, greywacke, turbidite, argillaceous limestone, matrix-supported conglomerate	Eastern Alaska, Yukon, Mackenzie region	58
91	13	Shale, chert, iron-formation, greywacke, turbidite, argillaceous limestone, matrix-supported conglomerate	Inuitian region, North Greenland	201
92	13	Shale, chert, iron-formation, greywacke, turbidite, argillaceous limestone, matrix-supported conglomerate	Interior western Alaska	29

	Lith.ID	Lithological class	Geographic domain	n
93	13	Shale, chert, iron-formation, greywacke, turbidite, argillaceous limestone, matrix-supported conglomerate	Okhotsk, Bering Sea, Pacific Alaska	90
94	14	Shale, chert, iron-formation, greywacke, turbidite, argillaceous limestone, matrix-supported conglomerate or metamorphosed equivalent	Arctic-North Atlantic region	2
95	14	Shale, chert, iron-formation, greywacke, turbidite, argillaceous limestone, matrix-supported conglomerate or metamorphosed equivalent	Brooks Range, Chukotka, Arctic Shelf	53
96	14	Shale, chert, iron-formation, greywacke, turbidite, argillaceous limestone, matrix-supported conglomerate or metamorphosed equivalent	Eastern Alaska, Yukon, Mackenzie region	143
97	14	Shale, chert, iron-formation, greywacke, turbidite, argillaceous limestone, matrix-supported conglomerate or metamorphosed equivalent	Inuitian region, North Greenland	107
98	14	Shale, chert, iron-formation, greywacke, turbidite, argillaceous limestone, matrix-supported conglomerate or metamorphosed equivalent	Interior western Alaska	71
99	14	Shale, chert, iron-formation, greywacke, turbidite, argillaceous limestone, matrix-supported conglomerate or metamorphosed equivalent	Okhotsk, Bering Sea, Pacific Alaska	41

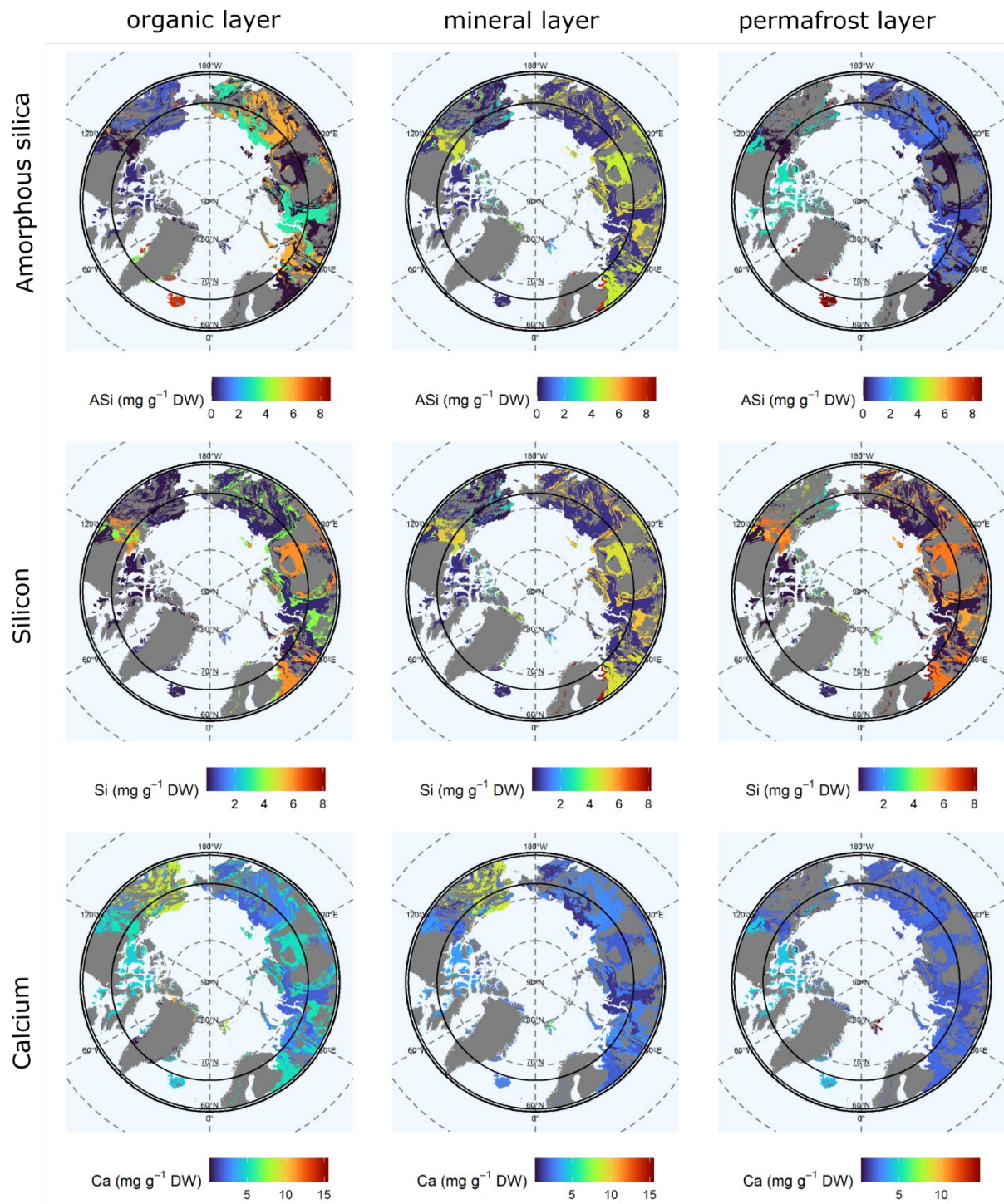


Fig. S6: Element concentrations of ASi, Si and Ca in organic, mineral (organic layer and mineral layer are part of the active layer) and Permafrost layer (left to right). Blue color represents low element concentrations, red color represent high element concentrations.

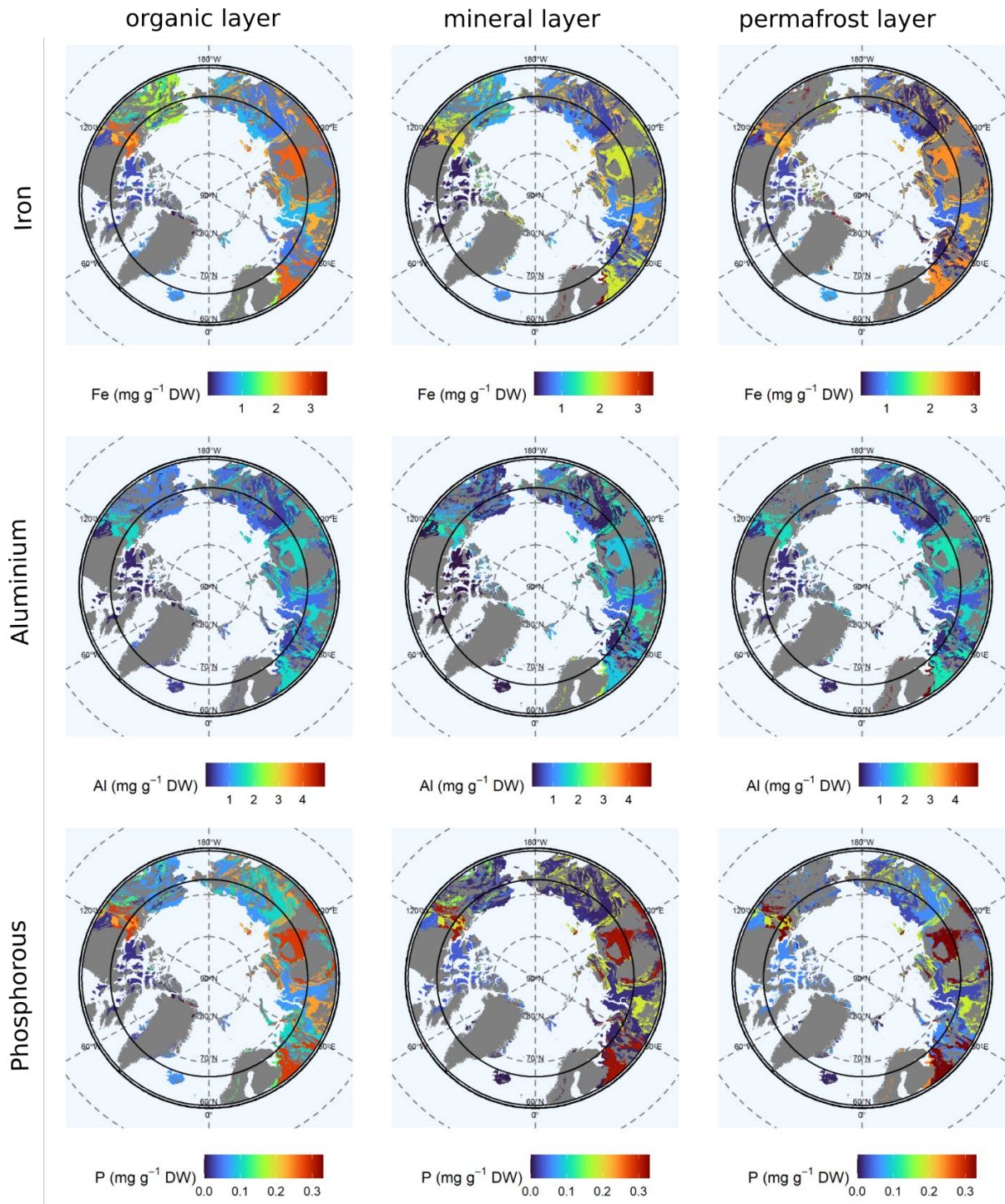


Fig. S7: Element concentrations of Fe, Al and P in organic, mineral and Permafrost layer (left to right). Blue color represents low element concentrations, red color represent high element concentrations.

3.2.2 Study 2: The importance of calcium and amorphous silica for Arctic soil CO₂ production.

Stimmler, Goeckede, Natali, et al. (2022)

Published 01.11.2022 in:

Front. Environ. Sci. 10:1019610.

(doi: 10.3389/fenvs.2022.1019610)



OPEN ACCESS

EDITED BY

Wei He,
China University of Geosciences, China

REVIEWED BY

Petr Semenov,
All Russian Research Institute of
Geology and Mineral Resources of the
World Ocean, Russia
Yinghui Wang,
Southern University of Science and
Technology, China

*CORRESPONDENCE

Jörg Schaller,
Joerg.Schaller@zalf.de

SPECIALTY SECTION

This article was submitted to
Biogeochemical Dynamics,
a section of the journal
Frontiers in Environmental Science

RECEIVED 15 August 2022

ACCEPTED 06 September 2022

PUBLISHED 01 November 2022

CITATION

Stimmler P, Göckede M, Natali SM,
Sonnentag O, Gilfedder BS, Perron N
and Schaller J (2022), The importance of
calcium and amorphous silica for arctic
soil CO₂ production.
Front. Environ. Sci. 10:1019610.
doi: 10.3389/fenvs.2022.1019610

COPYRIGHT

© 2022 Stimmler, Göckede, Natali,
Sonnentag, Gilfedder, Perron and
Schaller. This is an open-access article
distributed under the terms of the
[Creative Commons Attribution License
\(CC BY\)](https://creativecommons.org/licenses/by/4.0/). The use, distribution or
reproduction in other forums is
permitted, provided the original
author(s) and the copyright owner(s) are
credited and that the original
publication in this journal is cited, in
accordance with accepted academic
practice. No use, distribution or
reproduction is permitted which does
not comply with these terms.

The importance of calcium and amorphous silica for arctic soil CO₂ production

Peter Stimmler¹, Mathias Göckede², Susan M. Natali³,
Oliver Sonnentag⁴, Benjamin S. Gilfedder⁵, Nia Perron⁴ and
Jörg Schaller^{1*}

¹Centre for Agriculture Landscape Research e.V. (ZALF), Müncheberg, Germany, ²Max Planck Institute for Biogeochemistry, Jena, Germany, ³Woodwell Climate Research Center, Falmouth, MA, United States, ⁴Département de Géographie, Université de Montréal, Montréal, QC, Canada, ⁵Limnological Station, Bayreuth Center of Ecology and Environmental Research (BAYCEER), University of Bayreuth, Bayreuth, Germany

Future warming of the Arctic not only threatens to destabilize the enormous pool of organic carbon accumulated in permafrost soils but may also mobilize elements such as calcium (Ca) or silicon (Si). While for Greenlandic soils, it was recently shown that both elements may have a strong effect on carbon dioxide (CO₂) production with Ca strongly decreasing and Si increasing CO₂ production, little is known about the effects of Si and Ca on carbon cycle processes in soils from Siberia, the Canadian Shield, or Alaska. In this study, we incubated five different soils (rich organic soil from the Canadian Shield and from Siberia (one from the top and one from the deeper soil layer) and one acidic and one non-acidic soil from Alaska) for 6 months under both drained and waterlogged conditions and at different Ca and amorphous Si (ASi) concentrations. Our results show a strong decrease in soil CO₂ production for all soils under both drained and waterlogged conditions with increasing Ca concentrations. The ASi effect was not clear across the different soils used, with soil CO₂ production increasing, decreasing, or not being significantly affected depending on the soil type and if the soils were initially drained or waterlogged. We found no methane production in any of the soils regardless of treatment. Taking into account the predicted change in Si and Ca availability under a future warmer Arctic climate, the associated fertilization effects would imply potentially lower greenhouse gas production from Siberia and slightly increased greenhouse gas emissions from the Canadian Shield. Including Ca as a controlling factor for Arctic soil CO₂ production rates may, therefore, reduce uncertainties in modeling future scenarios on how Arctic regions may respond to climate change.

KEYWORDS

Arctic soil, climate change, GHG production, greenhouse gas emissions, silicon, soil respiration

1 Introduction

Near-surface air temperatures in northern high-latitude regions have been increasing twice as much as the global average within the last few decades and are also projected to increase further in the future (Allan, 2021). This temperature increase leads to thawing of the permafrost, i.e., perennially frozen ground (Brown and Romanovsky 2008; Romanovsky et al., 2010). Permafrost thaw may increase the release of greenhouse gases such as carbon dioxide (CO₂) and methane by accelerated soil organic-carbon mineralization (Schoor et al., 2015; Miner et al., 2022). The frozen ground of Arctic–boreal regions is the largest pool of soil organic-carbon, with ca. 1014 to 1035 Pg of organic carbon being stored within the upper 3 m in permafrost-affected regions (Hugelius et al., 2014; Mishra et al., 2021).

Thawing of permafrost may mobilize large amounts of nutrients stored in permafrost soils. In addition to primary nutrients such as nitrogen (N) or phosphorous (P), the thawing of permafrost may also mobilize elements such as calcium (Ca) and amorphous silicon (ASi) (Walker et al., 2001; Alfredsson et al., 2015; Stimmler et al., 2022a). Ca is known to potentially decrease soil respiration by cation bridging making the organic carbon in the soil (C_{org}) less available for microbial respiration (Whittinghill and Hobbie 2012; Rowley et al., 2018; Schaller et al., 2019). Reactive Si is stored in soils in the form of amorphous silica (Asi) as phytoliths from plant or microbial residuals (Schaller et al., 2021). Asi in soils can reduce hydraulic conductivity near saturation, increase hydraulic conductivity in dry soils, and is the main source of silicic acid (Schaller et al., 2020; Schaller et al., 2021). With this reduction in hydraulic conductivity near saturation, Asi may reduce the availability of electron acceptors leading to potentially more reduced conditions (Hömborg et al., 2021a; Hömborg et al., 2021b). Silicic acid competes with nutrients such as P and C_{org} for binding at the surface of iron minerals (Schaller et al., 2019; Hömborg et al., 2020). Through the effect of Asi mobilizing silicic acid, Asi can potentially increase P and C_{org} availability for microbial respiration (Reithmaier et al., 2017; Schaller et al., 2019).

The increasing and strongly decreasing effects of Si and Ca on the microbial respiration of Arctic soils, respectively, were shown only in one study so far on different Greenlandic soils (Schaller et al., 2019) and were further discussed by Stimmler et al. (2022b). However, Greenlandic soils feature a relatively low C_{org} pool, compared to soils from other Arctic regions, and therefore the potential increases in soil respiration under predicted future climates might be substantially less in Greenland than in Siberia, the Canadian Shield, or Alaska (Hugelius et al., 2014). Accordingly, the effects of Si and Ca on soil respiration of these vast Arctic regions with large C_{org} pools are poorly understood. Hence, knowledge about this

interdependency between Asi, Ca, and soil respiration may be crucial to reduce uncertainties for reliable modeling of future scenarios of how Arctic systems may respond to global warming. Additional important controls on the production of potent greenhouse gases such as CO₂ and CH₄ is the initial oxygen supply and associated drained or waterlogged conditions (Stein 2020). It was shown at the field scale that drainage increased soil-CO₂ emissions compared to waterlogged conditions (Kwon et al., 2019), and in an incubation study, it was shown that the large soil carbon storage in deep soil layers (Hugelius et al., 2014) was generally less vulnerable to soil respiration (Kwon et al., 2019).

Here, we assessed the relevance of both ASi and Ca for CO₂ and CH₄ production in soils collected from Siberia, the Canadian Shield, and Alaska. Five different soils from those regions were incubated under both drained and waterlogged conditions for 6 months under different Ca and ASi concentrations. For Alaska, we used soils from moist acidic and moist non-acidic tundras, as both soils differ substantially in available Ca in the active layer and permafrost layer (Walker et al., 2001). Especially for the moist acidic tundra, available Ca may increase with permafrost thaw as the permafrost layer contains much higher Ca concentrations compared to the active layer soil (Walker et al., 2001). For the Canadian Shield, we used organic-rich soil. For the soil from Siberia, we incubated two different soil depths to analyze the effect of soil depth on soil respiration.

2 Materials and methods

2.1 Sample collection and storage

The soil samples were collected using a spade or an auger from various sites (Table 1). All soils were stored at –20°C.

To prepare the soil for these incubation treatments, the frozen soil was crushed with a hammer and sieved to a particle size <650 µm. Subsequently, the sieved soil was homogenized, and for each sample, 5 g of soil was weighed into a 20 ml incubation vial (Ochs Laborbedarf, Bovenden, Germany).

2.2 Element extraction

For extraction of available concentrations of inorganic Si and Ca, the Mehlich III method was used (Mehlich 1984). In brief, 0.5–5 g of the original or freeze-dried soil sample was weighed in a 50 ml Falcon tube and mixed with 10 ml g⁻¹ Mehlich III (0.015 M NH₄F, 0.001 M EDTA, 0.25 M NH₄NO₃, 0.00325 M HNO₃, and 0.2 M HAc) extraction solution. The samples were shaken for 5 min at 200 min⁻¹ and centrifuged for 5 min at 10,000 g. The supernatant was collected with a

TABLE 1 Coordinates, soil sampling depth, ash content, and pH of the different soils used.

Region	Soil	Coordinates (latitude; longitude)	Depth	Ash content in %	pH
Siberia, Russia, Chersky	C1	68,61586°N; -161,35228°E	20–25 cm	94.3	6.5
Siberia, Russia, Chersky	C2	68,61685°N; -161,3504°E	50–60 cm	74.9	5.8
Alaska moist acidic tundra, Alaska, U.S.	MAT	69,42554°N; -148,69633°E	20–40 cm	75.0	6.6
Alaska moist non-acidic tundra, Alaska, U.S.	MNT	69,43303°N; -148,67435°E	0–25 cm	91.6	8.2
Canadian Shield, Canada	Ca1	69,22325°N; -104,90041°E	0–25 cm	13.3	6.7

syringe and filtered through a 0.2 µm cellulose acetate filter. The quantification of element concentrations was done by ICP-OES with all results given in mg g⁻¹ dry weight (DW).

For extraction of available biogenic ASi, alkaline extraction was used (DeMaster 1981). 30 mg of freeze-dried soil was weighted in falcon tubes and incubated for 1 h with 40 ml 0.1 M Na₂CO₃ solution at 85°C. After 1 h, 3 h, and 5 h, 10 ml of the supernatant was sampled and filtered through a 0.2 µm cellulose acetate filter. The silicon concentration in solution was quantified by ICP-OES. The ASi concentrations were calculated as the ordinate intercept of the linear function of silicon concentration over incubation time and are given in mg g⁻¹ dw⁻¹.

For total P analysis, 100 mg of the freeze-dried soil material was extracted using HNO₃/H₂O₂ followed by HNO₃/HCl 3:1 in a closed vessel microwave system. The extract was cleared with a 0.2 µm cellulose acetate filter and quantified with ICP-OES. For dry weight (DW) determination as the basis for element availability and concentrations on DW, 0.5–2 g of frozen material was weighed prior and after freeze-drying until a constant weight. All ICP-OES measurements were carried out using the iCAP 6000 Series (Thermo scientific) in the axial mode.

2.3 Incubation experiment

All soils were incubated with 16 treatments for different Si and Ca concentrations, supplemented by a control sample without modification of the ASi or Ca levels (control treatment). The treatments included all combinations of four different levels of ASi addition (0, 3, 6, or 10 mg g⁻¹ dw⁻¹, Aerosil 300[®], Evonik, Essen, Germany) and four different levels of Ca addition (0, 5, 10, and 15 mg g⁻¹ (DW)⁻¹ Ca (CaCl₂ × 2 H₂O, Grüssing, Filsum, Germany). Such an increase in ASi and Ca availability in the soil was shown to be within the expected natural range upon permafrost thaw (Stimmler et al. in revision). Each treatment was applied using 2 ml pure water. To examine the effect of this water addition on C cycle processes, the soils were incubated with and without pure water as reference. As

additional treatment, all the Si and Ca treatments and controls were incubated under both drained and waterlogged conditions (170 incubations in total for each soil type). After ASi and/or Ca addition and also for control the soil was saturated with a few millimeters of the water supernatant (waterlogged treatment). For the drained treatment the supernatant water was removed. All treatments were done with a replication of five.

To enable gas exchange but prevent water loss, vials were closed with Parafilm and stored at 5°C in an incubation fridge. The supernatant of the drained treatment was removed (the drained water) after 2 weeks to facilitate a more efficient oxygen entry.

2.4 Greenhouse gas analysis

After 4, 8, 12, and 24 weeks of the incubation experiment, the samples were closed with a rubber stopper and crimp caps 4 days before sampling of the gas phase. Next, the gas phase of each sample was collected from the head space using a syringe, and analyzed with GC-FID (8610C Gas Chromatograph, SRI Instruments, Bad Honnef, Germany) for the greenhouse gases such as CO₂ and CH₄. Calibration was done with 1,000 and 10,000 ppm of CH₄ and 5,000 and 50,000 ppm of CO₂ (Riessner Gase, Lichtenfels, Germany). The greenhouse gas production rates were calculated as follows:

$$c(Gas) \left[\frac{\mu\text{mol}}{\text{kg} \cdot \text{d}} \right] = \frac{\beta(Gas) [ppm] \cdot 101325 \left[\frac{\text{kg}}{\text{m}^3 \cdot \text{s}^2} \right] \cdot 0,000013 [\text{m}^3] \cdot 1000 \left[\frac{\text{g}}{\text{kg}} \right]}{8,1344 \cdot \left[\frac{\text{kg} \cdot \text{m}^2}{\text{s}^2 \cdot \text{mol} \cdot \text{K}} \right] \cdot 293 [\text{K}] \cdot 4 [\text{d}] \cdot m(\text{Soil}) [\text{g}]} \quad (1)$$

2.5 Statistical analysis and data visualization

For statistical analysis and visualization, the R computational environment was used (R_Core_Team, 2021). The data over all Ca and silica treatments were analyzed by a two-way analysis-of-variance (two-way ANOVA), using Si and Ca treatments as factors. Figures were plotted using the “geom_tile” function from the “ggplot2” package.

Chapter 3. Manuscripts

TABLE 2 Element concentrations of the five incubated soils. Ca and available P ($P_{\text{available}}$) were extracted with the Mehlich III method, ASi with the alkaline extraction, and total P (P_{total}) with the *aqua regia* extraction.

Location	Ca (mg g^{-1} DW)	ASi (mg g^{-1} DW)	$P_{\text{available}}$ (mg g^{-1} DW)	P_{total} (mg g^{-1} DW)
Chersky C1	0.25	4.00	0.01	1.30
Chersky C2	1.13	2.01	0.04	1.16
Canada Ca1	0.32	<0.01	<0.01	1.33
Alaska MNT	6.46	0.56	<0.01	1.12
Alaska MAT	2.35	0.45	<0.01	1.06

TABLE 3 CO_2 production for the different soils and Ca treatments compared to the control treatment in % difference from the treatment means.

	Drained	Waterlogged	
	Mean \pm SD	Mean \pm SD	Mean \pm SD
Chersky C1			
Ca+5	30 \pm 7	Ca+5	34 \pm 11
Ca+10	25 \pm 5	Ca+10	29 \pm 14
Ca+15	21 \pm 2	Ca+15	24 \pm 12
Chersky C2			
Ca+5	49 \pm 7	Ca+5	39 \pm 14
Ca+10	41 \pm 18	Ca+10	36 \pm 11
Ca+15	41 \pm 10	Ca+15	28 \pm 10
Canada			
Ca+5	34 \pm 11	Ca+5	38 \pm 18
Ca+10	30 \pm 12	Ca+10	27 \pm 19
Ca+15	37 \pm 18	Ca+15	NA
MNT			
Ca+5	56 \pm 21	Ca+5	72 \pm 40
Ca+10	58 \pm 36	Ca+10	45 \pm 18
Ca+15	43 \pm 22	Ca+15	49 \pm 3
MAT			
Ca+5	24 \pm 12	Ca+5	41 \pm 19
Ca+10	17 \pm 6	Ca+10	35 \pm 9
Ca+15	13 \pm 7	Ca+15	27 \pm 20

3 Results

3.1 Element concentrations

Samples from the Siberian site near Chersky (Chersky C1 and C2) were low in Ca. Alaska MNT showed the highest Ca concentration, followed by Alaska MAT, while ASi was low in both Alaskan samples. Soils from the Canadian Shield showed low Ca concentrations and ASi was nearly zero. In all samples, the available P in the Mehlich III extract was very low, whereas the total P amount was almost equal across regions (Table 2).

3.2 Greenhouse gas production for different soils

We found considerable differences in CO_2 production for the soils from three different Arctic regions for all Si and Ca treatments under drained and waterlogged conditions. In contrast, we detected no CH_4 production under the experimental conditions. The most pronounced and clear effects were found for Ca (Table 3). In most cases, even the lowest Ca addition (+5 mg Ca) led to a pronounced reduction in soil- CO_2 production. The differences between the different Ca-addition treatments and the initially drained and waterlogged conditions were small (Table 3).

3.3 Soil from Siberia Chersky C1

The CO_2 production in the Siberia soil Chersky C1 was constant after 12 weeks (compared to the measurements before, data not shown) under drained and waterlogged conditions. CO_2 production rates decreased significantly following Ca addition ($p < 0.001$, $F = 134.986$, $df = 3$). For example, CO_2 emissions were reduced from $228 \pm 59 \mu\text{mol d}^{-1} \text{kg}^{-1} \text{DW}$ in the control soil to $44\text{--}90 \mu\text{mol d}^{-1} \text{kg}^{-1} \text{DW}$ with Ca addition of +5 to +15 $\text{mg g}^{-1} \text{DW}$ soil under the initial drained conditions (Figure 1A). Nearly the same decrease in CO_2 production rates following Ca addition ($p < 0.001$, $F = 54.151$, $df = 3$) was found for Chersky C1 under the initial waterlogged conditions (Figure 1B). Addition of Si in the form of ASi significantly increased CO_2 production under waterlogged conditions ($p = 0.001$, $F = 6.051$, and $df = 3$), but no significant effects were observed under drained conditions ($p = 0.592$, $F = 0.641$, and $df = 3$) (Figures 1A,B). The interaction between Si and Ca addition was significant under waterlogged conditions ($p = 0.001$, $F = 3.601$, and $df = 9$) but not under drained conditions ($p = 0.476$, $F = 0.996$, and $df = 9$). Our reference treatment (no water addition) showed a CO_2 production rate of $178 \pm 59 \mu\text{mol d}^{-1} \text{kg}^{-1} \text{DW}$ after 12 weeks. With this, the CO_2 production rate of the reference without water addition is

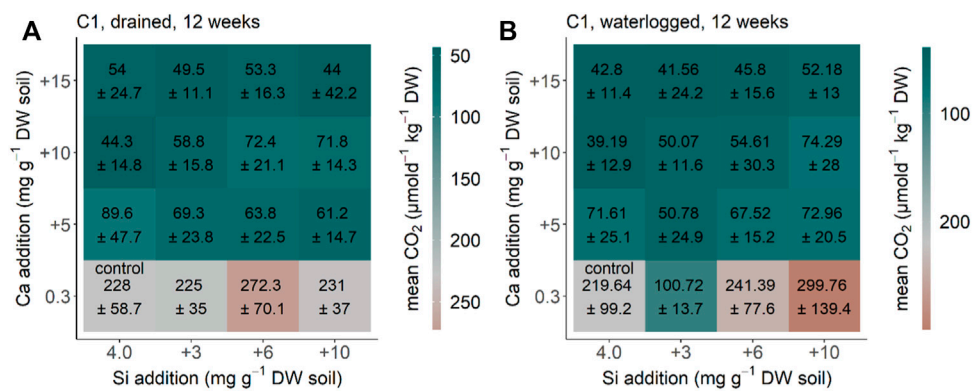


FIGURE 1

CO₂ production for the soil from Siberia Chersky C1, NE-Russia after 12 weeks (A) drained and (B) waterlogged incubation. Each square represents a treatment (n = 5) with Si (+0, +3, +6, and +10 mg g⁻¹ DW) and Ca (+0, +5, +10, and +15 mg g⁻¹ DW). Color represents the differences of the treatment of CO₂ production in comparison to the control treatment, with green–blue showing a decreased CO₂ production and red showing an increased CO₂ production in comparison to the control treatment.

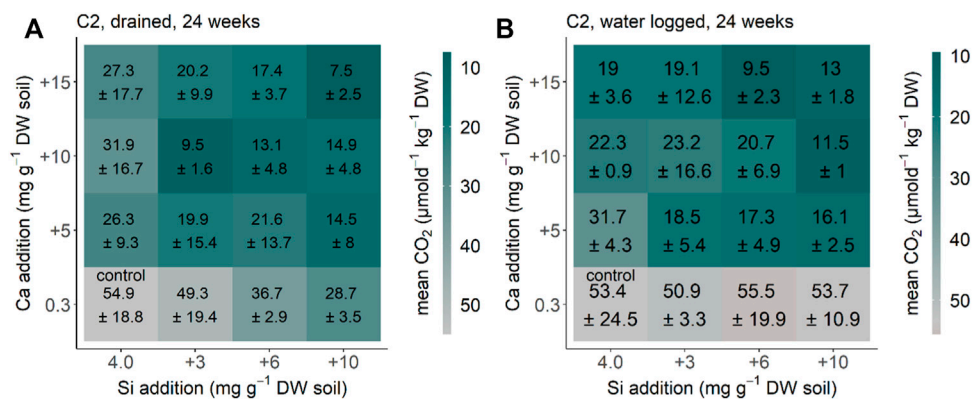


FIGURE 2

CO₂ production for the Siberia Chersky C2 from NE-Russia after 24 weeks (A) drained and (B) waterlogged incubation. Each square represents a treatment (n = 5) with Si (+0, +3, +6, and +10 mg g⁻¹ DW) and Ca (+0, +5, +10, and +15 mg g⁻¹ DW). Color represents the differences of the treatment CO₂ production in comparison to the control treatment, with green–blue showing a decreased CO₂ production and red showing an increased CO₂ production in comparison to the control treatment.

in the range between the control treatment of the drained and waterlogged treatments for the Siberia Chersky C1 soil.

3.4 Soil from Siberia Chersky C2

CO₂ production in the Siberia Chersky C2 soil equilibrated after 24 weeks (compared to the measurements before, data not shown) under drained and waterlogged conditions. The CO₂ production rate decreased significantly by Ca addition under the initial drained conditions ($p < 0.001$, $F = 21.049$, and $df = 3$) (Figure 2A). The same pattern with Ca addition decreasing the CO₂ production rate ($p < 0.001$, $F = 58.934$, and $df = 3$) was found

for Chersky C2 under initial waterlogged conditions (Figure 2B). Addition of ASi significantly decreased CO₂ production under drained conditions ($p < 0.001$, $F = 9.638$, and $df = 3$), but not significantly under waterlogged conditions ($p = 0.09$, $F = 2.221$, and $df = 3$) (Figures 2A,B). The interaction between Si and Ca addition was not significant under both drained conditions ($p = 0.371$, $F = 1.107$, and $df = 9$) and waterlogged conditions ($p = 0.49$, $F = 0.95$, and $df = 9$). Our reference treatment (no water addition) showed a CO₂ production rate of $7 \pm 3 \mu\text{mol d}^{-1}\text{kg}^{-1}$ DW after 24 weeks. With this, the CO₂ production rate of the reference without water addition is lower than the control treatment of the drained and waterlogged treatments for the Siberia Chersky C2 soil.

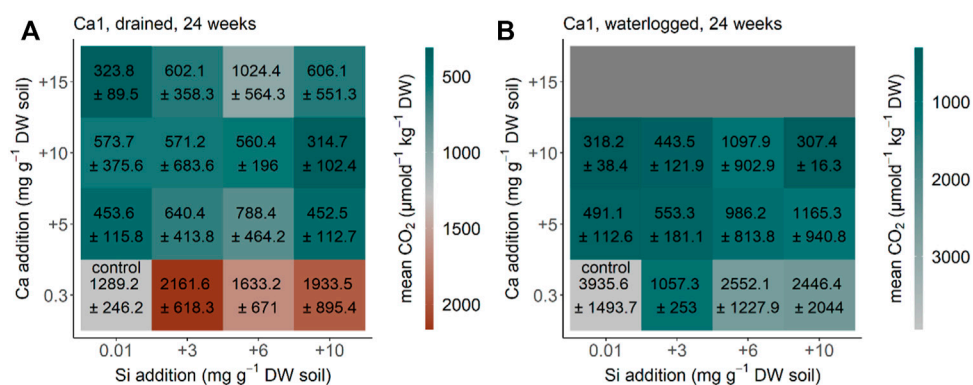


FIGURE 3

CO₂ production for the soil Ca1 from the Canadian Shield, Canada, Baffin Bay after 24 weeks (A) drained and (B) waterlogged incubation. Each square represents a treatment (n = 5) with Si (+0, +3, +6, and +10 mg g⁻¹ DW) and Ca (+0, +5, +10, and +15 mg g⁻¹ DW). Color represents mean and standard deviation of CO₂ production. A Ca+15 mg g⁻¹ DW was not possible for this soil under waterlogged conditions as we had too less soil material.

3.5 Soil from the Canadian Shield

For the soil from the Canadian Shield (Canada Ca1) the CO₂ production equilibrated after 24 weeks (compared to the measurements before, data not shown) under drained and waterlogged conditions. The CO₂ production rate decreased significantly after Ca addition under the initial drained conditions ($p < 0.001$, $F = 28.877$, and $df = 3$) (Figure 3A). The same pattern with Ca addition decreasing the CO₂ production rate ($p < 0.001$, $F = 24.637$, and $df = 3$) was found for the soil from Canada under the initial waterlogged conditions (Figure 3B). Addition of Si significantly increased CO₂ production under drained conditions in the treatments with no Ca addition, but changes were not significant considering all treatments ($p = 0.063$, $F = 2.569$, and $df = 3$), and were also not significant under waterlogged conditions ($p = 0.096$, $F = 2.245$, and $df = 3$) (Figures 3A,B). The interaction of Si and Ca addition was not significant under drained conditions ($p = 0.281$, $F = 1.254$, and $df = 9$) but under waterlogged conditions ($p = 0.019$, $F = 2.843$, and $df = 9$). Our reference treatment (no water addition) showed a CO₂ production rate of $2,210 \pm 1,440 \mu\text{mol d}^{-1} \text{kg}^{-1} \text{DW}$ after 24 weeks. With this, the CO₂ production rate of the reference without water addition is in the range between the control treatment of the drained and waterlogged treatments for the soils from the Canadian Shield.

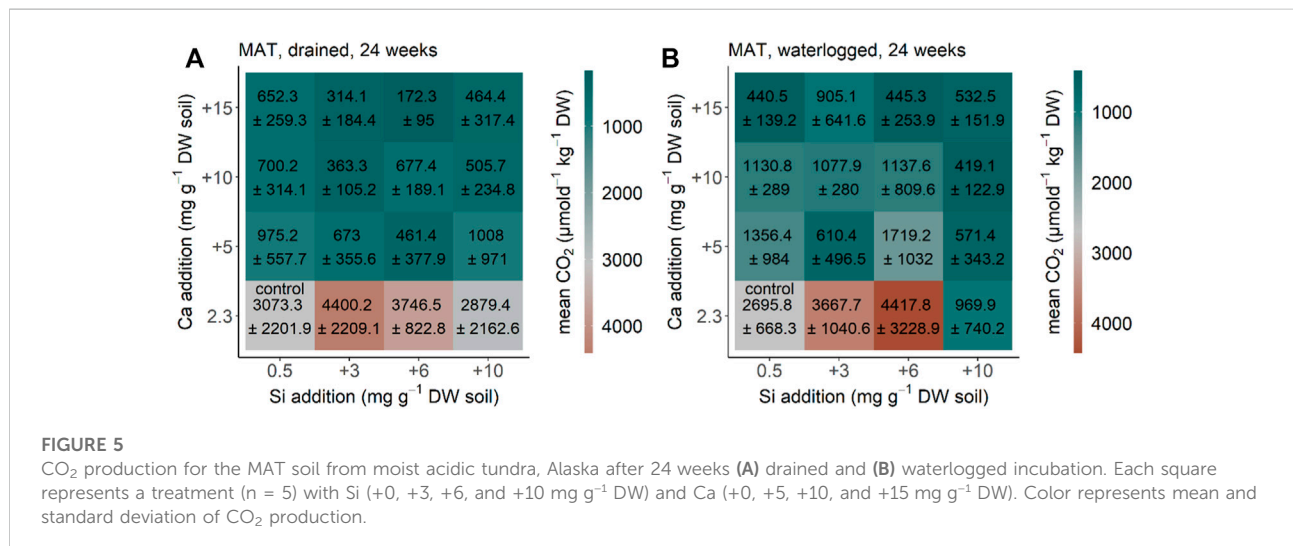
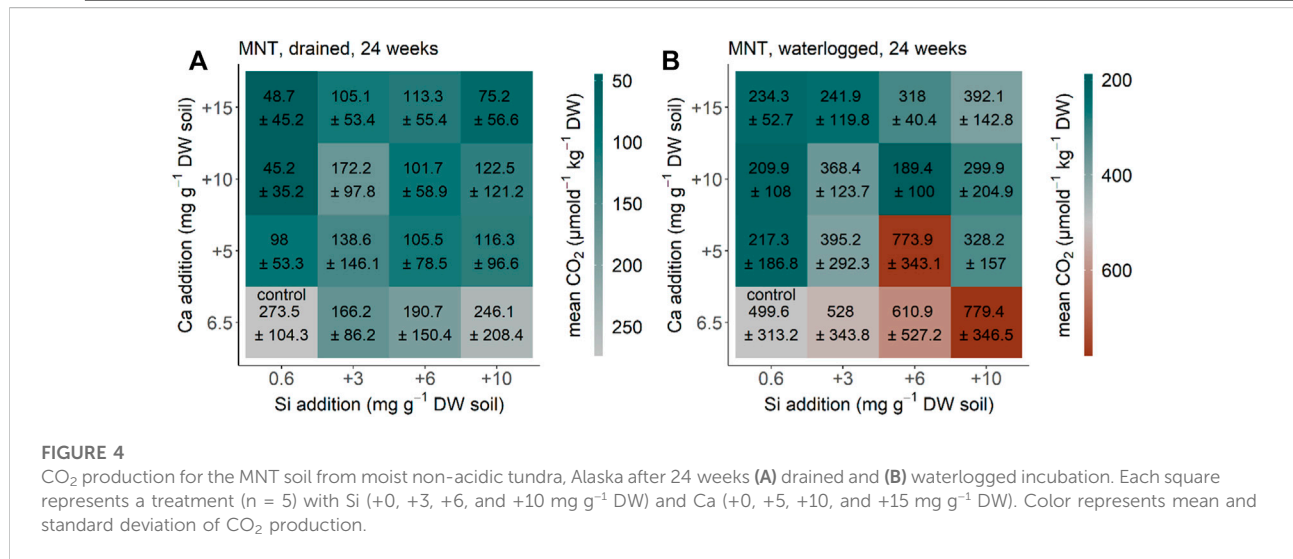
3.6 Soil from moist non-acidic tundra in Alaska (MNT)

CO₂ production in the MNT soil from Alaska equilibrated after 24 weeks (compared to the measurements before, data not

shown) under drained and waterlogged conditions. CO₂ production rate decreased significantly after Ca addition under the initial drained conditions ($p < 0.001$, $F = 6.905$, and $df = 3$) (Figure 4A). The same pattern with Ca addition decreasing the CO₂ production rate ($p < 0.001$, $F = 7.763$, $df = 3$) was found for MNT soil from Alaska under initial waterlogged conditions (Figure 4B). Addition of Si increased CO₂ production under drained conditions but not significantly ($p = 0.8338$, $F = 0.833$, and $df = 3$), and also not significantly under the initial waterlogged conditions ($p = 0.1$, $F = 2.186$, and $df = 3$) (Figures 4A, B). The interaction of Si and Ca addition was not significant under both drained conditions ($p = 0.485$, $F = 0.48$, and $df = 9$) and waterlogged conditions ($p = 0.116$, $F = 1.675$, and $df = 9$). Our reference treatment (no water addition) showed a CO₂ production rate of $331 \pm 38 \mu\text{mol d}^{-1} \text{kg}^{-1} \text{DW}$ after 24 weeks, which is in the range between the control treatment of the drained and waterlogged treatments for the soil from the moist non-acidic tundra from Alaska.

3.7 Soil from moist acidic tundra Alaska (MAT)

CO₂ production in the MAT soil from Alaska equilibrated after 24 weeks (compared to the measurements before, data not shown) under drained and waterlogged conditions. CO₂ production rate decreased significantly by Ca addition under initial drained conditions ($p < 0.001$, $F = 40.664$, $df = 3$) (Figure 5A). The same pattern with Ca addition decreasing CO₂ production rate ($p < 0.001$, $F = 25.163$, $df = 3$) was found for MAT soil from Alaska under initial waterlogged



conditions (Figure 5B). Addition of Si had no clear effect on CO₂ production under drained conditions ($p = 0.921$, $F = 0.164$, $df = 3$), and significantly decreased CO₂ production under initial waterlogged conditions ($p < 0.001$, $F = 7.098$, $df = 3$) (Figure 5A, B). The interaction of Si and Ca additions was not significant under initial drained conditions ($p = 0.527$, $F = 0.904$, $df = 9$) but under initial waterlogged conditions ($p = 0.003$, $F = 3.177$, $df = 9$). Our reference treatment (no water addition) showed a CO₂ production rate of $2,660 \pm 1,120 \mu\text{mol d}^{-1}\text{kg}^{-1}$ DW after 24 weeks, which is in the range between the control treatment of the drained and waterlogged treatments for the soil from the moist non-acidic tundra from Alaska.

4 Discussion and conclusion

For all soils, increasing Ca concentrations decreased the soil CO₂ production rate dramatically (Figures 1–5). The effect of Si was not clear, with Si increasing the soil CO₂ production rate for some treatments of some soils; for other soils, it decreased the soil CO₂ production rate, and for others it had no effect. The decrease of soil-CO₂ production rate by Ca agrees with earlier findings (Whittinghill and Hobbie 2012; Schaller et al., 2019). This effect may be explained by either cation-bridging of soil organic matter by Ca ions (Whittinghill and Hobbie 2012; Schaller et al., 2019), or by increasing the salinity by Ca addition potentially decreasing the activity of the microbial decomposer community (Mavi et al., 2012), or a

Chapter 3. Manuscripts

combination of both. The large response variation of the Si effect on the soil-CO₂ production rate (from increasing to decreasing) is in contrast to previous studies, reporting a positive effect of Si on soil respiration or organic-matter decomposition (Schaller et al., 2014; Marxen et al., 2015; Schaller et al., 2019). The effect of Si addition increased the soil-CO₂ production rate and might be explained by the silicic acid increasing both the soil phosphorus and soil's organic matter availability for microbial decomposers (Reithmaier et al., 2017; Schaller et al., 2019; Hömberg et al., 2020; Hömberg et al., 2021b). Polysilicic acid is competing with both dissolved organic carbon and phosphate for sorption sites at the surface of soil particles (Schaller et al., 2019; Hömberg et al., 2020; Schaller et al., 2021), mostly iron oxidic phases. The subsequent higher availability of both organic carbon and phosphate may result in an increase of greenhouse gas production by accelerating soil respiration afterward (Reithmaier et al., 2017; Schaller et al., 2019; Hömberg et al., 2021b; Hömberg et al., 2021c). A decreasing effect of Si on soil-CO₂ production rates was observed especially under waterlogged conditions. Such a decreasing effect might be due to the potential dissolution of iron oxides as a binding partner for phosphate, organic carbon, and silicic acid and afterward co-precipitating all those compounds in some form of silica (Liu et al., 2009).

We found no differences between drained and waterlogged conditions for Chersky C1 and C2 as well as MAT. However, for Ca1 and MNT soil, respiration increased from drained to waterlogged conditions. Both soils (Ca1 and MNT) are from the top layer, potentially consisting of younger organic carbon (Shi et al., 2020). The Ca effect on soil respiration was lowest for MNT, which might be explained by the fact that this soil has high ash content, hence having low organic carbon content. However, for the Chersky C1 soil, we did not find such a low effect of Ca on soil respiration despite its comparable ash content to the MNT soil. For the soil from Siberia (Chersky), the lower concentrations of both ASi and Ca in the uppermost part of the current permafrost layers suggest that deeper thaw, as a consequence of Arctic warming, would also lower the concentrations of these elements in the seasonally thawed and biogeochemically active layer by depletion (Stimmler et al. in revision). In this context, the soil ASi concentration are forecast to decrease more strongly than Ca concentrations (Stimmler et al. in revision), potentially leading to a domination of the effect of Ca on soil-CO₂ production and release over the Si effect, with its proceeding Arctic warming and associated permafrost thaw. Assuming the Chersky soils to be representative for a larger Arctic domain, this decrease in CO₂ production and release due to higher Ca availability in the future would lead to more potential CO₂ emissions than currently thought from Siberia in the future. Similarly, for the soil from the Canadian Shield (Canada Ca1) a slight decrease in soil-Ca concentrations is predicted (Stimmler

et al. in revision). Data from Walker et al. (2001) suggest a strong increased Ca concentration upon permafrost thaw (higher Ca concentration in the permafrost layer compared to the current active layer) for the moist acidic tundra in Alaska (MAT). This may lead to a strong decrease in the soil-CO₂ production rates for the acid soils from Alaska (MAT); whereas, for the non-acid tundra in Alaska (MNT), data from Walker et al. (2001) suggest a potential depletion of Ca concentration in those non-acidic soils (lower Ca concentration in the permafrost compared to the current active layer). Such a decrease in the soil-Ca concentration may lead to increased soil CO₂ production rates for the non-acid soils from Alaska (MNT). A potential explanation for the absence of CH₄ emissions are the extremely low temperatures and the low amounts of soil organic carbon used in the incubations.

Overall, our data suggest that the soil Ca concentration may be a main control on the soil CO₂ production rates for all the soils from the different regions of the Arctic. Including Ca as the main factor for Arctic soil-CO₂ production rates may reduce uncertainties when modeling future climate scenarios on how the Arctic system may respond to global warming and will make those models more reliable. The ASi effect seems to be complex and need further investigations. We did not find any CH₄ production under the used experimental conditions. This may be related to the sample size used in the experiments. As CH₄ is a very important greenhouse gas for Arctic systems (Treat et al., 2015) and was shown to also be abundant under field conditions in relation to waterlogging and drainage (Kwon et al., 2019), future experiments should be designed to reproduce the CH₄ production as observed natural field conditions (Corradi et al., 2005).

Data availability statement

The raw data supporting the conclusion of this article will be made available by the authors, without undue reservation.

Author contributions

JS and MG planned the experiment with help from PS. MG, SN, OS, and NP provided the soils. PS conducted the experiment. The measurements were carried out by PS with the help of BG. PS and JS wrote the first draft of the manuscript. All authors commented on and approved the manuscript.

Funding

This work was funded by the German Research Foundation (DFG), grant number SCHA 1822/12-1 to Jörg Schaller.

Acknowledgments

The authors would like to thank the staff at the Limnological station and the Agroecology department (both University Bayreuth) for their help with the experiment.

Conflict of interest

The authors declare that the research was conducted in the absence of any commercial or financial relationships that could be construed as a potential conflict of interest.

References

- Alfredsson, H., Hugelius, G., Clymans, W., Stadmark, J., Kuhry, P., and Conley, D. J. (2015). Amorphous silica pools in permafrost soils of the Central Canadian Arctic and the potential impact of climate change. *Biogeochemistry* 124, 441–459. doi:10.1007/s10533-015-0108-1
- Allan, R. P. (2021). *Climate change 2021: The physical science basis. Contribution of working group I to the sixth assessment report of the intergovernmental panel on climate change*. Geneva, Switzerland: WMO.
- Brown, J., and Romanovsky, V. E. (2008). Report from the international permafrost association: State of permafrost in the first decade of the 21st century. *Permafrost. Periglac. Process.* 19 (2), 255–260. doi:10.1002/ppp.618
- Corradi, C., Kolle, O., Walter, K., Zimov, S. A., and Schulze, E. D. (2005). Carbon dioxide and methane exchange of a north-east Siberian tussock tundra. *Glob. Change Biol.* 11, 1910–1925. doi:10.1111/j.1365-2486.2005.01023.x
- DeMaster, D. J. (1981). The supply and accumulation of silica in the marine environment. *Geochim. Cosmochim. Acta* 45, 1715–1732. doi:10.1016/0016-7037(81)90006-5
- Hömborg, A., Broder, T., Knorr, K.-H., and Schaller, J. (2021a). Divergent effect of silicon on greenhouse gas production from reduced and oxidized peat organic matter. *Geoderma* 386, 114916. doi:10.1016/j.geoderma.2020.114916
- Hömborg, A., Broder, T., Schaller, J., and Knorr, K. H. (2021b). Methane fluxes but not respiratory carbon dioxide fluxes altered under Si amendment during drying–rewetting cycles in fen peat mesocosms. *Geoderma* 404, 115338. doi:10.1016/j.geoderma.2021.115338
- Hömborg, A., Knorr, K.-H., and Schaller, J. (2021c). Methane production rate during anoxic litter decomposition depends on Si mass fractions, nutrient stoichiometry and carbon quality. *Plants (Basel)*. 10, 618. doi:10.3390/plants10040618
- Hömborg, A., Obst, M., Knorr, K.-H., Kalbitz, K., and Schaller, J. (2020). Increased silicon concentration in fen peat leads to a release of iron and phosphate and changes in the composition of dissolved organic matter. *Geoderma* 374, 114422. doi:10.1016/j.geoderma.2020.114422
- Hugelius, G., Strauss, J., Zubrzycki, S., Harden, J. W., Schuur, E. A. G., Ping, C. L., et al. (2014). Estimated stocks of circumpolar permafrost carbon with quantified uncertainty ranges and identified data gaps. *Biogeosciences* 11, 6573–6593. doi:10.5194/bg-11-6573-2014
- Kwon, M. J., Natali, S. M., Hicks Pries, C. E., Schuur, E. A. G., Steinhof, A., Crummer, K. G., et al. (2019). Drainage enhances modern soil carbon contribution but reduces old soil carbon contribution to ecosystem respiration in tundra ecosystems. *Glob. Change Biol.* 25, 1315–1325. doi:10.1111/gcb.14578
- Liu, M.-C., Sheu, H.-S., and Cheng, S. (2009). Anion-exchange induced phase transformation of mesostructured silica. *J. Am. Chem. Soc.* 131, 3998–4005. doi:10.1021/ja808025m
- Marxen, A., Klotzbücher, T., Jahn, R., Kaiser, K., Nguyen, V. S., Schmidt, A., et al. (2015). Interaction between silicon cycling and straw decomposition in a silicon deficient rice production system. *Plant Soil* 398, 153–163. doi:10.1007/s11104-015-2645-8
- Mavi, M. S., Marschner, P., Chittleborough, D. J., Cox, J. W., and Sanderman, J. (2012). Salinity and sodicity affect soil respiration and dissolved organic matter

Publisher's note

All claims expressed in this article are solely those of the authors and do not necessarily represent those of their affiliated organizations, or those of the publisher, the editors, and the reviewers. Any product that may be evaluated in this article, or claim that may be made by its manufacturer, is not guaranteed or endorsed by the publisher.

Supplementary material

The Supplementary Material for this article can be found online at: <https://www.frontiersin.org/articles/10.3389/fenvs.2022.1019610/full#supplementary-material>

- dynamics differentially in soils varying in texture. *Soil Biol. Biochem.* 45, 8–13. doi:10.1016/j.soilbio.2011.10.003
- Mehlich, A. (1984). Mehlich-3 soil test extractant - a modification of Mehlich-2 extractant. *Commun. Soil Sci. Plant Anal.* 15, 1409–1416. doi:10.1080/00103628409367568
- Miner, K. R., Turetsky, M. R., Malina, E., Bartsch, A., Tamminen, J., McGuire, A. D., et al. (2022). Permafrost carbon emissions in a changing Arctic. *Nat. Rev. Earth Environ.* 3, 55–67. doi:10.1038/s43017-021-00230-3
- Mishra, U., Hugelius, G., Shelef, E., Yang, Y., Strauss, J., Lupachev, A., et al. (2021). Spatial heterogeneity and environmental predictors of permafrost region soil organic carbon stocks. *Sci. Adv.* 7, eaaz5236. doi:10.1126/sciadv.aaz5236
- R_Core_Team. 2021. R: A language and environment for statistical computing.
- Reithmaier, G. M. S., Knorr, K. H., Arnhold, S., Planer-Friedrich, B., and Schaller, J. (2017). Enhanced silicon availability leads to increased methane production, nutrient and toxicant mobility in peatlands. *Sci. Rep.* 7, 8728. doi:10.1038/s41598-017-09130-3
- Romanovsky, V. E., Drozdov, D., Oberman, N. G., Malkova, G. V., Kholodov, A. L., Marchenko, S. S., et al. (2010). Thermal state of permafrost in Russia. *Permafrost. Periglac. Process.* 21, 136–155. doi:10.1002/ppp.683
- Rowley, M. C., Grand, S., and Verrecchia, É. P. (2018). Calcium-mediated stabilisation of soil organic carbon. *Biogeochemistry* 137, 27–49. doi:10.1007/s10533-017-0410-1
- Schaller, J., Cramer, A., Carminati, A., and Zarebanadkouki, M. (2020). Biogenic amorphous silica as main driver for plant available water in soils. *Sci. Rep.* 10, 2424. doi:10.1038/s41598-020-59437-x
- Schaller, J., Fauchere, S., Joss, H., Obst, M., Goeckede, M., Planer-Friedrich, B., et al. (2019). Silicon increases the phosphorus availability of Arctic soils. *Sci. Rep.* 9, 449. doi:10.1038/s41598-018-37104-6
- Schaller, J., Hines, J., Brackhage, C., Baucker, E., and Gessner, M. O. (2014). Silica decouples fungal growth and litter decomposition without changing responses to climate warming and N enrichment. *Ecology* 95, 3181–3189. doi:10.1890/13-2104.1
- Schaller, J., Puppe, D., Kaczorek, D., Ellerbrock, R., and Sommer, M. (2021). Silicon cycling in soils revisited. *Plants* 10, 295. doi:10.3390/plants10020295
- Schuur, E., McGuire, A., Schädel, C., Grosse, G., Harden, J. W., Hayes, D. J., et al. (2015). Climate change and the permafrost carbon feedback. *Nature* 520, 171–179. doi:10.1038/nature14338
- Shi, Z., Allison, S. D., He, Y., Levine, P. A., Hoyt, A. M., Beem-Miller, J., et al. (2020). The age distribution of global soil carbon inferred from radiocarbon measurements. *Nat. Geosci.* 13, 555–559. doi:10.1038/s41561-020-0596-z
- Stein, L. Y. (2020). The long-term relationship between microbial metabolism and greenhouse gases. *Trends Microbiol.* 28, 500–511. doi:10.1016/j.tim.2020.01.006
- Stimmler, P., Goeckede, M., Elberling, B., Natali, S., Kuhry, P., Perron, N., et al. (2022a). Pan-Arctic soil element bioavailability estimations. Earth System Science Data. Available at: <https://essd.copernicus.org/preprints/essd-2022-123/> (Accessed Apr 07, 2022).

Chapter 3. Manuscripts

Stimmler, P., Priemé, A., Elberling, B., Goeckede, M., and Schaller, J. (2022b). Arctic soil respiration and microbial community structure driven by silicon and calcium. *Sci. Total Environ.* 838, 156152. doi:10.1016/j.scitotenv.2022.156152

Treat, C. C., Natali, S. M., Ernakovich, J., Iversen, C. M., Lupascu, M., McGuire, A. D., et al. (2015). A pan-Arctic synthesis of CH₄ and CO₂ production from anoxic soil incubations. *Glob. Change Biol.* 21, 2787–2803. doi:10.1111/gcb.12875

Walker, D., Bockheim, J., Chapin, F., Eugster, W., Nelson, F., and Ping, C. (2001). Calcium-rich tundra, wildlife, and the "mammoth steppe". *Quat. Sci. Rev.* 20, 149–163. doi:10.1016/s0277-3791(00)00126-8

Whittinghill, K. A., and Hobbie, S. E. (2012). Effects of pH and calcium on soil organic matter dynamics in Alaskan tundra. *Biogeochemistry* 111, 569–581. doi:10.1007/s10533-011-9688-6

Supporting Information to:

The importance of calcium and amorphous silica for Arctic soil CO₂ production

Peter Stimmler¹, **Mathias Göckede**², **Susan M. Natali**³, **Oliver Sonnentag**⁴, **Benjamin S. Gilfedder**⁵, **Nia Perron**⁴, **Jörg Schaller**^{1,*}

¹ Centre for Agriculture Landscape Research e.V. (ZALF), Müncheberg, Germany

² Max Planck Institute for Biogeochemistry, Jena, Germany

³ Woodwell Climate Research Center, Falmouth, USA

⁴ Département de géographie, Université de Montréal, 1375 Avenue Thérèse-Lavoie-Roux, Montréal, QC H2V 0B3, Canada

⁵ Limnological Station, Bayreuth Center of Ecology and Environmental Research (BAYCEER), University of Bayreuth, Bayreuth, Germany

*** Correspondence:**

Jörg Schaller

Joerg.Schaller@zalf.de

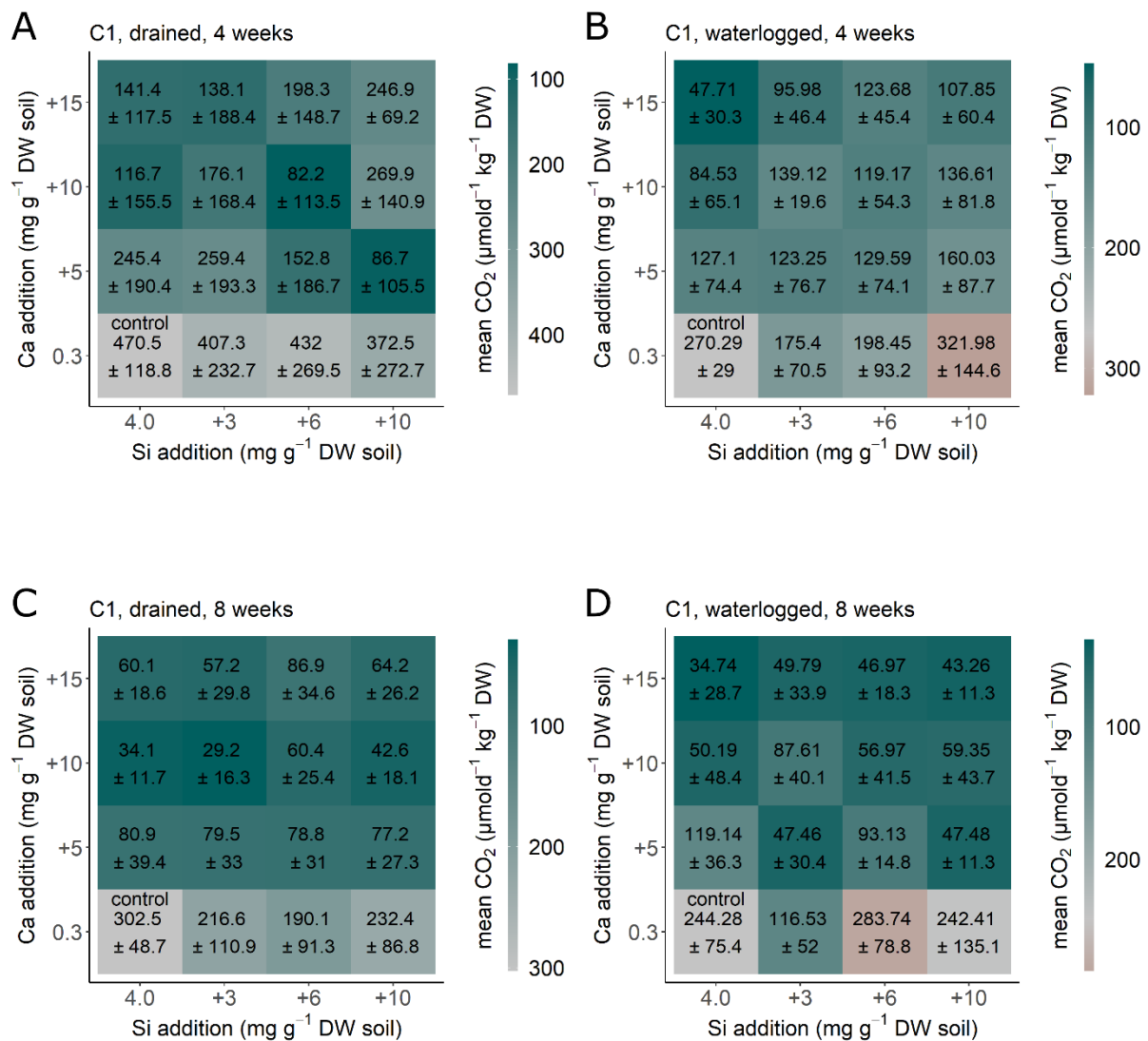


Fig. S1: CO₂ production for the soil from Siberia Chersky C1, NE-Russia after 4 weeks (A+B) and 8 weeks (C+D) under drained (A+C) and waterlogged (B+D) conditions. Each square represents a treatment (n=5) with Si (+0, +3, +6, and +10 mg g⁻¹ DW) and Ca (+0, +5, +10, and +15 mg g⁻¹ DW). Colour represents differences between the treatment CO₂ production in comparison to the control treatment, with green-blue showing a decreased CO₂ production and red showing an increased CO₂ production in comparison to the control treatment.

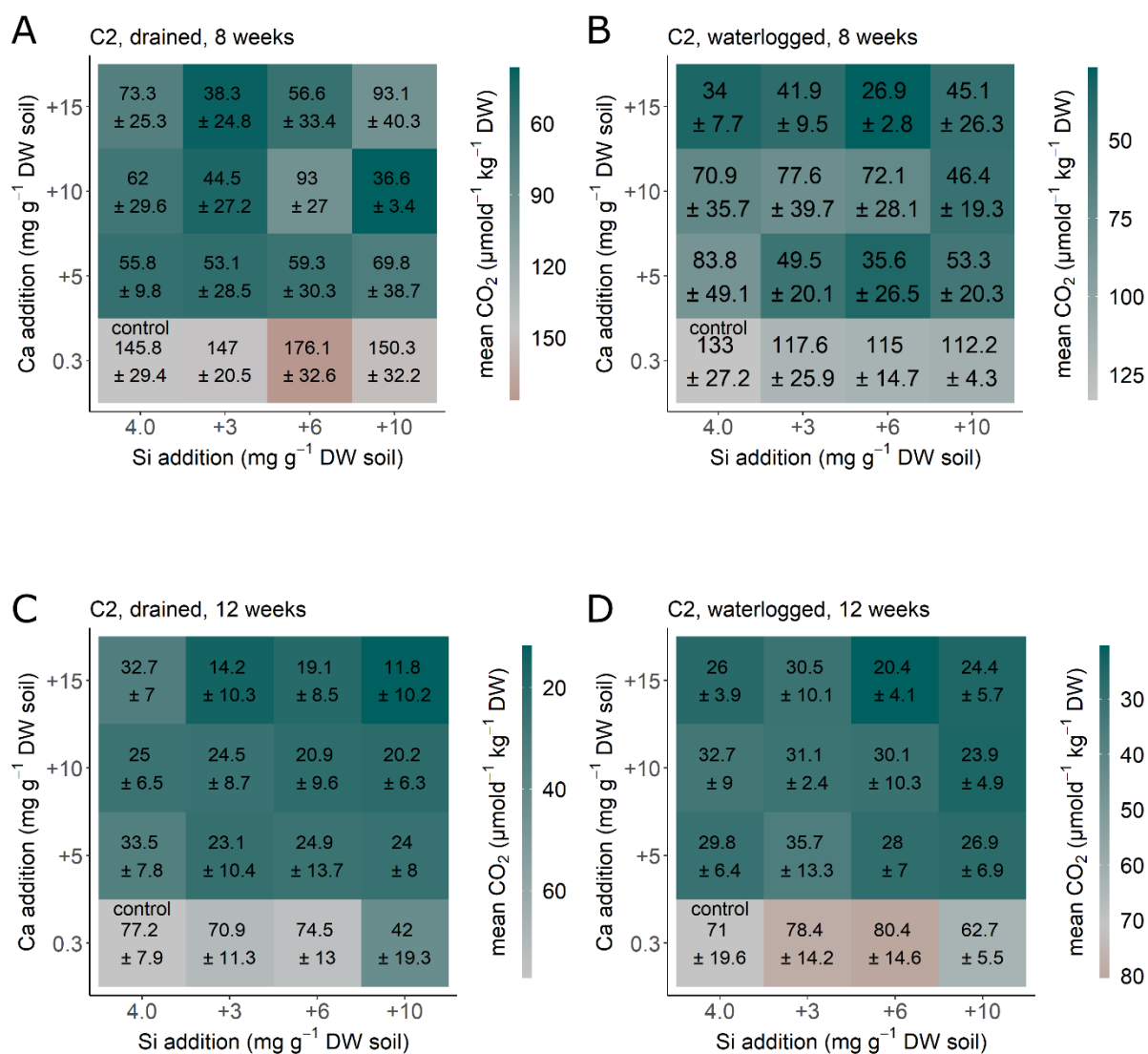


Fig. S2: CO₂ production for the soil from Siberia Chersky C2, NE-Russia after 8 weeks (A+B) and 12 weeks (C+D) under drained (A+C) and waterlogged (B+D) conditions. Each square represents a treatment (n=5) with Si (+0, +3, +6, and +10 mg g⁻¹ DW) and Ca (+0, +5, +10, and +15 mg g⁻¹ DW). Colour represents differences between the treatment CO₂ production in comparison to the control treatment, with green-blue showing a decreased CO₂ production and red showing an increased CO₂ production in comparison to the control treatment.

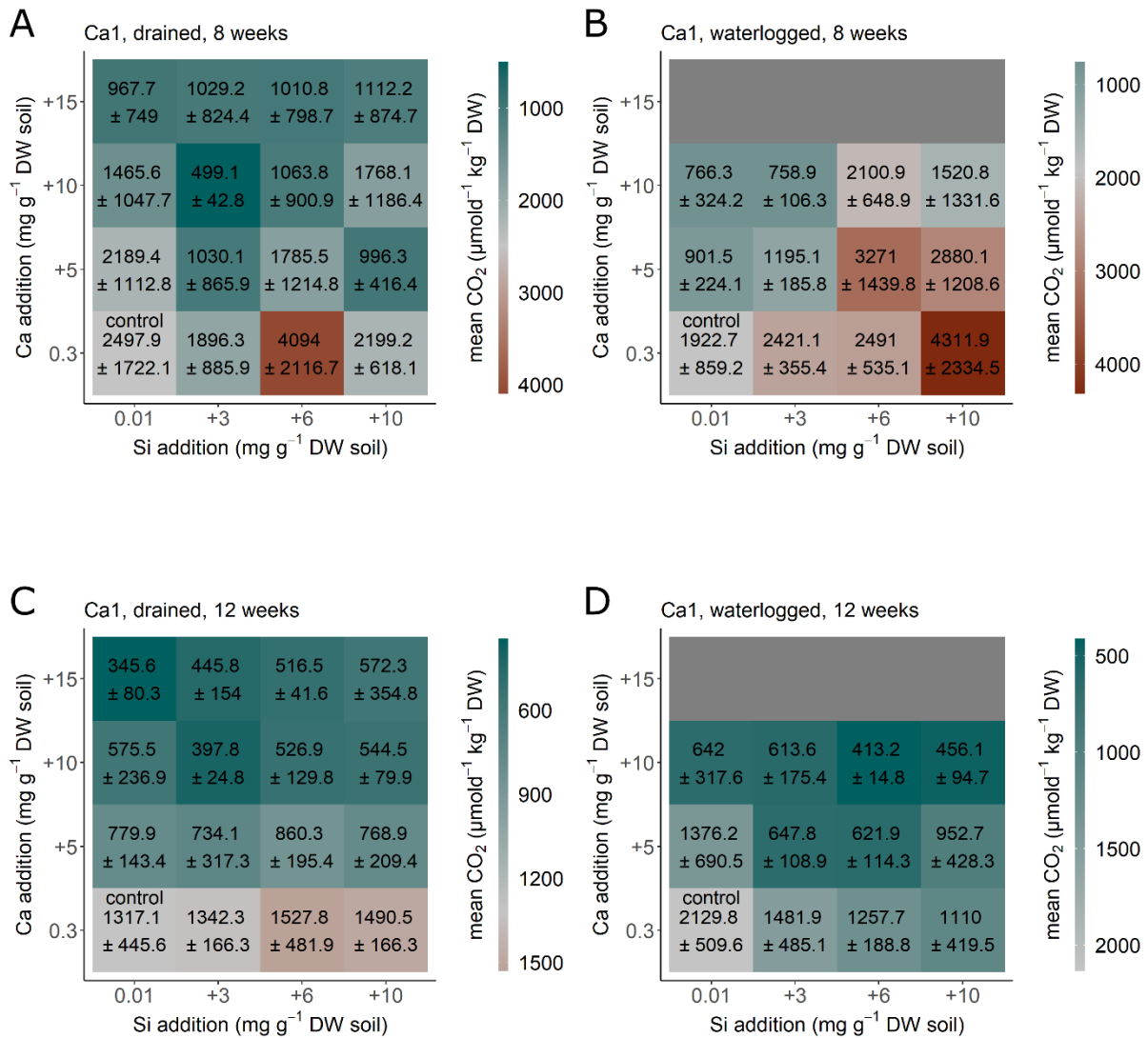


Fig. S3: CO₂ production for the soil Ca1 from the Canadian after 8 weeks (A+B) and 12 weeks (C+D) under drained (A+C) and waterlogged (B+D) conditions. Each square represents a treatment (n=5) with Si (+0, +3, +6, and +10 mg g⁻¹ DW) and Ca (+0, +5, +10, and +15 mg g⁻¹ DW). Colour represents differences between the treatment CO₂ production in comparison to the control treatment, with green-blue showing a decreased CO₂ production and red showing an increased CO₂ production in comparison to the control treatment.

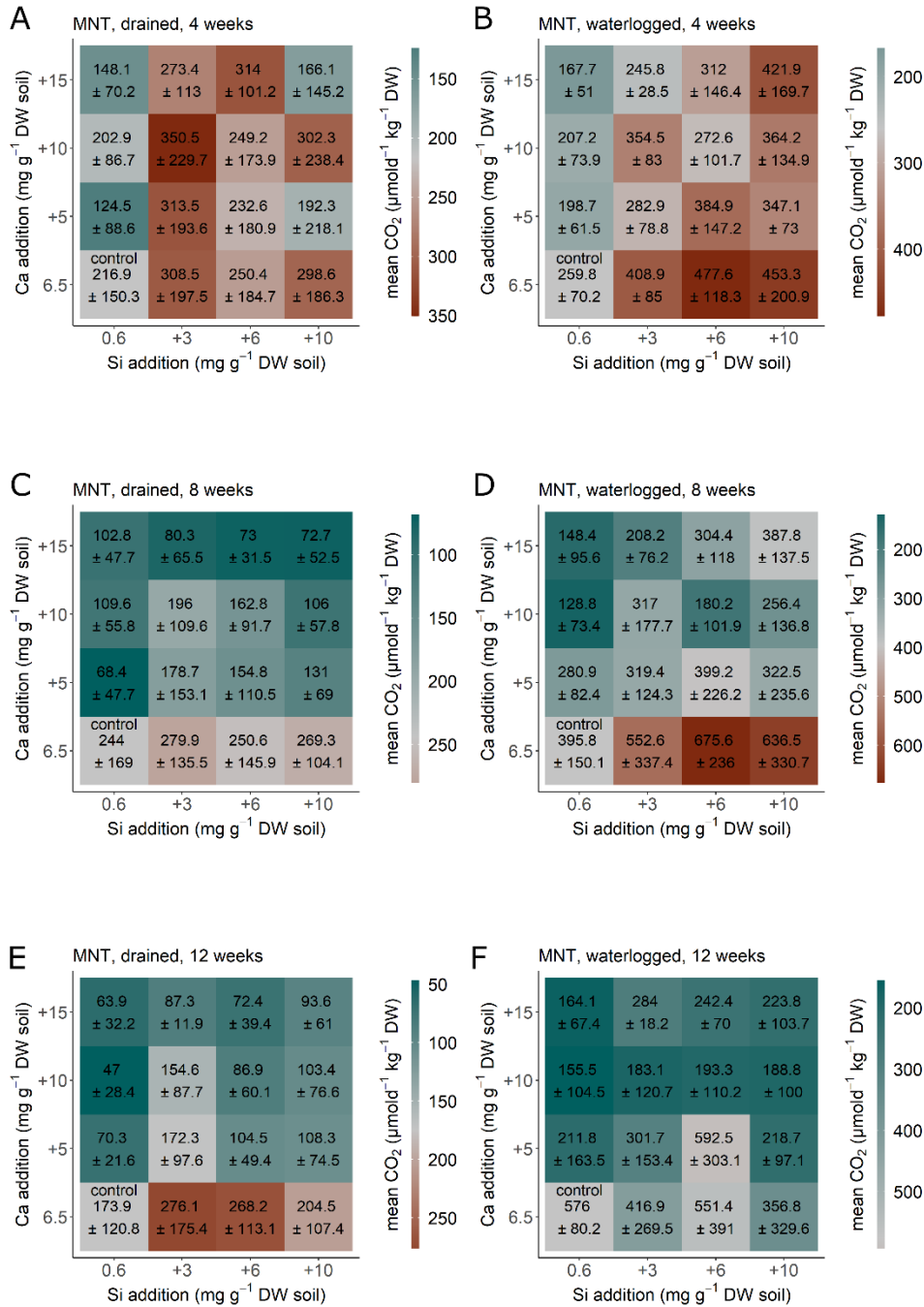


Fig. S4: CO₂ production for the soil from the moist acidic tundra (MAT), Alaska after 4 weeks (A+B), 8 weeks (C+D) and 12 weeks (E+F) under drained (A+C+E) and waterlogged (B+D+F) conditions. Each square represents a treatment (n=5) with Si (+0, +3, +6, and +10 mg g⁻¹ DW) and Ca (+0, +5, +10, and +15 mg g⁻¹ DW). Colour represents differences between the treatment CO₂ production in comparison to the control treatment, with green-blue showing a decreased CO₂ production and red showing an increased CO₂ production in comparison to the control treatment.

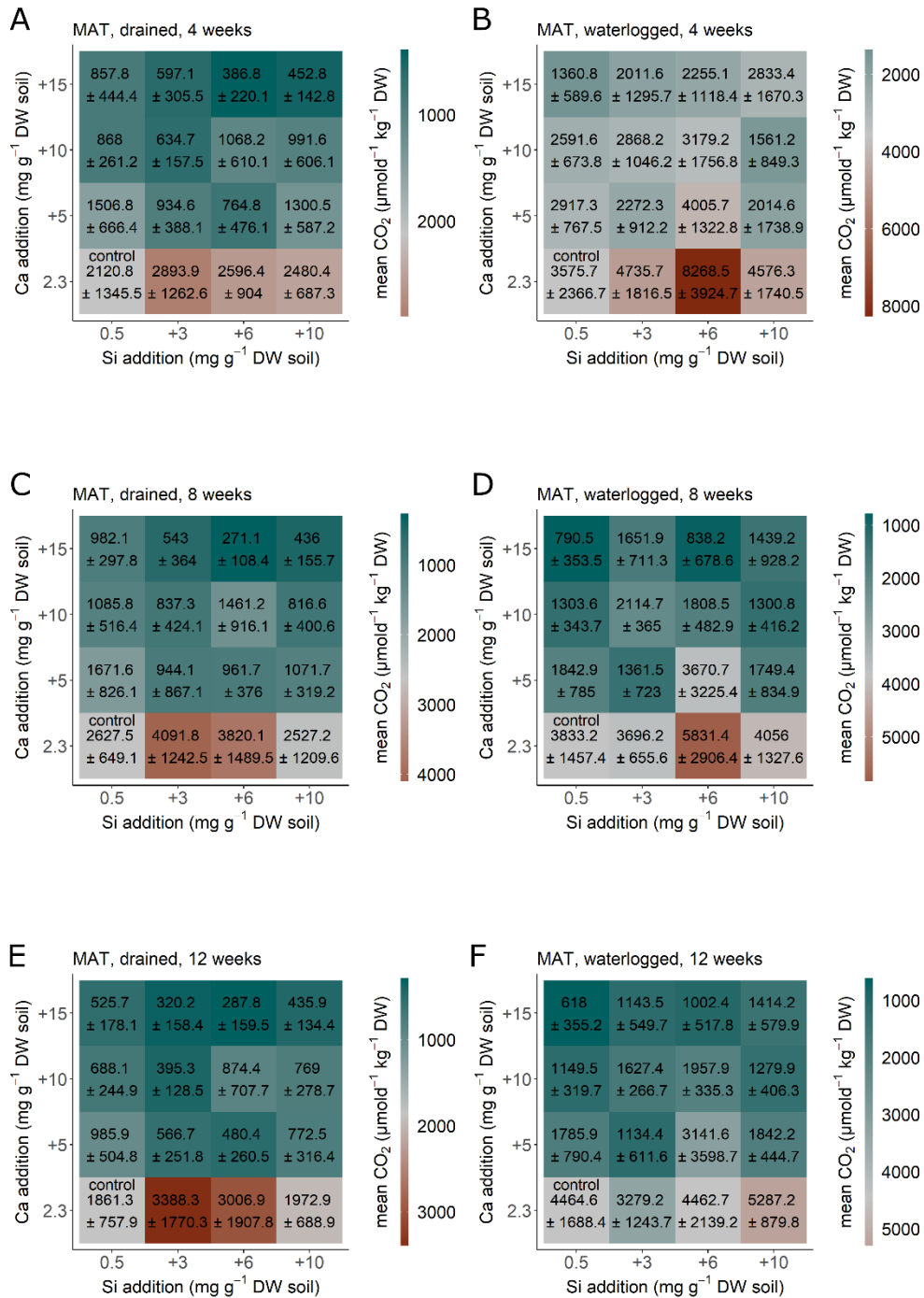


Fig. S5: CO₂ production for the soil from the moist non-acidic tundra (MNT), Alaska after 4 weeks (A+B), 8 weeks (C+D) and 12 weeks (E+F) under drained (A+C+E) and waterlogged (B+D+F) conditions. Each square represents a treatment (n=5) with Si (+0, +3, +6, and +10 mg g⁻¹ DW) and Ca (+0, +5, +10, and +15 mg g⁻¹ DW). Colour represents differences between the treatment CO₂ production in comparison to the control treatment, with green-blue showing a decreased CO₂ production and red showing an increased CO₂ production in comparison to the control treatment.

3.2.3 Study 3: Arctic soil CO₂ release during freeze-thaw cycles modulated by silicon and calcium.

Schaller, Stimmler, et al. (2022)

Published 20.04.2023 in:

Science of The Total Environment Volume 870, 161943

(<http://dx.doi.org/10.1016/j.scitotenv.2023.161943>)



Contents lists available at ScienceDirect

Science of the Total Environment

journal homepage: www.elsevier.com/locate/scitotenv

Arctic soil CO₂ release during freeze-thaw cycles modulated by silicon and calcium



Jörg Schaller^{a,*}, Peter Stimmler^a, Mathias Göckede^b, Jürgen Augustin^a, Fabrice Lacroix^{b,c}, Mathias Hoffmann^a

^a Leibniz Center for Agricultural Landscape Research (ZALF), 15374 Müncheberg, Germany

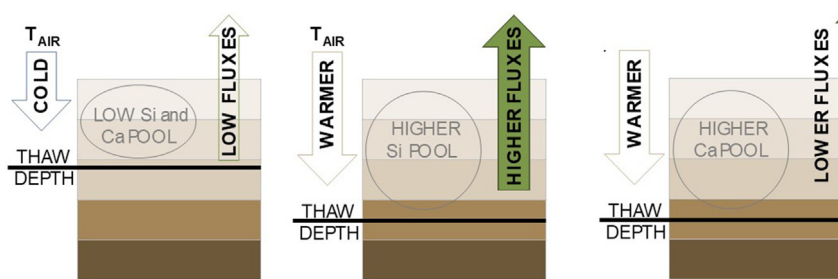
^b Max Planck Institute for Biogeochemistry, Jena, Germany

^c Climate and Environmental Physics, University of Bern, Bern, Switzerland

HIGHLIGHTS

- With each freeze-thaw cycle the CO₂ fluxes from the Arctic soils decreased.
- A considerable CO₂ emission is taking place below 0 °C.
- Si is increasing and Ca is decreasing CO₂ fluxes.
- Si is increasing Arctic soil CO₂ release especially when temperatures are below 0 °C.

GRAPHICAL ABSTRACT



ARTICLE INFO

Editor: Wei Shi

Keywords:

Amorphous silica
Arctic soil
Calcium
Climate change
Greenhouse gas release
Nutrient
Soil respiration

ABSTRACT

Arctic soils are the largest pool of soil organic carbon worldwide. Temperatures in the Arctic have risen faster than the global average during the last decades, decreasing annual freezing days and increasing the number of freeze-thaw cycles (temperature oscillations passing through zero degrees) per year as the temperature is expected to fluctuate more around 0 °C. At the same time, proceeding deepening of seasonal thaw may increase silicon (Si) and calcium (Ca) concentrations in the active layer of Arctic soils as the concentrations in the thawing permafrost layer might be higher depending on location. We analyzed the importance of freeze-thaw cycles for Arctic soil CO₂ fluxes. Furthermore, we tested how Si (mobilizing organic C) and Ca (immobilizing organic C) interfere with the soil CO₂ fluxes in the context of freeze-thaw cycles. Our results show that with each freeze-thaw cycle the CO₂ fluxes from the Arctic soils decreased. Our data revealed a considerable CO₂ emission below 0 °C. We also show that pronounced differences emerge in Arctic soil CO₂ fluxes with Si increasing and Ca decreasing CO₂ fluxes. Furthermore, we show that both Si and Ca concentrations in Arctic soils are central controls on Arctic soil CO₂ release, with Si increasing Arctic soil CO₂ release especially when temperatures are just below 0 °C. Our findings could provide an important constraint on soil CO₂ emissions upon soil thaw, as well as on the greenhouse gas budget of high latitudes. Thus we call for work improving understanding of freeze-thaw cycles as well as the effect of Ca and Si on carbon fluxes, as well as for increased consideration of those factors in wide-scale assessments of carbon fluxes in the high latitudes.

1. Introduction

There is large evidence from a variety of biomes covering temperate to higher latitudes that freeze-thaw cycles can strongly influence soil respira-

tion (Kurganova et al., 2007; Ouyang et al., 2015; Treat et al., 2021). While respiration is usually very low during the freeze phase, a brief strong CO₂ pulse often occurs during thaw, followed by a rapid decline in CO₂ release afterwards (Kim et al., 2012; Sapronov, 2021b; Zhang et al., 2022). Such strong CO₂ release after thawing is likely to be important for soils which store large amounts of organic carbon vulnerable for microbial respiration (Treat et al., 2021). Such soil with large amounts of vulnerable organic carbon are the soils in the Arctic (Hugelius et al., 2014).

* Corresponding author.

E-mail address: Joerg.Schaller@zalf.de (J. Schaller).

<http://dx.doi.org/10.1016/j.scitotenv.2023.161943>

Received 4 October 2022; Received in revised form 16 January 2023; Accepted 27 January 2023

Available online xxx

0048-9697/© 2023 Elsevier B.V. All rights reserved.

Arctic soils are the largest pool of soil organic carbon (C) worldwide (Strauss et al. 2017). Approximately, 1300 Tg of organic C are stored within the first 3 m (Hugelius et al., 2014). Temperatures in the high latitudes have risen faster as the global average in the last decades, decreasing annual freezing days (Henry, 2008; Rantanen et al., 2022; Stocker et al., 2014). Thawing of permafrost in Arctic soils due to climate warming exposes large amounts of organic C vulnerable to microbial degradation (Heslop et al., 2019; Mueller et al., 2015; Treat et al., 2021), thus potentially increasing C emissions of Arctic terrestrial systems, which potentially warms the climate through the greenhouse effect. Accordingly, CO₂ released from Arctic soils to the atmosphere as a result of soil organic matter degradation by microorganisms (heterotrophic respiration) could strongly impact future climate change, and should be considered for defining current climate goals (Anderson et al., 2016; Canadell et al., 2021; Schuur et al., 2015).

The few studies that have been conducted on Arctic soils during freeze-thaw cycles mostly follow the picture of experiments from other biomes showing a strong CO₂ release after each thaw event (Kim et al., 2012; Ludwig et al., 2006; Sapronov, 2021b; Schimel and Clein, 1996; Wang et al., 2014). Ludwig et al. (2006) found a consistent pronounced CO₂ release after thaw for every freeze-thaw cycle for soil from Russian tundra.

In deeper Arctic soils, which were previously permanently frozen, increased temperatures will firstly expose permanently frozen parts of the soil to freeze-thaw cycles and secondly increase the number of freeze-thaw cycles per year (oscillation around 0 °C), as the temperature is fluctuating more around 0 °C (Henry, 2008). Each thawing is accompanied by a strong increase in the concentration and quantities of both microbial degradable organic compounds and a number of other elements in the soil solution (Loiko et al., 2017; Payandi-Rolland et al., 2020). Such increase in element availability by thawing may be particularly important for silicon (Si) and calcium (Ca) altering the concentrations of both elements in the soil active layer (Alfredsson et al., 2016; Stimmler et al., in revision; Walker et al., 2001). Both elements may strongly interfere with soil organic C mineralization and soil CO₂ release (Schaller et al., 2019). Ca is known to bind organic C by cation bridging in Arctic soils (Whittinghill and Hobbie, 2012), while Si mobilizes organic C due to competition for binding at the surface of soil particles (Hömborg et al., 2020; Reithmaier et al., 2017; Schaller et al., 2019). These effects on organic C mobility have been reported to substantially affect the soil CO₂ release in incubation experiments of high-Arctic soils (Schaller et al., 2019; Stimmler et al., 2022). Consequently, we expect that Si increases and Ca decreases Arctic soil C fluxes.

However, up to now, no study analyzed the importance of freeze-thaw cycles (potentially mobilizing organic C) while considering effects caused by Si (mobilizing organic C) or Ca (immobilizing organic C) for Arctic soil CO₂ release especially under freezing conditions and upon thaw. In this study, we hypothesize that (i) every freeze-thaw cycle will lead to a consistent pronounced CO₂ release after thaw and (ii) Si is positively and Ca negatively related to Arctic soil CO₂ emissions. To investigate this, we used controlled laboratory incubation experiments to test the combination of freeze-thaw cycles, as well as Si and Ca for Arctic soil CO₂ release. To make the freeze-thaw experiments comparable with natural conditions we adapted the freeze-thaw regime to the natural freeze-thaw cycle of the Arctic soils to make sure that freezing as well as thawing periods allowed the soil microbes to adapt.

2. Materials and methods

2.1. Soil material used for experiments

The soil used for the present study was taken from a wet tussock tundra ecosystem near Chersky, Northeast Siberia, Russia (68,61,586°N; -161,35,228°E), underlain by continuous permafrost (Göckede et al., 2017; Göckede et al., 2019). The soil, which was sampled from the mineral active layer from 50 to 60 cm depth, was gently crushed in frozen state using a steel mortar in a first processing step. We used this soil layer as it is the deepest part of the active layer at this site and mostly affected by

changes in Si and Ca due to permafrost thaw. The frozen material was split and sieved under frozen conditions through a two mm sieve until all particles passed through the sieve. The soil had an amorphous Si content of 3 mg g⁻¹, and Mehlich(III) extractable concentrations of 0.08 mg g⁻¹ for Si, and 0.6 mg g⁻¹ for Ca (Stimmler et al., in revision). The soil was thawed and mixed with Ca and/or Si. We added 5 mg g⁻¹ Ca in form of CaCl₂ x 2H₂O and/or 6 mg g⁻¹ Si in form of an amorphous silica (Aerosil 300 Evonik, Germany), all replication of four and samples stabilized to the initial soil pH using HCl. The soil samples were completely saturated with 8 mL ultrapure water during the whole experiment. After this, the experiment immediately started.

2.2. Experimental design and analysis

To make the freeze-thaw experiments comparable with natural conditions, we adapted the laboratory freeze-thaw regime to the natural freeze-thaw cycle as observed within the Arctic soils at the sampling site near Chersky. For this, the soils were incubated at +5 °C until the CO₂ efflux was at equilibrium (Fig. 1). Afterwards, the soil temperature was decreased to +1 °C within two days. The temperature of +1 °C was held for two days. Afterwards, the temperature was decreased to -1 °C and held for two days, again. Thereafter, the temperature was decreased to -9 °C (Fig. 1). This temperature profile allows microbes to adapt to the temperatures is analog to field conditions. Such adaptation is important as microbes are sensitive toward freezing at too fast rates (Lipson et al., 2000). The chosen moderate temperature gradients prevent lysis as shown for such conditions before (Grogan et al., 2004). Linear extrapolated CO₂ flux rates, initially measured during -1 °C, were used in this study as a conservative estimate for CO₂ efflux during freeze periods.

2.3. Measurements and data analysis

We incubated four different sample treatments, namely a natural soil (control), and three further treatments with added silicon (+Si), added calcium (+Ca), and both added silicon and calcium (+Si + Ca). CO₂ fluxes from the samples were analyzed for three thaw periods (Table 1). For each treatment, four replicates of 20 g each were incubated in parallel using the incubation system described in detail by Rillig et al. (2021). The used incubation system works in a flow-through, steady-state mode corresponding to Livingston and Hutchinson (1995). It contains 16 airtight, cylindrical incubation vessels (50 mL PE centrifuge vials), for the samples to be incubated, and a control channel through which ambient air passes the incubation vessels directly from the pressure vessel to the gas analyzer (Picarro G2508; PICARRO, INC., Santa Clara, USA). Ambient air flows were continuously through the headspace of all incubation vessels via channels connecting the pressure vessel and the gas analyzer directly, using a multiplexer and a special circular channel. Air was circulated between the incubation unit headspace and the CRDS analyzer at 250 mL min⁻¹ using a low-leak diaphragm pump (A0702, Picarro, Santa Clara, CA, USA). To increase the sensitivity of the incubation system, flow rate and measurement time per channel were adjusted according to the expected CO₂ flux rate.

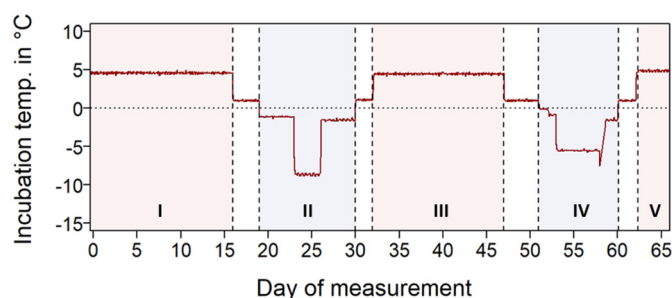


Fig. 1. Temperature (air) regime of the freeze-thaw-cycles simulated during the incubation experiment.

Table 1

average measured CO₂ fluxes for the different treatments during the repetitive freeze-thaw-cycle.

Period	Treatment	Temp.	Duration (d)	CO ₂
		°C		nmol m ⁻² s ⁻¹
1st thaw	control	4.0	19	52
	+Ca	4.0	19	25
	+Si	4.0	19	76
	+Ca + Si	4.0	19	35
1st freeze	control	-3.2	11	21
	+Ca	-3.5	11	34
	+Si	-3.4	11	61
	+Ca + Si	-3.2	11	51
2nd thaw	control	3.5	21	57
	+Ca	3.4	21	31
	+Si	3.5	21	49
	+Ca + Si	3.5	21	33
2nd freeze	control	-3.6	9	9
	+Ca	-3.8	9	13
	+Si	-3.8	9	16
	+Ca + Si	-3.5	9	6
3rd thaw	control	3.4	6	36
	+Ca	3.5	6	17
	+Si	3.6	6	26
	+Ca + Si	3.5	6	8

The temperature was controlled in the incubation vessels by means of a climate chamber. During the thawing phases, the samples were weighed several times to compensate for possible soil water losses. CO₂ fluxes were calculated from the measured CO₂ gas concentration in the respective channel, and the temporally corresponding concentration in the control channel according to Eq. (1):

$$F = \frac{(M * \rho * V * (\Delta c))}{(C * R * t * T)} \quad (1)$$

where F is the flux rate (µg CO₂-C core⁻¹ h⁻¹), M is the molar mass of CO₂, ρ the atmospheric pressure (Pa), V is the air flow rate into the headspace and the channels (m³ h⁻¹), Δc is the difference of CO₂ concentrations [mol] between outlet of a specific vessel and the corresponding, linear interpolated control channel CO₂ concentration, C is the soil sample area (m²), R the gas constant (m³ Pa K⁻¹ mol⁻¹), t is the time over which the concentration change was observed, and T the incubation temperature (K).

Fluxes were calculated using an R script (R_Core_Team, 2021). Influence of diurnal cycles in measured ambient air within the control channel on calculated CO₂ fluxes was minimized by linear interpolation of CO₂ concentrations measured for the control channel, rather than using adjacent control channel CO₂ concentration measurements only. To avoid bias caused by measurements on the previous channel, only values determined in the last minute of each channel measurement were used to calculate CO₂ fluxes. For calculation of CO₂ emissions, biased, negative CO₂ fluxes were rejected.

3. Results

3.1. CO₂ release decreased with progressing number of thaw-freeze periods

CO₂ fluxes during the whole incubation period generally decreased within all treatments as the number of thaw (Fig. 2) and freeze periods (Fig. 3) proceeds. Treatments of +Si and +CaSi however, decreased with -57% and -52% much more rapidly from the first to the last observed thaw period (period with temperature > 1 °C) compared to the control and +Ca treatment with -24% and -40%, respectively. The same was observed for the change from the first to the last observed freeze period (period with temperature < -1 °C), were +Si and +CaSi decreased by -82% and -70%, while CO₂ fluxes of the control and +Ca treatment decreased by -40% and -60%. As a result, differences between treatments during first and third freeze periods with +Si being

significantly higher diminished during the second freeze period ($p = 0.015$, compare the second and the third period) and were only significant different ($p < 0.01$) during thaw periods between treatments.

3.2. Silicon increased and calcium decreased CO₂ fluxes and emissions

CO₂ fluxes generally showed very high variability over time. Therefore, especially the effects of changing temperatures were not immediately recognizable at a glance (Fig. S1). However, average CO₂ fluxes during the whole incubation period in the +Si treatment with a median of 0.055 µmol m⁻² s⁻¹ were 22% higher and significantly different ($p = 0.01$, Wilcoxon test) compared to the control (0.045 µmol m⁻² s⁻¹). In comparison to the +Ca and the +Ca + Si treatments, which produced CO₂ flux medians of 0.021 µmol m⁻² s⁻¹ and 0.023 µmol m⁻² s⁻¹, respectively, the +Si treatment yielded also significantly higher CO₂ fluxes ($p < 0.01$, Wilcoxon test) (Fig. 4a). The same holds true for the CO₂ fluxes from the control treatment, which were also significantly higher ($p < 0.01$, Wilcoxon test) compared to the +Ca and the +Ca + Si treatments. No significant differences in CO₂ fluxes were found between the +Ca and the +Ca + Si treatment ($p = 0.015$; Wilcoxon test). Daily differences in CO₂ fluxes of the different treatments compared to control were shown in Fig. S1.

CO₂ fluxes above +1 °C of both the control treatment with a median of 0.043 µmol m⁻² s⁻¹ and the +Si treatment with a median of 0.049 µmol m⁻² s⁻¹ were significantly higher ($p < 0.01$, Wilcoxon test) compared to those of the +Ca with a median of 0.022 µmol m⁻² s⁻¹ and the +Ca + Si treatment with a median of 0.025 µmol m⁻² s⁻¹ (Fig. 4b). The CO₂ fluxes above +1 °C were no significantly different between control treatment and +Si and also not between the +Ca and the +Ca + Si treatment. Focusing on the CO₂ fluxes below -1 °C we found a strong and significant increase in CO₂ fluxes by 100% in the +Si treatment with a median of 0.030 µmol m⁻² s⁻¹ compared to the control treatment with a median of 0.015 µmol m⁻² s⁻¹. No significant difference were found between the control treatment and both the +Ca treatment with a median of 0.014 µmol m⁻² s⁻¹ and the +Ca + Si treatment with a median of 0.016 µmol m⁻² s⁻¹ (Fig. 4c). For the CO₂ fluxes above +1 °C the pattern was different compared with those fluxes below -1 °C.

Cumulative CO₂ emissions per treatment during the whole incubation period are shown in Fig. 5. Similar to average fluxes, the +Si treatment yielded 28% higher cumulative CO₂ emission (2.44 mg CO₂-C per sample) when compared to the control treatment (1.90 mg CO₂-C sample⁻¹). The +Ca and +Ca + Si treatments showed lower cumulative CO₂ emissions (1.13 and 1.47 mg CO₂-C sample⁻¹) compared to the control, with +Ca evidencing the lowest cumulative CO₂ emissions. Neither of both +Ca and +Ca + Si treatments showed a clear difference when compared to a proxy for the absence of frost-thaw, represented by the cumulative CO₂ emission, estimated based on the linear extrapolated, initially measured, average CO₂ flux of the control treatment at -1 °C incubation temperature. Only the +Si treatment yielded in substantially higher cumulative CO₂ emissions.

4. Discussion

The main finding of our study is that with each freeze-thaw cycle the CO₂ fluxes from the Arctic soils decreased, refuting hypothesis (i). We also found pronounced differences between the tested treatments with Si increasing and Ca decreasing Arctic soil CO₂ fluxes, confirming hypothesis (ii).

Frozen conditions prevent organic matter (OM) from microbial degradation (Mann et al., 2022). Our data revealed a considerable CO₂ emission below 0 °C, especially for the Si fertilized treatments. This is in line with earlier findings also showing CO₂ emission from Arctic soil until minus 5 °C (Ludwig et al., 2006; Sapronov, 2021b; Schimel and Clein, 1996; Wang et al., 2014). Zhang et al. (2022) found increased CO₂ emissions if the soil had been frozen to temperatures below -5°C, but no such effects if the freezing temperature was above -5°C. Consistent with our data, other

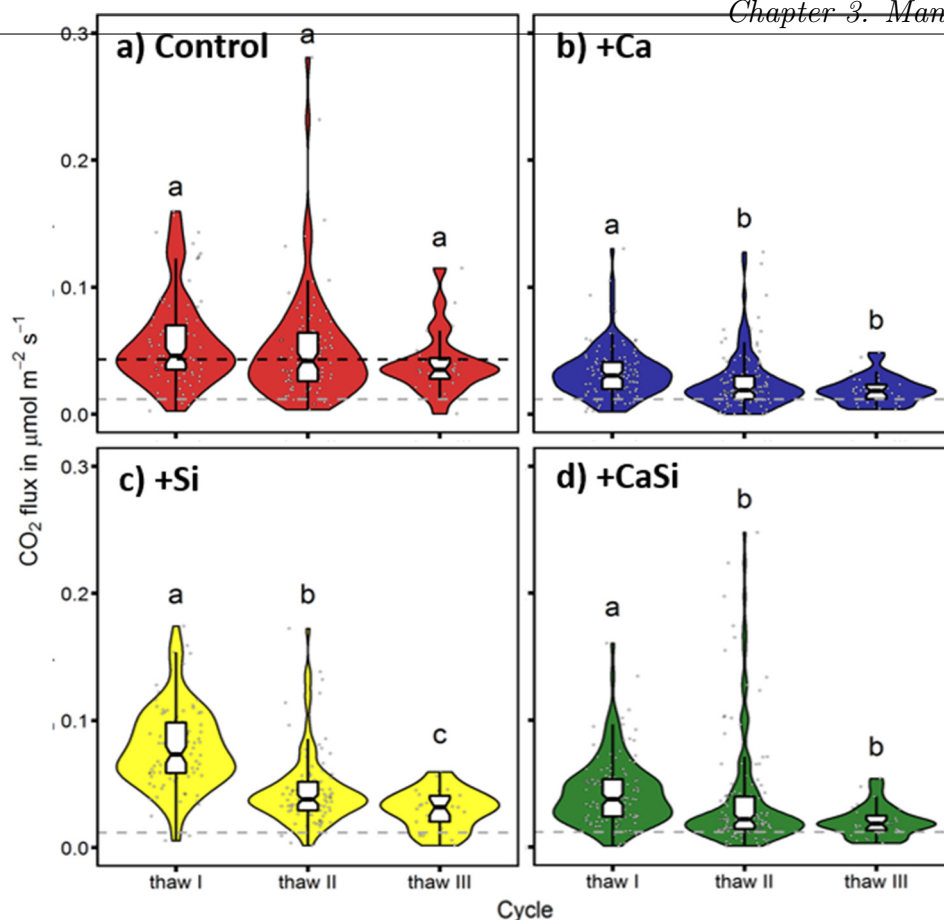


Fig. 2. Violin plot of measured CO_2 fluxes of the a) control, b) + Ca ($5 \text{ mg g}^{-1} \text{ Ca}$), c) + Si ($6 \text{ mg g}^{-1} \text{ Ca}$) and d) + Si + Ca ($5 \text{ mg g}^{-1} \text{ Ca}$; $6 \text{ mg g}^{-1} \text{ Si}$) treatment during the first, second and third thaw period (defined as incubation temperature $> +1^\circ \text{C}$ following freeze) within the incubation period. Boxplots show median CO_2 flux as well as 1st (25 %) and 3rd quartile (75 %). Whiskers represent the 0.05 (5 %) and 0.95 (95 %) quantile. The dashed black horizontal line indicated the median CO_2 flux of the control treatment (a), the dashed gray horizontal line the initially measured, average CO_2 flux of the control treatment at -1°C . Different letters indicate significant ($p < 0.05$) difference between CO_2 fluxes of the different thawing periods.

studies of Arctic soils also experienced a decrease in CO_2 release with increasing number of freeze-thaw cycles (Kurganova et al., 2007; Ludwig et al., 2006; Sapronov, 2021a; Schimel and Clein, 1996; Wang et al., 2014). This means that the labile organic carbon in Arctic soils is likely degraded rapidly, once the soil is thawed, needing only few freeze-thaw cycles to be mineralized and released to the atmosphere.

Consequently, higher Arctic temperatures with subsequent increased number of freeze-thaw cycles per year (oscillation around 0°C) (Henry, 2008) may contribute only to a minor extent to an increased soil CO_2 release in future, as long as no labile C input by e.g. plants occurs, since labile C may potentially increase the microbial organic C degradation and subsequent C release from Arctic soils (Hartley et al., 2010).

It is debated in literature how stable Arctic C is upon soil thaw and the timescale of organic C degradation in high latitude systems is still unknown (Schuur et al., 2015). Our results indicate that a strong response in CO_2 could take place rapidly after only few thawing cycles, thus soil thaw could have a direct impact on climate change in the near-future.

The effects of Si enhancing CO_2 fluxes from Arctic soils is in line with previous studies on Greenlandic soils (Schaller et al., 2019) or peatlands (Hömborg et al., 2021; Reithmaier et al., 2017). This enhanced CO_2 fluxes from Arctic soils by Si may be explained by an increase of available water (Schaller et al., 2020) without increasing salinity. Another potential mechanism underlying the enhancing CO_2 fluxes from Arctic soils by Si may be arising from the mobilization of silicic acid from the ASi (Schaller et al., 2021). Since silicic acid competes with phosphate for binding at the surfaces of soil particles, previously unavailable phosphate is potentially

mobilized reducing the phosphate limitation for the decomposing microbes (Hömborg et al., 2020; Schaller et al., 2019). As the strongest effect of +Si treatment enhancing CO_2 fluxes from Arctic soils was shown for temperatures below 0°C , the Si effect may have something to do with water availability below 0°C with increased “supercooled” water content under higher Si concentrations, which has been previously found for increased silt fractions enhancing the fractions of “supercooled” water at freezing conditions (Schaefer and Jafarov, 2016). Si in solution was found long time ago to reduce the water freezing point (Kahlenberg and Lincoln, 1898), which was confirmed recently (Kumar et al., 2019). This may lead to an increased water availability below 0°C by Si being a potential the reason for the higher CO_2 fluxes from the Arctic soil below 0°C in the +Si treatment (Fig. 4c) as microbes need available water.

The decrease of the soil CO_2 production rate by Ca is in line with earlier finding (Schaller et al., 2019; Whittinghill and Hobbie, 2012). This effect of Ca decreasing the soil CO_2 production rate may be explained by either cation bridging of soil organic matter by Ca ions (making the organic matter unavailable for microbial decomposition) (Schaller et al., 2019; Whittinghill and Hobbie, 2012) or by increasing salinity due to Ca addition potentially decreasing activity of microbial decomposer community (Mavi et al., 2012). It was recently shown that Si may be able to increase and Ca decrease the activity of microbial decomposers and change the microbial decomposer community structure (Stimmler et al., 2022).

We show that both Si and Ca concentrations in Arctic soils are a main controls on Arctic soil CO_2 release, with Si increasing soil CO_2 release especially when temperatures are below 0°C . High-Arctic permafrost soils store

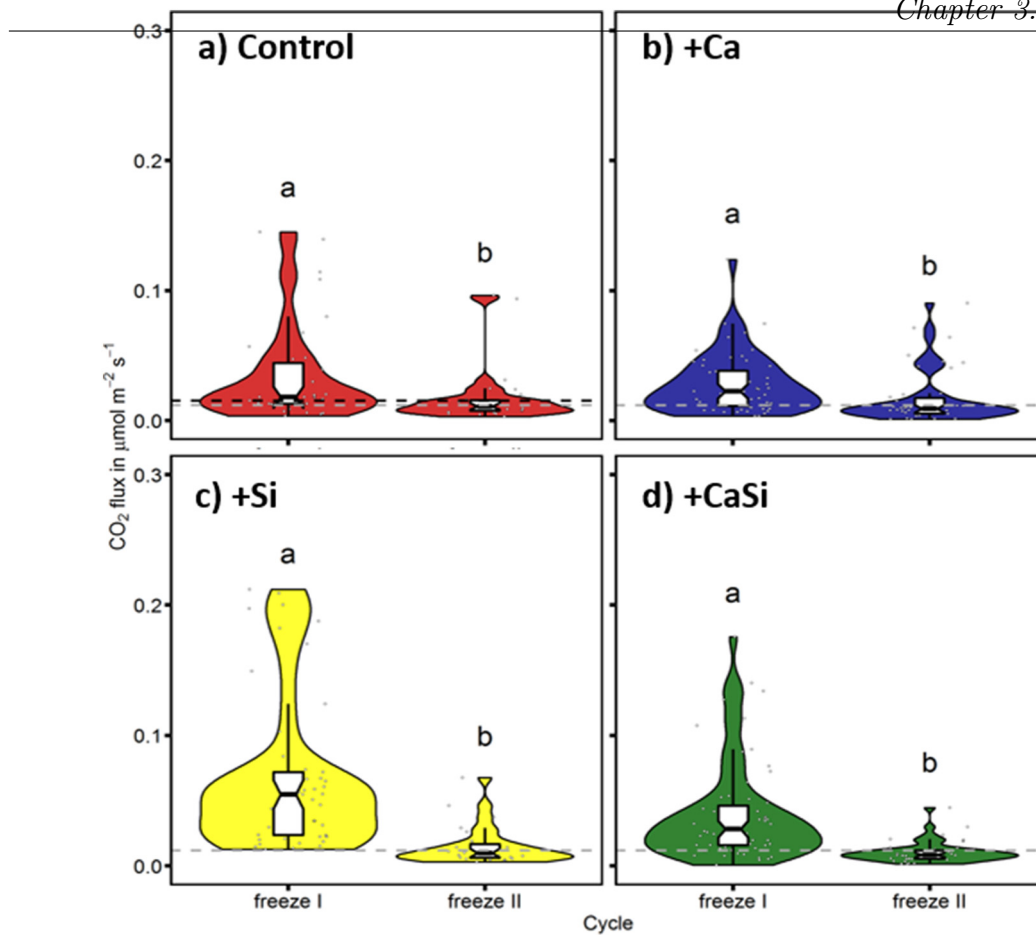


Fig. 3. Violin plot of measured CO₂ fluxes of the a) control, b) + Ca (5 mg g⁻¹ Ca), c) + Si (6 mg g⁻¹ Ca) and d) + Si + Ca (5 mg g⁻¹ Ca; 6 mg g⁻¹ Si) treatment during the first and second freeze period (defined as incubation temperature < -1 °C following thaw) within the incubation period. Boxplots show median CO₂ flux as well as 1st (25 %) and 3rd quartile (75 %). Whiskers represent the 0.05 (5 %) and 0.95 (95 %) quantile. The dashed black horizontal line indicates the median CO₂ flux of the control treatment (a). The dashed gray horizontal line indicates the initially measured, average CO₂ flux of the control treatment at -1 °C. Different letters indicate significant (p < 0.05) difference between CO₂ fluxes of the different freeze cycles.

vast amounts of Si and Ca (Alfredsson et al., 2016; Stimmler et al., in revision; Walker et al., 2001), which could be released upon thaw. These feedbacks which affect soil organic matter stabilization in Arctic soil

(potentially by Ca) are poorly understood and such effects of stabilization of organic matter by Ca potentially decreasing soil respiration and/or a mobilization of nutrient like phosphate by Si potentially increasing soil

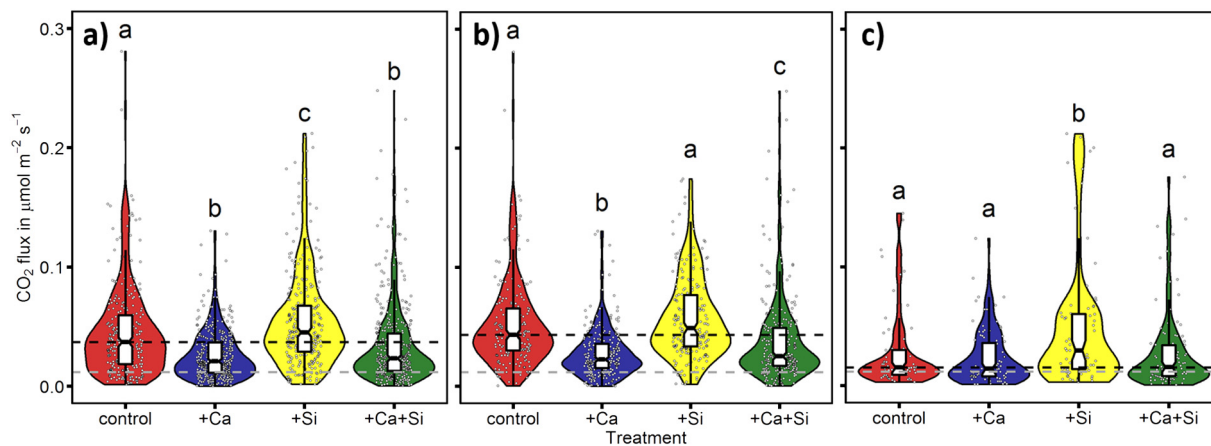


Fig. 4. Measured CO₂ fluxes of the a) different treatments for the entire incubation period; b) shows measured CO₂ fluxes for the different treatments when incubation temperature was above +1 °C and c) shows measured CO₂ fluxes for the different treatments when incubation temperature was below -1 °C. Boxplots show median CO₂ flux as well as 1st (25 %) and 3rd quartile (75 %). Whiskers represent the 0.05 (5 %) and 0.95 (95 %) quantile. The dashed black horizontal line indicated the median CO₂ flux of the control treatment, the dashed gray horizontal line the initially measured, average CO₂ flux of the control treatment at -1 °C incubation temperature. Different letters indicate significant (p < 0.05) differences between CO₂ fluxes of the different treatments.

Chapter 3. Manuscripts

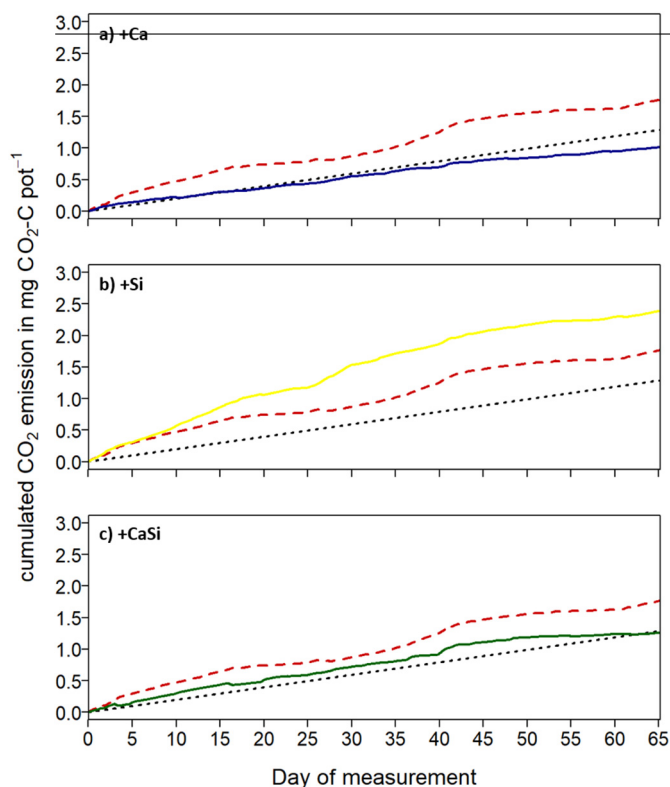


Fig. 5. Cumulative CO₂ emissions over the whole incubation period for the a) + Ca, b) + Si and c) + Ca + Si treatment. The dashed, red line represents the cumulative CO₂ emission of the control treatment. The dotted black line indicated the cumulative CO₂ flux based on the initially measured, average CO₂ flux of the control treatment at $-1\text{ }^{\circ}\text{C}$. (For interpretation of the references to colour in this figure legend, the reader is referred to the web version of this article.)

respiration are not taken into account in present global-scale assessments of the Arctic carbon budget (Canadell et al., 2021). If our findings regarding soil respiration effects of Si and Ca on Arctic soil organic matter turn out to be true on larger scales, they could provide an important constraint on soil CO₂ emissions upon soil thaw, as well as on the greenhouse gas budget of high latitudes. However, depending on the concentration of Si and Ca both effects (Si increasing and Ca decreasing soil CO₂ emissions) may offset each other. We thus call for work improving understanding on Ca and Si feedbacks on carbon fluxes, as well as for increased consideration of factors that affect the stability of Arctic soil carbon in wide-scale assessments.

A first step toward this is the development of an experimental design for the studies, which accurately captures the real conditions on thawed Arctic soils. An important impetus for this is the small post-thaw CO₂ pulse in our studies, which further decreased with proceeding freeze-thaw cycles. While a CO₂ pulse occurred in three of the studies that looked at the effect of freeze-thaw cycles on Arctic soils (Sapronov, 2021b; Schimel and Clein, 1996; Wang et al., 2014), it was also absent in (Ludwig et al., 2006). Apparently, this was because, in agreement with Ludwig et al. (2006), we had only slowly changed the temperature during the transition between freeze-thaw or vice versa, as actually occurring under natural conditions in Arctic soils. In other words, the CO₂ pulse observed by most other studies may be a result of an abrupt transition (no transition times between thawing and freezing) between temperature phases does not reflect the real situation on thawing Arctic soils. However, it is possible that the very high-frequency measurement of CO₂ fluxes used by our study and the study of Ludwig et al. (2006) simply made visible that CO₂ fluxes in Arctic soils fluctuate much more than previously perceived. The same holds true for the generalizability of the conclusions obtained in incubation experiments with small amounts of soil to the reduction of CO₂ release with increasing number of freeze-thaw cycles. At least, it cannot be excluded

that factors such as the presence of temperature and matter gradients in the soil profile, soil movements due to cryoturbation, and the diverse activities of plants alter the effects of freeze-thaw cycles on CO₂ release in the field (Mauritz et al., 2021; Olid et al., 2020; Treat et al., 2021). Therefore, the focus of future investigations should be to clarify exactly this.

Supplementary data to this article can be found online at <https://doi.org/10.1016/j.scitotenv.2023.161943>.

CRediT authorship contribution statement

JS, PS and MH designed the study. MG provided the soil. MH did the measurements. All authors discussed the results and contributed substantially to the manuscript.

Data availability

Data will be made available on request.

Declaration of competing interest

The authors declare no competing interests.

Acknowledgments

Special thanks to Mathias Lück (ZALF) for help with measurement and experimental setup. The work was funded by the German Research Foundation (DFG), grant number SCHA 1822/12-1 to Jörg Schaller.

References

- Alfredsson, H., Clymans, W., Hugelius, G., Kuhry, P., Conley, D.J., 2016. Estimated storage of amorphous silica (ASI) in soils of the circum-Arctic tundra region. *Glob. Biogeochem. Cycle* 30, 479–500.
- Anderson, T.R., Hawkins, E., Jones, P.D., 2016. CO₂, the greenhouse effect and global warming: from the pioneering work of Arrhenius and Callendar to today's Earth System Models. *Endeavour* 40, 178–187.
- Canadell, J.G., Monteiro, P.M., Costa, M.H., Da Cunha, L.C., Cox, P.M., Alexey, V., Henson, S., Ishii, M., Jaccard, S., Koven, C., Lohila, A., Patra, P., Piao, S., Rogelj, J., Syampungani, S., Zaehle, S., Zickfeld, K., 2021. Global carbon and other biogeochemical cycles and feedbacks. In: Masson-Delmotte, V., Zhai, P., Pirani, A., Connors, S., Péan, C., Berger, S., Caud, N., Chen, Y., Goldfarb, L., Gomis, M., Huang, M., Leitzell, K., Lonnoy, E., Matthews, J., Maycock, T., Waterfield, T., Yelekçi, O., Yu, R., Zhou, B. (Eds.), *Climate Change 2021: The Physical Science Basis. Contribution of Working Group I to the Sixth Assessment Report of the Intergovernmental Panel on Climate Change*. Cambridge University Press, Cambridge, United Kingdom, pp. 673–816.
- Göckede, M., Kittler, F., Kwon, M.J., Burjack, I., Heimann, M., Kolle, O., Zimov, N., Zimov, S., 2017. Shifted energy fluxes, increased Bowen ratios, and reduced thaw depths linked with drainage-induced changes in permafrost ecosystem structure. *Cryosphere* 11, 2975–2996.
- Göckede, M., Kwon, M.J., Kittler, F., Heimann, M., Zimov, N., Zimov, S., 2019. Negative feedback processes following drainage slow down permafrost degradation. *Glob. Chang. Biol.* 25, 3254–3266.
- Grogan, P., Michelsen, A., Ambus, P., Jonasson, S., 2004. Freeze-thaw regime effects on carbon and nitrogen dynamics in sub-arctic heath tundra mesocosms. *Soil Biol. Biochem.* 36, 641–654.
- Hartley, I.P., Hopkins, D.W., Sommerkorn, M., Wookey, P.A., 2010. The response of organic matter mineralisation to nutrient and substrate additions in sub-arctic soils. *Soil Biol. Biochem.* 42, 92–100.
- Henry, H.A., 2008. Climate change and soil freezing dynamics: historical trends and projected changes. *Clim. Chang.* 87, 421–434.
- Heslop, J.K., Winkel, M., Walter Anthony, K.M., Spencer, R.G.M., Podgorski, D.C., Zito, P., Kholodov, A., Zhang, M., Liebner, S., 2019. Increasing organic carbon biolability with depth in Yedoma permafrost: ramifications for future climate change. *J. Geophys. Res. Biogeosci.* 124, 2021–2038.
- Hömberg, A., Obst, M., Knorr, K.-H., Kalbitz, K., Schaller, J., 2020. Increased silicon concentration in fen peat leads to a release of iron and phosphate and changes in the composition of dissolved organic matter. *Geoderma* 374, 114422.
- Hömberg, A., Broder, T., Knorr, K.-H., Schaller, J., 2021. Divergent effect of silicon on greenhouse gas production from reduced and oxidized peat organic matter. *Geoderma* 386, 114916.
- Hugelius, G., Strauss, J., Zubrzycki, S., Harden, J.W., Schuur, E., Ping, C.-L., Schirmermeister, L., Grosse, G., Michaelson, G.J., Koven, C.D., 2014. Estimated stocks of circumpolar permafrost carbon with quantified uncertainty ranges and identified data gaps. *Biogeosciences* 11, 6573–6593.
- Kahlenberg, L., Lincoln, A., 1898. Solutions of silicates of the alkalis. *J. Phys. Chem.* 2, 77–90.

- Kim, D.G., Vargas, R., Bond-Lamberty, B., Turetsky, M.R., 2012. Effects of soil rewetting and thawing on soil gas fluxes: a review of current literature and suggestions for future research. *Biogeosciences* 9, 2459–2483.
- Kumar, A., Marcolli, C., Peter, T., 2019. Ice nucleation activity of silicates and aluminosilicates in pure water and aqueous solutions—part 2: quartz and amorphous silica. *Atmos. Chem. Phys.* 19, 6035–6058.
- Kurganova, I., Teepe, R., Lofffield, N., 2007. Influence of freeze-thaw events on carbon dioxide emission from soils at different moisture and land use. *Carbon Balance Manag.* 2, 1–9.
- Lipson, D.A., Schmidt, S.K., Monson, R.K., 2000. Carbon availability and temperature control the post-snowmelt decline in alpine soil microbial biomass. *Soil Biol. Biochem.* 32, 441–448.
- Livingston, G., Hutchinson, G., 1995. Enclosure-based measurement of trace gas exchange: applications and sources of error. *Biogenic Trace Gases: Measuring Emissions From Soil and Water*. 51, pp. 14–51.
- Loiko, S.V., Pokrovsky, O.S., Raudina, T.V., Lim, A., Kolesnichenko, L.G., Shirokova, L.S., Vorobyev, S.N., Kirpotin, S.N., 2017. Abrupt permafrost collapse enhances organic carbon, CO₂, nutrient and metal release into surface waters. *Chem. Geol.* 471, 153–165.
- Ludwig, B., Teepe, R., de Gerenyu, V.L., Flessa, H., 2006. CO₂ and N₂O emissions from gleyic soils in the Russian tundra and a German forest during freeze–thaw periods—a microcosm study. *Soil Biol. Biochem.* 38, 3516–3519.
- Mann, P.J., Strauss, J., Palmtag, J., Dowdy, K., Ogneva, O., Fuchs, M., Bedington, M., Torres, R., Polimene, L., Overduin, P., 2022. Degrading permafrost river catchments and their impact on Arctic Ocean nearshore processes. *Ambio* 51, 439–455.
- Mauritz, M., Pegoraro, E., Ogle, K., Ebert, C., Schuur, E.A.G., 2021. Investigating thaw and plant productivity constraints on old soil carbon respiration from permafrost. *J. Geophys. Res. Biogeosci.* 126.
- Mavi, M.S., Marschner, P., Chittleborough, D.J., Cox, J.W., Sanderman, J., 2012. Salinity and sodicity affect soil respiration and dissolved organic matter dynamics differentially in soils varying in texture. *Soil Biol. Biochem.* 45, 8–13.
- Mueller, C.W., Rethemeyer, J., Kao-Kniffin, J., Löppmann, S., Hinkel, K.M., Bockheim, G.J., 2015. Large amounts of labile organic carbon in permafrost soils of northern Alaska. *Glob. Chang. Biol.* 21, 2804–2817.
- Olid, C., Klaminder, J., Monteux, S., Johansson, M., Dorrepaal, E., 2020. Decade of experimental permafrost thaw reduces turnover of young carbon and increases losses of old carbon, without affecting the net carbon balance. *Glob. Chang. Biol.* 26, 5886–5898.
- Ouyang, W., Lai, X., Li, X., Liu, H., Lin, C., Hao, F., 2015. Soil respiration and carbon loss relationship with temperature and land use conversion in freeze–thaw agricultural area. *Sci. Total Environ.* 533, 215–222.
- Payandi-Rolland, D., Shirokova, L.S., Nakhle, P., Tesfa, M., Abdou, A., Causserand, C., Lartiges, B., Rols, J.-L., Guérin, F., Bénéthéz, P., Pokrovsky, O.S., 2020. Aerobic release and biodegradation of dissolved organic matter from frozen peat: effects of temperature and heterotrophic bacteria. *Chem. Geol.* 536.
- R_Core_Team, 2021. R: A Language and Environment for Statistical Computing.
- Rantanen, M., Karpechko, A.Y., Lipponen, A., Nordling, K., Hyvärinen, O., Ruosteenoja, K., Vihma, T., Laaksonen, A., 2022. The Arctic has warmed nearly four times faster than the globe since 1979. *Commun. Earth Environ.* 3, 1–10.
- Reithmaier, G.M.S., Knorr, K.H., Armhold, S., Planer-Friedrich, B., Schaller, J., 2017. Enhanced silicon availability leads to increased methane production, nutrient and toxicant mobility in peatlands. *Sci. Rep.* 7, 8728.
- Rillig, M.C., Hoffmann, M., Lehmann, A., Liang, Y., Lück, M., Augustin, J., 2021. Microplastic fibers affect dynamics and intensity of CO₂ and N₂O fluxes from soil differently. *Microplast. Nanoplast.* 1, 1–11.
- Sapronov, D., 2021a. The CO₂ emission during laboratory freezing-thawing of soils from various natural zones of Russia. *Eurasian Soil Sci.* 54, 1196–1205.
- Sapronov, D.V., 2021b. The CO₂ emission during laboratory freezing-thawing of soils from various natural zones of Russia. *Eurasian Soil Sci.* 54, 1196–1205.
- Schaefer, K., Jafarov, E., 2016. A parameterization of respiration in frozen soils based on substrate availability. *Biogeosciences* 13, 1991–2001.
- Schaller, J., Fauchere, S., Joss, H., Obst, M., Goeckede, M., Planer-Friedrich, B., Peiffer, S., Gilfedder, B., Elberling, B., 2019. Silicon increases the phosphorus availability of Arctic soils. *Sci. Rep.* 9, 449.
- Schaller, J., Cramer, A., Carminati, A., Zarebanadkouki, M., 2020. Biogenic amorphous silica as main driver for plant available water in soils. *Sci. Rep.* 10, 2424.
- Schaller, J., Puppe, D., Kaczorek, D., Ellerbrock, R., Sommer, M., 2021. Silicon cycling in soils revisited. *Plants* 10, 295.
- Schimel, J.P., Clein, J.S., 1996. Microbial response to freeze-thaw cycles in tundra and taiga soils. *Soil Biol. Biochem.* 28, 1061–1066.
- Schuur, E., McGuire, A., Schädel, C., Grosse, G., Harden, J., Hayes, D., Hugelius, G., Koven, C., Kuhry, P., Lawrence, D., Natali, S., Olefeldt, D., Romanovsky, V., Schaefer, K., Turetsky, M., Treat, C., Vonk, V., 2015. Climate change and the permafrost carbon feedback. *Nature* 520, 171–179.
- Stimmler, P., Priemé, A., Elberling, B., Goeckede, M., Schaller, J., 2022. Arctic soil respiration and microbial community structure driven by silicon and calcium. *Sci. Total Environ.* 838, 156152.
- Stimmler et al., n.d. Stimmler P, Goeckede M, Elberling B, Natali S, Kuhry P, Perron N, Lacroix F, Hugelius G, Sonnentag O, Strauss J, Minions C, Sommer M, Schaller J. Pan-Arctic soil element bioavailability estimations. *Earth System Science Data* in revision.
- Stocker, T., Qin, D., Plattner, G.-K., Tignor, M., Allen, S.K., Boschung, J., Nauels, A., Xia, Y., Bex, V., Midgley, P.M., 2014. *Climate Change 2013: The Physical Science Basis*. Cambridge University Press, Cambridge, UK, and New York.
- Strauss, J., Schirrmeyer, L., Grosse, G., Fortier, D., Hugelius, G., Knoblauch, C., Romanovsky, V., Schädel, C., von Deimling, T.S., Schuur, E.A., 2017. Deep Yedoma permafrost: a synthesis of depositional characteristics and carbon vulnerability. *Earth-Sci. Rev.* 172, 75–86.
- Treat, C.C., Jones, M.C., Alder, J., Sannel, A.B.K., Camill, P., Frolking, S., 2021. Predicted vulnerability of carbon in permafrost peatlands with future climate change and permafrost thaw in Western Canada. *J. Geophys. Res. Biogeosci.* 126, e2020JG005872.
- Walker, D., Bockheim, J., Chapin, F., Eugster, W., Nelson, F., Ping, C., 2001. Calcium-rich tundra, wildlife, and the “Mammoth Steppe”. *Quat. Sci. Rev.* 20, 149–163.
- Wang, J., Song, C., Hou, A., Wang, L., 2014. CO₂ emissions from soils of different depths of a permafrost peatland, Northeast China: response to simulated freezing–thawing cycles. *J. Plant Nutr. Soil Sci.* 177, 524–531.
- Whittinghill, K.A., Hobbie, S.E., 2012. Effects of pH and calcium on soil organic matter dynamics in Alaskan tundra. *Biogeochemistry* 111, 569–581.
- Zhang, J., Hong, J., Wei, D., Wang, X., 2022. Severe freezing increases soil respiration during the thawing period: a meta-analysis. *Eur. J. Soil Sci.* 73, e13161.

Supplementary information to:

Arctic soil CO₂ release during freeze-thaw cycles modulated by silicon and calcium

Authors

Jörg Schaller^{1}, Peter Stimmeler¹, Mathias Göckede², Jürgen Augustin¹, Fabrice Lacroix^{2, 3} and Mathias Hoffmann¹*

Affiliations

¹ Leibniz Center for Agricultural Landscape Research (ZALF), 15374 Müncheberg, Germany

² Max Planck Institute for Biogeochemistry, Jena, Germany

³ Climate and Environmental Physics, University of Bern, Bern, Switzerland

*Corresponding author Email: Joerg.Schaller@zalf.de

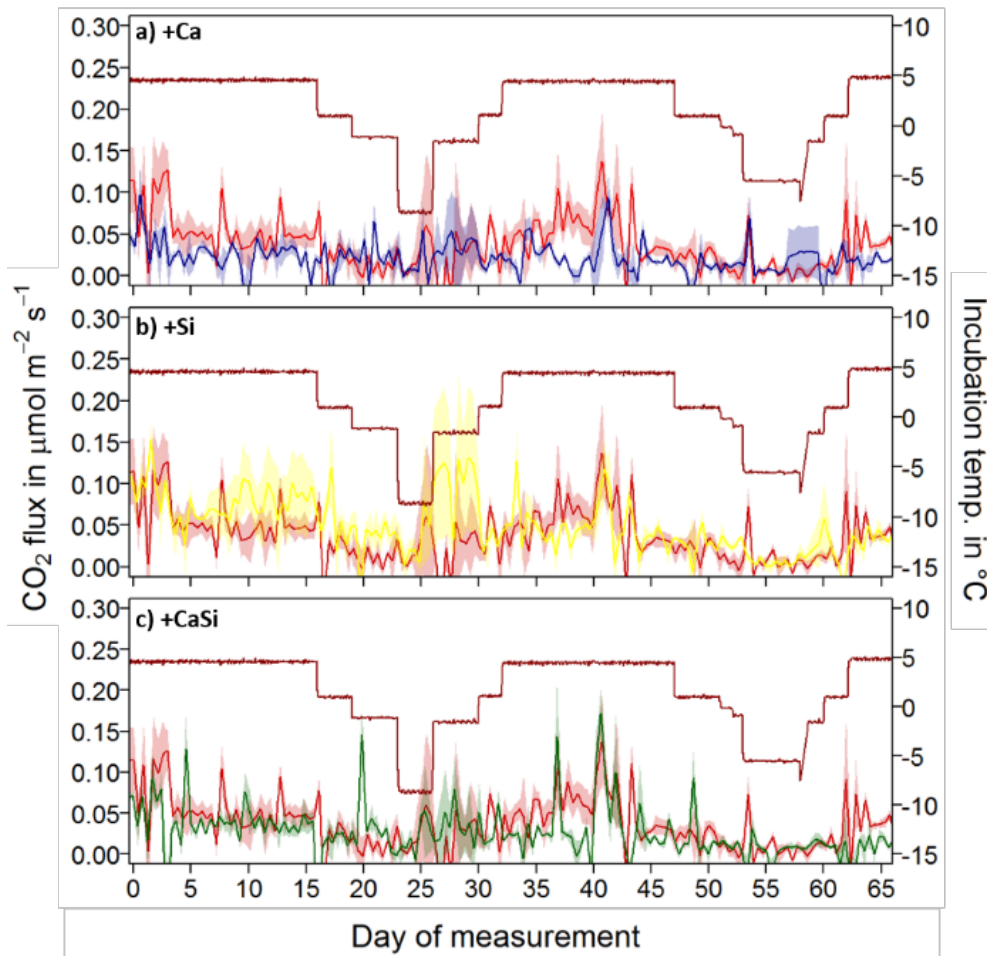


Fig. S1: Measured CO₂ flux dynamic \pm SD (shaded area) for a) +Ca (blue), b) +Si (yellow) and c) +CaSi (green) vs. control (bright red line), each averaged over the four replicates per treatment. Solid, dark red line represents the temperature during the incubation period.

3.2.4 Study 4: Arctic soil respiration and microbial community structure driven by silicon and calcium

Stimmler, Priemé, et al. (2022)

Published 10.09.2022 in:

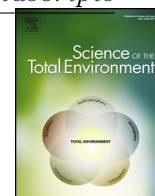
Science of the Total Environment, Volume 838, Part 2, 161943

(<http://dx.doi.org/10.1016/j.scitotenv.2022.156152>)



Contents lists available at ScienceDirect

Science of the Total Environment

journal homepage: www.elsevier.com/locate/scitotenv

Arctic soil respiration and microbial community structure driven by silicon and calcium



Peter Stimmler^{a,*}, Anders Priemé^{b,c}, Bo Elberling^{c,d}, Mathias Goeckede^e, Joerg Schaller^{a,*}

^a Leibniz Centre for Agricultural Landscape Research (ZALF), Eberswalder Str. 84, 15374 Müncheberg, Germany

^b Department of Biology, University of Copenhagen, 1350 Copenhagen, Denmark

^c Center for Permafrost, Department of Geosciences and Natural Resource Management, University of Copenhagen, 1350 Copenhagen, Denmark

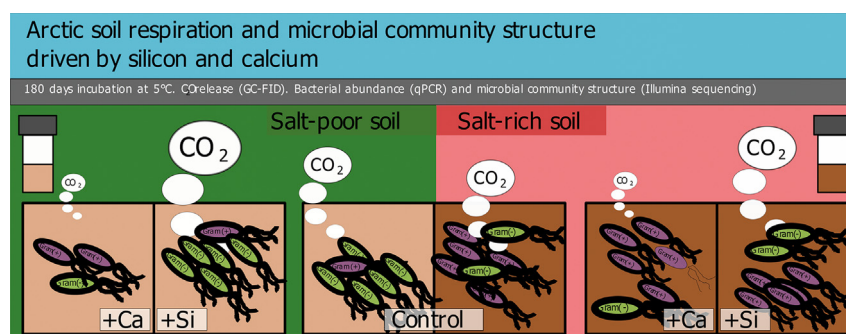
^d Department of Geosciences and Natural Resource Management, University of Copenhagen, 1350 Copenhagen, Denmark

^e Max Planck Institute for Biogeochemistry, 07701 Jena, Germany

HIGHLIGHTS

- Amorphous silica (Si) positively and Ca negatively affect microbial community.
- Spore-forming bacteria increased by Si.
- Ca promotes spore-forming bacteria.
- Ca decreased and Si increased CO₂ production by altering nutrient availability or MCS.

GRAPHICAL ABSTRACT



ARTICLE INFO

Editor: Wei Shi

Keywords:

Carbon cycle
Greenhouse gas emissions
Halo-tolerance
Microbial community structure
Salinity
Silica
Permafrost

ABSTRACT

Global warming is most pronounced in the Arctic region. Greenhouse gas (GHG) release from Arctic soils increase due to global warming. By this, the Arctic may change from currently being a carbon sink to a future source. To improve accurate predictions of future GHG release from Arctic soils, it is important to unravel factors controlling both the microbial community structure and activity. Soil microbial activity is important for Arctic greenhouse gas production, but depends on soil conditions such as salinity being increased by calcium (Ca) and decreased by amorphous silica (Si) potentially enhancing water availability. In the Arctic, climate changes may alter salinity by changing Si and Ca concentrations upon permafrost thaw as a result of global warming with Si potentially decreasing and Ca potentially increasing salinity. Here, we show that higher Si concentration increased and higher Ca concentrations decreased the microbial CO₂ production for both a salt-poor and a salt-rich soil from Greenland. In the salt-rich soil, Si amendment increased CO₂ production and the abundance of gram-negative bacteria. However, the bacterial community became dominated by spore-forming gram-positive Firmicutes and Actinobacteria. The CO₂ release from soils was directly affected by the abundance of bacteria and fungi, and their community structure. Our results highlight the importance of the soil Si and Ca concentration on organic carbon turnover by strongly changing microbial abundance and community structure, with consequences for CO₂ release in the Arctic. Consequently, Ca and Si and their relation to Arctic soil microbial community structure has to be considered when estimating pan-Arctic carbon budgets.

* Corresponding authors.

E-mail addresses: peter.stimmler@zalf.de (P. Stimmler), aprieme@bio.ku.dk (A. Priemé), be@ign.ku.dk (B. Elberling), mgoeck@bgc-jena.mpg.de (M. Goeckede), joerg.schaller@zalf.de (J. Schaller).

<http://dx.doi.org/10.1016/j.scitotenv.2022.156152>

Received 17 December 2021; Received in revised form 18 March 2022; Accepted 18 May 2022

Available online 21 May 2022

0048-9697/© 2022 Elsevier B.V. All rights reserved.

1. Introduction

The increased greenhouse gas (GHG) release from Arctic soils due to global warming is dominated by CO₂ (Schädel et al., 2016). To facilitate accurate simulations of future GHG release from Arctic soils, it is important to unravel factors controlling both the microbial community structure and activity (Coolen and Orsi, 2015). Abiotic factors including availability of nutrients like phosphorous (DeForest and Scott, 2010) and composition of the organic matter (Biasi et al., 2005), have been shown to change microbial community structure in Arctic soils and by this GHG emissions. The carbon (C) cycling in Arctic soils is strongly influenced by the microbial community structure and its metabolic capacities (Monteux et al., 2020; Qin et al., 2021). Thawing permafrost mediated by ongoing climate change has been shown to lead to altered microbial community structure and a metabolic shift from survival in frozen soil to enhanced metabolic activity in thawed soil. Thawing leads to an up regulation of microbial C and nitrogen (N) cycling pathways (Mackelprang et al., 2011), while further warming after thawing increases the amount of enzymes involved in soil organic matter decomposition (Jansson and Hofmøckel, 2020). By this, the Arctic may change from currently being a C sink (Virkkala et al., 2021) to a future source (Hugelius et al., 2020), which may accelerate global warming.

Arctic soil microorganisms are challenged by large fluctuations in environmental conditions and stressors like drought, freezing and salinity. Salinity can be high in Arctic soils, particular in high Arctic desert soils and at sub-zero temperatures, the latter due to salt exclusion during freezing. The liquid water between ice and soil is a main habitat of Eutectophiles (Deming, 2002) that can be physiological active until $-20\text{ }^{\circ}\text{C}$ (Rivkina et al., 2000). The concentration of elements like calcium (Ca) decreases the freezing point of water and leads to liquid water with high salinity between ice and soil particles (Jessen et al., 2014). Amorphous silica (Si) is the main source for available silica in soils (Schaller et al., 2021) and decreases freezing temperature, too (Ishizaki et al., 1996). Microbes have evolved different strategies to enhance survival and sustain activity e.g. during freezing, thawing, and at high salinity. Modified membrane fluidity ensures viscosity at low temperatures (Denich et al., 2003), cold shock proteins prevent formation of secondary mRNA structures (Suetin et al., 2009) and osmolytes enable microbes to be metabolic active in salt-rich environments (Sleator and Hill, 2002).

A partial thaw of the uppermost permafrost layer of Arctic soils due to climate change induced by thermic insolation and higher air temperatures may increase the concentration of Si or Ca depending on location and geochemistry of specific regions of the Arctic (Stimmler et al., in preparation; Alfredsson et al., 2016; Walker et al., 2001). This may change the microbial community structure of Arctic soils, because of the potential effects of both elements on microbes (Song et al., 2021; Ye et al., 2016) and will potentially alter microbial GHG emissions linked to changes in the concentration of Si and Ca (Schaller et al., 2019). Soluble ions like Ca increase osmolytic stress for microbes. In contrast to Ca, Si may decrease salt stress for microbes as it was shown already for plants (Coskun et al., 2016; Yan et al., 2021).

To better understand the effect of Si and Ca on soil microbial community structure and activity, and their relation to salt conditions in soils we incubated a Greenlandic soil with high extractable Ca concentration (salt-rich) and a soil with low extractable Ca concentration (salt-poor) under different soil Si and Ca concentrations. In these experiments, we analyzed the responses of the microbial community structure and the corresponding CO₂ production rates. Our hypotheses were: (i) microbial community structure differs between original salt-rich and salt-poor Arctic soils, (ii) Ca increases salinity stress and therefore promotes a halotolerant microbial community structure, (iii) Si reduces salinity stress and leads to halo-intolerant microbial community structure, and (iv) Ca and Si concentration can interact in relation to the effects on microbial community structure, and corresponding CO₂ production rate.

2. Materials and methods

2.1. Incubation experiments

For each sample 5 g soil were incubated at 5 °C in a 25-mL glass vial with 2 mL of deionized water. To simulate Ca induced salt stress, we incubated with +0, +5, +10, +15 mg Ca g⁻¹ DW (from CaO, pH adapted with HCl to initial soil pH). The Ca treatments are equal to growth conditions of slightly halophilic (1.0–1.2 M NaCl), moderately halophilic (1.0–1.2 to 2.0–2.5 M NaCl) and extremely halophilic (2.0–2.5 M NaCl) bacteria (Zahran, 1997). To investigate salt stress reduction by Si, we added +0, +3, +6, +10 mg Si g⁻¹ DW (from Si fertilizer Aerosil-300, Evonik, Germany). The different treatments did not change soil pH. In addition, we included controls involving soil incubated with 1 mg g⁻¹ DW (Peary Land) or 3 mg g⁻¹ DW (Disko) Na₂HPO₄. This phosphorus addition treatment was done to separate a direct Si effect from an indirect effect of Si via Si mobilizing phosphorus as shown before (Schaller et al., 2019). A reference incubation without added water was also included.

2.2. DNA isolation, PCR and preparation for amplicon sequencing

Raw soil material was freeze dried and ground with a mill until a fine powder was obtained using a Retsch, MM 2000 mill. Every sample was replicated three times. DNA was isolated from 100 mg material per sample using “DNeasy Power Soil Pro Kit” (Qiagen, Vedbæk, Denmark). The success of the DNA isolations was checked on a 0.7% agarose gel.

Amplicon sequencing libraries were prepared using a two-step PCR, targeting 16S rRNA gene V3-V4 regions for prokaryotic communities and the ITS2 for fungal communities. First PCR amplification of the V3-V4 region was performed using primers Uni341F (5'-CCTAYGGGRBGCASCAG-3') and Uni806R (5'-GGACTACNNGGGTATCTAAT-3') (Caporaso et al., 2011). PCR amplification of ITS2 was performed with the primers gITS7 (5'-GTGARTCATCGARTCTTG-3') (Ihrmark et al., 2012; Nguyen et al., 2016) and ITS4ngs (5'-TCCGTAGGTGAACCTGCGG-3').

PCR products were checked on a 1% agarose gel. First PCR amplification products were purified using HighPrep PCR clean-up (MagBio Genomics, Galthersburg, USA). A second PCR reaction was performed to add Illumina sequencing adapters and sample-specific dual indexes (IDT Integrated DNA technologies, Coralville, USA) using PCRBio HiFi (PCR Biosystems Ltd., London, UK) for 15 amplification cycles. Products from the second PCR were purified with HighPrep PCR Clean Up System, as described for the first PCR. Sample concentrations were normalized using the SequalPrep Normalization Plate Kit (Thermo Fisher Scientific, Hvidovre, Denmark). The libraries were pooled and up-concentrated using DNA Clean and Concentrator-5 Kit (Zymo Research, Irvine, USA). The concentration of the pooled PCR products was determined using a Qubit 2.0 Fluorometer (Life Technologies, Carlsbad, USA). The libraries were denatured and sequenced following the manufacturer's instructions using a 250 paired-end Illumina MiSeq platform (Illumina, San Diego, USA). Raw data on DNA sequences for bacteria and fungi can be found on Erda.dk (<https://sid.erd.dk/sharelink/BvOzKefXwG> for the 16S data and <https://sid.erd.dk/sharelink/AriM6hncZ4> for the fungal ITS2 data).

2.3. Generation of operational taxonomic units (OTUs)

Sequences were trimmed of primer sequences and barcodes and assembled using Usearch (Edgar, 2010). Sequences which could not be assembled, singletons, chimeras, and sequences with a quality score less than 25 were discarded. Sequences were denoised to generate operational taxonomic units (OTUs). The 16S rRNA gene fragments and ITS2 sequences were mapped back with a 97% similarity threshold and were classified using the SILVA (Pruesse et al., 2007) and UNITE (Abarenkov et al., 2010) database, respectively.

2.4. qPCR

Prokaryotic 16S rRNA gene and (fungal) ITS2 copy numbers were estimated using quantitative PCR (qPCR). The Uni341F (5'-CCTAYGGGRBGCASCAG-3') and 518R (5'-ATTACCGCG GCTGCTGG-3') (Muyzer et al., 1993) primers were used for 16S rRNA gene quantification. The PCR protocol involved a total volume of 20 μ L containing 10 μ L of 2 \times Brilliant III Ultra-Fast SYBR[®] Green QPCR Master Mix (Agilent Technologies, Cedar Creek, TX, USA), 1 μ L of forward and reverse primers (final concentration 10 μ M), 1 μ L of a diluted DNA template, and 7 μ L of ddH₂O. Cycling conditions consisted of 2 min at 95 °C followed by 40 cycles of denaturation at 95 °C for 5 s and combined annealing and extension at 60 °C for 20 s. In order to estimate the abundance of fungal ITS2 we used the primers gITS7 and ITS4ngs. The PCR setup and cycling conditions were the same as for 16S rRNA. All qPCR assays included three technical replicates per sample. No template controls (NTC) for all assays were used to exclude the possibility of contamination. All reactions were carried out in LightCycler[®] 96 Instrument (Roche Life Science, Hvidovre, Denmark). Prior to gene quantification, all samples were diluted 100 times in order to avoid inhibition of amplification efficiency. Known quantities of a pUC19 plasmid with the cloned gene of interest were used as standards in the qPCR assays. Partial 16S rRNA gene was cloned from *Escherichia coli*, while ITS2 region was cloned from *Aureobasidium pullulans* (Dahl et al., 2017); see SI text for the DNA sequence of the standards. In order to account for non-target sequences such as DNA co-extracted from chloroplasts and mitochondria, final qPCR results were adjusted for amplified based on the relative abundance of chloroplasts and mitochondria DNA (less than 1.51 \pm 0.37% of total sequence reads in any sample) in the 16S rRNA gene amplicon sequencing data.

We performed permutational multivariate analysis of variance based on Bray–Curtis dissimilarity matrices to test treatment differences (10,000 permutations) using the ANOSIM function in Primer7 (Clarke and Gorley, 2015). Primer7 was also used to generate metric multidimensional (mMDS) plots based on the Bray–Curtis dissimilarity matrices.

2.5. Statistics

For Disko soil samples the relative abundance of the four most common bacterial phyla (Acidobacteria, Actinobacteria, Chloroflexi, Firmicutes and Proteobacteria) and the three most common fungal phyla (Ascomycota, Basidiomycota and Mortierellomycota) were calculated. Bacterial taxa assigned to Actinobacteria, Chloroflexi and Firmicutes (excluding members of Negativicutes and Halanaerobiales, which in contrast to the majority of Firmicutes are gram-negative; reads assigned to Negativicutes were found in negligible numbers in the Peary Land soil and in small numbers in the Disko soil, while no reads were assigned to members of Halanaerobiales (Tables S1–S4) were summarized as gram-positive bacteria, while all other bacterial taxa were summarized as gram-negative bacteria (see Megrian et al. 2020 for a discussion of the division of gram negative and positive bacteria). Descriptive statistics of relative and absolute bacterial and fungal abundance (minimum, maximum, median, standard deviation and first and third quarter) were calculated in R Studio (version 1.2.5033, 2019, RStudio, Inc) using the function “favstats” from the package “mosaic” (version 1.8.3). Boxplots were plotted with the package “graphics” (version 3.6.3). The data was analyzed using an ANOVA, followed by a pairwise Tukey-HSD as post-hoc test (package “stats”, version 3.6.3). Linear regression of samples were calculated and plotted by the function “stator” from the package “ggpubr” (version 0.4.0) and “ggplot2” (version 3.6.3). Comparison of fungal and bacterial abundance was done with an undirected *t*-test on a 95% confidence interval using the function “t.test” from the package “mosaic” (version 1.8.3). For quantifying biodiversity of the microbial community structure of the original soil the Shannon Index was calculated using the function “diversity” from the package “vegan” (version 2.5–7). The structural equation model was generated using the “lavaan” package (version 0.6–9) and visualized using the “semPlot” package (version 1.1.2).

3. Results

3.1. Characterization of sampling sites

The effects of Si and Ca on microbial community structure and CO₂ production rates were analyzed on incubated soils from two sites in Greenland; Brønlundhus, Peary Land, North Greenland (82° 6' N, 32° 33' W) representing a carbonate-based soil and Disko, West Greenland (69° 15' N, 53° 34' W) representing an weathered basaltic soil. In Disko the vegetation cover consists of dwarf shrubs (*Betula nana*, *Vaccinium uliginosum* and *Salix glauca*). The soils are characterized by a low pH at ~5.6, high alkaline extractable Si (5.2 mg g⁻¹ dry weight (DW)), low Mehlich-3 extractable Ca (1.7 mg g⁻¹ DW) and low Mehlich-3 extractable P (0.13 mg g⁻¹ DW). The total P concentration in the soil was 1.5 mg g⁻¹ DW. The total C was 16.5%, the total N 0.8%, the water content 20.8% and conductivity was low with 72 μ S cm⁻¹. Peary Land is a dry polar desert with a thin soil cover of 5–20 cm and very spare vegetation cover. The soil showed a high pH-value at ~8.4 and contained low alkaline extractable Si (1.4 mg g⁻¹ DW), but high Mehlich-3 extractable Ca (15.6 mg g⁻¹ DW). Mehlich-3 extractable P was very low (0.01 mg g⁻¹ DW), and soil total P concentration was 0.6 mg g⁻¹ DW. The total C (3.1%), total N (0.03%) and water content (0.7%) were low, the conductivity was high (2253 μ S cm⁻¹).G.

3.2. Si and Ca affect absolute microbial abundance

In the salt-poor Disko soil, the abundance of bacterial 16S rRNA gene was significant (undirected *t*-test: *t* = 5.24, *P* < 0.001, *df* = 68) higher than fungal ITS2 copy number. On average, 1.7 \times 10¹² g⁻¹ DW bacterial 16S rRNA gene copies were found, compared to 1.3 \times 10⁶ g⁻¹ DW fungal ITS2 copies. All Ca treatments (Fig. 1a) lead to a significant decrease (*P* < 0.001, *df* = 6, *F* = 15.6 + 53) of the bacterial 16S rRNA gene copy number from 3.1 \times 10¹² \pm 1.7 \times 10¹² g⁻¹ DW at 1.7 mg Ca g⁻¹ DW to 1.6 \times 10¹⁰ \pm 1.6 \times 10¹⁰ g⁻¹ DW at 1.7 + 15 mg Ca g⁻¹ DW as mean of all Si levels. Water only (2.6 \times 10¹² \pm 2.4 \times 10¹² g⁻¹ DW) and P addition (3.9 \times 10¹² \pm 2.7 \times 10¹² g⁻¹ DW) treatments did not differ from the non-amended reference (no addition of water, Si and Ca with 4.4 \times 10¹² \pm 1.7 \times 10¹² g⁻¹ DW). Compared to the bacterial abundance, fungal ITS2 copy numbers decreased less dramatically from 1.9 \times 10⁶ \pm 1.6 \times 10⁶ g⁻¹ DW for 1.7 mg Ca g⁻¹ DW to 0.5 \times 10⁶ \pm 0.2 \times 10⁶ g⁻¹ DW (*P* = 0.13, *df* = 6, *F* = 2.2) at 1.7 + 15 mg Ca g⁻¹ DW (Fig. 1b). Si addition treatments had no significant effect on bacterial or fungal abundance compared to controls (Fig. S1). The raw qPCR data including standards can be found on Erda.dk (<https://sid.erda.dk/sharelink/BvOzKefXwG> for the 16S data and <https://sid.erda.dk/sharelink/AriM6hncC4> for the fungal ITS2 data).

In the Peary Land soil, an increase in Si concentration to 1.4 + 10 mg g⁻¹ DW Si increased the bacterial 16S rRNA gene copy number significantly (*P* < 0.001, *df* = 6, *F* = 30.0) from 0.3 \pm 0.4 \times 10⁶ \pm 5.2 \pm 2.9 \times 10⁶ g⁻¹ DW, while the number of fungal ITS2 copies (*P* = 0.01, *df* = 6, *F* = 2.9) decreased from 4.6 \pm 4.0 \times 10³ to 1.7 \pm 0.8 \times 10³ g⁻¹ DW (Fig. 2). In both cases, the highest Si concentration showed copy numbers similar to those of the reference treatment without addition of water, Ca or Si (5.4 \times 10⁶ \pm 1.1 \times 10⁶ bacterial 16S rRNA gene copies g⁻¹ DW and 1.8 \times 10³ \pm 0.8 \times 10³ fungal ITS2 gene copies g⁻¹ DW). The soil Ca concentration had no significant effect on the number of fungal ITS2 copies, while the bacterial abundance was significantly higher in the water only control treatment (only water addition) (Fig. S2A and B) compared to the non-amended reference treatment (5.4 \pm 1.1 \times 10⁶ bacterial 16S rRNA gene copies g⁻¹ DW, and 1.7 \pm 0.8 \times 10⁶ fungal ITS2 gene copies g⁻¹ DW) (*P* < 0.01, *df* = 6, *F* = 5.7).

3.3. Si and Ca affect bacterial community structure

In Disko soils, we measured 3989–24,445 reads of bacterial 16S rRNA V3-V4 regions per sample averaging 15,737 \pm 4242 reads per sample. The composition of the microbial communities changed dramatically with the Si and Ca additions. In the untreated soils (reference), the most common

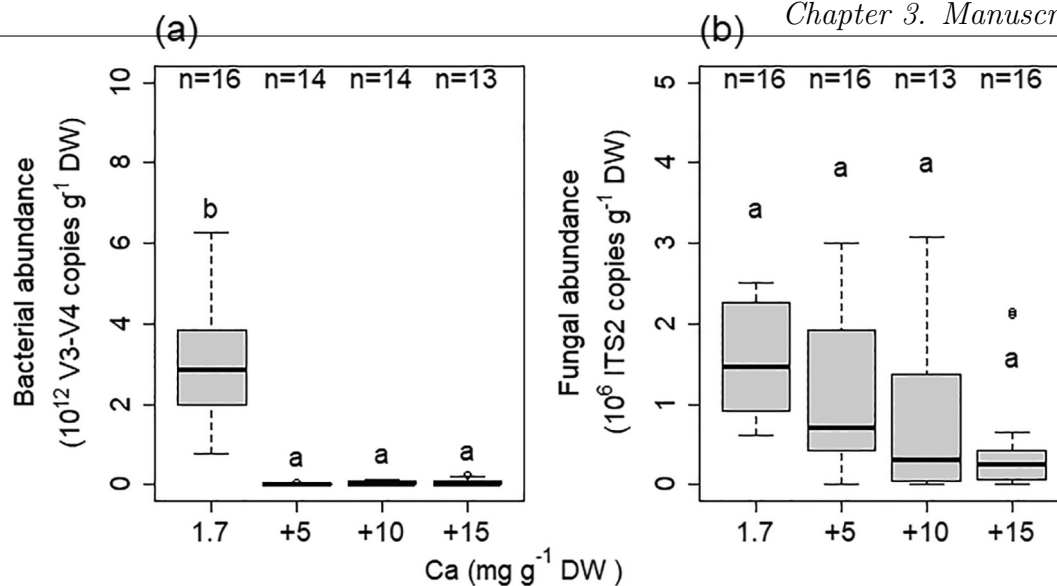


Fig. 1. The effect of Ca on copy numbers in Disko soils. (a) Bacterial 16S rRNA and (b) fungal ITS2 gene fragments in treatments using soil from Disko based on qPCR data. Data are shown as boxplots with median, 25% and 75% quartile and upper and lower whisker showing minimum and maximum values. Different letters indicate significant ($P < 0.05$) differences between treatments.

phyla were Acidobacteria, Actinobacteria, Firmicutes and Proteobacteria (alpha-, gamma-, delta-proteobacterial classes), whereas Archaea and Chloroflexi had only a minor abundance (Fig. S3). Increasing the Ca concentration had a significant (ANOSIM, $P = 0.002$) effect on the bacterial community as the community structure in treatments with elevated Ca concentration were clearly separated from those without Ca addition (Fig. S4). Increasing P availability had no significant effect on the bacterial community structure.

Increasing Ca concentration changed the microbial community structure significantly at the original Si concentration of $5.2 \text{ mg g}^{-1} \text{ DW Si}$ (no Si added). The relative abundance of Acidobacteria and Proteobacteria decreased at $1.7 + 5 \text{ mg g}^{-1} \text{ DW Ca}$ and increased with further enhanced Ca concentrations (Fig. 3a-b). In contrast, Actinobacteria (mostly represented by the order Micrococcales) and Firmicutes (mainly Clostridiales) showed the opposite pattern (Fig. 3c-d). The water-addition treatment only

significantly affected the relative abundance of Proteobacteria ($P < 0.01$, $F = 86.2$; $df = 6$) compared to the non-amended reference treatment ($5.2 \pm 2.4\%$).

A linear interdependency of different phyla to the different soil Ca concentrations was found. The relative abundance of Acidobacteria ($P < 0.001$, $R = 0.83$) and Chloroflexi ($P < 0.001$, $R = 0.77$) decreased significantly with increasing relative abundance of Firmicutes (Fig. S5a-b). In this context, the abundances of Acidobacteria and Chloroflexi varied proportional to each other ($P < 0.001$, $R = 0.91$) (Fig. S5c). A linear correlation was found, although bacterial 16S rRNA gene copies varied significantly between Ca amendments (Fig. 1).

In Peary Land soils, 10,491–64,786 reads of bacterial 16S rRNA V3-V4 regions per sample with $30,027 \pm 15,606$ reads per sample in average were measured. The diversity in original soil samples from Peary Land (Shannon Diversity Index, $H = 0.64 \pm 0.13$) showed a significant less ($P < 0.001$,

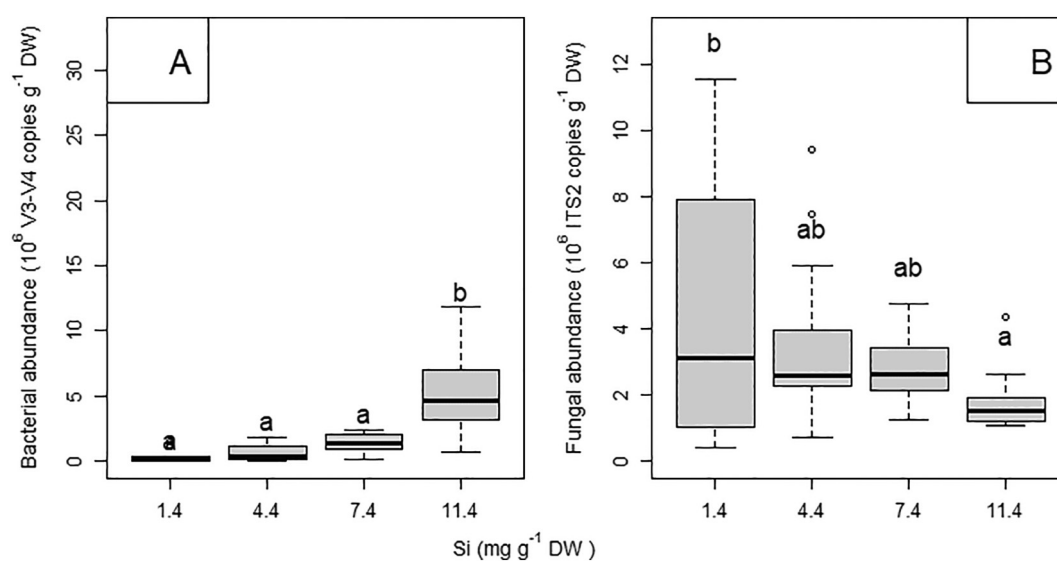


Fig. 2. The effect of Si on copy numbers in Peary Land soils. (a) Bacterial 16S rRNA and (b) fungal ITS2 gene fragments in treatments using soil from Peary Land, based on qPCR data. Shown are the boxplots with median, 25% and 75% quartile and upper and lower whisker. Different letters indicate significant difference between treatments at 5% significance level.

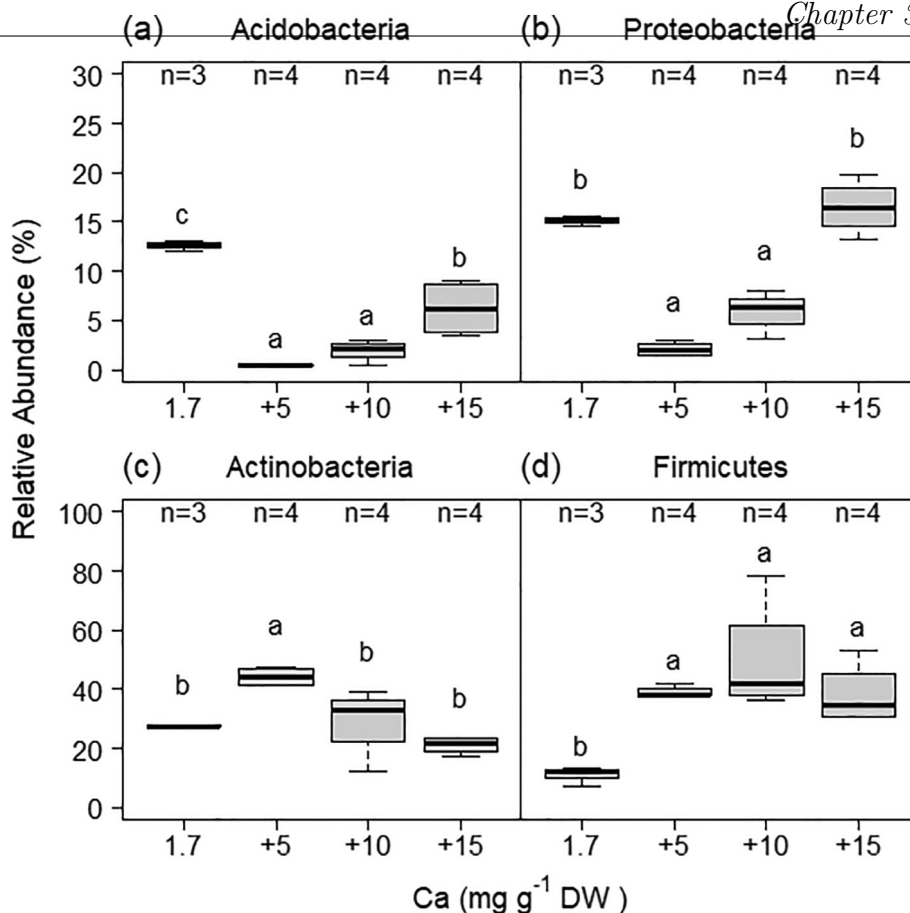


Fig. 3. Relative abundances of the most common bacterial phyla at different Ca amendments in soil samples from Disko (a) Acidobacteria, (b) Proteobacteria, (c) Actinobacteria, and (d) Firmicutes. The boxes represent the treatments at the original Si concentration of $5.2 \text{ mg g}^{-1} \text{ DW}$. Data are shown as boxplots with median, 25% and 75% quartile and upper and lower whisker showing minimum and maximum values. Different letters indicate significant difference between treatments at 5% significance level.

$df = 6, t = 43.9$) diverse taxonomic community compared to those from Disko ($H = 3.48 \pm 0.02$). The most common OTUs in the untreated (reference treatment) Peary Land soil were representatives of the phyla Firmicutes, Actinobacteria, Bacteroidetes, and Proteobacteria (Fig. S6). The P addition increased the share of Bacteroidetes and Chloroflexi. The mMDS cluster analysis showed no significant differences within the different Ca and Si treatments (Fig. S7). The relative abundance of Firmicutes decreased significantly due to the addition of water, compared to the reference in the Ca treatments ($P < 0.001, df = 6, F = 165.1$) and Si treatments ($P < 0.001, df = 6, F = 856.2$). An addition of $10 \text{ mg Ca g}^{-1} \text{ DW}$ led to a significant increase of Firmicutes ($P < 0.001, df = 6, F = 165.1$) (Fig. 4a). Moreover, at $1.4 + 6$ and $1.4 + 10 \text{ mg Si g}^{-1} \text{ DW}$, Firmicutes increased significantly ($P < 0.001, df = 6, F = 856.2$) from a relative abundance of $4.9 \pm 2.8\%$ to become the dominant phylum at $77.6 \pm 3.5\%$ (Fig. 4c). OTUs of the order Bacillales had the largest share of the Firmicutes ($93.6 \pm 16.9\%$). The Bacteroidetes and Proteobacteria decreased along with the increase of the Firmicutes. At a concentration of $15.6 + 10 \text{ mg Ca g}^{-1} \text{ DW}$, Proteobacteria decreased significantly compared to lower soil Ca concentrations ($P < 0.001, df = 6, F = 96.8$) from $61.9 \pm 12.0\%$ to $38.7 \pm 5.5\%$ (Fig. 4b). At $1.4 + 6 \text{ mg Si g}^{-1} \text{ DW}$, Proteobacteria decreased significantly in comparison to lower Si concentrations ($P < 0.001, df = 6, F = 98.53$) from $61.9 \pm 12.0\%$ to $13.6 \pm 2.0\%$ (Fig. 4d). Further, the relative abundance of gram-positive bacteria correlated positively with Si at all Ca concentrations, too (Fig. S14).

The relative abundance of Firmicutes showed a negative linear correlation with Bacteroidetes ($P < 0.001, R = -0.90$) and Proteobacteria ($P < 0.001, R = -0.94$) (Fig. S8 a-b). Furthermore, the relative abundance of

Proteobacteria was directly proportional to the relative abundance of Bacteroidetes (Fig. S8 c) ($P < 0.001, R = 0.84$).

3.4. Si and Ca affect fungal community structure

In Disko soils, we measured 3358–39,919 reads of fungal ITS2 copies per sample with $29,838 \pm 15,990$ reads per sample on average. As for the bacterial community, the fungal community structure of Disko soils was strongly affected by the soil Ca concentration (Fig. S9). In soils with no Si addition ($1.4 \text{ mg g}^{-1} \text{ DW Si}$), Ascomycota dominated, but their relative abundance decreased significantly ($P = 0.02, df = 6, F = 5.7$) from $79.8 \pm 13.8\%$ at $1.7 \text{ mg g}^{-1} \text{ DW Ca}$ to $30.0 \pm 22.8\%$ at $1.7 + 15 \text{ mg g}^{-1} \text{ DW Ca}$ (Fig. 5a). The largest share of the Ascomycota was made of the order Helotiales together with the order Sordariales. The Basidiomycota (mostly represented by the orders Agaricales and Boletales) increased significantly ($P < 0.01, df = 6, F = 8.6$) from $2.5 \pm 2.5\%$ at $1.7 \text{ mg g}^{-1} \text{ DW Ca}$ to $64.5 \pm 31.6\%$ at $1.7 + 15 \text{ mg g}^{-1} \text{ DW Ca}$ (Fig. 5b). The phylum Mortierellomycota was only represented by the species *Mortierella gemmifera*, which decreased from $11.5 \pm 2.5\%$ at $1.7 \text{ mg g}^{-1} \text{ DW Ca}$ to $1.1 \pm 2.1\%$ at $1.7 + 15 \text{ mg g}^{-1} \text{ DW Ca}$ (Fig. 5c).

In Peary Land soils, 5701–66,857 reads of fungal ITS2 copies per sample with $39,362 \pm 16,142$ on average we measured. We found no significant effect of changes in either Si or Ca treatment on fungal community structure of Peary Land soils (Fig. S10). Also, the number of fungal ITS2 copies was very low ($<10^4$ ITS2 copies $\text{g}^{-1} \text{ DW soil}$) in all treatments.

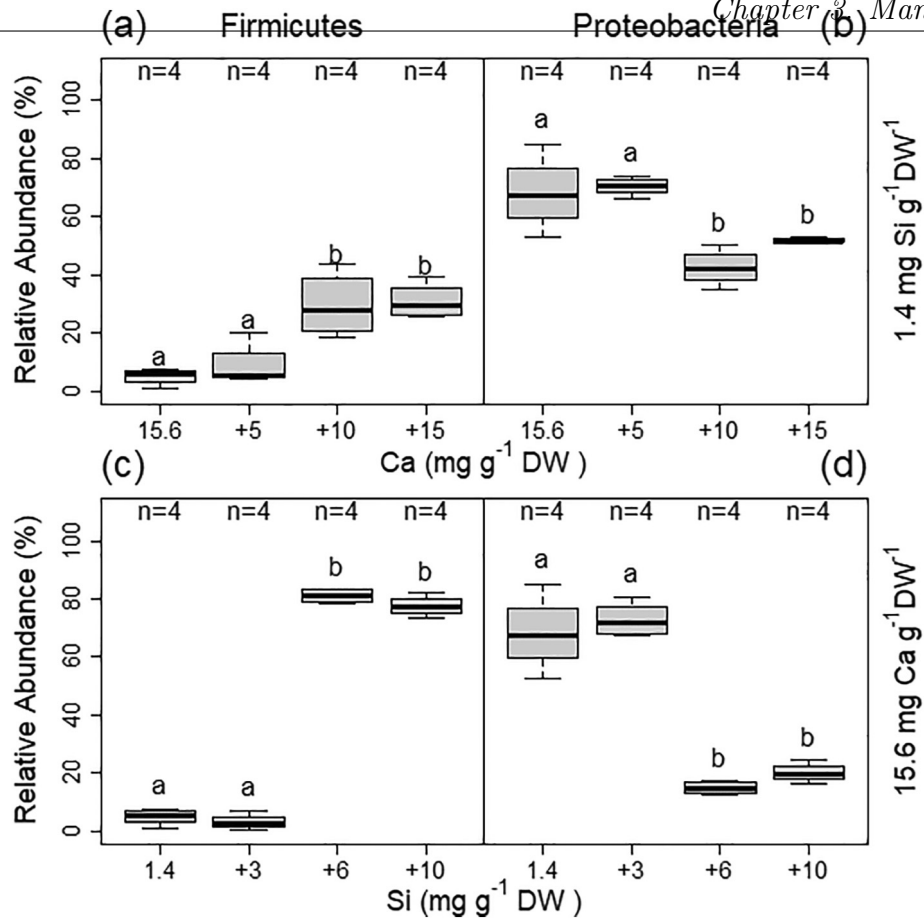


Fig. 4. Relative abundances of the most common bacterial phyla in the soil samples from Peary Land. Firmicutes (a + c) and Proteobacteria (b + d). The boxes represent the treatments with 15.6, 15.6 + 5 and 15.6 + 10 and 15.6 + 15 mg Ca g⁻¹ DW at 1.4 mg g⁻¹ DW Si and Si treatments with 1.4, 1.4 + 3, 1.4 + 6, 1.4 + 10 mg Si g⁻¹ DW at 15.6 mg g⁻¹ DW Ca. Shown are the boxplots with median, 25% and 75% quartile and upper and lower whisker. Different letters indicate significant difference between treatments at 5% significance level.

3.5. Microbial community structure correlates with CO₂ release

The CO₂ production in the Disko soils showed a significant negative correlation with the Ca concentration ($R = -0.54, P < 0.001$) in all treatments

(Fig. 6a), while Si concentration showed no effect on CO₂ production. The CO₂ production correlated positively with the abundance of bacteria (Fig. 6b) and fungi (Fig. S11), but not with the abundance of any bacterial phyla.

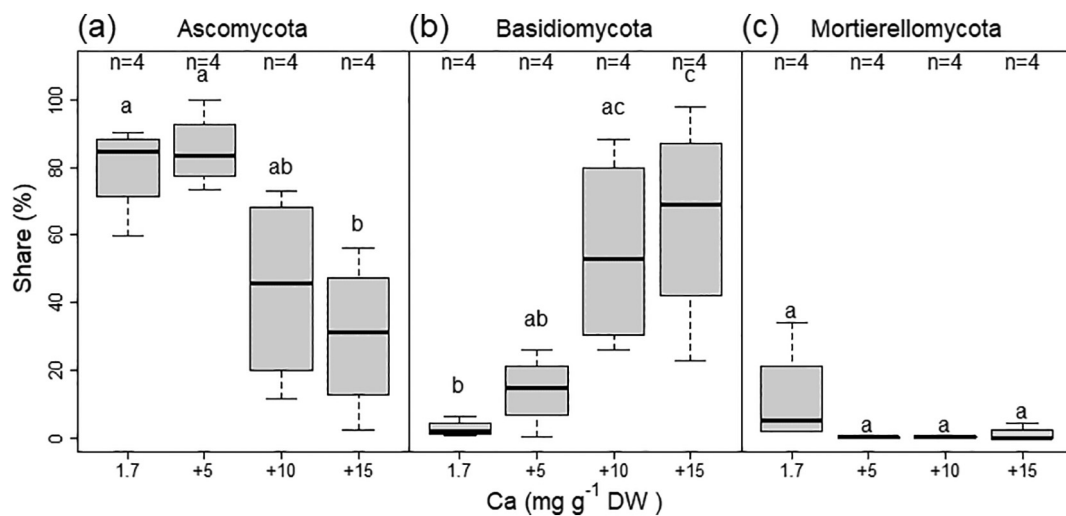


Fig. 5. Relative abundance of the most common fungal phyla in the soil samples from Disko. (a) Ascomycota, (b) Basidiomycota and (c) Mortierellomycota. The boxes represent the treatments with 1.7, 1.7 + 5, 1.7 + 10 and 1.7 + 15 mg Ca g⁻¹ DW at 5.2 mg Si g⁻¹ DW treatments. Median, 25% and 75% quartile and upper and lower whisker are shown on the boxplots. Different letters indicate significant difference between treatments at 5% significance level.

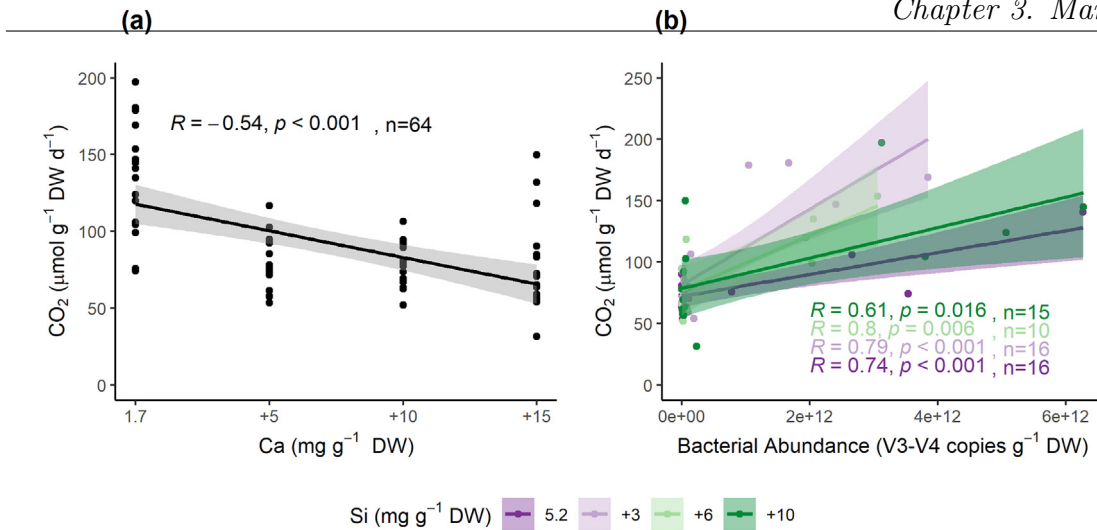


Fig. 6. CO₂ production in the Disko soils. (a) Significant negative correlation with Ca concentration. (b) Significant positive correlation with bacterial abundance, grouped by Si treatments.

In Peary Land soils, the CO₂ production correlated negatively with Ca concentrations (Fig. S12) and positively with Si concentrations at 15.6 + 10–15.6 + 15 mg Ca g⁻¹ DW (Fig. 7a). Furthermore, CO₂ production was positively correlated with the share of gram-negative bacteria (Fig. 7b). At 15.6 + 15 mg Ca g⁻¹ DW, the CO₂ production correlated positively with the share of gram-positive bacteria (Fig. S13).

The structural equation model supported these findings. In Disko soils, Ca had a stronger negative effect (-0.67) on bacterial 16S RNA gene copy numbers than on CO₂ production (-0.29) (Fig. 8a). Also, the positive effect of bacterial 16S RNA gene copy numbers on CO₂ production was stronger (0.42) than the negative effect of Ca on CO₂ production (-0.29). In Peary Land soils, the negative effect of Ca on CO₂ production was strongest (-0.75), compared to all other effects (Fig. 8b). Si had a strong positive effect on the number of bacterial 16S RNA gene copy numbers (0.70), but the effect of 16S RNA gene copy numbers on CO₂ was negligible (-0.18).

4. Discussion

4.1. Microbial community structure differs in the salt-rich and -poor soils

In both the salt-poor soil from Disko and the salt-rich soil from Peary Land, Ca amendment increased the relative abundance of spore-forming gram-positive Actinobacteria and Firmicutes (excluding members of Negativicutes) and decreased gram-negative bacteria. This was linked to a decrease of CO₂ production and indicates that the changes in CO₂ production was not just a consequence of overall decrease in microbial abundance, but also of microbial community structure changes. In Peary Land soil, Ca additionally had a direct effect on CO₂ production by reducing P availability, as found earlier (Schaller et al., 2019). The effect of Si amendment differed among the two soils. In the salt-poor Disko soil, Si promoted gram-negative bacteria, while in the salt-rich Peary Land soil, Si increased relative and absolute abundance of gram-positive bacteria.

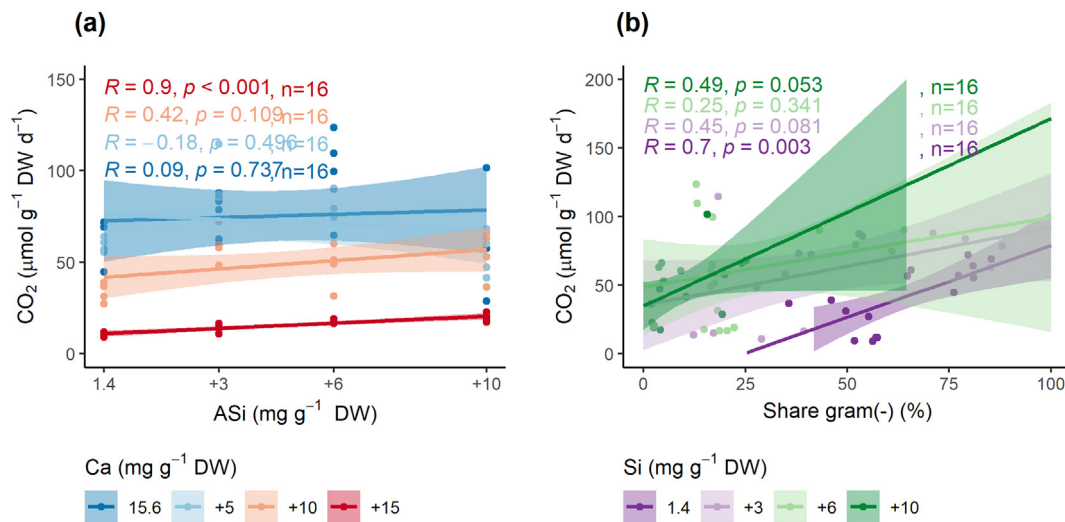


Fig. 7. CO₂ production of Peary Land soils. (a) Significant positive correlation with Si concentration at 15.6–15.6 + 15 mg Ca g⁻¹ DW. (b) Significant positive correlation with share of gram-negative bacteria, grouped by Si treatments.

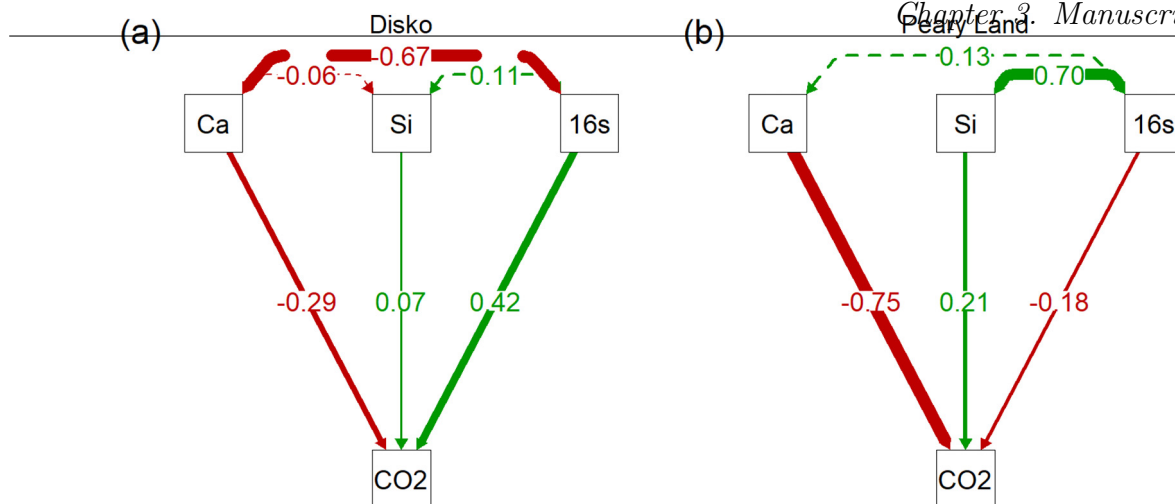


Fig. 8. Structural equation model. (a) Salt-poor soils from Disko (b) salt-rich soils from Peary Land. Green arrows show positive effects, red arrows show negative effects. Ca denotes Ca concentration, Si denotes Si concentration, 16S denotes number of 16S rRNA gene copies, and CO₂ denotes CO₂ production rates.

For both soils, the bacterial community structure is in accordance with other studies showing a predominance of gram-negative Acidobacteria and Proteobacteria as well as of gram-positive Firmicutes and Actinobacteria in Arctic soils (Jansson and Taş, 2014). Also, in both soils, 16S rRNA gene copies outnumbered fungal ITS2 copies, like in other Arctic soils (Margesin and Collins, 2019). The initial microbial community structure of the salt-rich and the salt-poor soils differed substantially and differences in nutrient availability are known to influence Arctic soil microbial community structure (Biasi et al., 2005; Voříšková et al., 2019). As a consequence, the microbial community structure can react differently to environmental changes, for example changes in Si or Ca concentrations. These changes in microbial community structure may be explained by the fact that Ca is known to increase salinity (Jessen et al., 2014) and Si is increasing water availability soils, potentially decreasing salinity (Schaller et al., 2021).

The mMDS of the microbial community reflected these changes in microbial community structure, as it showed different patterns in both soils after changed Ca and Si concentrations.

4.2. Ca affects microbial community structure more than Si in Disko soils

The acidic salt-poor soil from Disko (pH = 5.6) with high concentration of Si (5.2 mg g⁻¹ DW) and low concentration of Ca (1.7 mg g⁻¹ DW) was dominated by Chloroflexi and Acidobacteria. After increasing the Ca concentrations, the absolute abundance of bacteria decreased and the gram-positive Intrasporangiaceae (Actinobacteria) as well as Clostridiaceae (Firmicutes) dominated. Both families include spore-forming taxa (Barka et al., 2016; Rosenberg et al., 2014). This suggests that Ca addition to salt-poor adapted bacterial community leads to a physiological more inactive microbial community structure dominated by members surviving the enhanced salt-stress by elevated Ca concentration in a dormant state. Ca amendment decreased fungal abundance and changed the community structure, too. At initial Si concentration, Ascomycota dominated at 1.7 mg Ca g⁻¹ DW, whereas at 1.7 + 15 mg Ca g⁻¹ DW, Basidiomycota dominated. Our results suggest that bacterial abundance reacted stronger to changing Si and Ca concentrations than fungal abundance. The less marked decrease in fungal abundance indicates that fungi potentially benefit from the severely depleted and possibly physiological inactive bacterial community. Fungi are known to require Ca and many taxa can tolerate high concentrations (Pitt and Ugalde, 1984). The initial fungal community was dominated by Ascomycota and Mortierellomycota. Taxa within the latter group are known to adapt well to cold habitats by producing linoleic and arachidonic acid (Hassan et al., 2016). Moderate Ca concentrations of 1.7 + 5 mg Ca g⁻¹ DW in the Disko soil led to a decrease in Mortierellomycota

and continued a dominance of Ascomycota, whereas high concentrations of 1.7 + 10–1.7 + 15 mg Ca g⁻¹ DW led to a dominance of Basidiomycota. Zumsteg et al. (2012) found a similar shift of Ascomycota dominating young soils in an Alpine glacial forefield to Basidiomycota dominating older soils. Bacteria and fungi often use different carbon sources in soil. While many soil bacteria prefer labile, simple carbon sources, many soil fungi mineralize more complex organic matter (Voříšková et al., 2019). In consequence, Si and Ca could affect mineralization of different soil organic material differently. Both, the bacterial and the fungal abundance correlated positively with CO₂ production. Gram-positive bacteria correlated negative with absolute bacterial abundance, whereas gram-negative bacteria correlated positively with CO₂ production. This hints that Ca has an indirect negative effect on CO₂ production in salt-poor soils by reducing the abundance of gram-negative bacteria. The results from the structural equation modelling support this suggestion (Fig. 8).

4.3. Si promotes salt-adapted microbes in Peary Land soils

In the alkaline salt-rich soil from Peary Land (pH 8.4) with low Si (1.4 mg g⁻¹ DW) and high Ca (15.6 mg g⁻¹ DW) *Staphylococcus* (phylum Firmicutes) was the dominating genus. *Staphylococcus* spp. are known to grow under high salinity conditions in soils by modifying extracellular polysaccharides and membrane lipids (Qurashi, 2011). It is also known, that gram-positive bacteria in general contain higher concentrations of potassium and glutamate and by this a higher turgor pressure (Whatmore and Reed, 1990). This enables these bacteria to live under higher salinity levels in a dormant state. As a consequence, increased Ca concentrations had no effect on absolute abundance of bacteria. The addition of low amounts of Si and Ca increased the relative abundance of gram-negative Pseudomonadaceae (Gamma-Proteobacteria), while higher Si and Ca concentrations increased the relative abundance of *Staphylococcus* spp. again. The low water availability of the original untreated soil would select for a xero- and halotolerant microbial community structure. This is indicated by the strong dominance of Firmicutes. The addition of Si at low concentration may have killed many halotolerant members of the original bacterial community due to osmotic shock. This led to a microbial community dominated by presumed less halotolerant bacteria, e.g. Pseudomonadaceae, at low Si treatment levels. Our data is in accordance with previous studies showing an increase of the abundance of gram-positive bacteria in soils at high Si concentration (Schaller et al., 2016; Song et al., 2021). The CO₂ production rates at low Si concentrations of 1.4 and 1.4 + 3 mg g⁻¹ DW correlated positively with the share of gram-negative bacteria, indicating that gram-negative bacteria are the main driver for the CO₂ production. Furthermore, gram-positive bacteria correlated positively with CO₂ production

at highest Ca concentration. Like in Disko soils, Ca increased relative abundance of gram-positive bacteria and decreased gram-negative bacteria. Additionally to this indirect effect of Ca on CO₂ production, the structural equation modelling showed a strong direct negative effect of Ca on CO₂ production. This could be explained by cation-bridging of organic matter and phosphate co-precipitation with carbonate precipitation. In summary, it seems that Si benefits physiological activity of gram-negative bacteria at low Si concentrations. At high Ca concentrations gram-positive bacteria benefit from increased Si levels and increase their activity, which leads to increased CO₂ production rates.

5. Conclusion

In summary, the effects of Ca and Si on soil microbial community structure are affected by the local geology and soil element concentrations. Our data showed that the bacterial community of a salt-rich Arctic soil was dominated by gram-positive bacteria and a salt-poor soil was dominated by gram-negative bacteria, verifying hypothesis (i). The microbial community structure of the salt-poor soil responded strongly to Ca treatment, confirming hypothesis (ii). The effect of Ca on bacteria and fungi was negligible for the salt- and Ca-rich Peary Land soil, whereas in the salt- and Ca-poor Disko soil it significantly decreased bacterial 16S rRNA gene copy numbers and increased the relative abundance of Firmicutes and Acidobacteria. As CO₂ production rates were positively correlated with the relative abundance of gram-positive bacteria at high Ca concentration in the salt- and Ca-rich Peary Land, these bacteria may have been physiological active, whereas in salt- and Ca-poor Disko soil the gram-positive bacteria may have formed spores and hence were inactive. The microbial abundance and community structure of the Disko soil were not affected by Si, whereas the bacterial abundance of the Peary Land soil increased significantly in response to high Ca concentration. This finding leads to a rejection of hypothesis (iii), no halo-intolerant bacteria benefitted from increased Si concentrations, while halotolerant bacteria benefitted. In this case, Si may enable bacteria to outcompete fungi. On the contrary, in the salt- and Ca-poor soil, fungi may not be outcompeted by bacteria at high Ca concentrations. This indicates that the effects of Si and Ca on microbial community structure of bacteria and fungi are complex, confirming hypothesis (iv). The CO₂ release was directly affected by the abundance of microbes and their community structure. This confirms hypothesis (v) and indicates that Si and Ca affected CO₂ release not only by nutrient mobilization, but also by changing microbial community structure. On one hand, it seems that Si can reduce Ca-induced salt stress in halotolerant microbes. On the other hand, high initial Si concentrations are not able to protect gram-negative bacteria from Ca-induced salt stress. Both elements have the potential to change microbial community structure in Arctic soils by the suggested change in their concentration due to on-going Arctic warming and active layer deepening altering both Si and Ca availability in the Arctic soils dependent on lithology (Stimmler et al., in preparation). Increasing thawing depth and elevated weathering rates (driven by climate changes) may not only release phosphorus and other well-known nutrients, but may also release Si and Ca in quantities which depending on the parent material may be released in quantities which can directly influence soil organic matter decomposition and microbial respiration through changes in microbial community structure and activity. With this our data showed an important interdependency between Si and Ca availability on one hand and microbial community structure related to soil CO₂ production on the other hand. Such changes in microbial community structure related to soil CO₂ production should be considered when estimating future carbon feedback under the predicted climate change.

Supplementary data to this article can be found online at <https://doi.org/10.1016/j.scitotenv.2022.156152>.

CRedit authorship contribution statement

The study was initiated by J.S, A.P and B.E. B.E. supplied soil samples, A.P analyzed the microbial community structure. P.S. made the data

analysis and wrote main part of the manuscript. All authors contributed to the manuscript and approved the submitted version of the manuscript.

Availability

All data needed to evaluate the conclusions in the paper are present in the paper and/or the Supplementary Materials. The data that support the findings of this study are available from the corresponding author upon reasonable request.

Declaration of competing interest

All authors contributed to the manuscript and approved the submitted version of the manuscript. The authors declare that they have no competing interests. German Research Foundation grant SCHA 1822/12-1.

References

- Abarenkov, K., Nilsson, H., Kõljalg, U., 2010. The UNITE database for molecular identification of fungi – recent updates and future perspectives. *New Phytol.* 281.
- Alfredsson, H., Clymans, W., Hugelius, G., Kuhry, P., Conley, D.J., 2016. Estimated storage of amorphous silica in soils of the circum-Arctic tundra region. *Glob. Biogeochem. Cycles* 30, 479.
- Barka, E.A., Vatsa, P., Sanchez, L., Gaveau-Vaillant, N., Jacquard, C., Meier-Kolthoff, J.P., Klenk, H.-P., Clément, C., Ouhdouch, Y., van Wezel, G.P., 2016. Taxonomy, physiology, and natural products of actinobacteria. *Microbiol. Mol. Biol. Rev.* 80, 1.
- Biasi, C., Rusalimova, O., Meyer, H., Kaiser, C., Wanek, W., Barsukov, P., Junger, H., Richter, A., 2005. Temperature-dependent shift from labile to recalcitrant carbon sources of arctic heterotrophs. *Rapid Commun. Mass Spectrom.* 19, 1401.
- Caporaso, J.G., Lauber, C.L., Walters, W.A., Berg-Lyons, D., Lozupone, C.A., Turnbaugh, P.J., Fierer, N., Knight, R., 2011. Global patterns of 16S rRNA diversity at a depth of millions of sequences per sample. *Proc. Nat. Acad. Sci. U.S.A.*, p. 4516.
- Clarke, K.R., Gorley, R.N., 2015. *Primer v7: User Manual/Tutorial*, p. 300.
- Coolen, M.J.L., Orsi, W.D., 2015. The transcriptional response of microbial communities in thawing Alaskan permafrost soils. *Front. Microbiol.* 6, 197.
- Coskun, D., Britto, D.T., Huynh, W.Q., Kronzucker, H.J., 2016. The role of silicon in higher plants under salinity and drought stress. *Front. Plant Sci.* 7, 1072.
- Dahl, M.B., Priemé, A., Brejnrod, A., Brusvang, P., Lund, M., Nymand, J., Kramshøj, M., Røpoulsen, H., Haugwitz, M.S., 2017. Warming, shading and a moth outbreak reduce tundra carbon sink strength dramatically by changing plant cover and soil microbial activity. *Sci. Rep.* 16035.
- DeForest, J.L., Scott, L.G., 2010. Available organic soil phosphorus has an important influence on microbial community composition. *Soil Sci. Soc. Am. J.* 74, 2059.
- Deming, J.W., 2002. Psychrophiles and polar regions. *Curr. Opin. Microbiol.* 5, 301.
- Denich, T.J., Beaudette, L.A., Lee, H., Trevors, J.T., 2003. Effect of selected environmental and physico-chemical factors on bacterial cytoplasmic membranes. *J. Microbiol. Methods* 52, 149.
- Edgar, R.C., 2010. Search and clustering orders of magnitude faster than BLAST. *Bioinformatics* 2460.
- Hassan, N., Rafiq, M., Hayat, M., Shah, A.A., Hasan, F., 2016. Psychrophilic and psychrotrophic fungi: a comprehensive review. *Rev. Environ. Sci. Biotechnol.* 15, 147.
- Hugelius, G., Loisel, J., Chadburn, S., Jackson, R.B., Jones, M., MacDonald, G., Maruschak, M., Olefeldt, D., Packalen, M., Siewert, M.B., Treat, C., Turetsky, M., Voigt, C., Yu, Z., 2020. Large stocks of peatland carbon and nitrogen are vulnerable to permafrost thaw. *Proc. Natl. Acad. Sci. U. S. A.* 117, 20438.
- Ihrmark, K., Bodeker, I.T.M., Cruz-Martinez, K., Friberg, H., Kubartova, A., Schenck, J., Strid, Y., Stenlid, J., Brandström-Durling, M., Clemmensen, K.E., Lindahl, B.D., 2012. New primers to amplify the fungal ITS2 region—evaluation by 454-sequencing of artificial and natural communities. *FEMS Microbiol. Ecol.* 666.
- Ishizaki, T., Maruyama, M., Furukawa, Y., Dash, J.G., 1996. Premelting of ice in porous silica glass. *J. Cryst. Growth* 163, 455.
- Jansson, J.K., Hofmøckel, K.S., 2020. Soil microbiomes and climate change. *Nat. Rev. Microbiol.* 18, 35.
- Jansson, J.K., Taş, N., 2014. The microbial ecology of permafrost. *Nat. Rev. Microbiol.* 12, 414.
- Jessen, S., Holmslykke, H.D., Rasmussen, K., Richardt, N., Holm, P.E., 2014. Hydrology and pore water chemistry in a permafrost wetland, Ilulissat, Greenland. *Water Resour. Res.* 50, 4760.
- Mackelprang, R., Waldrop, M.P., DeAngelis, K.M., David, M.M., Chavarria, K.L., Blazewicz, S.J., Rubin, E.M., Jansson, J.K., 2011. Metagenomic analysis of a permafrost microbial community reveals a rapid response to thaw. *Nature* 480, 368.
- Margesin, R., Collins, T., 2019. Microbial ecology of the cryosphere (glacial and permafrost habitats): current knowledge. *Appl. Microbiol. Biotechnol.* 103, 2537.
- Megrian, D., Taib, N., Witwinowski, J., Beloin, C., Gribaldo, S., 2020. One or two membranes? Diderm Firmicutes challenge the Gram-positive/Gram-negative divide. *Mol. Microbiol.* 113 (3), 659–671. <https://doi.org/10.1111/mmi.14469>.
- Monteux, S., Keuper, F., Fontaine, S., Gavazov, K., Hallin, S., Juhanson, J., Krab, E.J., Revalliot, S., Verbruggen, E., Walz, J., Weedon, J.T., Dorrepaal, E., 2020. Carbon and nitrogen cycling in Yedoma permafrost controlled by microbial functional limitations. *Nat. Geosci.* 13, 794.

- Muyzer, G., Waal, E.C., Uitterlinden, A.G., Muyzer, G., Waal, E.C., Uitterlinden, A.G., 1993. Profiling of complex microbial populations by denaturing gradient gel electrophoresis analysis of polymerase chain reaction-amplified genes coding for 16S rRNA. *Appl. Environ. Microbiol.* 59, 695.
- Nguyen, N.H., Song, Z., Bates, S.T., Branco, S., Tedersoo, L., Menke, J., Schilling, J.S., Kennedy, P.G., 2016. FUNGuild: an open annotation tool for parsing fungal community datasets by ecological guild. *Fungal Ecol.* 20, 241.
- Pitt, Ugalde, U.O., 1984. Calcium in fungi. *Plant Cell Environ.* 467.
- Pruesse, E., Quast, C., Knittel, K., Fuchs, B.M., Ludwig, W., Peplies, J., Glöckner, F.O., 2007. SILVA: a comprehensive online resource for quality checked and aligned ribosomal RNA sequence data compatible with ARB. *Nucleic Acids Res.* 7188.
- Qin, S., Kou, D., Mao, C., Chen, Y., Chen, L., Yang, Y., Qin, S., Kou, D., Mao, C., Chen, Y., Chen, L., Yang, Y., 2021. Temperature sensitivity of permafrost carbon release mediated by mineral and microbial properties. *Sci. Adv.* 7, eabe3596.
- Qurashi, A.W., 2011. Osmoadaptation and plant growth promotion by salt tolerant bacteria under salt stress. *Afr. J. Microbiol. Res.* 5.
- Rivkina, E.M., Friedmann, E.I., McKay, C.P., Gilichinsky, D.A., 2000. Metabolic activity of permafrost bacteria below the freezing point. *Appl. Environ. Microbiol.* 66, 3230.
- Rosenberg, E., DeLong, E.F., Lory, S., Stackebrandt, E., Thompson, F., 2014. *The Prokaryotes*, p. 1018.
- Schädel, C., Bader, M.K.-F., Schuur, E.A.G., Biasi, C., Bracho, R., Čapek, P., Baets, S., Diáková, K., Ernakovich, J., Estop-Aragones, C., Graham, D.E., Hartley, I.P., Iversen, C.M., Kane, E., Knoblauch, C., Lupascu, M., Martikainen, P.J., Natali, S.M., Norby, R.J., Wickland, K.P., 2016. Potential carbon emissions dominated by carbon dioxide from thawed permafrost soils. *Nat. Clim. Chang.* 6, 950.
- Schaller, J., Böttger, R., Dudel, G., Ruess, L., 2016. Reed litter Si content affects microbial community structure and the lipid composition of an invertebrate shredder during aquatic decomposition. *Limnologia* 57, 14.
- Schaller, J., Faucherre, S., Joss, H., Obst, M., Goeckede, M., Planer-Friedrich, B., Peiffer, S., Gilfedder, B., Elberling, B., 2019. Silicon increases the phosphorus availability of Arctic soils. *Sci. Rep.* 9, 449.
- Schaller, J., Puppe, D., Kaczorek, D., Ellerbrock, R., Sommer, M., 2021. Silicon cycling in soils revisited. *MDPI Plants* 10.
- Sleator, R.D., Hill, C., 2002. Bacterial osmoadaptation: the role of osmolytes in bacterial stress and virulence. *FEMS Microbiol. Rev.* 26, 49.
- Song, A., Li, Z., Liao, Y., Liang, Y., Wang, E., Wang, S., Li, X., Bi, J., Si, Z., Lu, Y., Nie, J., Fan, F., 2021. Soil bacterial communities interact with silicon fraction transformation and promote rice yield after long-term straw return. *Soil Ecol. Lett.* 3, 395–408. <https://doi.org/10.1007/s42832-021-0076-4>.
- Stimmler et al., in prep. P. Stimmler M. Goeckede B. Elberling S. Natali P. Kuhry P. Perron et al (in prep.): Pan-Arctic element availability estimations. In preparation.
- Suetin, S.V., Shcherbakova, V.A., Chuvilskaya, N.A., Rivkina, E.M., Suzina, N.E., Lysenko, A.M., Gilichinsky, D.A., 2009. *Clostridium tagluense* sp. nov., a psychrotolerant, anaerobic, spore-forming bacterium from permafrost. *Int. J. Syst. Evol. Microbiol.* 59, 1421.
- Virkkala, A.-M., Aalto, J., Rogers, B.M., Tagesson, T., Treat, C.C., Natali, S.M., Watts, J.D., Potter, S., Lehtonen, A., Mauritz, M., Schuur, E.A.G., Kochendorfer, J., Zona, D., Oechel, W., Kobayashi, H., Humphreys, E., Goeckede, M., Iwata, H., Laflour, P.M., Luoto, M., 2021. Statistical upscaling of ecosystem CO₂ fluxes across the terrestrial tundra and boreal domain: regional patterns and uncertainties. *Glob. Chang. Biol.* 4040–4059.
- Voříšková, J., Elberling, B., Priemé, A., 2019. Fast response of fungal and prokaryotic communities to climate change manipulation in two contrasting tundra soils. *Environ. Microbiome* 14.
- Walker, D.A., Bockheim, J.G., Chapin III, F.S., Eugster, W., Nelson, F.E., Ping, C.L., 2001. Calcium-rich tundra, wildlife, and the “Mammoth Steppe”. *Quat. Sci. Rev.* 20, 149.
- Whatmore, A.M., Reed, R.H., 1990. Determination of turgor pressure in *Bacillus subtilis*: a possible role for K⁺ in turgor regulation. *J. Gen. Microbiol.* 136, 2521.
- Yan, G., Fan, X., Tan, L., Yin, C., Li, T., Liang, Y., 2021. Root silicon deposition and its resultant reduction of sodium bypass flow is modulated by OsLsi1 and OsLsi2 in rice. *Plant Physiol. Biochem.* 158, 219.
- Ye, C., Yang, X., Zhao, F.-J., Ren, L., 2016. The shift of the microbial community in activated sludge with calcium treatment and its implication to sludge settleability. *Bioresour. Technol.* 207, 11.
- Zahrán, H.H., 1997. Diversity, adaptation and activity of the bacterial flora in saline environments. *Biol. Fertil. Soils* 25, 211.
- Zumsteg, A., Luster, J., Göransson, H., Smittenberg, R.H., Brunner, I., Bernasconi, S.M., Zeyer, J., Frey, B., 2012. Bacterial, archaeal and fungal succession in the forefield of a receding glacier. *Microb. Ecol.* 63, 552.

Supporting information to:

Arctic soil respiration and microbial community structure driven by silicon and calcium

AUTHORS

Peter Stimmler^{1*}, Anders Priemé^{2,3}, Bo Elberling^{2,3}, Mathias Goeckede⁴, Jörg Schaller¹

AFFILIATIONS

1. Leibniz Centre for Agricultural Landscape Research (ZALF), Eberswalder Str. 84, 15374 Müncheberg, Germany, *corresponding Author: Peter Stimmler, email: Peter.Stimmler@zalf.de; Jörg Schaller, email: joerg.schaller@zalf.de
2. University of Copenhagen, Department of Biology, University of Copenhagen, 1350 Copenhagen, Denmark. Anders Priemé, email: aprieme@bio.ku.dk
3. Center for Permafrost, Copenhagen, Denmark, Center for Permafrost, Department of Geosciences and Natural Resource Management, University of Copenhagen, 1350 Copenhagen, Denmark, Bo Elberling, email: be@ign.ku.dk
4. Department of Geosciences and Natural Resource Management, University of Copenhagen, 1350 Copenhagen, Denmark
5. Max Planck Institute for Biogeochemistry, Department of Biogeochemical Signals, 07701 Jena, Germany, email: mgoeck@bgc-jena.mpg.de

SUPPORTING INFORMATION

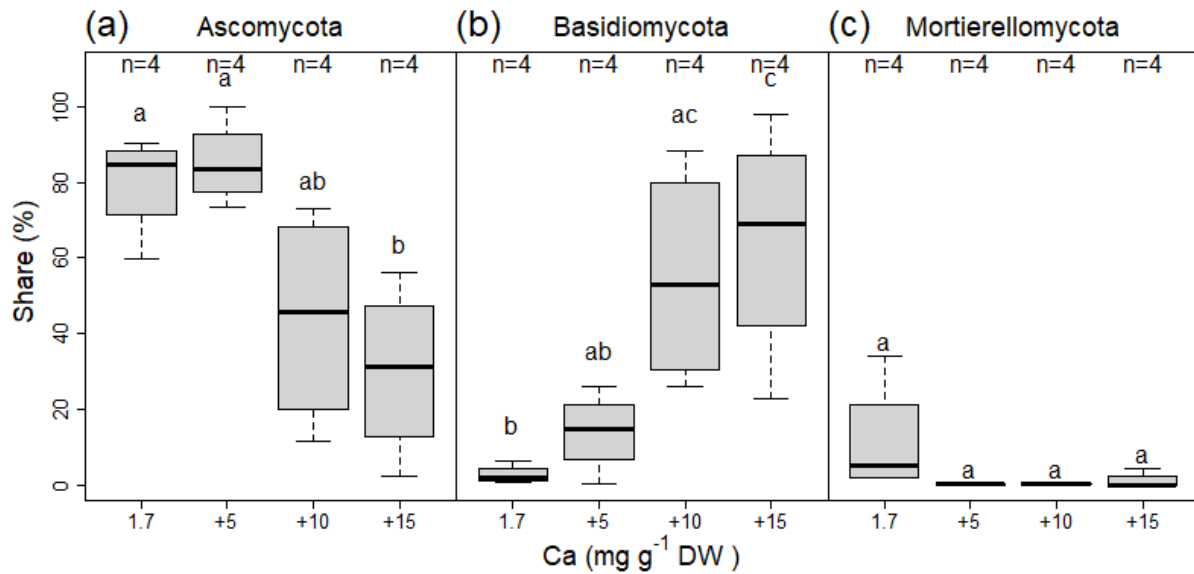


Figure S1: qPCR of Disko soils. (a) Bacterial 16S rRNA gene copies and (b) Fungal ITS2 copies, grouped by Si treatments over all Ca concentrations. Increased Si concentration had no significant effect on the bacterial and fungal abundance. Data are shown as boxplots with median, 25% and 75% quartile and upper and lower whisker showing minimum and maximum values. Different letters indicate significant ($P < 0.05$) differences between treatments.

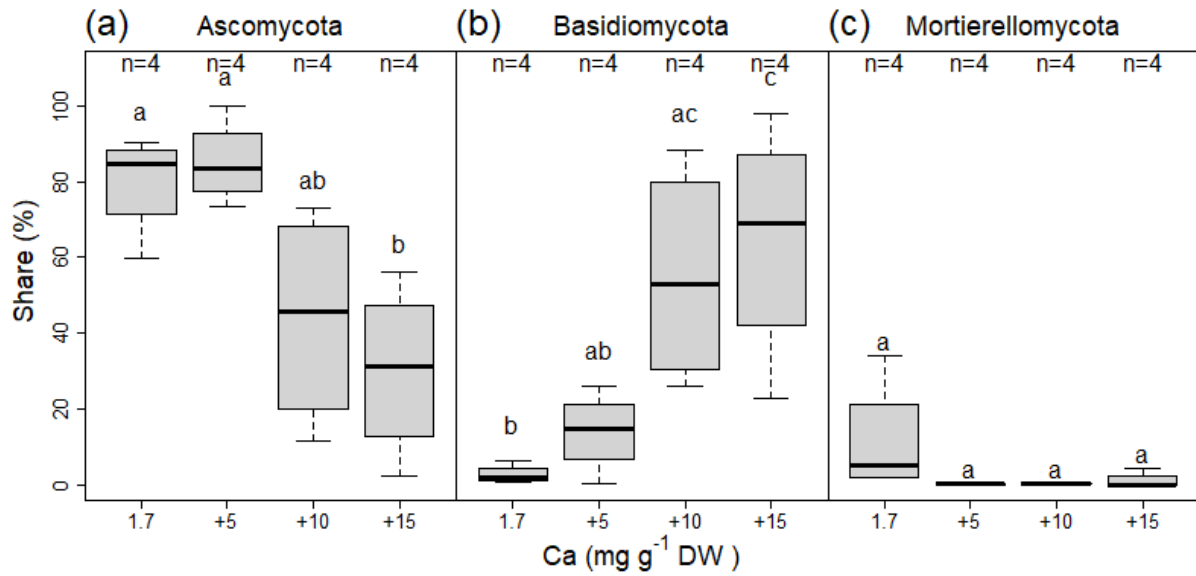


Figure S2: qPCR of Peary Land soil. (a) Bacterial 16S rRNA gene copies and (b) Fungal ITS2 copies. Increased Ca concentration had little effect on the bacterial and fungal abundance over all Si concentrations. Shown are the boxplots with median, 25% and 75% Quartile and upper and lower whisker. Different letters indicate significant difference between treatments at 5% significance level.

Disko 16S rDNA community structure at phylum level (and proteobacterial class level)

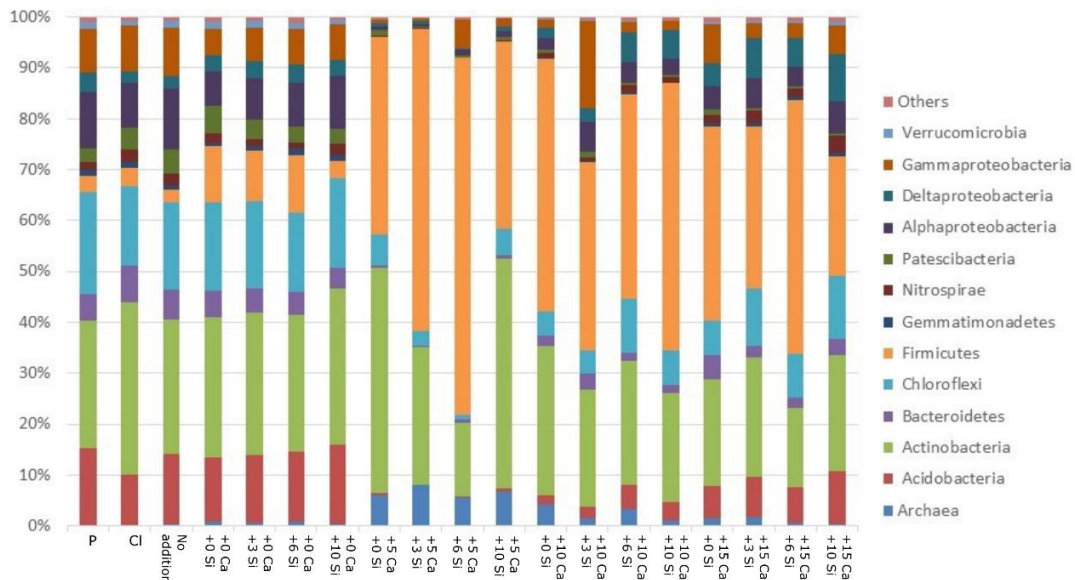


Figure S3: 16S rRNA gene-based bacterial community structure of incubated Disko soil. Shown was the most common bacteria at phylum level and proteobacterial class level of the incubated soil from Disko. Data show the relative abundances of the most common phyla, while uncommon phyla are combined in "Others". The columns represent the single treatments ($n=4$) with the combinations of 1.7, 1.7+5, 1.7+10 and 1.7+15 $\text{mg}^{-1} \text{g}^{-1} \text{DW Ca}$ and 5.2, 5.2+3, 5.2+6 and 5.2+10 $\text{mg}^{-1} \text{g}^{-1} \text{DW Si}$ availability. The P treatment with additional phosphorous (3 mg NaH_2PO_4 per sample), Cl control (4 mg NaCl per sample) and the reference with no water added (No addition) can be found at the left side. Bacterial community structure of Disko soils at different Ca and Si treatments. Most common phyla were gram-negative Acidobacteria, Chloroflexi, Proteobacteria and gram-positive Actinobacteria and Firmicutes.

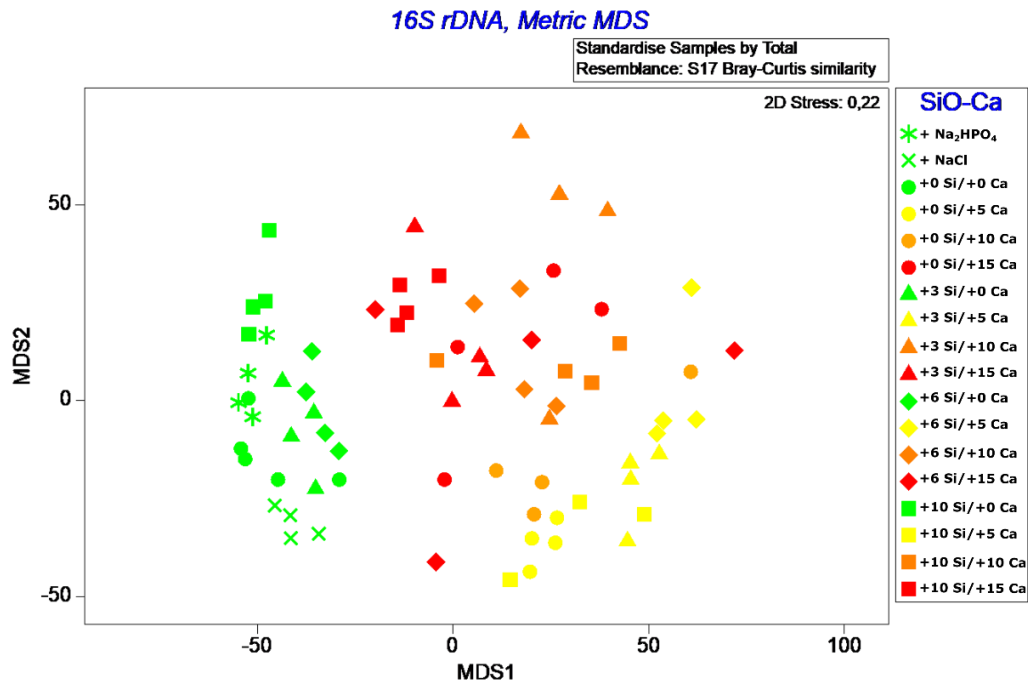


Figure S4: Metric Multidimensional Scaling (mMDS) of bacterial community structure in Disko soil. Community structure based on 16S rRNA gene of the incubated soil from Disko (2D Stress: 0.22). The Ca treatments are colored in green ($1.7 \text{ mg}^{-1} \text{ g}^{-1} \text{ DW Ca}$), yellow ($1.7+5 \text{ mg}^{-1} \text{ g}^{-1} \text{ DW Ca}$), orange ($1.7+10 \text{ mg}^{-1} \text{ g}^{-1} \text{ DW Ca}$) and red ($1.7+15 \text{ mg}^{-1} \text{ g}^{-1} \text{ DW Ca}$). The Si treatments are plotted as circles ($5.2 \text{ mg}^{-1} \text{ g}^{-1} \text{ DW Si}$), triangles ($5.2+3 \text{ mg}^{-1} \text{ g}^{-1} \text{ DW Si}$), rhombus ($5.2+6 \text{ mg}^{-1} \text{ g}^{-1} \text{ DW Si}$) and square ($5.2+10 \text{ mg}^{-1} \text{ g}^{-1} \text{ DW Si}$). Further P control with additional phosphorous ($3 \text{ mg Na}_2\text{HPO}_4$ per sample, asterisk symbol) and Cl control (4 mg NaCl per sample, cross symbol) are shown. Metric Multidimensional Scaling (mMDS) of the bacterial community structure in Disko soils showed clear patterns with Ca concentrations.

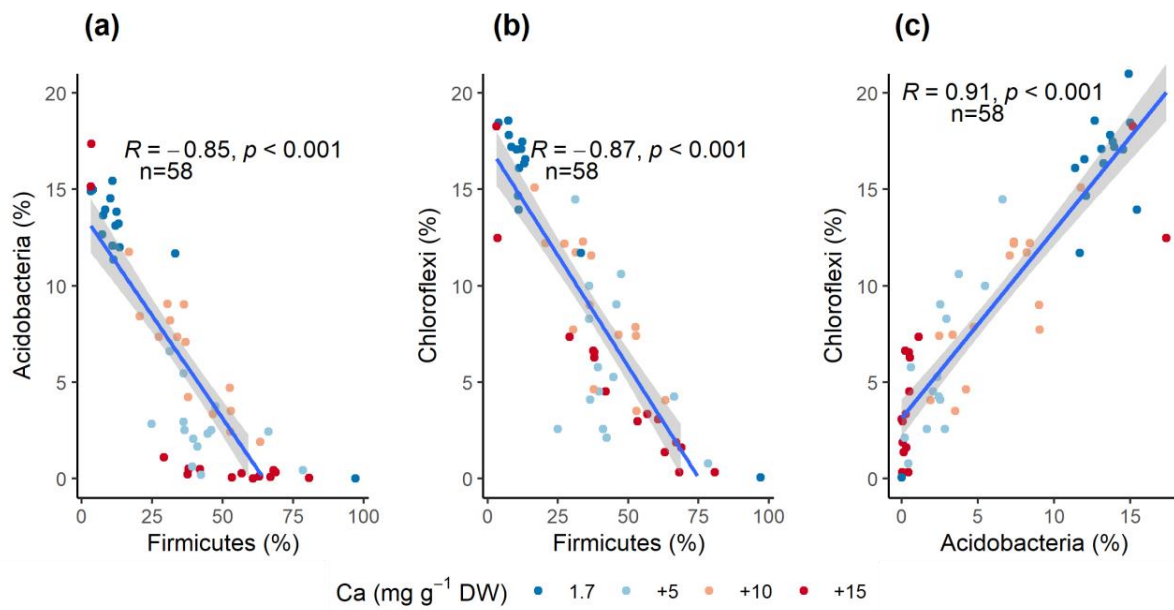


Figure S5: Correlation between the relative abundance. Selected bacterial phyla in the soil samples from Disko over all Si treatments ($n=58$). Ca treatments are colored from low (blue) to high (red) concentrations. (a) Acidobacteria versus Firmicutes, (b) Chloroflexi versus Firmicutes, and (c) Acidobacteria versus Chloroflexi.

Peary Land 16S rDNA community structure at phylum level (and proteobacterial class level)

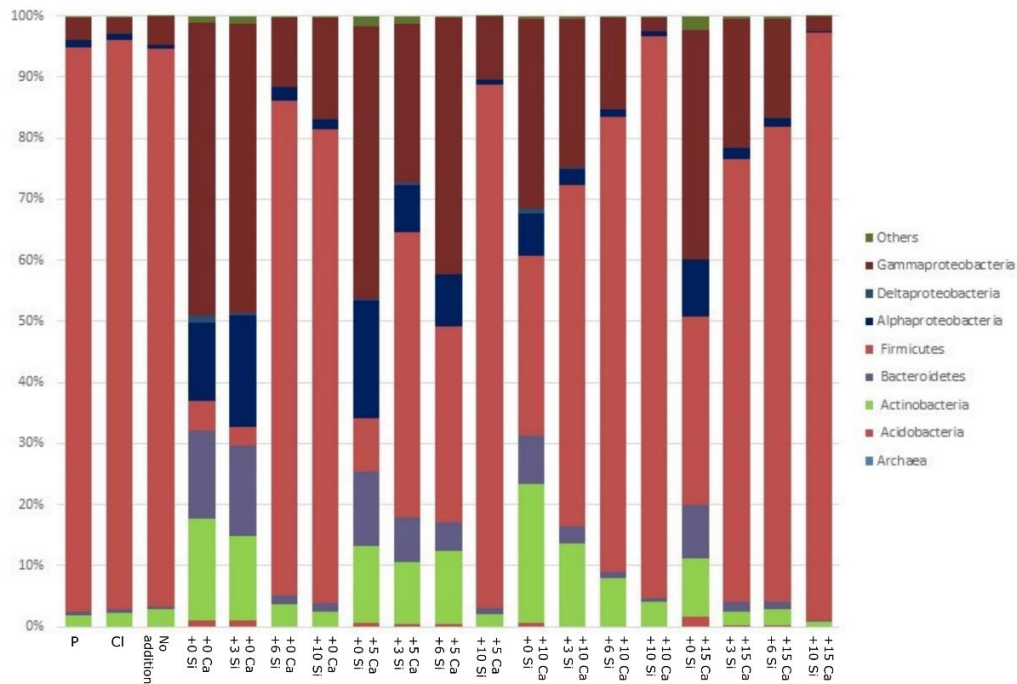


Figure S6: 16S rRNA gene-based bacteria community structure of incubated Peary Land soil. Shown are the most common bacteria at phyla level and proteobacterial class level of the incubated soil from Peary Land. The data show the relative abundances of the most common phyla, while uncommon phyla are grouped as “Others”. The columns represent the single treatments with the combinations of 15.6, 15.6+5, 15.6+10 and 15.6+15 mg g⁻¹ DW⁻¹ Ca and 1.4, 1.4+3, 1.4+6 and 1.4+10 mg g⁻¹ DW Si availability. The P control with additional phosphorous (1 mg Na₂HPO₄ per sample), the Cl control (5 mg NaCl per sample) addition and the negative control with no water added (No water) can be found at the left side. Bacterial community structure of Peary Land soils. Most common phyla were gram-negative Proteobacteria and Proteobacteria and gram-positive Actinobacteria and Firmicutes.

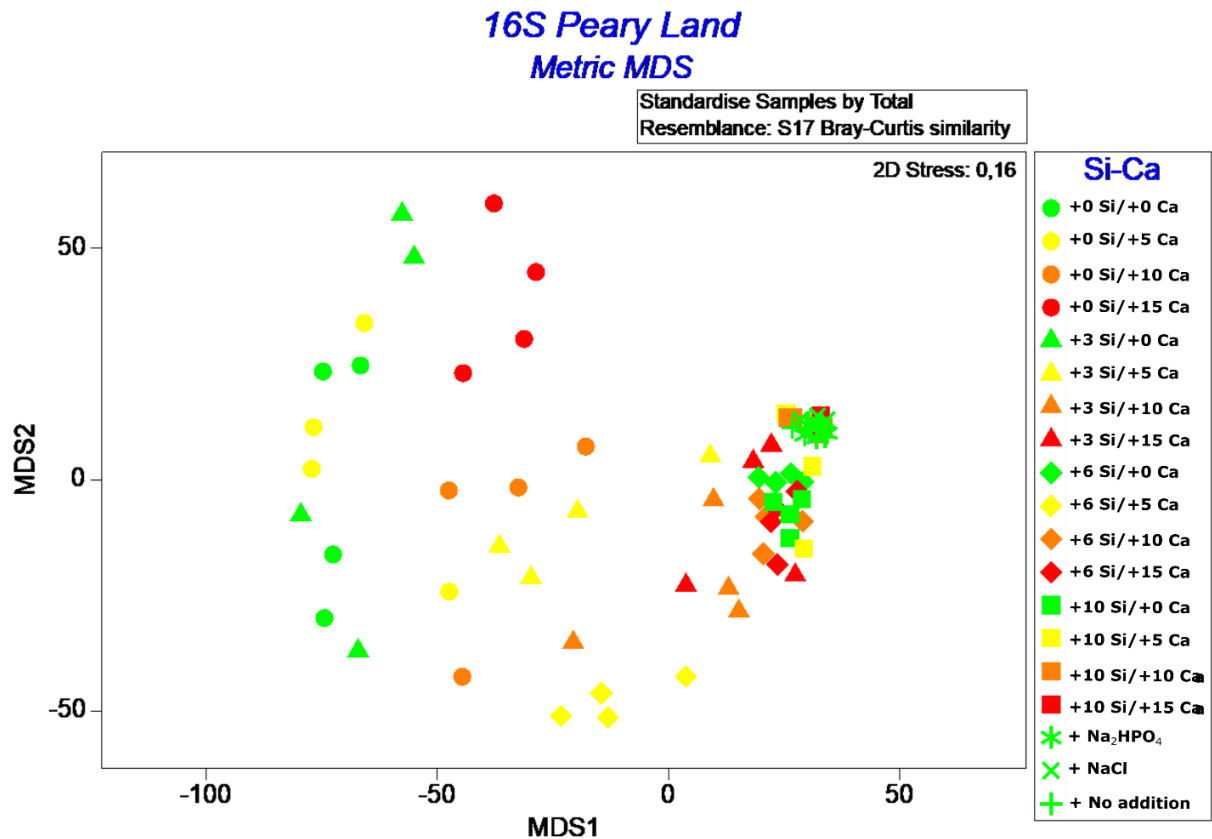


Figure S7: Metric Multidimensional Scaling (mMDS) of bacterial community structure in Peary Land soil. Community structure based on the 16S rDNA genes of the incubated soil from Peary Land (2D Stress: 0.16). The Ca treatments are colored in green ($15.6 \text{ mg g}^{-1} \text{ DW}^{-1} \text{ Ca}$), yellow ($15.6+5 \text{ mg g}^{-1} \text{ DW}^{-1} \text{ Ca}$), orange ($15.6+10 \text{ mg g}^{-1} \text{ DW}^{-1} \text{ Ca}$) and red ($15.6+15 \text{ mg g}^{-1} \text{ DW}^{-1} \text{ Ca}$). The Si treatments are plotted as circles ($1.4 \text{ mg g}^{-1} \text{ DW Si}$), triangles ($1.4+3 \text{ mg g}^{-1} \text{ DW Si}$), rhombus ($1.4+6 \text{ mg g}^{-1} \text{ DW Si}$) and square ($1.4+10 \text{ mg g}^{-1} \text{ DW Si}$). Further the no addition treatment with no water added (plus symbol, Reference), P control with additional phosphorous ($1 \text{ mg Na}_2\text{HPO}_4$ per sample, asterisk symbol) and Cl control (5 mg NaCl per sample, cross symbol) are shown. Metric Multidimensional Scaling (mMDS) of the bacterial community structure in Disko soils showed clear patterns with Ca concentrations.

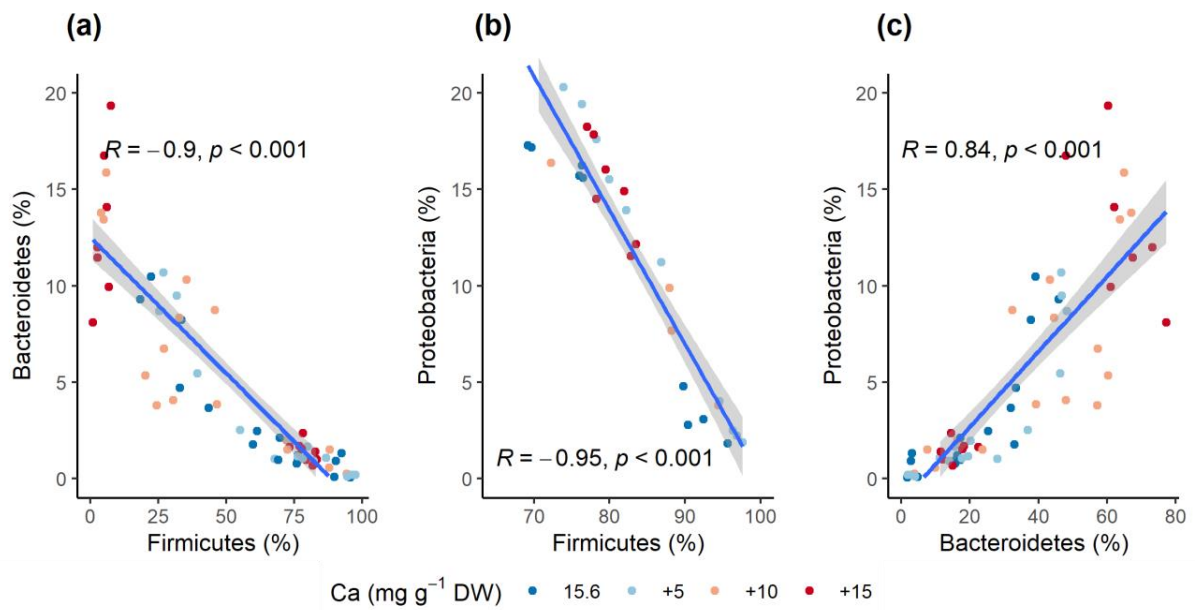


Figure S8: Correlation between the relative abundances. Selected bacterial phyla in the soil samples from Peary Land over all Si treatments ($n=64$). Ca treatments are colored from low (blue) to high (red) concentrations. (a) Bacteroidetes versus Firmicutes, (b) Proteobacteria versus Firmicutes, and (c) Proteobacteria versus Bacteroidetes.

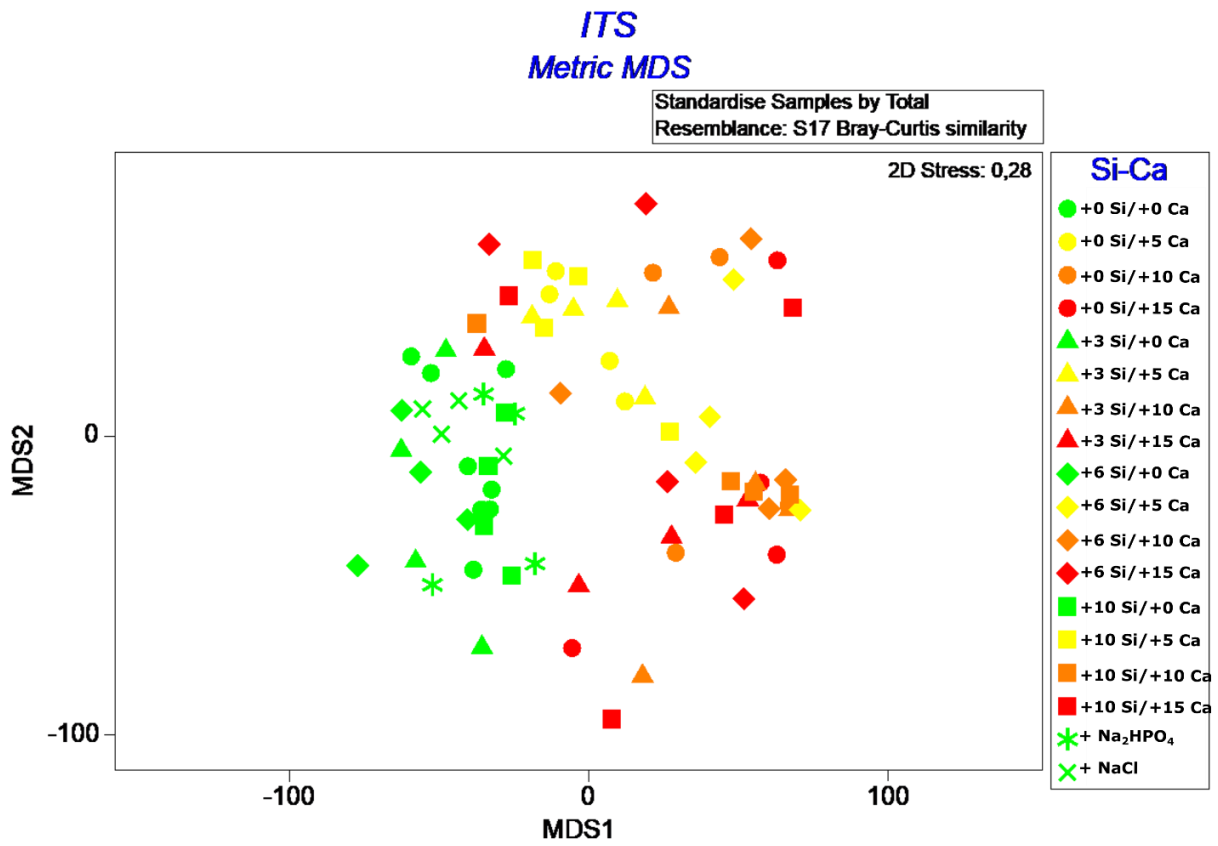


Figure S9: Metric Multidimensional Scaling (mMDS) of the ITS2 fungal community structure in Disko soil. Community structure based on fungal ITS2 genes of the incubated soil from Disko (2D Stress: 0.28). The Ca treatments are colored in green ($1.7 \text{ mg}^{-1} \text{ g}^{-1} \text{ DW Ca}$), yellow ($1.7+5 \text{ mg}^{-1} \text{ g}^{-1} \text{ DW Ca}$), orange ($1.7+10 \text{ mg}^{-1} \text{ g}^{-1} \text{ DW Ca}$) and red ($1.7+15 \text{ mg}^{-1} \text{ g}^{-1} \text{ DW Ca}$). The Si treatments are plotted as circles ($1.4 \text{ mg}^{-1} \text{ g}^{-1} \text{ DW Si}$), triangles ($1.4+3 \text{ mg}^{-1} \text{ g}^{-1} \text{ DW Si}$), rhombus ($1.4+6 \text{ mg}^{-1} \text{ g}^{-1} \text{ DW Si}$) and square ($1.4+10 \text{ mg}^{-1} \text{ g}^{-1} \text{ DW Si}$). Further P control with additional phosphorous ($3 \text{ mg Na}_2\text{HPO}_4$ per sample, asterisk symbol) and Cl symbol (4 mg NaCl per sample, cross symbol). Metric Multidimensional Scaling (mMDS) of the bacterial community structure in Disko soils showed clear patterns with Ca concentrations.

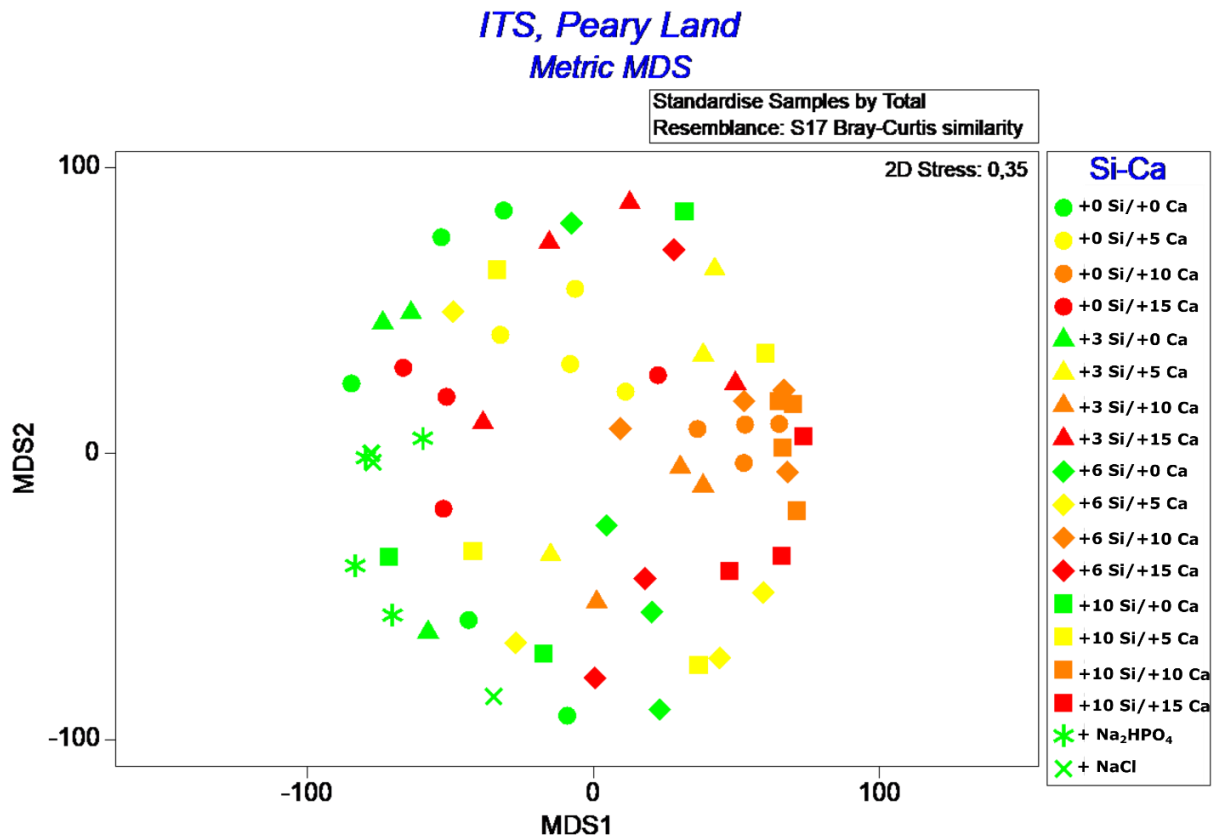


Figure S10: Metric Multidimensional Scaling (mMDS) of the ITS2 fungal community structure in Peary Land soil. Community structure based on fungal ITS2 genes from incubated Peary Land soils. (2D Stress: 0.35). The Ca treatments are colored in green ($5.6 \text{ mg}^{-1} \text{ g}^{-1} \text{ DW Ca}$), yellow ($5.6+5 \text{ mg}^{-1} \text{ g}^{-1} \text{ DW Ca}$), orange ($5.6+10 \text{ mg}^{-1} \text{ g}^{-1} \text{ DW Ca}$) and red ($5.6+15 \text{ mg}^{-1} \text{ g}^{-1} \text{ DW Ca}$). The Si treatments are plotted as circles ($1.4 \text{ mg}^{-1} \text{ g}^{-1} \text{ DW Si}$), triangles ($1.4+3 \text{ mg}^{-1} \text{ g}^{-1} \text{ DW Si}$), rhombus ($1.4+6 \text{ mg}^{-1} \text{ g}^{-1} \text{ DW Si}$) and square ($1.4 \text{ mg}^{-1} \text{ g}^{-1} \text{ DW Si}+10$). Further, P control with additional phosphorous ($1 \text{ mg Na}_2\text{HPO}_4$ per sample, asterisk symbol) and Cl control (5 mg NaCl per sample, cross symbol) can be found at the left side. Metric Multidimensional Scaling (mMDS) of the bacterial community structure in Disko soils showed clear patterns with Ca concentrations.

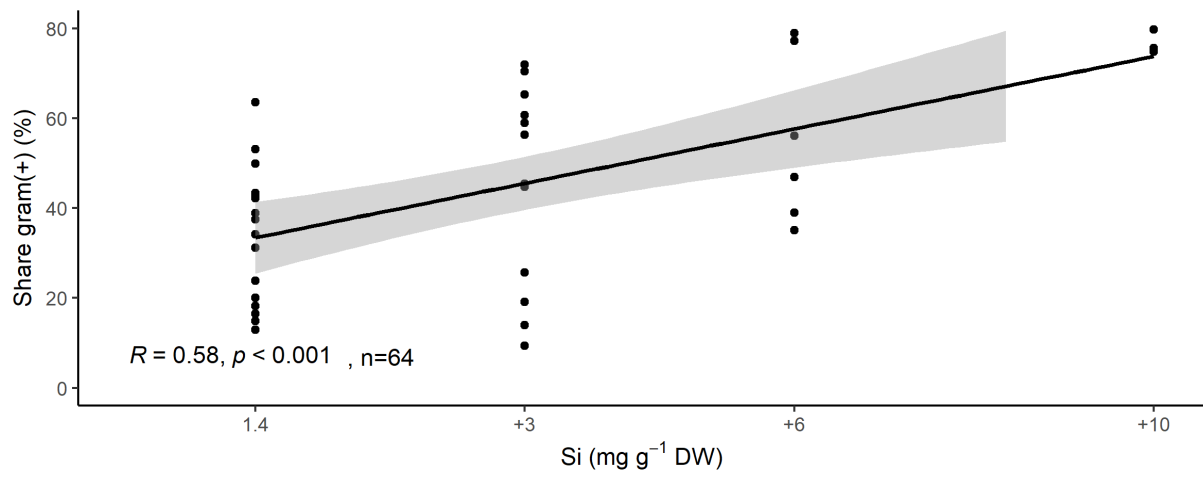


Figure S11: Fungal abundance and CO₂ production in Disko soil. Significant positive correlation of fungal abundance and - production over all Ca treatments in Disko soils, grouped by Si treatment.

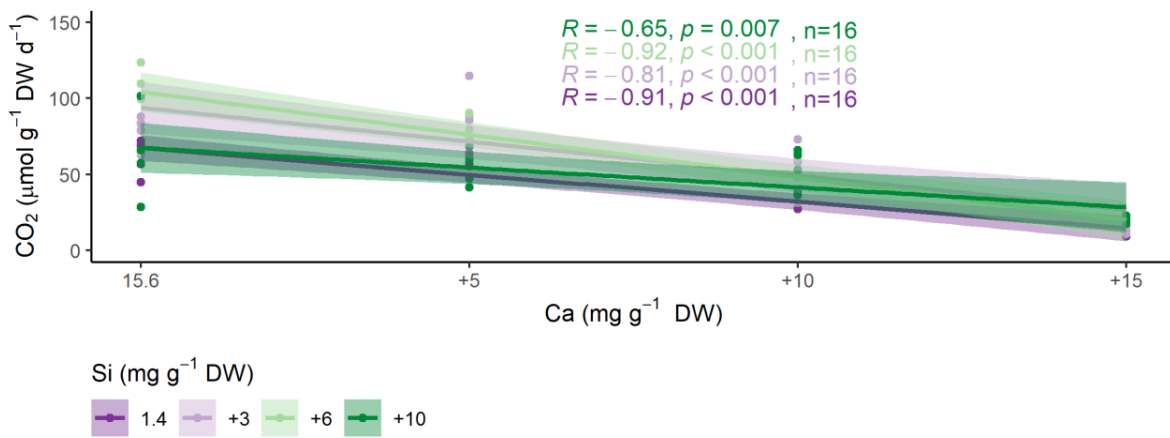


Figure S12: CO₂ production correlates significant negatively over all Si treatments in Peary Land soils.

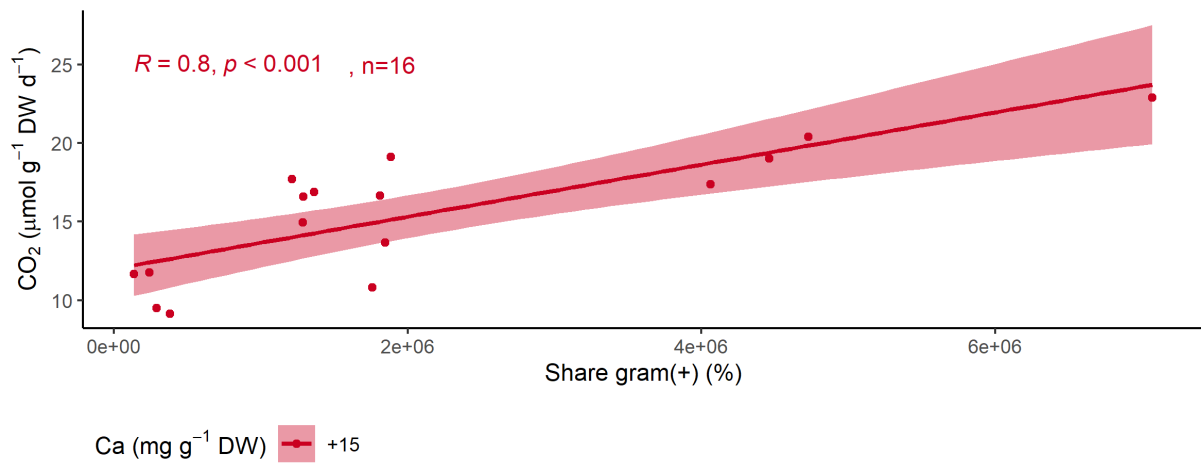


Figure S13: Gram-positive bacteria correlated positive with CO₂ production at highest Ca levels in Peary Land soils.

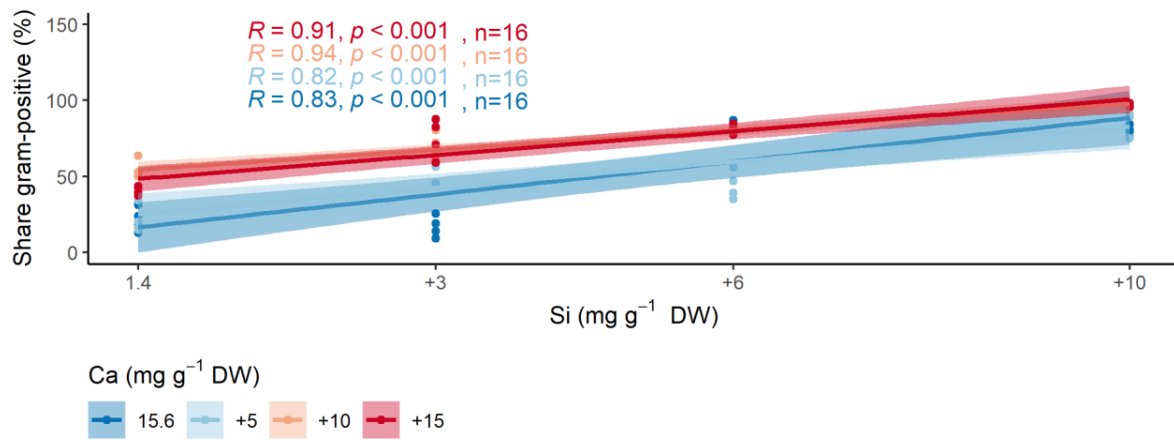


Figure S14: Si concentration and share of gram-positive bacteria in Peary Land soils. Si increased the share of gram-positive bacteria significantly under all Ca concentrations.

3.2.5 Study 5: Silicon and calcium controls on iron and aluminum availability in Arctic soils

Stimmler, M. Obst, Stein, et al. (2023)

Published 30.05.2023 in:

Chemosphere 335 (2023) 139087

(<https://doi.org/10.1016/j.chemosphere.2023.139087>)



Contents lists available at ScienceDirect

Chemosphere

journal homepage: www.elsevier.com/locate/chemosphere

Silicon and calcium controls on iron and aluminum mobility in Arctic soils

Peter Stimmler^a, Martin Obst^b, Mathias Stein^a, Mathias Goeckede^c, Kerstin Hockmann^{b,d},
Joerg Schaller^{a,*}

^a Leibniz Centre for Agricultural Landscape Research (ZALF), Eberswalder Str. 84, 15374, Müncheberg, Germany

^b Experimental Biogeochemistry, Bayreuth Center for Ecology and Environmental Research (BayCEER), University of Bayreuth, Bayreuth, Germany

^c Biogeochemical Signals (BSI), Max Planck Institute for Biogeochemistry, Jena, Germany

^d Department of Hydrology, Bayreuth Center for Ecology and Environmental Research (BayCEER), University of Bayreuth, Bayreuth, Germany

HIGHLIGHTS

- Si increased Al availability in acidic and neutral pH soils.
- Si decreased Al availability in alkaline soils.
- Si increased Fe availability by increasing Fe(II) phases.
- Ca decreased Al availability in Arctic soils.
- Si and Ca have to be considered for Fe and Al availability in Arctic soils.

GRAPHICAL ABSTRACT

	Siberia (pH 5.8)	Canada (pH 6.7)	Alaska (pH 6.6)	Alaska (pH 8.0)
Si effects on Fe	0	0	+	+
Si effects on Al	+	+	+	-
Ca effects on Fe	+	-	-	0
Ca effects on Al	-	-	-	-

ARTICLE INFO

Handling Editor: Prof. X. Cao

Keywords:
Aluminum
Iron speciation
Nutrients
Permafrost
Silica
SROAS

ABSTRACT

Arctic permafrost soils store large amounts of organic carbon and nutrients. With deepening of the perennial thawing upper active layer due to rising temperatures in the Arctic, not only the mobility of organic matter (OM), but also those of elements like silicon (Si) or calcium (Ca) may increase. It is known that major elements like Si and Ca can affect mineralization rates of OM, consequently influencing the carbon cycle. But only little is known about the interactions of Si and Ca with inorganic nutrients like iron (Fe) or potentially toxic elements like aluminum (Al) in Arctic soils. In this study, we analyzed the effect of Si and Ca fertilization in laboratory incubation experiments with soil samples from several Arctic regions. Our results show a significant increase in Fe and Al mobility (Mehlich-3 extractable) after increasing Si. Using high resolution X-ray microscopy (STXM/NEXAFS), we show that Si promotes Fe(II) phases and by this increases Fe mobility. Al mobility was increased for acidic and neutral pH soils but decreased for alkaline soils after increasing Si. Furthermore, we show a decreased Al mobility after increasing Ca, independent on the original pH values and the OM content of the soils. These results demonstrate the importance of interactions between Si and Ca on one hand and Fe and Al mobility on the other hand for Arctic soils.

* Corresponding author.

E-mail address: Joerg.Schaller@zalf.de (J. Schaller).

<https://doi.org/10.1016/j.chemosphere.2023.139087>

Received 15 March 2023; Received in revised form 26 May 2023; Accepted 29 May 2023

Available online 30 May 2023

0045-6535/© 2023 Elsevier Ltd. All rights reserved.

Author contribution statement

J.S. and M.G. conceived the study. P.S. conducted the experiment and analyzed the data. M.O., P.S., K.H. and M.S. did the XAS measurements and analyzed the data. P.S. wrote the first draft of the manuscript. J.S., M.O., M.S., K.H. and M.G. revised the manuscript. All author agreed on the final version of the manuscript.

1. Introduction

The permafrost soils of the Northern Hemisphere store 1014 to 1035 Pg of organic carbon (Hugelius et al., 2014; Mishra et al., 2021). As temperatures are rising twice as fast in northern regions compared with the global average (IPCC, 2021), about 13.9×10^6 km² of the Arctic permafrost soils (Obu et al., 2019) show deeper perennial thaw of the active layer and increasing soil temperatures (Romanovsky et al., 2010; Abramov et al., 2021). As a result, emissions of greenhouse gases (GHG) like CO₂ and CH₄ are altered (Schoor et al., 2015; Virkkala et al., 2021). Deepening of the active layer by thawing of the underlying permafrost layer may mobilize elements like silicon (Si), calcium (Ca), iron (Fe) and potentially toxic elements (PTEs) like aluminum (Al) from deeper soil horizons modifying the mobility in the upper soil layer. This new mobilized pool of Si, Ca, Fe and Al holds the potential for further feedbacks with element cycle processes.

For organic rich peatland soils it was shown that Si can mobilize elements like Fe (Reithmaier et al., 2017). On the one hand, the presence of amorphous silica (ASi) was shown to increase the share of Fe(II) phases by potentially reducing hydraulic conductivity, thus, promoting the use of Fe minerals as electron acceptors (Schaller et al., 2022). On the other hand, ASi may stabilize short-range ordered Fe phases and preventing them from mineralization by exchanging OH-groups with monomeric silicate species (Kanematsu et al., 2018). Moreover, silicic acid may alter the formation and transformation of Fe (oxy)hydroxides in soils due to the formation of silicic acid-associated Fe (oxy)hydroxides e.g., ferrihydrite. Consequently, Si may stabilize ferrihydrite against transformation even under Fe-reducing conditions (Schulz et al., 2022). In presence of dissolved Si, Al can form short-range ordered aluminosilicates (SROAS) in solutions at pH < 5 and >7 (Wada and Kubo, 1975; Schaller et al., 2021). Solid phase Al(OH)₃ may also react with silicic acid forming SROAS (Yokoyama et al., 2002). Most recently a strong effect of both elements on soil respiration of Arctic soils was found with Si increasing, and Ca decreasing soil respiration (Stimmeler et al., 2022; Schaller et al., 2023). For several regions of the Arctic, it is suggested that Si and/or Ca mobility may increase due to permafrost thaw (Stimmeler et al., 2023). Such increased Ca concentration in soil solution may increase the pH, potentially decreasing Fe mobility as its solubility decreases with increasing pH (Marschner, 2003). At anoxic conditions Ca ions may compete with Fe(II) bound to e.g., clay mineral surfaces (Van Groeningen et al., 2020), potentially releasing Fe in solution via cation exchange. Moreover, Ca may interact with Fe in regard to binding to organic matter and increases the sorption capacity of Fe-OM associations (Beauvois et al., 2021). Al mobility in soils may decrease with increasing Ca concentrations, as the precipitation of Al(OH)₃ is favored at increasing pH (Kryzevicius et al., 2019).

However, it is unknown whether the Si effects on Fe mobility exist beyond organic rich peatland soils in mineral dominated soils and over which soil pH range. It is also not clear under which condition the effect of Si limiting Al mobility by the precipitating SROAS occurs in thawing permafrost soils. Furthermore, it is unknown whether Ca, being potentially important for soil respiration, is also important for the mobility of Fe and Al for different Arctic soils differing in pH and Al and Fe contents. Such understanding is crucial, as Fe is a nutrient for plants and microbes and Al is a PTE for such organisms (especially under low pH conditions), to predict effects on future ecosystem performance in the Arctic e.g., biomass production or soil respiration.

To test for the interdependency between Si and Ca concentration on

Chapter 3. Manuscripts

Fe and Al mobility (Mehlich-3 extractable) we incubated four Arctic soils differing in soil pH and initial Si, Ca, Fe and Al mobility, with Si and Ca addition in the range of expected changes in Arctic soils due to permafrost thaw, estimated by another study (Stimmeler et al., 2023). Our hypotheses were that (i) Si increases Fe and decreases Al mobility, and (ii) Ca decreases both Fe and Al mobility in Arctic soils.

2. Material and methods

2.1. Sample collection and storage

All four soil samples were collected in the field with a spade or auger. The samples were transported frozen and stored for less than 4 weeks at -20 °C until the experiments started. These four different soils were chosen because of the differences in pH and element mobility. Coordinates and sampling depth of the five locations are shown in Table 1. Before incubation the soil samples were crushed with a hammer under frozen conditions. To ensure homogeneity the crushed soil was sieved to a particle size < 6.5 mm. The total element concentration of the soils were for C2 (25% Si, 0.8% Ca, 3.8% Fe, 5.6% Al, and 0.07% P), MAT (23% Si, 0.9% Ca, 3.4% Fe, 3.5% Al, and 0.06% P), MNT (23% Si, 4.6% Ca, 2.6% Fe, 3.6% Al, and 0.05% P), and Ca1 (9% Si, 5.3% Ca, 0.8% Fe, 0.8% Al, and 0.17% P); all measurements were done using XRF (NITON XRF-Analyzer XL3 SDD, Analyticon Instruments GmbH, Rosbach, Germany). The soils were chosen because of the differences in pH, Si, Ca, Fe, and Al concentrations to test if effects by Si and Ca are common for all or specific for certain soil conditions.

2.2. Incubation experiment

To analyze the effects of Si and Ca on Fe and Al mobilization, soil was fertilized with four levels of Si (+0, +3, +6 and +10 mg g⁻¹ DW soil, using Aerosil-300, Evonik, Germany) and Ca (+0, +5, +10 and +15 mg g⁻¹ DW soil, as CaCl₂ x 2H₂O) to cover the potential changes in Si and Ca mobility due to permafrost thaw (Stimmeler et al., 2023). Aerosil-300 is an amorphous Si which has comparable properties to natural occurring amorphous Si (Lindner et al., 2022). Therefore, 5 g soil were weighed into 20 ml incubation vials (Ochs Laborbedarf, Bovenden, Germany) and gently mixed after adding 2 ml fertilization solution. For control 5 g soil was mixed with 2 ml pure water and the vial was closed with parafilm. For simulation of a thawing active layer the incubation of all treatments was examined under waterlogged conditions for 24 weeks at 5 °C in the dark. After 24 weeks soil samples were taken, freeze dried, and analyzed. A subsample was taken for STXM measurements.

2.3. Mehlich-3 extraction

For analysis of available Si, Ca, Fe and Al the Mehlich-3 extraction was used (Mehlich, 1984). Therefore, 2 g of freeze-dried soil were exposed to 20 ml Mehlich-3 extractant (0.25 M NH₄NO₃, 0.015 M NH₄F, 0.001 M EDTA, 0.2 M acetic acid, 0.013 M HNO₃) and shaken at room temperature for 5 min at 120 rounds per minute. Samples were centrifuged for 2 min at 10,000 g and filtered using a 0.2 µm cellulose acetate

Table 1

Information to locations, soil type and depths of incubated soils.

Region	Soil	Coordinates	Depth [cm]
Chersky, Siberia, Russia; Umbric cryosol	C2	68,61685°N, 161,3504°E	50–60
moist acidic tundra, Alaska, US; Histic cryosol	MAT	69,42554°N, 148,69633°E	20–40
moist non-acidic tundra, Alaska, US; Turbic cryosol	MNT	69,43303°N, 148,67435°E	0–25
Canadian Shield, Canada; Histic cryosol	Ca1	69,22325°N, 104,90041°E	0–25

syringe filter (Chromafil Xtra-CA-20/25, Macherey-Nagel, Düren, Germany). Element concentrations in extract were analyzed by Inductively coupled plasma atomic emission spectrometry (ICP-iCAP 6300 DUO, ThermoFisher SCIENTIFIC, Waltham, Massachusetts, USA).

2.4. Scanning transmission X-ray microscopy measurements

To elucidate the underlying biogeochemical mechanisms, explaining the changing element availabilities, spatially resolved quantification of the involved chemical species is required. Therefore, we used scanning transmission (soft) X-ray microscopy (STXM) at beamline 10ID-1 at the Canadian Light Source. Soil samples were suspended in de-ionized water and wet-deposited onto Formvar coated, 300 mesh Cu TEM grids (Plano GmbH, Wetzlar, Germany), blotted, and dried immediately. For quantification and characterization of the involved iron phases along the gradient from the inside to the surface of individual particles, the Fe $L_{3,2}$ absorption edges at 706.8 and 719.9 eV were chosen (scanning energy range: 699–740 eV) as they turned out to provide most valuable spatially resolved information efficiently in previous studies (Schaller et al., 2019; Sowers et al., 2020). For analysis, the near-edge X-ray fine structure (NEXAFS) spectra were linearly decomposed using reference spectra of ferrihydrite and goethite as potential Fe(III)-phases and vivianite and siderite as potential Fe(II)-phases. The lowest standard deviations were achieved by a combination of ferrihydrite and vivianite. Therefore, normalized spectra (1 nm thickness) of these two phases were used for quantitative mapping of the phases and for spectral fitting. For these analyses the aXis2000 software package (www.unicorn.mcmaster.ca), Hitchcock (2017) was used.

2.5. Statistics

2.5.1. Element mobility

Statistics were done using R (R Core Team, 2021). For statistics, element mobility was calculated in mg g^{-1} DW soil and data higher or lower the mean \pm threefold standard deviation were deleted as outliers. Graphs were generated with the *geom_smooth* function from the “ggplot2” (version 3.3.6) package, correlations were performed with the *stat_cor* function from the “ggpubr” (version 0.4.0) package with a probability of $p = 0.001$ and a correlation coefficient of $r = 0.01$. The metric multidimensional scaling (mMDS) was calculated using the functions *dist* and *cmdscale* and *kmeans* from the “stats” package (version 4.1.3) and plotted with *ggscatter* from the “ggpubr” package.

2.5.2. STXM-NEXAFS data

Spectra of goethite, ferrihydrite, siderite, vivianite as reference materials and a non-Fe background modelled as organic carbon CH_2O from the atomic scattering factors (Henke et al., 1993), all normalized to a 1 nm layer thickness, were used in different combinations for curve fitting (CGO function) of the average spectra of the sample. The combination ferrihydrite, vivianite and CH_2O showed the lowest standard deviation. These were used in the SVD function to create maps of vivianite, ferrihydrite and CH_2O . Using the vivianite map masks with areas containing optical densities of 1.0–2.0 nm, 2.1–4.0 nm, 4.1–10 nm and 11–16 nm were generated. These maps were used to extract the spectra from areas with specific optical densities (ODs) of the average sample. These area specific spectra were fitted with the CGO function to calculate the theoretical layer thickness of vivianite, ferrihydrite and CH_2O . The ratio of vivianite to total iron was calculated using the following equation:

$$\text{ratio} = \frac{\text{vivianite}[\text{nm}]}{\text{vivianite}[\text{nm}] + \text{ferrihydrite}[\text{nm}]}$$

The ratios of single ODs were grouped and mean, and standard deviation was calculated for every soil. Significances were calculated with a one-way ANOVA at the 95% confidence interval for single ODs. The heatmap was plotted using the *geom_tile* function of the “ggplot2” package.

3. Results

3.1. Initial soil properties

The soils differed in their element mobility and differed significantly (ANOSIM, $p < 0.001$, $R = 0.235$) in the metric multidimensional scaling (mMDS) plot (Fig. S1). In the mMDS plot the data were plotted based on the Euclidian distances that is given on the axis. A close distance between samples points to higher similarity based on the given parameters (here mobility of Si, Ca, Fe and P at different Si and Ca contents). The weak acidic soil from Chersky, Siberia, Russia (C2) was tested to have an element mobility comparable to the soil from Alaska, moist acidic tundra (MAT). Both soils showed low initial Si and Ca contents and a weak acidic to neutral pH as seen in Table 2. However, the soils from Alaska, moist non-acidic tundra (MNT) characterized by alkaline pH ($\text{pH} = 8.0$), high Ca contents, low Si contents and thus showed a higher Euclidian distance from all other soils. The soil from the Canadian Shield (Ca1) consisted mainly of peat and was clearly separated in the mMDS plot. The pH was nearly neutral ($\text{pH} = 6.7$), the Ca content was high ($7.39 \pm 0.56 \text{ mg g}^{-1}$ DW) and the Si content low ($0.09 \pm < 0.01 \text{ mg g}^{-1}$ DW).

3.2. Mobility of Si, Ca, Fe and Al in the Arctic soils

Overall, the pattern of Si and Ca effects on both Fe and Al were different for the examined soils, except of the effect of Ca on Al mobility which was negatively correlated for all soils (Table 3).

In the soil C2 from Siberia the Fe mobility ranged from 0.50 to 0.90 mg g^{-1} DW over all treatments. There was no significant correlation with Si concentration. However, Ca was weak but significant positive correlated with Fe (Pearson, $p = 0.002$, $R = 0.37$) (Fig. 1A–C). When single Ca treatments were considered, strong positive correlations (Pearson, $R = 0.45$ – 0.7) but lower p values were found. Iron and silicon correlated significantly positive in every single Si treatment ($R = 0.74$ – 0.87 , $p < 0.001$) (Fig. S2). Aluminum contents ranged from 0.52 to 0.92 mg g^{-1} DW and increased significantly over all Si contents (Pearson, $R = 0.63$, $p < 0.001$) (Fig. 1B). This was shown for single Si treatments, too (Fig. S2). For Ca we found a significant negative correlation with Al (Pearson, $R = -0.76$, $p < 0.001$) over all Ca treatments (Fig. 1D). Fe and Al correlated significant positively, but only for single Ca treatments separately (Fig. S6).

The MAT soil showed Mehlich 3 extractable Fe contents of 0.32–0.70 mg g^{-1} DW. The Fe contents were significantly positive correlated with Si contents over all Si treatments (Pearson, $R = 0.58$, $p < 0.001$) (Fig. 2A) and even better in single Si treatments ($R = 0.74$ – 0.87 , see Fig. S3). For Ca weak but significant negative correlation with Fe was found over all treatments ($R = -0.23$, $p = 0.046$, Fig. 2C). However, when single Ca treatments were analyzed, significant positive correlations were found for +0 and +10 mg g^{-1} DW Ca (Fig. S2). Aluminum contents ranged from 0.54 to 1.13 mg g^{-1} DW and were significantly

Table 2

Initial mobility of Si, Ca, Fe, Al, and pH in incubated soils extracted with the Mehlich-3 method given as mean with standard deviation in mg g^{-1} DW soil. Soils from Siberia: Chersky (C2, Siberia, Russia), Canadian Shield (Ca1, Canada), moist acidic tundra (MAT, Alaska, US) and moist non-acidic tundra (MNT, Alaska, US) were analyzed after incubation under waterlogged conditions. Each with a replication of five.

	Si	Ca	Fe	Al	pH
C2	0.16 ± 0.02	1.14 ± 0.06	0.65 ± 0.06	0.84 ± 0.04	5.8
Ca1	0.17 ± 0.04	6.77 ± 0.42	1.44 ± 0.04	0.12 ± 0.04	6.7
MAT	0.07 $\pm < 0.01$	4.16 ± 0.25	0.50 ± 0.05	0.93 ± 0.06	6.6
MNT	0.09 $\pm < 0.01$	7.94 ± 0.51	0.17 $\pm < 0.01$	0.18 ± 0.03	8.0

Table 3

Summary of the Si and Ca effects on both Fe and Al mobility in the different soils considering all different Si and Ca treatments and not considering the interdependency in the single Si and Ca treatments.

	C2 (Siberia)	Ca1 (Canada)	MAT (Alaska)	MNT (Alaska)
Si effects on Fe	0	0	+	+
Si effects on Al	+	+	+	-
Ca effects on Fe	+	-	-	0
Ca effects on Al	-	-	-	-

positive correlated with Si over all treatments (Pearson, $R = 0.36$, $p = 0.001$, see Fig. 2B). For the different Si treatments the correlation of Al and Si was even higher (Pearson, $R = 0.38$ – 0.71 , see Fig. S2). With increasing Ca concentrations, the Al mobility decreased significantly (Pearson, $R = -0.56$, $p < 0.001$) (Fig. 2D). However, for single Ca concentrations a significant positive correlation of Ca and Al was found (Fig. S2). Fe and Al were significant positively correlated (Pearson, $R = 0.76$, $p < 0.001$) over all treatments and in every single Ca treatment (Fig. S6).

For the MNT soil the Fe mobility increased significantly (Pearson, $R = 0.31$, $p = 0.007$) from 0.14 to 0.22 mg g^{-1} DW when Si concentrations increased (Fig. 3A). Even higher R values were found for single Si treatments (Fig. S4). With increasing Ca concentrations, Fe mobility showed no clear pattern over all treatments (Fig. 3C). However, for single Ca treatments a significant positive correlation was shown for Ca and Fe contents (Fig. S4). Aluminum content ranged from 0.04 mg g^{-1} DW to 0.23 mg g^{-1} DW and significantly decreased with increasing Si concentrations (Pearson, $R = -0.46$, $p < 0.001$) (Fig. 3C). The correlation was significantly negative for all single Ca treatments, too (Fig. S4). Within all Ca treatments Al decreased significantly (Pearson, $R = -0.26$, $p = 0.026$) (Fig. 3D). However, considering the single Ca treatment no clear pattern was found regarding Al mobility as positive and negative correlations were found (Fig. S4). Aluminum and Fe mobility correlated

weak and not significantly, neither considering all nor single treatments (Fig. S6).

Soil Ca1 differed from the three others soils because of its very high organic carbon and low mineral content, as it consisted mainly of peat (Stimmeler et al., 2022). The Fe contents ranged from 1.11 to 1.51 mg g^{-1} DW and showed no clear relationship with Si contents (Fig. 4A). When single Si treatments were considered, a significant positive correlation was found for Fe for two of four treatments (Fig. S5). The Fe contents decreased significantly (Pearson, $R = -0.73$, $p < 0.001$) with increasing Ca contents (Fig. 4C). Considering the single Ca treatments, no clear pattern was shown as one treatment correlated positively, one negatively and another treatment showed no effect (Fig. S5). Aluminum content was lowest with no Si addition (0.001 mg g^{-1} DW Al) and increased up to 0.83 mg g^{-1} DW with Si addition. There was a significant positive correlation (Pearson, $R = 0.39$, $p = 0.002$) for Si and Al contents (Fig. 4B) and similar pattern were found for single Si treatments (Fig. S4). With increasing Ca concentration Al mobility decreased significantly (Pearson, $R = -0.7$, $p < 0.001$) (Fig. 4D). But considering single Ca treatments no clear effect on Al mobility was found as one treatment showed positive correlation and the other two treatments showed no correlation (Fig. S5). Aluminum and Fe contents correlated significantly positive (Pearson, $R = 0.62$, $p < 0.001$) over all treatments, R values were even higher when single Ca treatments were considered (Fig. S6).

3.3. STXM-NEXAFS analysis of the iron phases

Soil C2 was analyzed by scanning transmission X-ray microscopy (STXM), which is an approach that employs spatially resolved near edge X-ray absorption fine structure (NEXAFS) spectroscopy to identify, map and quantify chemical species (Schaller et al., 2019, 2022; Hömberg et al., 2020). The analysis was done for the control, the highest Si ($+10$ mg g^{-1} DW) and the highest Ca ($+15$ mg g^{-1} DW) treatments (Fig. 5A–J). Compared to the control, the samples of the Si treatment

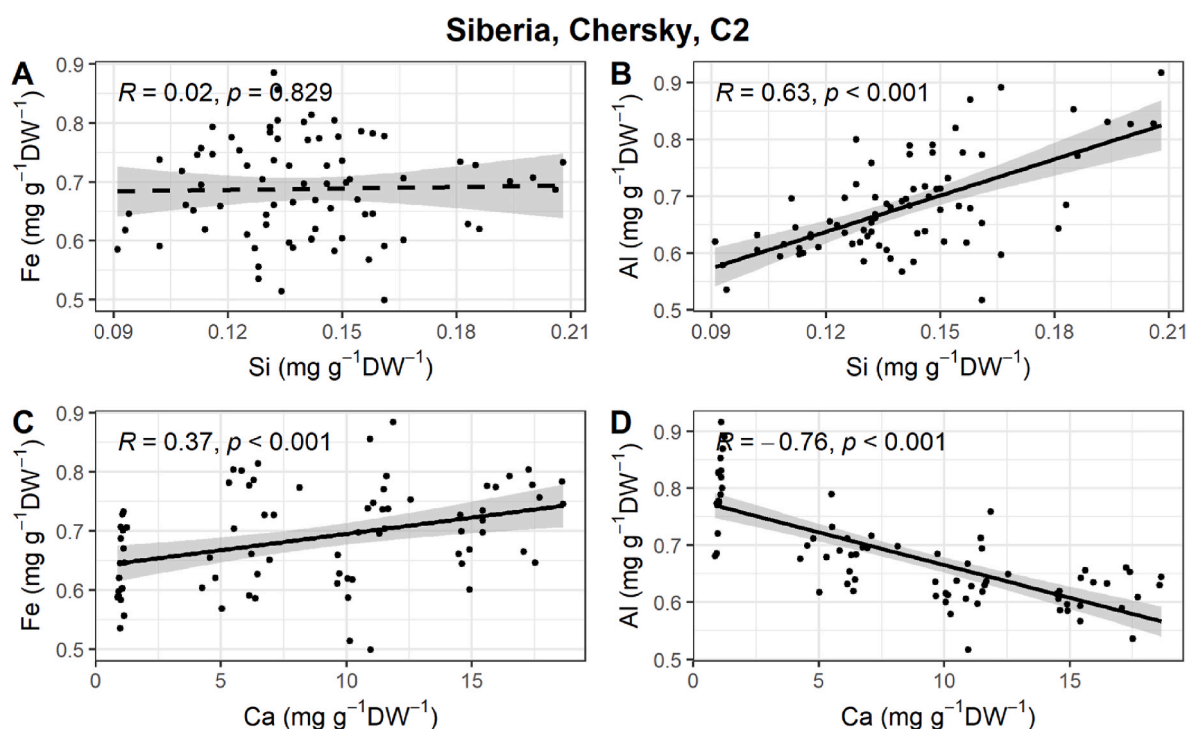


Fig. 1. Soil C2. Mobility of Fe and Al with Si (A + B) and Ca (C + D) addition after 24 weeks of incubation under waterlogged conditions. For extraction Mehlich 3 method was used and contents are given in mg g^{-1} DW. Data shown contains all treatments of Si ($+0$, $+3$, $+6$, $+10$ mg g^{-1} DW) and Ca ($+0$, $+5$, $+10$, $+15$ mg g^{-1} DW). For statistics p value at the 95% confidence interval and the Pearson correlation were used. Solid lines show significant correlation whereas dashed lines show non-significant correlation.

Alaska, mosist acidic tundra (MAT)

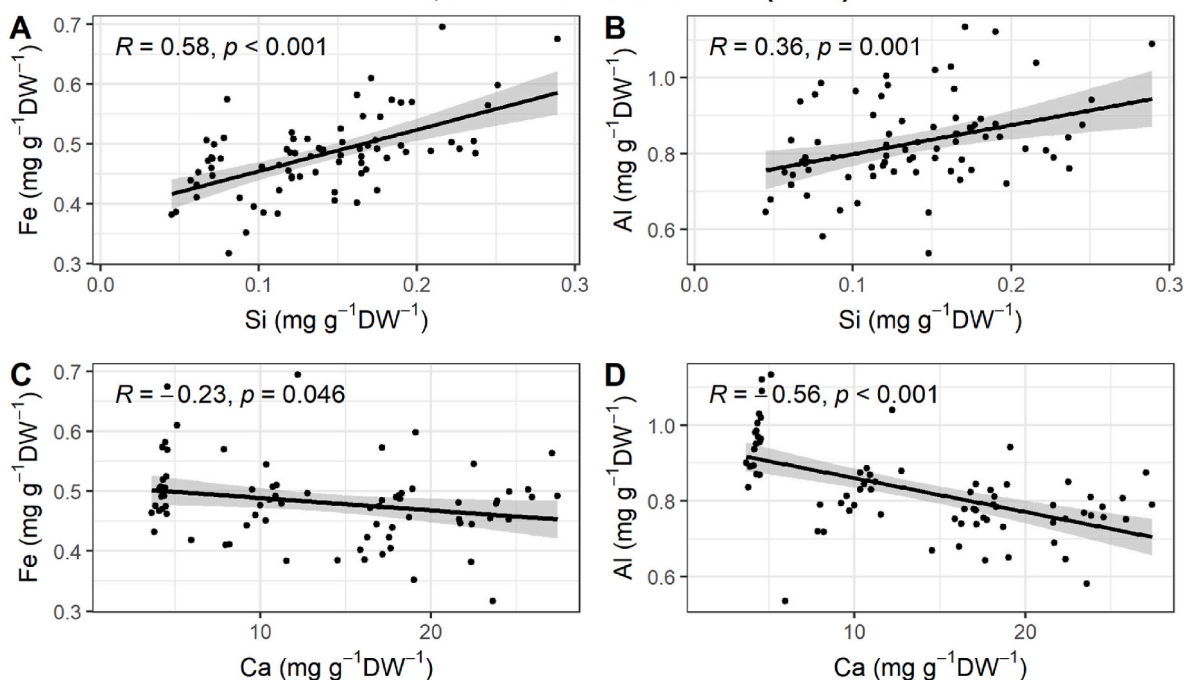


Fig. 2. Soil MAT. Mobility of Fe and Al with Si (A + B) and Ca (C + D) after 24 weeks of incubation under waterlogged conditions. For extraction Mehlich 3 method was used. Contents are given in mg g⁻¹ DW. Data shown contain all treatments of Si (+0, +3, +6, +10 mg g⁻¹ DW) and Ca (+0, +5, +10, +15 mg g⁻¹ DW). For statistics p value at the 95% confidence interval and the Pearson correlation were used. Solid lines show significant correlation.

Alaska, moist-nonacidic tundra (MNT)

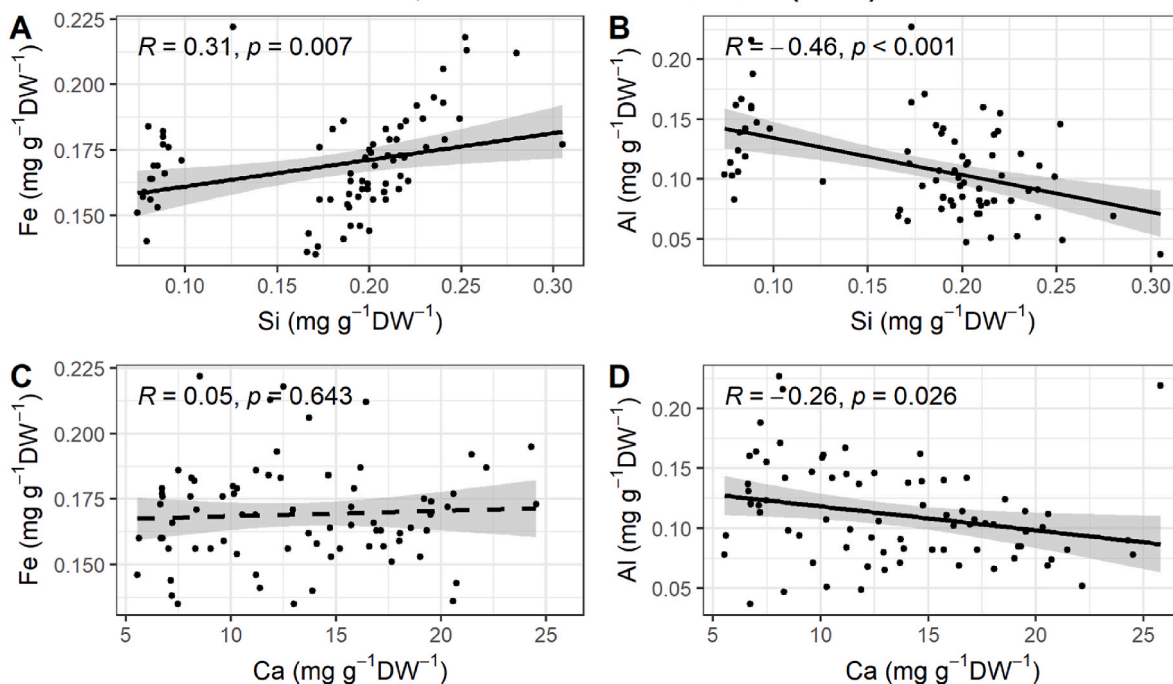


Fig. 3. Soil MNT. Mobility of Fe and Al with Si (A + B) and Ca (C + D) after 24 weeks of incubation under waterlogged conditions. For extraction Mehlich 3 method was used, concentrations are given in mg g⁻¹ DW. Data shown contain all treatments of Si (+0, +3, +6, +10 mg g⁻¹ DW) and Ca (+0, +5, +10, +15 mg g⁻¹ DW). For statistics p value at the 95% confidence interval and the Pearson correlation were used. Solid lines show significant correlation whereas dashed lines show non-significant correlation.

contained a higher amount of ferrous phases (Fe(II)), spectroscopically similar to vivianite (red lines at 708 eV and 720 eV) than of a ferric phase (Fe(III)) similar to ferrihydrite (green lines at 710 eV and 723 eV).

The fitted, species-specific maps of the Si treatment (Fig. 5B) showed large amount of the vivianite-like phases (red areas), whereas the control sample (Fig. 5E) contained mainly the ferrihydrite-like phases

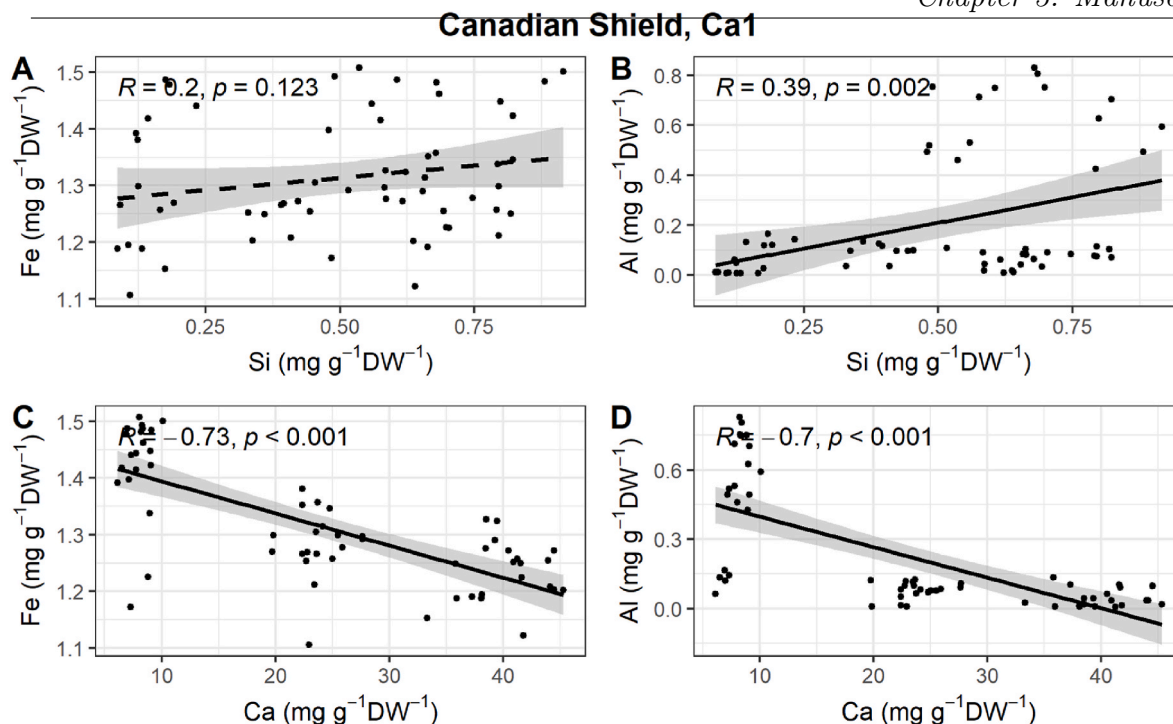


Fig. 4. Soil Ca1. Mobility of Fe and Al with Si (A + B) and Ca (C + D) after 24 weeks of incubation under waterlogged conditions. For extraction Mehlich 3 method was used, contents are given in $\text{mg g}^{-1} \text{DW}$. Data shown contain all treatments of Si (+0, +3, +6, +10 $\text{mg g}^{-1} \text{DW}$) and Ca (+0, +5, +10, +15 $\text{mg g}^{-1} \text{DW}$). For statistics p value at the 95% confidence interval and the Pearson correlation were used. Solid lines show significant correlation whereas dashed lines show non-significant correlation.

(green areas) (see also Fig. S7 for reference spectra). The samples of the Ca treatment (Fig. 5H) showed similar amounts of the ferrihydrite-like phase (green areas) like the control soil and a higher amount of a non-Fe phase that was fitted as a model of organic carbon (blue areas). The spectra of the Si treatments showed a higher linear absorbance at energies of that of vivianite-specific (red lines at 708 eV and 720 eV) compared to the control soil and the Ca treatment (Fig. 5J). In the Si treatment (Fig. 5J, dashed lines) the content of vivianite-like phases differed within the particle. The content of vivianite-like phases was higher in areas representing the inner bulk particle (10–16 nm of vivianite, shown in pink, also see Fig. 5C, F and I) compared to areas representing the surface of the particle (1–2 nm vivianite, shown in red). In the control treatment (continuous line) and Ca treatment (dotted line) this effect was much weaker. When all treatments (control, Si and Ca) were considered, a significant increase (ANOVA, $p < 0.001$, $df = 3$, $F = 23.5$) in the ratio vivianite-like $\text{Fe}/\text{Fe}_{\text{total}}$ was observed from 0.27 ± 0.03 in surface areas (1–2 nm vivianite) to 0.47 ± 0.09 in areas representing the bulk (10–16 nm vivianite) (Fig. 9A).

The STXM-NEXAFS analysis was done for the control and the highest Ca (+10 $\text{mg g}^{-1} \text{DW}$) treatment for the MAT soil (Fig. 6A–G). The fitted, species-specific maps of the bulk showed a high non-iron content for both, control and Ca treatment (Fig. 6B + E, blue areas) and a similar amount of vivianite-like phases (red areas) and ferrihydrite-like phases (green areas). The spectra of the control (continuous line) and Ca treatment (dotted line) showed similar intensities of vivianite-like phases (708 eV, 720 eV) and ferrihydrite-like phases (710 eV, 723 eV) (Fig. 6G, see also Fig. S7 for reference spectra). With all treatments the ratio of vivianite-like to total iron phases increased significantly (ANOVA, $p < 0.05$, $df = 3$, $F = 3.7$) from 0.28 ± 0.10 in areas representing the particle surface (1–2 nm vivianite, shown in red, see also Fig. 6C + F) to 0.36 ± 0.08 in areas representing mainly the bulk (10–16 nm vivianite, shown in pink) (Fig. 9A).

The STXM-NEXAFS analysis were done for the control and the Si treatment of the MNT soil (Fig. 7A–G). The bulk samples of the Si

treatment showed a higher amount of vivianite-like phases (red areas) compared to the control (Fig. 7B + E). The spectra of the Si treatment (Fig. 7G, blue dashed line) showed higher linear absorbance for vivianite-like phases (red lines at 708 eV and 720 eV) in areas representing the bulk particle (4–10 nm, shown in blue see also Fig. 7C + F) compared to the control soil (blue continuous line). In areas representing the surface (1–2 nm vivianite-like phases (shown in red) the control and Si treatment did not differ in the spectra anymore. The ratio vivianite-like iron to total Fe increased significantly (ANOVA, $p < 0.01$, $df = 3$, $F = 6.7$) from 0.21 ± 0.02 in outer particle areas containing 1–2 nm vivianite to 0.39 ± 0.12 in inner particle areas containing 10–16 nm vivianite (Fig. 9A).

The STXM-NEXAFS analysis were done for the control and the highest Ca (+10 $\text{mg g}^{-1} \text{DW}$) treatment of the soil from Canada (Ca1). The fitted species-specific maps of the bulk (Fig. 8G) showed larger areas of vivianite-like phases (red areas) in the Si treatment, compared to the control (Fig. 8B + E). The surface area of the particles (1–2 nm vivianite, shown in red, see also Fig. 8C + F) of the Si treatment (dashed line) showed a higher ratio of vivianite-like Fe to total Fe compared to the control soil (continuous line). The spectra of the bulk particle (Figs. 8G, 4–10 nm, shown in blue) showed lower ratio of vivianite-like Fe to total Fe compared to the surface area (1–2 nm, shown in red). For the control and Si treatment together the ratio of vivianite-like Fe to total Fe ranged between 0.40 ± 0.1 and 0.43 ± 0.08 (Fig. S7).

Fig. 9A shows the ratio of thickness in nm of Fe(II)phosphate to total Fe from the species-specific curve fitting of spectra of single ODs of all treatments in the soils from Chersky (Siberia, Russia, C2), the Canadian Shield (Ca1) and moist acidic tundra and moist-nonacidic tundra (MAT and MNT Alaska, USA). Over all soils (C2, MAT, MNT, Ca1) and all treatments (control, +10 $\text{mg g}^{-1} \text{DW}$ Si and +15 $\text{mg g}^{-1} \text{DW}$ Si Ca treatments) there was a significant positive correlation (Pearson, $R = 0.46$, $p = 0.04$) between the ratio of vivianite-like iron to total iron and the total iron (Fig. 9B).

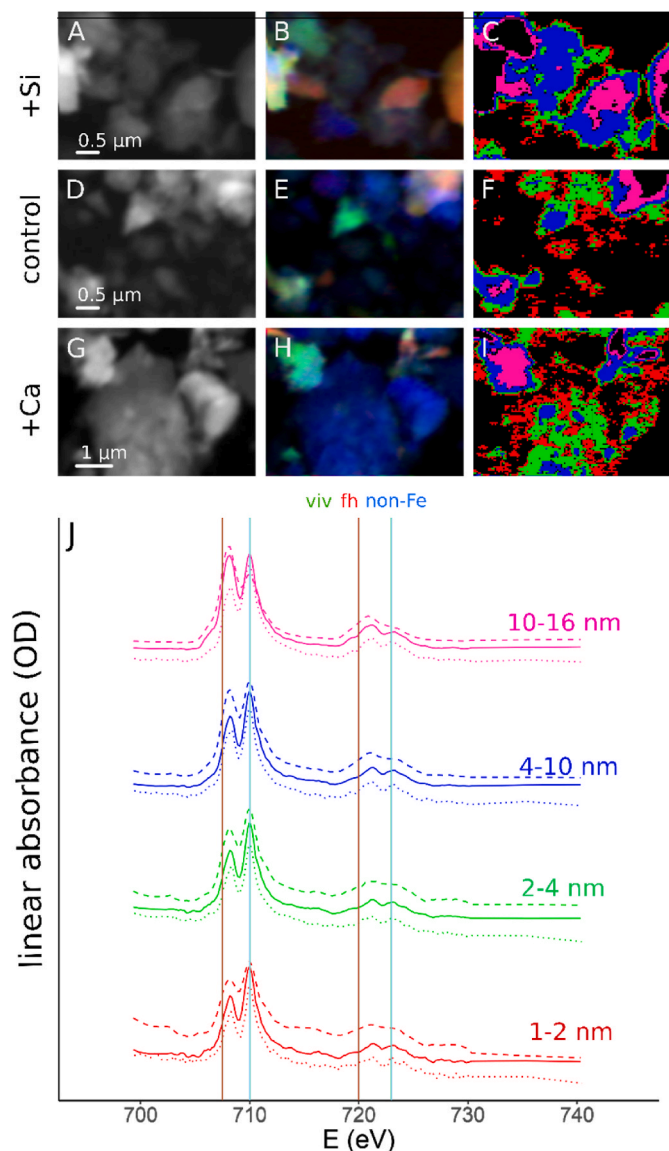


Fig. 5. STXM-NEXAFS measurements of the soil C2. Images show soils with addition of Si (A–C), control soil without treatment (D–F), and soil with addition of Ca (G–I). Figures A, D and G show averaged linear absorbance maps across the Fe2p edges of soil particles of the different treatments analyzed. Figures B, E and H show quantitative red/green/blue (RGB) composite maps of vivianite-like phases (red), ferrihydrite-like phases (green) and non-Fe background (blue), derived from linear decomposition of the image stacks using respective spectra of reference compounds. In the region of interest maps C, F and I colors represent areas with same thickness (red: 1–2 nm, green: 2–4 nm, blue: 4–10 nm, pink: 10–16 nm) of vivianite. Figure J shows the linear absorbance (OD) for areas with same thickness of vivianite for control (continuous line), Si treatment (dashed line) and Ca treatment (dotted line). Vertical light brown lines at 708 eV and 720 eV represent specific absorbance maxima for vivianite, vertical blue lines at 710 eV and 723 eV represent specific absorbance maxima for ferrihydrite. (For interpretation of the references to color in this figure legend, the reader is referred to the Web version of this article.)

4. Discussion

Hypothesis (i) was partially confirmed with Si increasing Fe mobility for the soils from Alaska (MAT and MNT), but decreasing Al mobility only for the MNT soil with a pH of 8.0 but increasing Al mobility for all soils with a pH ≤ 6.7 and. The hypothesis (ii) was also only partially confirmed with Ca decreasing Al mobility for all soils but Ca showing no clear effect on Fe mobility. However, considering single Si and Ca

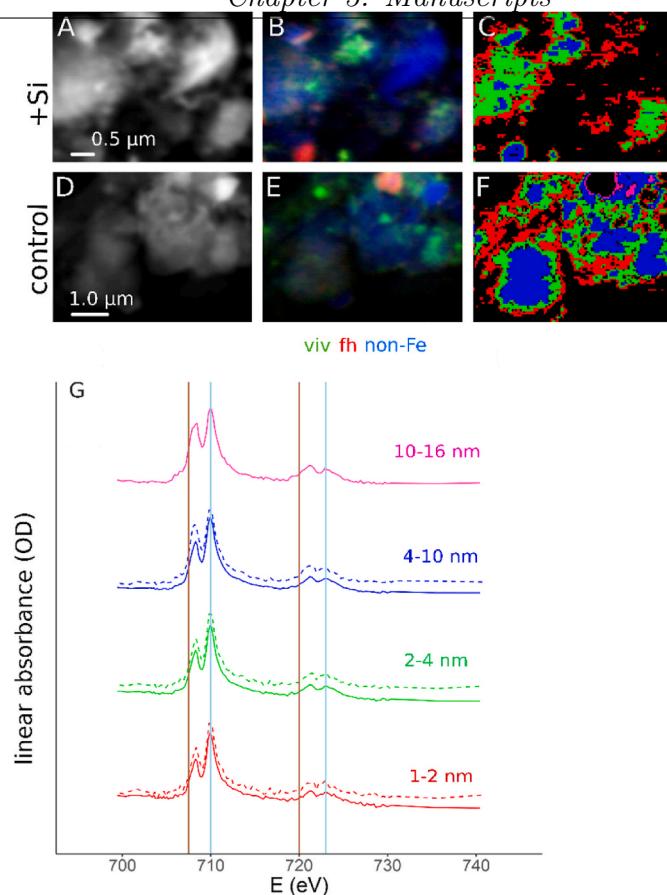


Fig. 6. STXM-NEXAFS measurements of the soil MAT. Images show soils with addition of Ca (A–C), control soil without treatment (D–F). Figures A and D show averaged linear absorbance maps across the Fe2p edges of soil particles of the different treatments analyzed. Figures B and E show quantitative red/green/blue (RGB) composite maps of vivianite-like phases (red), ferrihydrite-like phases (green) and non-Fe background (blue), derived from linear decomposition of the image stacks using respective spectra of reference compounds. In the region of interest maps C and F colors represent areas with same thickness (red: 1–2 nm, green: 2–4 nm, blue: 4–10 nm, pink: 10–16 nm) of vivianite. Figure G shows the linear absorbance (OD) for areas with same thickness of vivianite for control (continuous line) and Ca treatment (dotted line). Vertical light brown lines at 708 eV and 720 eV represent specific absorbance maxima for vivianite, vertical blue lines at 710 eV and 723 eV represent specific absorbance maxima for ferrihydrite. (For interpretation of the references to color in this figure legend, the reader is referred to the Web version of this article.)

treatments we found sometimes other directions of interdependencies compared to correlations considering all treatments together (see above).

Iron contents in soils correlated significantly positive with the Si contents for the MAT (pH 6.6) and the MNT (pH 8.0) soils, both with initial low available Si. It seems that iron may be mobilized from soils by increasing ASI. The largest share of Fe in soils is bound in the crystal lattice of primary minerals (e.g., olivine, augite, hornblende and biotite). By weathering of these minerals Fe oxides/hydroxides like ferrihydrite and goethite Fe may be mobilized (Schwertmann and Cornell, 2008). In solution Si may form Fe complexes ($\text{Fe}_{\text{aq}}\text{OSi}(\text{OH})_2^+$) and prevent precipitation of iron hydroxides in a pH range from 6 to 8 (Perry and Keeling-Tucker, 1998). Furthermore, Fe minerals tend to a lower crystallinity in the presence of ASI (Gauger et al., 2016). This may lead to a higher solubility of Fe and, consequently, to higher Fe mobility, too. However, under anoxic conditions Fe(II) may adsorb on clay mineral surfaces (Van Groeningen et al., 2020). Increasing silicic acid

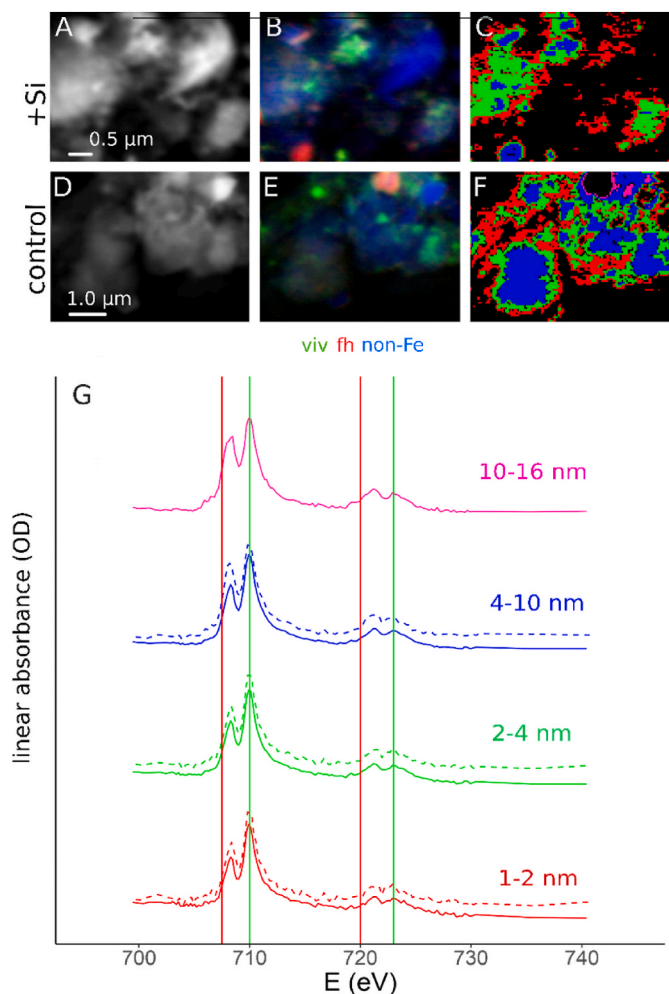


Fig. 7. STXM-NEXAFS measurements of the soil MNT. Images show soils with addition of Si (A–C), control soil without treatment (D–F). Figures A and D show averaged linear absorbance maps across the Fe2p edges of soil particles of the different treatments analyzed. Figures B and E show quantitative red/green/blue (RGB) composite maps of vivianite-like phases (red), ferrihydrite-like phases (green) and non-Fe background (blue), derived from linear decomposition of the image stacks using respective spectra of reference compounds. In the region of interest maps C and F colors represent areas with same thickness (red: 1–2 nm, green: 2–4 nm, blue: 4–10 nm, pink: 10–16 nm) of vivianite. Figure G shows the linear absorbance (OD) for areas with same thickness of vivianite for control (continuous line) and Si treatment (dashed line). Vertical light brown lines at 708 eV and 720 eV represent specific absorbance maxima for vivianite, vertical blue lines at 710 eV and 723 eV represent specific absorbance maxima for ferrihydrite. (For interpretation of the references to color in this figure legend, the reader is referred to the Web version of this article.)

concentrations in the surrounding pore water may alter the surface chemistry of those minerals (see STXM-NEXAFS discussion below). Furthermore, it was shown in other studies that ASI may increase soil respiration rates (Schaller et al., 2019; Stimmeler et al., 2022) and decreases hydraulic conductivity (Schaller et al., 2020; Zarebanadkouki et al., 2022), thus favoring anoxic conditions. Consequently the demand of electron acceptors due to the increased respiration may increase and the decrease of exchange rates of electron acceptors due to decreased hydraulic conductivity (limiting the transport of dissolved electron acceptors to a specific spot) may promote Fe minerals as electron acceptors. To analyze the effect of Si on redox state of iron phases, we conducted STXM-NEXAFS analysis of soil particles after incubation with and without Si and Ca. Addition of ASI stimulated the formation of

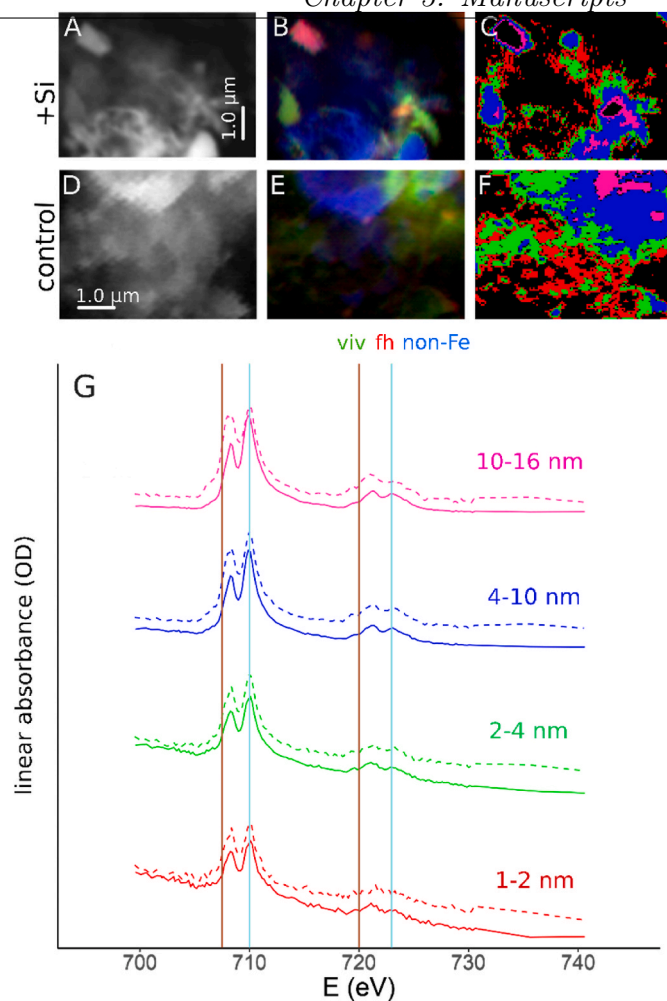


Fig. 8. STXM-NEXAFS measurements from the soil Ca1. Images show soils with addition of Si (A–C), control soil without treatment (D–F), and soils with addition of Ca (G–I). Figures A, D and G show averaged linear absorbance maps across the Fe2p edges of soil particles of the different treatments analyzed. Figures B, E and H show quantitative red/green/blue (RGB) composite maps of vivianite-like phases (red), ferrihydrite-like phases (green) and non-Fe background (blue), derived from linear decomposition of the image stacks using respective spectra of reference compounds. In the region of interest maps C, F and I colors represent areas with same thickness (red: 1–2 nm, green: 2–4 nm, blue: 4–10 nm, pink: 10–16 nm) of vivianite. Figure J shows the linear absorbance (OD) for areas with same thickness of vivianite for control (continuous line), Si treatment (dashed line) and Ca treatment (dotted line). Vertical light brown lines at 708 eV and 720 eV represent specific absorbance maxima for vivianite, vertical blue lines at 710 eV and 723 eV represent specific absorbance maxima for ferrihydrite. (For interpretation of the references to color in this figure legend, the reader is referred to the Web version of this article.)

vivianite-like Fe(II) phases in mineral soil C2 (Fig. 5 B + E). Vivianite-like Fe(II) phases were not limited to the surface of the particles but were also present in the bulk volume of the individual particles. For our soils used in the experiment, reduction of Fe phases seems to be independent of the soil pH (considering the different used soils), as higher abundances of vivianite-like phases after Si addition were found in the weak acidic soil C2 (pH 5.8, Fig. 5J), soil from MAT (pH 6.6) (Fig. 6G) and weak alkaline soil MNT (pH 8.0) (Fig. 7G). Further, effects of Si seem not to be limited to mineral soils, as the organic soil Ca1 showed also higher abundance of vivianite-like phases after incubation with Si (Fig. 8 B + E + G). This is in accordance with other studies showing that Si can increase the abundance of vivianite-like phases in the bulk volume of paddy soils particles (Schaller et al., 2022).

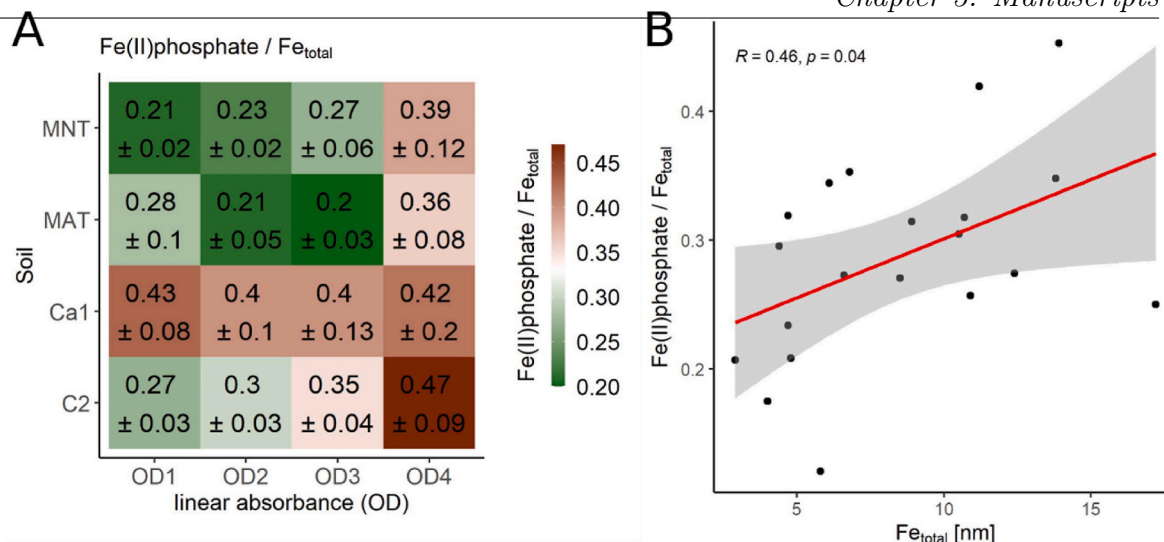


Fig. 9. A) Ratio of thickness in nm of Fe(II)phosphate to total Fe from the species-specific curve fitting of spectra of single ODs of all treatments in the soils from Chersky (Siberia, Russia, C2); from the Canadian Shield (Ca1) and moist acidic tundra and moist-nonacidic tundra (MAT and MNT Alaska, US). Given are the mean and standard deviation. B) Ratio of Fe(II)phosphate/Fe_{total} of all soils and treatments in regression to total iron. Given is also the Pearson correlation at a confidence interval of 95%.

Incubation over longer time span led to reduction not only of the surface of the particle, but also of the bulk volume of the particles (more Fe(II) in higher optical densities Fig. 9). In summary, Si can mobilize Fe by promoting Fe(II) phases with lower crystallinity and higher solubility (Picard et al., 2016; Kanematsu et al., 2018; Schaller et al., 2022). Hence, Si seems to be able to increase the mobility of Fe.

The interdependency between Si and Al mobility seemed to depend on the soil pH. In the weak acidic (pH 5.8) soil C2 (Fig. S6B), in the MAT soil (pH 6.6) and in the Ca1 soil (pH 6.7) (Fig. 2B) Al mobility increased with increasing Si. At low pH values Al mobility increases due to formation of ions (Rengel, 2004) and a potentially binding competition between Si and Al may result in an increase of Al mobility (see discussion below). In the weak alkaline soil MNT (Fig. 3B) Si decreased the Al mobility. This may be explained due to the pH dependency of the solubility and reactivity of silicic acid. The high reactivity of deprotonated silicic acid at alkaline pH values may enhance the formation of SROAS (Wada and Kubo, 1975; Schaller et al., 2021) and by this decrease concentration of free Al. In weak acidic and neutral soils the solubility of silicic acid is lower and by this processes may take much longer and hence may not be measurable during the incubation time of 24 weeks. Yokoyama et al. (2002) showed the formation of aluminum silicates under presence of silicic acid and Al(OH)₃ phases in a pH range from 6 to 10. They showed the substitution of Al by Si in solid Al phases leading to an increase of free Al ions with simultaneous decrease of free Si.

However, Ca led to a decrease of Al mobility in all soils, in the mineral, weak acidic soil C2 (pH 5.8 (Fig. 1D), mineral MAT soil (pH 6.6) (Fig. 2D), mineral weak alkaline soil MNT (pH 8.0 (Fig. 3D) and in the organic soil Ca1 (pH 6.7) (Fig. 4D) organic. This effect was most pronounced in soils with high content of OM. This may be a hint, that the formation of OM complexes with Ca with a further complexation of Al may be the reason for the decreased Al mobility (Gregor et al., 1996).

5. Conclusion

We report here on the effect of Ca and amorphous silica (Si) on Fe and Al mobility in four Arctic soils differing in soil pH. Our results show that Fe mobility correlates positively with Si. Amorphous silica promotes vivianite-like Fe(II) phases in the outer and deeper layer of the particles by increasing soil respiration rates and with this increasing the demand of electron acceptors on the one hand and decreasing hydraulic

conductivity and with this decreased exchange rates of electron acceptors on the other hand may promote Fe minerals as electron acceptors. Mobilization of Al by Si depends on soil pH. At weak acidic and neutral pH Si increased Al mobility, potentially by mobilization of Al from mineral binding sites in Al(OH)₃ and aluminum silicates. In weak alkaline soils formation of aluminum silicates by deprotonated silicic acid may be a sink for Al ions. This is an important result as it shows the importance of indirect effects of Si on soil chemistry. The formation of Ca-OM complexes with a further complexation and immobilization of Al may be the reason for the decreasing mobility of Al after Ca addition. As Fe is a micro nutrient for plants and microbes and Al is a PTE for such organisms, to predict effects on future ecosystem performance in the Arctic e.g., biomass production or soil respiration. In summary, both Si and Ca have to be considered regarding the mobility of Fe and Al in Arctic soils and with this the ecosystem performance of Arctic systems.

Declaration of competing interest

The authors declare no competing interest.

Data availability

Data will be made available on request.

Acknowledgements

The work was funded by the German Research Foundation (DFG), grant number SCHA 1822/12-1 to Jörg Schaller. Part of the research described in this paper was performed using a beamline at the Canadian Light Source, a national research facility of the University of Saskatchewan, which is supported by the Canada Foundation for Innovation (CFI), the Natural Sciences and Engineering Research Council (NSERC), the National Research Council (NRC), the Canadian Institutes of Health Research (CIHR), the Government of Saskatchewan, and the University of Saskatchewan.

Appendix A. Supplementary data

Supplementary data to this article can be found online at <https://doi.org/10.1016/j.chemosphere.2023.139087>.

References

- Abramov, A., Davydov, S., Ivashchenko, A., Karelina, D., Kholodov, A., Kraev, G., Lupachev, A., Maslakov, A., Ostroumov, V., Rivkina, E., 2021. Two decades of active layer thickness monitoring in northeastern Asia. *Polar Geogr.* 44, 186–202.
- Beauvois, A., Vantelon, D., Jestin, J., Bouhnik-Le Coz, M., Catrouillet, C., Briois, V., Bizien, T., Davranche, M., 2021. How crucial is the impact of calcium on the reactivity of iron-organic matter aggregates? Insights from arsenic. *J. Hazard Mater.* 404, 124127.
- Gauger, T., Byrne, J.M., Konhauser, K.O., Obst, M., Crowe, S., Kappler, A., 2016. Influence of organics and silica on Fe (II) oxidation rates and cell–mineral aggregate formation by the green-sulfur Fe (II)-oxidizing bacterium *Chlorobium ferrooxidans* KoF0x—Implications for Fe (II) oxidation in ancient oceans. *Earth Planet Sci. Lett.* 443, 81–89.
- Gregor, J., Fenton, E., Brokenshire, G., Van Den Brink, P., O’Sullivan, B., 1996. Interactions of calcium and aluminium ions with alginate. *Water Res.* 30, 1319–1324.
- Henke, B.L., Gullikson, E.M., Davis, J.C., 1993. X-ray interactions: photoabsorption, scattering, transmission, and reflection at $E = 50\text{--}30,000$ eV, $Z = 1\text{--}92$. *Atomic Data Nucl. Data Tables* 54, 181–342.
- Hitchcock, A.P., 2017. *aXis 2000 - Analysis of X-Ray Images and Spectra*. <http://unicorn.mcmaster.ca/aXis2000.html>.
- Hömborg, A., Obst, M., Knorr, K.-H., Kalbitz, K., Schaller, J., 2020. Increased silicon concentration in fen peat leads to a release of iron and phosphate and changes in the composition of dissolved organic matter. *Geoderma* 374, 114422.
- Hugelius, G., Strauss, J., Zubrzycki, S., Harden, J.W., Schuur, E., Ping, C.-L., Schirmer, L., Grosse, G., Michaelson, G.J., Koven, C.D., 2014. Estimated stocks of circumpolar permafrost carbon with quantified uncertainty ranges and identified data gaps. *Biogeosciences* 11, 6573–6593.
- IPCC, 2021. *Climate Change 2021: the Physical Science Basis. Contribution of Working Group I to the Sixth Assessment Report of the Intergovernmental Panel on Climate Change*. Climate Change, p. 236.
- Kanematsu, M., Waychunas, G., Boily, J.-F., 2018. Silicate binding and precipitation on iron oxyhydroxides. *Environ. Sci. Technol.*
- Kryzevicius, Z., Karcauskienė, D., Álvarez-Rodríguez, E., Zukauskaitė, A., Slepetienė, A., Volungevičius, J., 2019. The effect of over 50 years of liming on soil aluminium forms in a Retisol. *J. Agric. Sci.* 157, 12–19.
- Lindner, G.G., Drexler, C.-P., Sälzer, K., Schuster, T.B., Krueger, N., 2022. Comparison of biogenic amorphous silicas found in common horsetail and oat husk with synthetic amorphous silicas. *Front. Public Health*, 1598.
- Marschner, H., 2003. *Mineral Nutrition of Higher Plants*. Academic Press, London.
- Mehlich, A., 1984. Mehlich-3 soil test extractant - a modification of Mehlich-2 extractant. *Commun. Soil Sci. Plant Anal.* 15, 1409–1416.
- Mishra, U., Hugelius, G., Shelef, E., Yang, Y., Strauss, J., Lupachev, A., Harden, J.W., Jastrow, J.D., Ping, C.-L., Riley, W.J., 2021. Spatial heterogeneity and environmental predictors of permafrost region soil organic carbon stocks. *Sci. Adv.* 7 eaaz5236.
- Obu, J., Westermann, S., Bartsch, A., Berdnikov, N., Christiansen, H.H., Dashtseren, A., Delaloye, R., Elberling, B., Eitzelmüller, B., Kholodov, A., 2019. Northern Hemisphere permafrost map based on TTOP modelling for 2000–2016 at 1 km² scale. *Earth Sci. Rev.* 193, 299–316.
- Perry, C.C., Keeling-Tucker, T., 1998. Aspects of the bioinorganic chemistry of silicon in conjunction with the biomaterials calcium, iron and aluminium. *J. Inorg. Biochem.* 69, 181–191.
- Picard, A., Obst, M., Schmid, G., Zeitvogel, F., Kappler, A., 2016. Limited influence of Si on the preservation of Fe mineral-encrusted microbial cells during experimental diagenesis. *Geobiology* 14, 276–292.
- R_Core_Team, 2021. *R: A Language and Environment for Statistical Computing*.
- Reithmaier, G.M.S., Knorr, K.H., Arnold, S., Planer-Friedrich, B., Schaller, J., 2017. Enhanced silicon availability leads to increased methane production, nutrient and toxicant mobility in peatlands. *Sci. Rep.* 7, 8728.
- Rengel, Z., 2004. Aluminium cycling in the soil-plant-animal-human continuum. *Biomaterials* 17, 669–689.
- Romanovsky, V.E., Drozdov, D., Oberman, N.G., Malkova, G., Kholodov, A.L., Marchenko, S., Moskalenko, N.G., Sergeev, D., Ukraintseva, N., Abramov, A., 2010. Thermal state of permafrost in Russia. *Permafrost. Periglac. Process.* 21, 136–155.
- Schaller, J., Cramer, A., Carminati, A., Zarebanadkouki, M., 2020. Biogenic amorphous silica as main driver for plant available water in soils. *Sci. Rep.* 10, 2424.
- Schaller, J., Fauchere, S., Joss, H., Obst, M., Goeckede, M., Planer-Friedrich, B., Peiffer, S., Gilfedder, B., Elberling, B., 2019. Silicon increases the phosphorus availability of Arctic soils. *Sci. Rep.* 9, 449.
- Schaller, J., Puppe, D., Kaczorek, D., Ellerbrock, R., Sommer, M., 2021. Silicon cycling in soils revisited. *Plants* 10, 295.
- Schaller, J., Stimmeler, P., Goeckede, M., Augustin, J., Lacroix, F., Hoffmann, M., 2023. Arctic soil CO₂ release during freeze-thaw cycles modulated by silicon and calcium. *Sci. Total Environ.*, 161943.
- Schaller, J., Wu, B., Amelung, W., Hu, Z., Stein, M., Lehnendorff, E., Obst, M., 2022. Silicon as a potential limiting factor for phosphorus availability in paddy soils. *Sci. Rep.* 12, 16329.
- Schulz, K., ThomasArrigo, L.K., Kaegi, R., Kretzschmar, R., 2022. Stabilization of ferrihydrite and lepidocrocite by silicate during Fe (II)-catalyzed mineral transformation: impact on particle morphology and silicate distribution. *Environ. Sci. Technol.* 56, 5929–5938.
- Schuur, E., McGuire, A., Schädel, C., Grosse, G., Harden, J., Hayes, D., Hugelius, G., Koven, C., Kuhry, P., Lawrence, D., Natali, S., Olefeldt, D., Romanovsky, V., Schaefer, K., Turetsky, M., Treat, C., Vonk, V., 2015. Climate change and the permafrost carbon feedback. *Nature* 520, 171–179.
- Schwertmann, U., Cornell, R.M., 2008. *Iron Oxides in the Laboratory: Preparation and Characterization*. John Wiley & Sons.
- Sowers, T.D., Wani, R.P., Coward, E.K., Fischel, M.H., Betts, A.R., Douglas, T.A., Duckworth, O.W., Sparks, D.L., 2020. Spatially resolved organomineral interactions across a permafrost chronosequence. *Environ. Sci. Technol.* 54, 2951–2960.
- Stimmeler, P., Goeckede, M., Natali, S.M., Sonnentag, O., Gilfedder, B.S., Perron, N., Schaller, J., 2022. The importance of calcium and amorphous silica for arctic soil CO₂ production. *Front. Environ. Sci.* 10, 1019610.
- Stimmeler, P., Goeckede, M., Elberling, B., Natali, S., Kuhry, P., Perron, N., Lacroix, F., Hugelius, G., Sonnentag, O., Strauss, J., Minions, C., Sommer, M., Schaller, J., 2023. Pan-Arctic soil element bioavailability estimations. *Earth Syst. Sci. Data* 15, 1059–1075.
- Van Groeningen, N., ThomasArrigo, L.K., Byrne, J.M., Kappler, A., Christl, I., Kretzschmar, R., 2020. Interactions of ferrous iron with clay mineral surfaces during sorption and subsequent oxidation. *Environ. Sci.: Process. Impacts* 22, 1355–1367.
- Virkkala, A.M., Aalto, J., Rogers, B.M., Tagesson, T., Treat, C.C., Natali, S.M., Watts, J.D., Potter, S., Lehtonen, A., Mauritz, M., 2021. Statistical upscaling of ecosystem CO₂ fluxes across the terrestrial tundra and boreal domain: regional patterns and uncertainties. *Global Change Biol.* 27, 4040–4059.
- Wada, K., Kubo, H., 1975. Precipitation of amorphous aluminosilicates from solutions containing monomeric silica and aluminium ions. *J. Soil Sci.* 26, 100–111.
- Yokoyama, T., Ueda, A., Kato, K., Mogi, K., Matsuo, S., 2002. A study of the alumina-silica gel adsorbent for the removal of silicic acid from geothermal water: increase in adsorption capacity of the adsorbent due to formation of amorphous aluminosilicate by adsorption of silicic acid. *J. Colloid Interface Sci.* 252, 1–5.
- Zarebanadkouki, M., Hosseini, B., Gerke, H.H., Schaller, J., 2022. Amorphous silica amendment to improve sandy soils’ hydraulic properties for sustained plant root access under drying conditions. *Front. Environ. Sci.* 10, 935012.

Supplementary material to:

Silicon and calcium controls on iron and aluminium availability in Arctic soils

Peter Stimmler¹, Martin Obst ², Mathias Stein¹, Mathias Goeckede³, Kerstin Hockmann^{2, 4}, and Joerg Schaller^{1, *}

¹ Leibniz Centre for Agricultural Landscape Research (ZALF), Eberswalder Str. 84, 15374 Müncheberg, Germany

² Experimental Biogeochemistry, Bayreuth Center for Ecology and Environmental Research (*BayCEER*), University of Bayreuth, Bayreuth, Germany

⁴ Biogeochemical Signals (BSI), Max Planck Institute for Biogeochemistry, Jena, Germany

⁴ Department of Hydrology, Bayreuth Center for Ecology and Environmental Research (*BayCEER*), University of Bayreuth, Bayreuth, Germany

* corresponding author: Jörg Schaller (Joerg.Schaller@zalf.de)

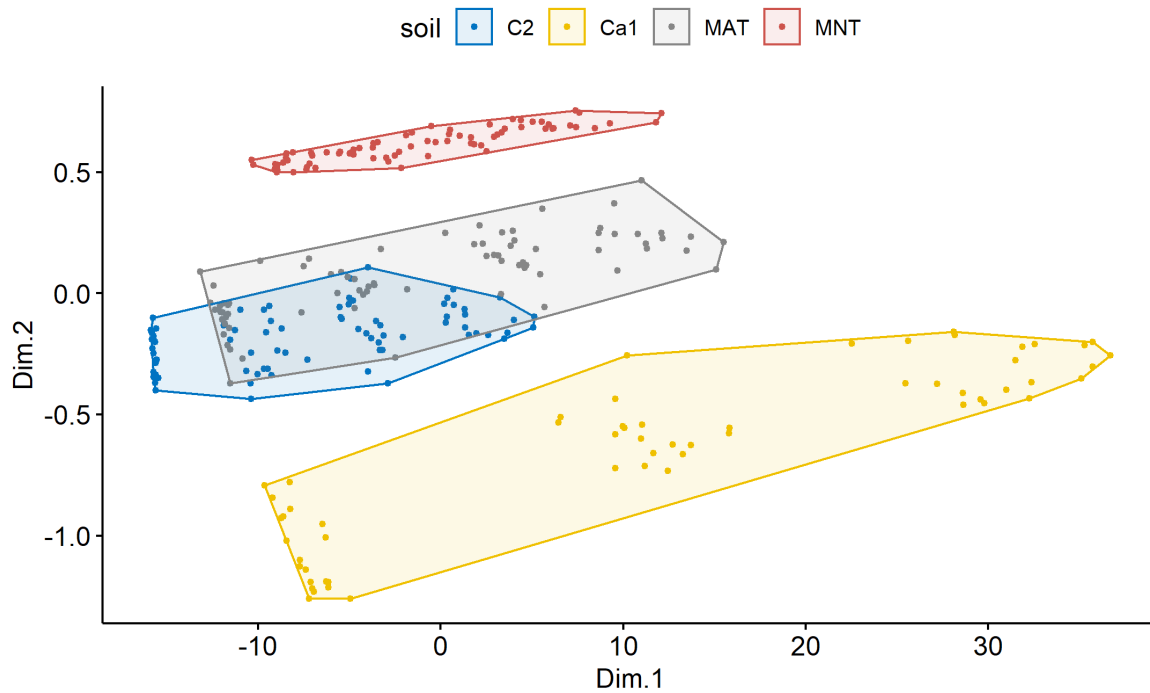


Fig. S1: Metric multidimensional scaling (mMDS) of soils from Chersky (Siberia, Russia, C2, blue), from the moist acidic tundra (MAT, Alaska, US, grey), from the moist non-acidic tundra (MNT, Alaska, US, yellow) and from the Canadian Shield (Ca1, red) over all treatments of Si (+0, +3, +6, +10 mg g⁻¹ DW) and Ca (+0, +5, +10, +15 mg g⁻¹ DW) under waterlogged conditions. All soils differ significantly (ANOSIM, $p < 0.001$, $R = 0.235$) from each other.

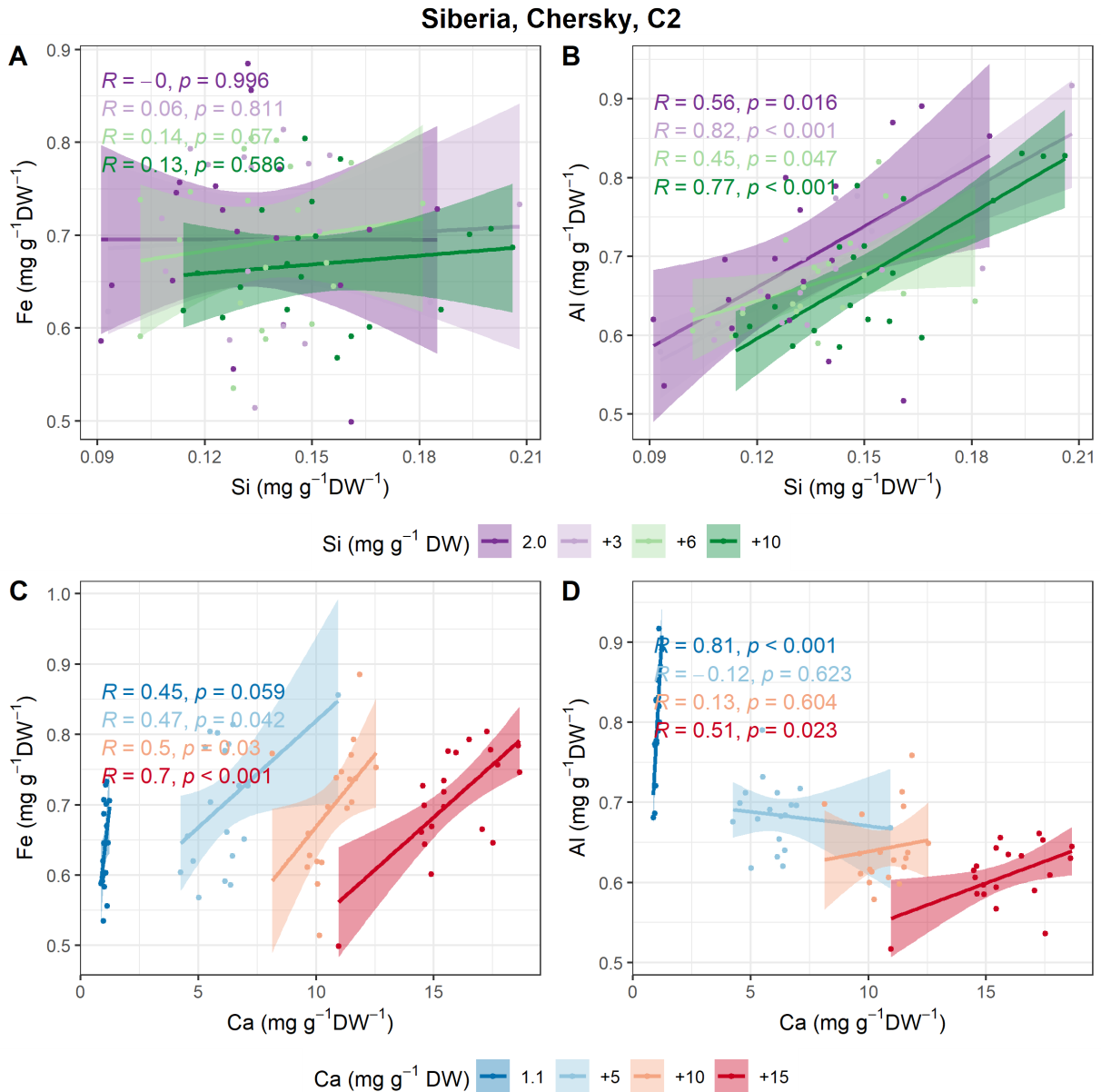


Fig. S2: Soil C2. Availability of Fe and Al with Si (A+B) and Ca (C+D) after 24 weeks of incubation under water logged conditions. For extraction, the Mehlich-3 method was used. Concentrations were given in $\text{mg g}^{-1} \text{DW}$. Colours represent treatments of Si (2.0, +3, +6, +10 $\text{mg g}^{-1} \text{DW}$) and Ca (1.1, +5, +10, +15 $\text{mg g}^{-1} \text{DW}$). For statistics p value at the 95% confidence interval and the Pearson correlation were given.

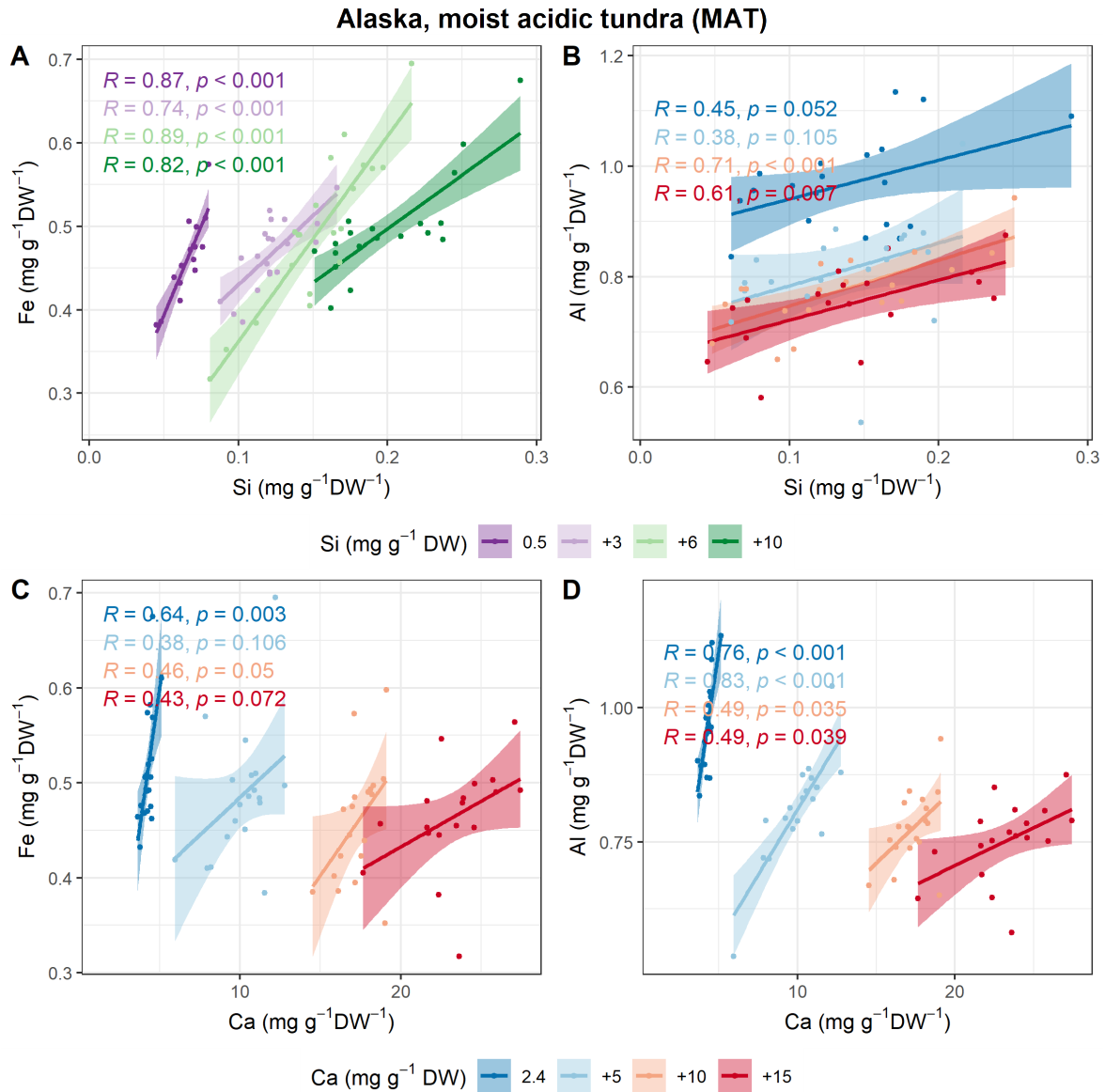


Fig. S3: Soil MAT. Availability of Fe and Al with Si (A+B) and Ca (C+D) after 24 weeks of incubation under water logged conditions. For extraction, the Mehlich-3 method was used. Concentrations were given in $\text{mg g}^{-1} \text{DW}$. Colours represent treatments of Si (0.5, +3, +6, +10 $\text{mg g}^{-1} \text{DW}$) and Ca (2.4, +5, +10, +15 $\text{mg g}^{-1} \text{DW}$). For statistics p value at the 95% confidence interval and the Pearson correlation were given.

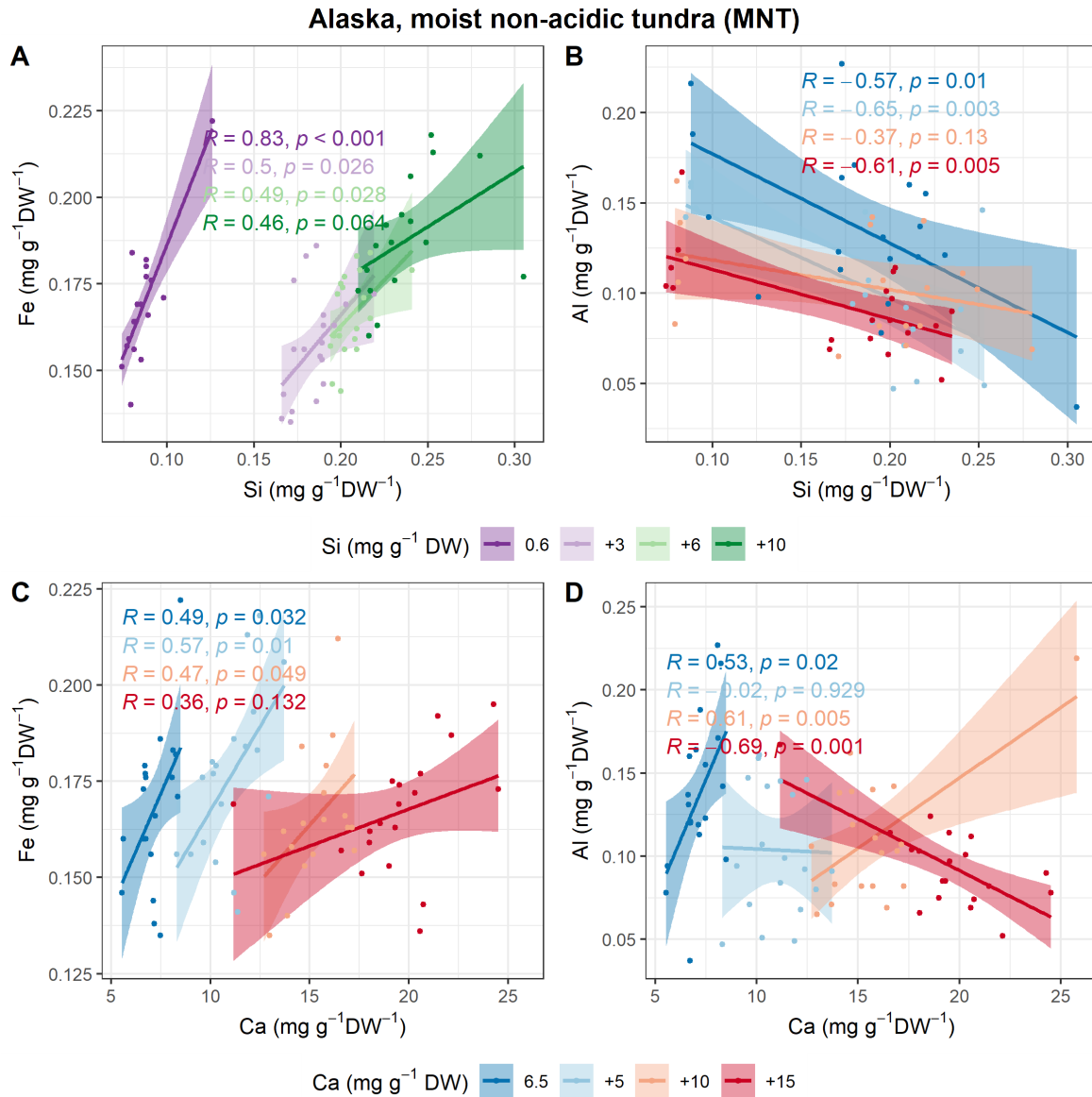


Fig. S4: Soil MNT. Availability of Fe and Al with Si (A+B) and Ca (C+D) after 24 weeks of incubation under water logged conditions. For extraction, the Mehlich-3 method was used. Concentrations were given in $\text{mg g}^{-1}\text{DW}$. Colours represent treatments of Si (0.6, +3, +6, +10 $\text{mg g}^{-1}\text{DW}$) and Ca (6.5, +5, +10, +15 $\text{mg g}^{-1}\text{DW}$). For statistics p value at the 95% confidence interval and the Pearson correlation were given.

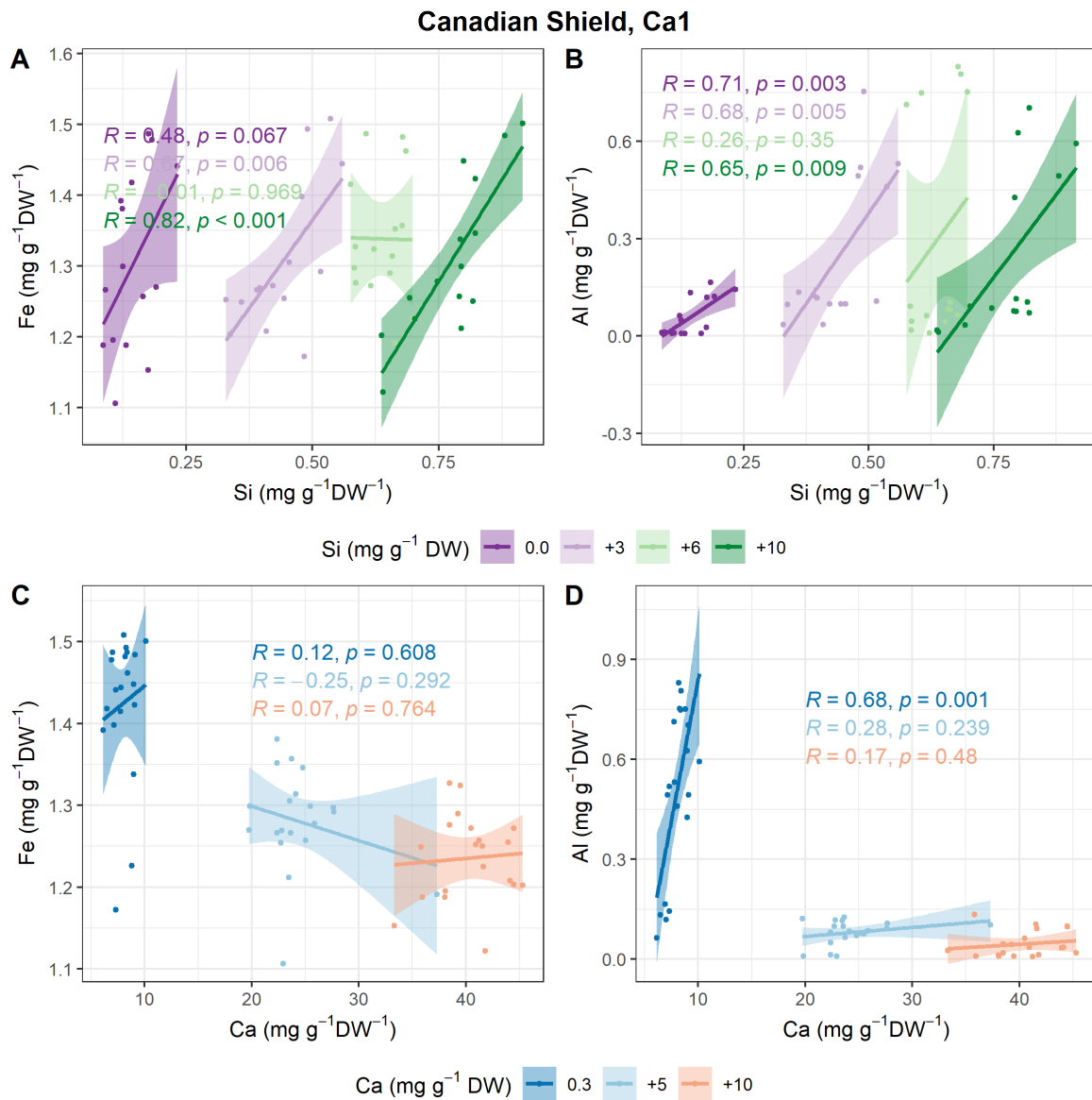


Fig. S5: Soil Ca1. Availability of Fe and Al with Si (A+B) and Ca (C+D) after 24 weeks of incubation under water logged conditions. For extraction, the Mehlich-3 method was used. Concentrations were given in $\text{mg g}^{-1}\text{DW}$. Colours represent treatments of Si (0.0, +3, +6, +10 $\text{mg g}^{-1}\text{DW}$) and Ca (0.3, +5, +10 $\text{mg g}^{-1}\text{DW}$). For statistics p value at the 95% confidence interval and the Pearson correlation were given.

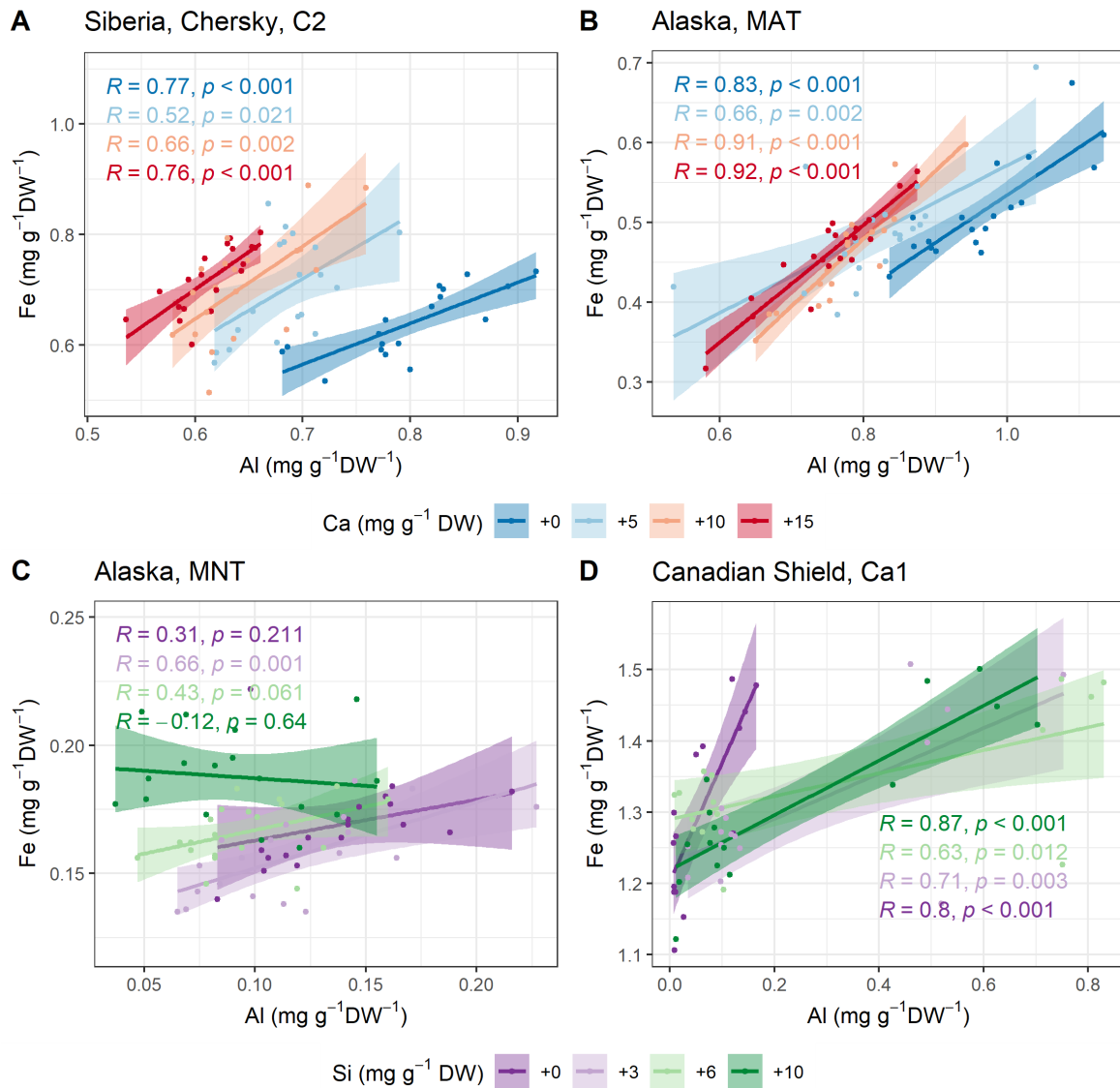


Fig. S6: Concentrations of Mehlich 3 extractable Fe given in mg g⁻¹ DW in soils from Chersky (Siberia, Russia, C2) (A), moist acidic tundra (MAT, Alaska, US) (B), moist non-acidic tundra (MNT, Alaska, US) (C) and Canadian Shield (Ca1) (D) after 24 weeks of incubation under water logged conditions. Colours represent treatments of Ca (+0, +5, +10, +15 mg g⁻¹ DW) (A+B) and Si (+0, +3, +6, +10 mg g⁻¹ DW) (C+D). For statistics *p* value at the 95% confidence interval and the Pearson correlation were used.

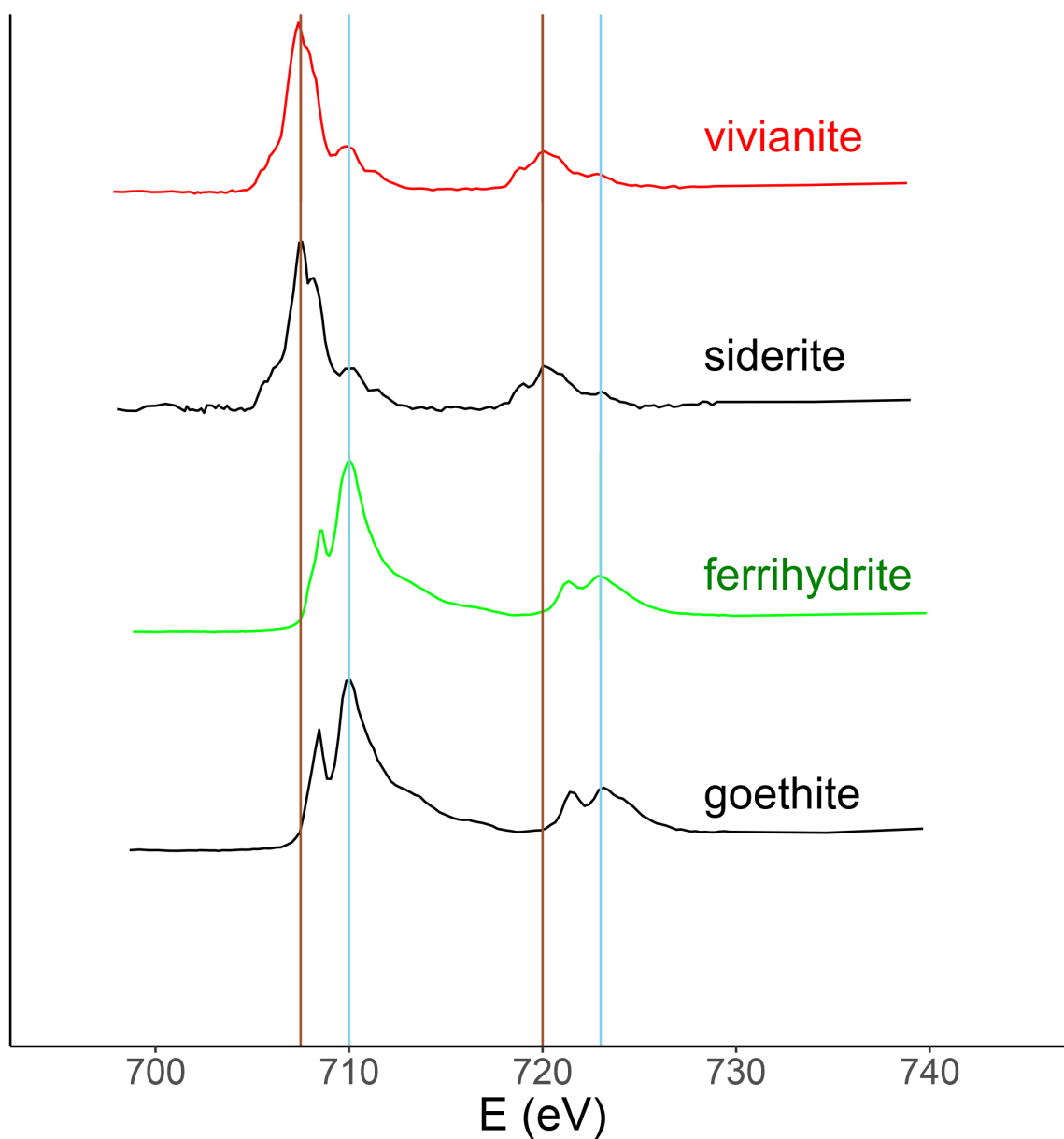


Fig. S7: X-Ray absorption spectra of the iron minerals vivianite, ferrihydrite, siderite and goethite. Shown are also lines at the specific absorption maxima of vivianite in brown (708 eV, 720 eV) and ferrihydrite in light blue (710 eV and 723 eV).

Chapter 4

Review and outlook

Bringing things together

4.1– Conclusion

4.2– List of studies

4.3 – List of references

4.4 – List of figures

4.4 – Index

4.5 – Danksagung

?? – Eidesstatt

4.1 Conclusion

The importance of the Arctic for future climate scenarios can not be overestimated. In my research I clearly show the impact of Si and Ca on microbes, mineral phases, nutrient availability and GHG release in arctic soils. Many studies focus on the pool of organic C and its potential mobilization from thawed permafrost soils to predict potential GHG release to the atmosphere in a warming Arctic. Only few studies take other elements like N and P into account, although these are often the limiting factor for microbial decomposition processes. In my research I highlight the importance of Si and Ca for GHG release from Arctic soils and point out the diverse and complex biogeochemical processes defining the element availability. The first estimation of available element concentrations of ASi, Si, Ca, Fe, Al and P will help to predict element mobilization from thawing permafrost. In-silico approaches and ESM like "QUINCY" already take the effects of Si and Ca on the C cycling and GHG release into account. Changed future climatic conditions can alter weathering processes and the rates of mineral trans- and neo-formation. I clearly show that Si and Ca change the availabilities of C, Fe, Al and P by interacting with mineral surfaces. This makes clear, that not only total element contents and lithology defines element availability. The degree of crystallinity and the interactions of elements with the mineral surfaces can have a huge impact on the availability of nutrients and organic C and by this on GHG release. Future research on Arctic soils should focus more on the elements that form mineral phases, as the biggest share of C and nutrients in the soil is associated with these phases. The C is decomposed by microbes and Si and Ca directly alter MCS. Processes like these are as important for GHG release as the availability of C and nutrients. A deeper understanding of the interactions of lifeforms with their inorganic environment can hold the key to unravel complex and small-scale patterned GHG release from the Arctic.

4.2 List of studies

1. Stimmler, Peter; Goeckede, Mathias; Elberling, Bo; Natali, Susan; Kuhry, Peter; Perron, Nia et al. (2023): Pan-Arctic soil element bioavailability estimations. In: *Earth Syst. Sci. Data* 15 (3), S. 1059–1075. DOI: 10.5194/essd-15-1059-2023 . (Stimmler, Goeckede, Elberling, et al. 2022)
2. Stimmler, Peter; Goeckede, Mathias; Natali, Susan M.; Sonnentag, Oliver; Gilfedder, Benjamin S.; Perron, Nia; Schaller, Jörg (2022): The importance of calcium and amorphous silica for arctic soil CO₂ production. In: *Front. Environ. Sci.* 10, Artikel 1019610. DOI: 10.3389/fenvs.2022.1019610 . (Stimmler, Goeckede, Natali, et al. 2022)
3. Schaller, Jörg; Stimmler, Peter; Goeckede, Mathias; Augustin, Jürgen; Lacroix, Fabrice; Hoffmann, Mathias (2022): Arctic Soil CO₂ Release During Freeze-Thaw Cycles Modulated by Silicon and Calcium. In: *SSRN Journal*. DOI: 10.2139/ssrn.4257915 . (Schaller, Stimmler, et al. 2022)
4. Stimmler, Peter; Priemé, Anders; Elberling, Bo; Goeckede, Mathias; Schaller, Joerg (2022): Arctic soil respiration and microbial community structure driven by silicon and calcium. In: *The Science of the total environment* 838 (Pt 2), S. 156152. DOI: 10.1016/j.scitotenv.2022.156152 . (Stimmler, Priemé, et al. 2022)

5. Stimmler, P.; Obst, M.; Goeckede, M.; Hockmann, K.; Stein, M.; Schaller, J. (In preparation): Silicon and calcium controls on iron and aluminum availability in Arctic soils. In: *Chemosphere*. (Stimmler, M. Obst, Stein, et al. 2023)
6. Stimmler, P.; Obst, M.; Goeckede, M.; Hockmann, K.; Stein, M.; Schaller, Joerg (In preparation): Reduced greenhouse gas emissions from Arctic soils due to aragonite formation from CO₂ and free calcium. (Stimmler, M. Obst, Goeckede, et al. n.d.)
7. Lacroix, Fabrice; Zaehle, Sönke; Caldararu, Silvia; Schaller, Jörg; Stimmler, Peter; Holl, David et al. (2022): Mismatch of N release from the permafrost and vegetative uptake opens pathways of increasing nitrous oxide emissions in the high Arctic. In: *Global change biology* 28 (20), S. 5973–5990. DOI: 10.1111/gcb.16345 . (Lacroix et al. 2022)

4.3 List of references

- Abbott, B. W. et al. (2015). *Patterns and persistence of hydrologic carbon and nutrient export from collapsing upland permafrost*. Copernicus GmbH. DOI: 10.5194/bgd-12-2063-2015.
- Abramov, A., T. Vishnivetskaya, and E. Rivkina (2021). “Are permafrost microorganisms as old as permafrost?” In: *FEMS microbiology ecology* 97.2. DOI: 10.1093/femsec/fiaa260.
- Alfred Wegener Institut (2023). *Permafrost - An introduction: What is permafrost?* URL: <https://www.awi.de/en/focus/permafrost/permafrost-an-introduction.html> (visited on 03/06/2023).
- Alfredsson, H., W. Clymans, et al. (2016). “Estimated storage of amorphous silica in soils of the circum-Arctic tundra region”. In: *Global Biogeochemical Cycles* 30.3, pp. 479–500. ISSN: 08866236. DOI: 10.1002/2015GB005344.
- Alfredsson, H., G. Hugelius, et al. (2015). “Amorphous silica pools in permafrost soils of the Central Canadian Arctic and the potential impact of climate change”. In: *Biogeochemistry* 124.1-3, pp. 441–459. ISSN: 0168-2563. DOI: 10.1007/s10533-015-0108-1.
- Alloway, Brian J. (2013). “Bioavailability of Elements in Soil”. In: *Essentials of Medical Geology*. Ed. by Olle Selinus. Springer, Dordrecht, pp. 351–373. ISBN: 978-94-007-4375-5. DOI: 10.1007/978-94-007-4375-5_15. URL: https://link.springer.com/chapter/10.1007/978-94-007-4375-5_15.
- Andreev, A., P. E. Tarasov, et al. (2016). “Millennial-scale vegetation changes in the north-eastern Russian Arctic during the Pliocene/Pleistocene transition (2.7–2.5 Ma) inferred from the pollen record of Lake El’gygytyn”. In: *Quaternary Science Reviews* 147, pp. 245–258. ISSN: 02773791. DOI: 10.1016/j.quascirev.2016.03.030.
- Andreev, A., PAVEL E. Tarasov, et al. (2003). “Late Pleistocene and Holocene vegetation and climate on the northern Taymyr Peninsula, Arctic Russia”. In: *Boreas* 32.3, pp. 484–505. ISSN: 0300-9483. DOI: 10.1080/03009480310003388.
- ASGR (1988). “Glossary of permafrost and related ground-ice terms”. In: *Permafrost Subcommittee National Research Council of Canada*.
- Barka, Essaid Ait et al. (2016). “Taxonomy, Physiology, and Natural Products of Actinobacteria”. In: *Microbiology and molecular biology reviews : MMBR* 80.1, pp. 1–43. DOI: 10.1128/MMBR.00019-15.
- Al-Barrak, K. and D. L. Rowell (2006). “The solubility of gypsum in calcareous soils”. In: *Geoderma* 136.3-4, pp. 830–837. ISSN: 00167061. DOI: 10.1016/j.geoderma.2006.06.011. URL: <https://www.sciencedirect.com/science/article/pii/S0016706106001935>.

- Barreto, Matheus Sampaio C. et al. (2021). “Calcium enhances adsorption and thermal stability of organic compounds on soil minerals”. In: *Chemical Geology* 559, p. 119804. ISSN: 00092541. DOI: 10.1016/j.chemgeo.2020.119804.
- Bäuerlein, Edmund, M. Epple, and P. Behrens, eds. (2007). *Handbook of biomineralization*. Weinheim: Wiley-VCH. ISBN: 978-3527-31804-9. DOI: 10.1002/9783527619443. URL: <http://dx.doi.org/10.1002/9783527619443>.
- Beauvois, Anthony et al. (2021). “How crucial is the impact of calcium on the reactivity of iron-organic matter aggregates? Insights from arsenic”. In: *Journal of hazardous materials* 404.Pt A, p. 124127. DOI: 10.1016/j.jhazmat.2020.124127.
- Bernard, E., Y. Yan, and B. Lothenbach (2021). “Effective cation exchange capacity of calcium silicate hydrates (C-S-H)”. In: *Cement and Concrete Research* 143, p. 106393. ISSN: 00088846. DOI: 10.1016/j.cemconres.2021.106393.
- Berner, Logan T. et al. (2020). “Summer warming explains widespread but not uniform greening in the Arctic tundra biome”. In: *Nature communications* 11.1, p. 4621. DOI: 10.1038/s41467-020-18479-5.
- Biasi, C. et al. (2005). “Temperature-dependent shift from labile to recalcitrant carbon sources of arctic heterotrophs”. In: *Rapid communications in mass spectrometry : RCM* 19.11, pp. 1401–1408. ISSN: 0951-4198. DOI: 10.1002/rcm.1911.
- Biskaborn, Boris K. et al. (2019). “Permafrost is warming at a global scale”. In: *Nature communications* 10.1, p. 264. DOI: 10.1038/s41467-018-08240-4.
- Blume-Werry, Gesche et al. (2019). “Dwelling in the deep - strongly increased root growth and rooting depth enhance plant interactions with thawing permafrost soil”. In: *The New phytologist* 223.3, pp. 1328–1339. DOI: 10.1111/nph.15903.
- Bockheim (2007). “Importance of Cryoturbation in Redistributing Organic Carbon in Permafrost-Affected Soils”. In: *Soil Science Society of America Journal* 71.4, pp. 1335–1342. ISSN: 03615995. DOI: 10.2136/sssaj2006.0414N.
- Bockheim, J.G and C. Tarnocai (1998). “Recognition of cryoturbation for classifying permafrost-affected soils”. In: *Geoderma* 81.3-4, pp. 281–293. ISSN: 00167061. DOI: 10.1016/S0016-7061(97)00115-8.
- Boehm, Hanns-P. (1980). “The Chemistry of Silica. Solubility, Polymerization, Colloid and Surface Properties, and Biochemistry. VonR. K. Iler. John Wiley and Sons, Chichester 1979. XXIV, 886 S., geb. £ 39.50”. In: *Angewandte Chemie* 92.4, p. 328. ISSN: 0044-8249. DOI: 10.1002/ange.19800920433.
- Box, J. E. et al. (2019). “Key indicators of Arctic climate change: 1971–2017”. In: *Environmental Research Letters* 14.4, p. 045010. ISSN: 1748-9326. DOI: 10.1088/1748-9326/aafc1b. URL: <https://iopscience.iop.org/article/10.1088/1748-9326/aafc1b/meta>.

- Brigatti, Maria Franca et al. (2011). *Structure and mineralogy of layer silicates*. DOI: 10.1180/EMU-notes.11.1. URL: https://pubs.geoscienceworld.org/minersoc/books/edited-volume/943/chapter-pdf/3746856/9780903056458_ch01.pdf.
- Bughio, Mansoor Ahmed et al. (2017). “Neoformation of pedogenic carbonate and conservation of lithogenic carbonate by farming practices and their contribution to carbon sequestration in soil”. In: *Journal of Plant Nutrition and Soil Science* 180.4, pp. 454–463. ISSN: 1522-2624. DOI: 10.1002/jpln.201500650. URL: <https://onlinelibrary.wiley.com/doi/pdf/10.1002/jpln.201500650>.
- Callaghan, T. V., R. o Cazzolla G., and G. Phoenix (2022). “The need to understand the stability of arctic vegetation during rapid climate change: An assessment of imbalance in the literature”. In: *AMBIO* 51.4, pp. 1034–1044. DOI: 10.1007/s13280-021-01607-w.
- Capek, P. et al. (2015). “The effect of warming on the vulnerability of subducted organic carbon in arctic soils”. In: *Soil Biology and Biochemistry* 90, pp. 19–29. ISSN: 00380717. DOI: 10.1016/j.soilbio.2015.07.013.
- Colombo, N. et al. (2018). “Review: Impacts of permafrost degradation on inorganic chemistry of surface fresh water”. In: *Global and Planetary Change* 162, pp. 69–83. ISSN: 09218181. DOI: 10.1016/j.gloplacha.2017.11.017.
- Coolen, M. J. L. and W. D. Orsi (2015). “The transcriptional response of microbial communities in thawing Alaskan permafrost soils”. In: *Frontiers in microbiology* 6, p. 197. DOI: 10.3389/fmicb.2015.00197.
- Coskun, D. et al. (2016). “The Role of Silicon in Higher Plants under Salinity and Drought Stress”. In: *Frontiers in plant science* 7, p. 1072. ISSN: 1664-462X. DOI: 10.3389/fpls.2016.01072.
- Dahl, M. B. et al. (2017). “Warming, shading and a moth outbreak reduce tundra carbon sink strength dramatically by changing plant cover and soil microbial activity”. In: *Scientific reports*, p. 16035. DOI: 10.1038/s41598-017-16007-y.
- Daniels, C. J. et al. (2018). “A global compilation of coccolithophore calcification rates”. In: *Earth System Science Data* 10.4, pp. 1859–1876. DOI: 10.5194/essd-10-1859-2018.
- DeMaster, D J. (1981). “The supply and accumulation of silica in the marine environment”. In: *Geochimica et Cosmochimica Acta* 45, pp. 1715–1732. ISSN: 00167037.
- Deming, J. W. (2002). “Psychrophiles and polar regions”. In: *Current Opinion in Microbiology* 5.3, pp. 301–309. ISSN: 13695274. DOI: 10.1016/S1369-5274(02)00329-6.
- Denich, T.J et al. (2003). “Effect of selected environmental and physico-chemical factors on bacterial cytoplasmic membranes”. In: *Journal of microbiological methods* 52.2, pp. 149–182. ISSN: 0167-7012. DOI: 10.1016/s0167-7012(02)00155-0. URL: <https://pubmed.ncbi.nlm.nih.gov/12459238/>.

- Dessert, C. et al. (2003). “Basalt weathering laws and the impact of basalt weathering on the global carbon cycle”. In: *Chemical Geology* 202.3-4, pp. 257–273. ISSN: 00092541. DOI: 10.1016/j.chemgeo.2002.10.001.
- Dobiński, W. (2020). “Northern Hemisphere permafrost extent: Drylands, glaciers and sea floor. Comment to the paper: Obu, J., et al. 2019. Northern Hemisphere permafrost map based on TTOP modeling for 2000–2016 at 1 km² scale, Earth Science Reviews, 193, 299–316”. In: *Earth-Science Reviews* 203, p. 103037. ISSN: 00128252. DOI: 10.1016/j.earscirev.2019.103037.
- Dutta et al. (2006). “Potential carbon release from permafrost soils of Northeastern Siberia”. In: *Global change biology* 12.12, pp. 2336–2351. DOI: 10.1111/j.1365-2486.2006.01259.x.
- Faucherre, S. et al. (2018). “Short and Long-Term Controls on Active Layer and Permafrost Carbon Turnover Across the Arctic”. In: *Journal of Geophysical Research: Biogeosciences* 123.2, pp. 372–390. ISSN: 21698953. DOI: 10.1002/2017JG004069.
- Fischer, Joseph C. von et al. (2010). “Vegetation height and other controls of spatial variability in methane emissions from the Arctic coastal tundra at Barrow, Alaska”. In: *Journal of Geophysical Research* 115.G4. ISSN: 0148-0227. DOI: 10.1029/2009JG001283. URL: <https://onlinelibrary.wiley.com/doi/pdf/10.1029/2009JG001283>.
- Fuchs, M. et al. (2018). “Carbon and nitrogen pools in thermokarst-affected permafrost landscapes in Arctic Siberia”. In: *Biogeosciences* 15.3, pp. 953–971. ISSN: 1726-4189. DOI: 10.5194/bg-15-953-2018.
- Gal, J. Y. et al. (1996). “Calcium carbonate solubility: a reappraisal of scale formation and inhibition”. In: *Talanta* 43.9, pp. 1497–1509. ISSN: 0039-9140. DOI: 10.1016/0039-9140(96)01925-X. URL: <https://www.sciencedirect.com/science/article/pii/003991409601925X>.
- Gavryushkin, Pavel N. et al. (2021). “Metastable structures of CaCO₃ and their role in transformation of calcite to aragonite and postaragonite”. In: *Crystal Growth & Design* 21.1, pp. 65–74. ISSN: 1528-7483. DOI: 10.1021/acs.cgd.0c00589.
- Göckede, M., Fanny Kittler, et al. (2017). “Shifted energy fluxes, increased Bowen ratios, and reduced thaw depths linked with drainage-induced changes in permafrost ecosystem structure”. In: *The Cryosphere* 11.6, pp. 2975–2996. DOI: 10.5194/tc-11-2975-2017.
- Göckede, M., Min Jung Kwon, et al. (2019). “Negative feedback processes following drainage slow down permafrost degradation”. In: *Global change biology* 25.10, pp. 3254–3266. DOI: 10.1111/gcb.14744.
- Goldman, Charles R. et al., eds. (2013). *Climatic Change and Global Warming of Inland Waters: Impacts and Mitigation for Ecosystems and Societies*. 1st ed. Chichester,

- West Sussex, UK: John Wiley & Sons Inc. ISBN: 9781119968665. DOI: 10.1002/9781118470596.
- Grogan, P. et al. (2004). “Freeze–thaw regime effects on carbon and nitrogen dynamics in sub-arctic heath tundra mesocosms”. In: *Soil Biology and Biochemistry* 36.4, pp. 641–654. ISSN: 00380717. DOI: 10.1016/j.soilbio.2003.12.007.
- Harrison, J. C. et al. (2011). *Geological map of the Arctic*. DOI: 10.4095/287868. URL: <https://geoscan.nrcan.gc.ca/starweb/geoscan/servlet.starweb?path=geoscan/download.web&search1=R=287868> (visited on 08/27/2019).
- Hassan, Noor et al. (2016). “Psychrophilic and psychrotrophic fungi: a comprehensive review”. In: *Reviews in Environmental Science and Bio/Technology* 15.2, pp. 147–172. ISSN: 1569-1705. DOI: 10.1007/s11157-016-9395-9.
- Hassol, Susan Joy, ed. (2005). *Impacts of a warming Arctic*. Cambridge: Cambridge University Press. ISBN: 0521617782.
- Henry, Hugh A. L. (2008). “Climate change and soil freezing dynamics: historical trends and projected changes”. In: *Climatic Change* 87.3-4, pp. 421–434. ISSN: 0165-0009. DOI: 10.1007/s10584-007-9322-8.
- Höfle, S. et al. (2013). “Organic matter composition and stabilization in a polygonal tundra soil of the Lena Delta”. In: *Biogeosciences* 10.5, pp. 3145–3158. ISSN: 1726-4189. DOI: 10.5194/bg-10-3145-2013.
- Hömberg, Annkathrin, Tanja Broder, et al. (2021). “Divergent effect of silicon on greenhouse gas production from reduced and oxidized peat organic matter”. In: *Geoderma* 386, p. 114916. ISSN: 00167061. DOI: 10.1016/j.geoderma.2020.114916.
- Hömberg, Annkathrin, Martin Obst, et al. (2020). “Increased silicon concentration in fen peat leads to a release of iron and phosphate and changes in the composition of dissolved organic matter”. In: *Geoderma* 374, p. 114422. ISSN: 00167061. DOI: 10.1016/j.geoderma.2020.114422.
- Hugelius, G., Julie Loisel, et al. (2020). “Large stocks of peatland carbon and nitrogen are vulnerable to permafrost thaw”. In: *Proceedings of the National Academy of Sciences of the United States of America* 117.34, pp. 20438–20446. DOI: 10.1073/pnas.1916387117.
- Hugelius, G., J. Strauss, et al. (2014). “Estimated stocks of circumpolar permafrost carbon with quantified uncertainty ranges and identified data gaps”. In: *Biogeosciences* 11.23, pp. 6573–6593. ISSN: 1726-4189. DOI: 10.5194/bg-11-6573-2014.
- Ikeda, Takeshi (2021). “Bacterial biosilicification: a new insight into the global silicon cycle”. In: *Bioscience, biotechnology, and biochemistry* 85.6, pp. 1324–1331. DOI: 10.1093/bbb/zbab069.

- Imai, Ryozo, ed. (2013). *Plant and Microbe Adaptations to Cold in a Changing World: Proceedings from Plant and Microbe Adaptations to Cold 2012*. 1st ed. New York, NY: Springer New York. ISBN: 978-1-4614-8252-9. DOI: 10.1007/978-1-4614-8253-6.
- IPCC (2022). *The Ocean and Cryosphere in a Changing Climate: Special Report of the Intergovernmental Panel on Climate Change*. Cambridge University Press. ISBN: 9781009157964. DOI: 10.1017/9781009157964. URL: <https://www.cambridge.org/core/product/A05E6C9F8638FA7CE1748DE2EB7B491B> (visited on 01/11/2023).
- Jansson, Janet K. and Kirsten S. Hofmockel (2020). “Soil microbiomes and climate change”. In: *Nature reviews. Microbiology* 18.1, pp. 35–46. DOI: 10.1038/s41579-019-0265-7.
- Jansson, Janet K. and Neslihan Taş (2014). “The microbial ecology of permafrost”. In: *Nature Reviews Microbiology* 12.6, pp. 414–425. DOI: 10.1038/nrmicro3262.
- Jessen, Søren et al. (2014). “Hydrology and pore water chemistry in a permafrost wetland, Ilulissat, Greenland”. In: *Water Resources Research* 50.6, pp. 4760–4774. ISSN: 00431397. DOI: 10.1002/2013WR014376.
- Jin, Xiao-Ying et al. (2020). “Impacts of climate-induced permafrost degradation on vegetation: A review”. In: *Advances in Climate Change Research*. ISSN: 16749278. DOI: 10.1016/j.accre.2020.07.002.
- Jobbágy, E. and R. B. Jackson (2001). “The distribution of soil nutrients with depth: Global patterns and the imprint of plants”. In: *Biogeochemistry* 53, pp. 51–77. ISSN: 0168-2563. URL: <https://link.springer.com/article/10.1023/A:1010760720215> (visited on 01/17/2023).
- Johnson, Sarah (2022). *Conservation of Arctic Flora and Fauna*. Uppsala. URL: <https://www.polartrec.com/expeditions/international-arctic-buoy-program/journals/2022-03-31> (visited on 06/27/2023).
- Kahlenberg, L. and A. T. Lincoln (1898). “Solutions of Silicates of the Alkalies”. In: *The Journal of Physical Chemistry* 2.2, pp. 77–90. ISSN: 0092-7325. DOI: 10.1021/j150002a001.
- Kaiser, C. et al. (2007). “Conservation of soil organic matter through cryoturbation in arctic soils in Siberia”. In: *Journal of Geophysical Research* 112.G2. ISSN: 0148-0227. DOI: 10.1029/2006JG000258.
- Kanematsu, Masakazu, Glenn A. Waychunas, and Jean-François Boily (2018). “Silicate Binding and Precipitation on Iron Oxyhydroxides”. In: *Environmental science & technology* 52.4, pp. 1827–1833. DOI: 10.1021/acs.est.7b04098.
- Katz, O. et al. (2021). “Silicon in the Soil-Plant Continuum: Intricate Feedback Mechanisms within Ecosystems”. In: *Plants (Basel, Switzerland)* 10.4, p. 652. ISSN: 2223-7747. DOI: 10.3390/plants10040652. URL: <https://www.mdpi.com/2223-7747/10/4/652/pdf?version=1617938009>.

- Kim, D.-G. et al. (2012). “Effects of soil rewetting and thawing on soil gas fluxes: a review of current literature and suggestions for future research”. In: *Biogeosciences* 9.7, pp. 2459–2483. ISSN: 1726-4189. DOI: 10.5194/bg-9-2459-2012.
- King, Jennifer Y., W. S. Reeburgh, and Shannon K. Regli (1998). “Methane emission and transport by arctic sedges in Alaska: Results of a vegetation removal experiment”. In: *Journal of Geophysical Research* 103.D22, pp. 29083–29092. ISSN: 0148-0227. DOI: 10.1029/98JD00052.
- Köhler, P., J. Hartmann, and Dieter A. Wolf-Gladrow (2010). “Geoengineering potential of artificially enhanced silicate weathering of olivine”. In: *Proceedings of the National Academy of Sciences of the United States of America* 107.47, pp. 20228–20233. DOI: 10.1073/pnas.1000545107.
- Köppen, W. (1931). *Grundriß der Klimakunde*. Reprint 2019. Berlin and Boston: de Gruyter. ISBN: 9783111667751. DOI: 10.1515/9783111667751.
- Kosolov, Roman, A.toly Prokushkin, and Oleg Pokrovsky (2016). “Major anion and cation fluxes from the Central Siberian Plateau watersheds with underlying permafrost”. In: *IOP Convergence Series: Earth and Environmental Science*.
- Koven, C. D. et al. (2011). “Permafrost carbon-climate feedbacks accelerate global warming”. In: *Proceedings of the National Academy of Sciences* 108.36, pp. 14769–14774. ISSN: 0027-8424. DOI: 10.1073/pnas.1103910108.
- Krause, Jeffrey W. et al. (2018). “Biogenic silica production and diatom dynamics in the Svalbard region during spring”. In: *Biogeosciences* 15.21, pp. 6503–6517. ISSN: 1726-4189. DOI: 10.5194/bg-15-6503-2018.
- Kryzevicius, Z. et al. (2019). “The effect of over 50 years of liming on soil aluminium forms in a Retisol”. In: *The Journal of Agricultural Science* 157.1, pp. 12–19. ISSN: 0021-8596. DOI: 10.1017/S0021859619000194. URL: <https://www.cambridge.org/core/services/aop-cambridge-core/content/view/DB5B296B820E79A0C9D9F6C52834F244/S0021859619000194a.pdf/div-class-title-the-effect-of-over-50-years-of-liming-on-soil-aluminium-forms-in-a-retisol-div.pdf>.
- Kumar, A.nd, Claudia M.lli, and T. P. (2019). “Ice nucleation activity of silicates and aluminosilicates in pure water and aqueous solutions – Part 2: Quartz and amorphous silica”. In: *Atmospheric Chemistry and Physics* 19.9, pp. 6035–6058. DOI: 10.5194/acp-19-6035-2019.
- Kurganova, Irina, R. Teepe, and N. Loftfield (2007). “Influence of freeze-thaw events on carbon dioxide emission from soils at different moisture and land use”. In: *Carbon balance and management* 2, p. 2. DOI: 10.1186/1750-0680-2-2.

- Lacroix, Fabrice et al. (2022). “Mismatch of N release from the permafrost and vegetative uptake opens pathways of increasing nitrous oxide emissions in the high Arctic”. In: *Global change biology* 28.20, pp. 5973–5990. DOI: 10.1111/gcb.16345.
- Lamhonwah, D. et al. (2017). “Multi-year impacts of permafrost disturbance and thermal perturbation on High Arctic stream chemistry”. In: *Arctic Science* 3.2, pp. 254–276. ISSN: 2368-7460. DOI: 10.1139/as-2016-0024.
- Larsen, K., S. Jasson, and A. Michelsen (2002). “Repeated freeze–thaw cycles and their effects on biological processes in two arctic ecosystem types”. In: *Applied Soil Ecology* 21.3, pp. 187–195. ISSN: 09291393. DOI: 10.1016/S0929-1393(02)00093-8.
- Liang, Yongchao et al. (2015). *Silicon in Agriculture: From Theory to Practice*. 1st ed. 2015. Dordrecht: Springer Netherlands and Imprint: Springer. ISBN: 9789401799782.
- Loiko, S. V. et al. (2017). “Abrupt permafrost collapse enhances organic carbon, CO₂, nutrient and metal release into surface waters”. In: *undefined*. URL: <https://www.semanticscholar.org/paper/Abrupt-permafrost-collapse-enhances-organic-carbon%2C-Loiko-Pokrovsky/68b202a9f0b5b6c6d5f1e3e3082404fbdb1ca931>.
- Luo, Dongliang et al. (2016). “Recent changes in the active layer thickness across the northern hemisphere”. In: *Environmental Earth Sciences* 75.7. ISSN: 1866-6280. DOI: 10.1007/s12665-015-5229-2.
- Mackelprang, R. et al. (2011). “Metagenomic A.lysis of a permafrost microbial community reveals a rapid response to thaw”. In: *Nature* 480.7377, pp. 368–371. DOI: 10.1038/nature10576.
- Mann, P. J. et al. (2022). “Degrading permafrost river catchments and their impact on Arctic Ocean nearshore processes”. In: *AMBIO*. DOI: 10.1007/s13280-021-01666-z.
- Margesin, R. and T. Collins (2019). “Microbial ecology of the cryosphere (glacial and permafrost habitats): current knowledge”. In: *Applied microbiology and biotechnology* 103.6, pp. 2537–2549. DOI: 10.1007/s00253-019-09631-3.
- Marschner, H. and P. Marschner (2012). *Marschner’s Mineral Nutrition of Higher Plants (Mineral Nutrition of Higher Plants)*. Academic Press. ISBN: 978-0-12-384905-2.
- Mauclet, E. et al. (2022). “Changing sub-Arctic tundra vegetation upon permafrost degradation: impact on foliar mineral element cycling”. In: *Biogeosciences* 19.9, pp. 2333–2351. ISSN: 1726-4189. DOI: 10.5194/bg-19-2333-2022.
- Mavi, M. S. et al. (2012). “Salinity and sodicity affect soil respiration and dissolved organic matter dynamics differentially in soils varying in texture”. In: *Soil biology & biochemistry* 45, pp. 8–13. ISSN: 0038-0717. DOI: 10.1016/j.soilbio.2011.10.003.
- McCarty, Jessica L. et al. (2021). “Reviews and syntheses: Arctic fire regimes and emissions in the 21st century”. In: *Biogeosciences* 18.18, pp. 5053–5083. ISSN: 1726-4189. DOI: 10.5194/bg-18-5053-2021.

- Merbold, L. et al. (2009). “Artificial drainage and associated carbon fluxes (CO₂/CH₄) in a tundra ecosystem”. In: *Global change biology* 15.11, pp. 2599–2614. DOI: 10.1111/j.1365-2486.2009.01962.x.
- Miner, Kimberley R. et al. (2022). “Permafrost carbon emissions in a changing Arctic”. In: *Nature Reviews Earth & Environment* 3.1, pp. 55–67. DOI: 10.1038/s43017-021-00230-3.
- Mishra, Umakant et al. (2021). “Spatial heterogeneity and environmental predictors of permafrost region soil organic carbon stocks”. In: *Science Advances* 7.9. ISSN: 2375-2548. DOI: 10.1126/sciadv.aaz5236.
- Monhonval, A., E. Mauclet, et al. (2021). “Mineral Element Stocks in the Yedoma Domain: A Novel Method Applied to Ice-Rich Permafrost Regions”. In: *Frontiers in Earth Science* 9. DOI: 10.3389/feart.2021.703304.
- Monhonval, A., J. Strauss, C. Hirst, et al. (2022). “Thermokarst processes increase the supply of stabilizing surfaces and elements (Fe, Mn, Al, and Ca) for mineral–organic carbon interactions”. In: *Permafrost and Periglacial Processes* 33.4, pp. 452–469. ISSN: 10456740. DOI: 10.1002/ppp.2162.
- Monhonval, A., J. Strauss, E. Mauclet, et al. (2021). “Iron Redistribution Upon Thermokarst Processes in the Yedoma Domain”. In: *Frontiers in Earth Science* 9. DOI: 10.3389/feart.2021.703339.
- Monteux, S. et al. (2020). “Carbon and nitrogen cycling in Yedoma permafrost controlled by microbial functional limitations”. In: *Nature Geoscience* 13.12, pp. 794–798. ISSN: 1752-0894. DOI: 10.1038/s41561-020-00662-4.
- Mueller, Carsten W. et al. (2015). “Large amounts of labile organic carbon in permafrost soils of northern Alaska”. In: *Global change biology* 21.7, pp. 2804–2817. DOI: 10.1111/gcb.12876.
- Nezat, Carmen A. et al. (2008). “Mineral Sources of Calcium and Phosphorus in Soils of the Northeastern United States”. In: *Soil Science Society of America Journal* 72.6, pp. 1786–1794. ISSN: 03615995. DOI: 10.2136/sssaj2007.0344.
- Obu, Jaroslav et al. (2019). “Northern Hemisphere permafrost map based on TTOP modelling for 2000–2016 at 1 km² scale”. In: *Earth-Science Reviews* 193, pp. 299–316. ISSN: 00128252. DOI: 10.1016/j.earscirev.2019.04.023.
- Olefeldt, D, Mikael Hovemyr, et al. (2021). “The Boreal–Arctic Wetland and Lake Dataset (BAWLD)”. In: *Earth System Science Data* 13.11, pp. 5127–5149. DOI: 10.5194/essd-13-5127-2021.
- Olefeldt, D, Merritt R. Turetsky, et al. (2013). “Environmental and physical controls on northern terrestrial methane emissions across permafrost zones”. In: *Global change biology* 19.2, pp. 589–603. DOI: 10.1111/gcb.12071.

- Opdekamp, W. et al. (2012). “Tussocks: Biogenic Silica Hot-Spots in a Riparian Wetland”. In: *Wetlands* 32.6, pp. 1115–1124. ISSN: 1943-6246. DOI: 10.1007/s13157-012-0341-5. URL: <https://link.springer.com/content/pdf/10.1007/s13157-012-0341-5.pdf>.
- Otsuki, A. and R. Wetzel (1972). “Cocprecipitation of phosphate with carbonates in a marl lake”. In: *Limnology and Oceanography* 17.5, pp. 763–767. ISSN: 00243590. DOI: 10.4319/lo.1972.17.5.0763.
- Overland, J. E. (2020). “Less climatic resilience in the Arctic”. In: *Weather and Climate Extremes* 30, p. 100275. ISSN: 22120947. DOI: 10.1016/j.wace.2020.100275.
- Patzner, Monique S., Nora Kainz, et al. (2022). “Seasonal Fluctuations in Iron Cycling in Thawing Permafrost Peatlands”. In: *Environmental science & technology* 56.7, pp. 4620–4631. DOI: 10.1021/acs.est.1c06937.
- Patzner, Monique S., Carsten W. Mueller, et al. (2020). “Iron mineral dissolution releases iron and associated organic carbon during permafrost thaw”. In: *Nature communications* 11.1, p. 6329. DOI: 10.1038/s41467-020-20102-6.
- Perry, C. C. and T. Keeling-Tucker (1998). “Aspects of the bioinorganic chemistry of silicon in conjunction with the biometals calcium, iron and aluminium”. In: *Journal of Inorganic Biochemistry* 69.3, pp. 181–191. ISSN: 01620134. DOI: 10.1016/S0162-0134(97)10017-4.
- Petkowski, Janusz Jurand, William Bains, and Sara Seager (2020). “On the Potential of Silicon as a Building Block for Life”. In: *Life (Basel, Switzerland)* 10.6. ISSN: 2075-1729. DOI: 10.3390/life10060084.
- Picard, A. et al. (2016). “Limited influence of Si on the preservation of Fe mineral-encrusted microbial cells during experimental diagenesis”. In: *Geobiology* 14.3, pp. 276–292. ISSN: 1472-4677. DOI: 10.1111/gbi.12171.
- Ping, C. L. et al. (2008). “Cryogenesis and soil formation along a bioclimate gradient in Arctic North America”. In: *Journal of Geophysical Research* 113.G3. ISSN: 0148-0227. DOI: 10.1029/2008JG000744.
- Pitt and U.O Ugalde (1984). “Calcium in fungi”. In: *Plant, Cell and Environment* 7, pp. 467–475.
- Qurashi, Aisha Waheed (2011). “Osmoadaptation and plant growth promotion by salt tolerant bacteria under salt stress”. In: *African Journal of Microbiology Research* 5.21, pp. 3546–3554. DOI: 10.5897/AJMR11.736.
- Rantanen, Mika et al. (2022). “The Arctic has warmed nearly four T.es faster than the globe since 1979”. In: *Communications Earth & Environment* 3.1. DOI: 10.1038/s43247-022-00498-3.

- Raynolds, Martha K. et al. (2019). “A raster version of the Circumpolar Arctic Vegetation Map (CAVM)”. In: *Remote Sensing of Environment* 232, p. 111297. ISSN: 00344257. DOI: 10.1016/j.rse.2019.111297.
- Reimann, C. et al. (2001). “Multi-element, multi-medium regional geochemistry in the European Arctic: element concentration, variation and correlation”. In: *Applied Geochemistry* 16, pp. 759–780.
- Reithmaier, Gloria-Maria Susanne et al. (2017). “Enhanced silicon availability leads to increased methane production, nutrient and toxicant mobility in peatlands”. In: *Scientific reports* 7.1, p. 8728. DOI: 10.1038/s41598-017-09130-3.
- Rivkina, E. M. et al. (2000). “Metabolic activity of permafrost bacteria below the freezing point”. In: *Applied and environmental microbiology* 66.8, pp. 3230–3233. ISSN: 0099-2240. DOI: 10.1128/aem.66.8.3230-3233.2000.
- Rohde, Manfred (2019). “The Gram-Positive Bacterial Cell Wall”. In: *Microbiology spectrum* 7.3. DOI: 10.1128/microbiolspec.GPP3-0044-2018.
- Rooney, Erin C. et al. (2022). “The Impact of Freeze–Thaw History on Soil Carbon Response to Experimental Freeze–Thaw Cycles”. In: *Journal of Geophysical Research: Biogeosciences* 127.5. ISSN: 2169-8953. DOI: 10.1029/2022JG006889.
- Rosenberg, Eugene et al. (2014). *The Prokaryotes*. Berlin, Heidelberg: Springer Berlin Heidelberg. ISBN: 978-3-642-30137-7. DOI: 10.1007/978-3-642-30138-4.
- Rowley, Mike C., Stéphanie Grand, and Éric P. Verrecchia (2018). “Calcium-mediated stabilization of soil organic carbon”. In: *Biogeochemistry* 137.1-2, pp. 27–49. ISSN: 0168-2563. DOI: 10.1007/s10533-017-0410-1.
- Sale, Richard and Per Michelsen (2018). *The Arctic*. Dunbeath, Caithness: Whittles Publishing. ISBN: 9781849953429.
- Sapronov, D. V. (2021). “The CO_2 Emission during Laboratory Freezing-Thawing of Soils from Various Natural Zones of Russia”. In: *Eurasian Soil Science* 54.8, pp. 1196–1205. ISSN: 1064-2293. DOI: 10.1134/S1064229321080147.
- Schaefer, Kevin and Elchin Jafarov (2016). “A parameterization of respiration in frozen soils based on substrate availability”. In: *Biogeosciences* 13.7, pp. 1991–2001. ISSN: 1726-4189. DOI: 10.5194/bg-13-1991-2016. URL: <https://bg.copernicus.org/articles/13/1991/2016/>.
- Schaetzl, Randall J. and M. L. Thompson (2015). *Soils: Genesis and geomorphology*. 2. ed. New York, NY: Cambridge Univ. Press. ISBN: 9781107016934.
- Schaller, J., Rita Böttger, et al. (2016). “Reed litter Si content affects microbial community structure and the lipid composition of an invertebrate shredder during aquatic decomposition”. In: *Limnologia* 57, pp. 14–22. ISSN: 00759511. DOI: 10.1016/j.limno.2015.12.002.

- Schaller, J., A. Cramer, et al. (2020). “Biogenic amorphous silica as main driver for plant available water in soils”. In: *Scientific reports* 10.1, p. 2424. DOI: 10.1038/s41598-020-59437-x.
- Schaller, J., S. Faucherre, et al. (2019). “Silicon increases the phosphorus availability of Arctic soils”. In: *Scientific reports* 9.1, p. 449. DOI: 10.1038/s41598-018-37104-6.
- Schaller, J., D. Puppe, et al. (2021). “Silicon Cycling in Soils Revisited”. In: *MDPI Plants* 10.2. DOI: 10.3390/plants10020295.
- Schaller, J., P. Stimmler, et al. (2022). “Arctic Soil CO₂ Release During Freeze-Thaw Cycles Modulated by Silicon and Calcium”. In: *SSRN Electronic Journal*. ISSN: 1556-5068. DOI: 10.2139/ssrn.4257915.
- Schirrmeister, L. et al. (2011). “Sedimentary characteristics and origin of the Late Pleistocene Ice Complex on north-east Siberian Arctic coastal lowlands and islands – A review”. In: *Quaternary International* 241.1-2, pp. 3–25. ISSN: 10406182. DOI: 10.1016/j.quaint.2010.04.004.
- Schulz, Katrin et al. (2022). “Stabilization of Ferrihydrite and Lepidocrocite by Silicate during Fe(II)-Catalyzed Mineral Transformation: Impact on Particle Morphology and Silicate Distribution”. In: *Environmental science & technology* 56.9, pp. 5929–5938. DOI: 10.1021/acs.est.1c08789.
- Schuur, E. A. G., B. W. Abbott, et al. (2013). “Expert assessment of vulnerability of permafrost carbon to climate change”. In: *Climatic Change* 119.2, pp. 359–374. ISSN: 0165-0009. DOI: 10.1007/s10584-013-0730-7.
- Schuur, E. A. G., A. D. McGuire, et al. (2015). “Climate change and the permafrost carbon feedback”. In: *Nature* 520.7546, pp. 171–179. ISSN: 1476-4687. DOI: 10.1038/nature14338. URL: <https://www.nature.com/articles/nature14338>.
- Sims, J. T. (1989). “Comparison of mehlich 1 and mehlich 3 extractants for P, K, Ca, Mg, Mn, Cu and Zn in atlantic coastal plain soils”. In: *Communications in Soil Science and Plant Analysis* 20.17-18, pp. 1707–1726. ISSN: 0010-3624. DOI: 10.1080/00103628909368178.
- Singh, V. P., Ingrid Stober, and Kurt Bucher (2002). *Water-Rock Interaction*. Vol. 40. Dordrecht: Springer Netherlands. ISBN: 978-94-010-3906-2. DOI: 10.1007/978-94-010-0438-1.
- Smith, Sharon L. et al. (2022). “The changing thermal state of permafrost”. In: *Nature Reviews Earth & Environment* 3.1, pp. 10–23. DOI: 10.1038/s43017-021-00240-1.
- Song, Alin et al. (2021). “Soil bacterial communities interact with silicon fraction transformation and promote rice yield after long-term straw return”. In: *Soil Ecology Letters*. ISSN: 2662-2289. DOI: 10.1007/s42832-021-0076-4.

- Sowers, Tyler D. et al. (2020). “Spatially Resolved Organomineral Interactions across a Permafrost Chronosequence”. In: *Environmental science & technology* 54.5, pp. 2951–2960. DOI: 10.1021/acs.est.9b06558.
- Stamm, Franziska M., Andre Baldermann, et al. (2023). “Unravelling the formation paths of amorphous hydroxyaluminosilicates and hydrous ferric silicates: Evidence from silicon isotopes”. In: *EGU-23*.
- Stamm, Franziska M., T. Zambardi, et al. (2019). “The experimental determination of equilibrium Si isotope fractionation factors among H₄SiO₄, H₃SiO₄– and amorphous silica (SiO₂·0.32 H₂O) at 25 and 75 °C using the three-isotope method”. In: *Geochimica et Cosmochimica Acta* 255, pp. 49–68. ISSN: 00167037. DOI: 10.1016/j.gca.2019.03.035.
- Stimmler, P., M. Goeckede, B. Elberling, et al. (2022). *Pan-Arctic soil element availability estimations*. DOI: 10.5194/essd-2022-123.
- Stimmler, P., M. Goeckede, Susan M. Natali, et al. (2022). “The importance of calcium and amorphous silica for arctic soil CO₂ production”. In: *Frontiers in Environmental Science* 10. DOI: 10.3389/fenvs.2022.1019610.
- Stimmler, P., M. Obst, M. Goeckede, et al. (n.d.). “Reduced greenhouse gas emissions from Arctic soils due to aragonite formation from CO₂ and free calcium”. In: ().
- Stimmler, P., M. Obst, M. Stein, et al. (2023). “Silicon and calcium controls on iron and aluminum mobility in Arctic soils”. In: *Chemosphere* 335, p. 139087. ISSN: 00456535. DOI: 10.1016/j.chemosphere.2023.139087. URL: <https://www.sciencedirect.com/science/article/pii/S0045653523013541>.
- Stimmler, P., A. Priemé, et al. (2022). “Arctic soil respiration and microbial community structure driven by silicon and calcium”. In: *The Science of the total environment* 838.Pt 2, p. 156152. DOI: 10.1016/j.scitotenv.2022.156152.
- Strauss, J. et al. (2017). “Deep Yedoma permafrost: A synthesis of depositional characteristics and carbon vulnerability”. In: *Earth-Science Reviews* 172, pp. 75–86. ISSN: 00128252. DOI: 10.1016/j.earscirev.2017.07.007.
- Strauss, Jens et al. (2013). “The deep permafrost carbon pool of the Yedoma region in Siberia and Alaska”. In: *Geophysical research letters* 40.23, pp. 6165–6170. ISSN: 0094-8276. DOI: 10.1002/2013GL058088.
- Suetin, S. V. et al. (2009). “Clostridium tagluense sp. nov., a psychrotolerant, A.erobic, spore-forming bacterium from permafrost”. In: *International journal of systematic and evolutionary microbiology* 59.Pt 6, pp. 1421–1426. ISSN: 1466-5026. DOI: 10.1099/ijs.0.002295-0.

- Sun, Zhaoan, Fanqiao Meng, and Biao Zhu (2023). “Influencing factors and partitioning methods of carbonate contribution to CO₂ emissions from calcareous soils”. In: *Soil Ecology Letters* 5.1, pp. 6–20. ISSN: 2662-2289. DOI: 10.1007/s42832-022-0139-1.
- Terhaar, J. et al. (2021). “Around one third of current Arctic Ocean primary production sustained by rivers and coastal erosion”. In: *Nature communications* 12.1, p. 169. DOI: 10.1038/s41467-020-20470-z.
- Thum, Tea et al. (2019). *A new terrestrial biosphere model with coupled carbon, nitrogen, and phosphorus cycles (QUINCY v1.0; revision 1772)*. DOI: 10.5194/gmd-2019-49.
- Treat, Claire C. et al. (2021). “Predicted Vulnerability of Carbon in Permafrost Peatlands With Future Climate Change and Permafrost Thaw in Western CA,da”. In: *Journal of Geophysical Research: Biogeosciences* 126.5, e2020JG005872. ISSN: 2169-8961. DOI: 10.1029/2020JG005872.
- Turekian, K. K. and K. H. Wedepohl (1961). “Distribution of the Elements in Some Major Units of the Earth’s Crust”. In: *GSA Bulletin* 72.2, p. 175. ISSN: 0016-7606. DOI: 10.1130/0016-7606(1961)72[175:DOTEIS]2.0.CO;2. URL: <https://pubs.geoscienceworld.org/gsa/gsabulletin/article-pdf/72/2/175/3416820/i0016-7606-72-2-175.pdf>.
- Vandenbergh, J. (2013). “PERMAFROST AND PERIGLACIAL FEATURES | Cryoturbation Structures”. In: *Encyclopedia of Quaternary Science*. Elsevier, pp. 430–435. ISBN: 9780444536426. DOI: 10.1016/B978-0-444-53643-3.00096-0.
- Vasskog, K. et al. (2015). “The Greenland Ice Sheet during the last glacial cycle: Current ice loss and contribution to sea-level rise from a palaeoclimatic perspective”. In: *Earth-Science Reviews* 150, pp. 45–67. ISSN: 00128252. DOI: 10.1016/j.earscirev.2015.07.006.
- Villani, Maëlle et al. (2022). “Mineral element recycling in topsoil following permafrost degradation and a vegetation shift in sub-Arctic tundra”. In: *Geoderma* 421, p. 115915. ISSN: 00167061. DOI: 10.1016/j.geoderma.2022.115915.
- Virkkala, Anna-Maria et al. (2021). “Statistical upscaling of ecosystem CO₂ fluxes across the terrestrial tundra and boreal domain: regional patterns and uncertainties”. In: *Global change biology* 27, pp. 4040–4059. DOI: 10.1111/gcb.15659.
- Voigt, Carolina et al. (2020). “Nitrous oxide emissions from permafrost-affected soils”. In: *Nature Reviews Earth & Environment* 1.8, pp. 420–434. DOI: 10.1038/s43017-020-0063-9. URL: <https://www.nature.com/articles/s43017-020-0063-9.pdf>.
- Wada, KOJI (1988). “Synthesis and Characterization of a Hollow Spherical Form of Monolayer Aluminosilicate”. In: *Clays and Clay Minerals* 36.1, pp. 11–18. ISSN: 00098604. DOI: 10.1346/CCMN.1988.0360102. URL: <https://link.springer.com/content/pdf/10.1346/CCMN.1988.0360102.pdf>.

- Wada, KOJI and HIROSHI KUBO (1975). “Precipitation of amorphous aluminosilicates from solutions containing monomeric silica and aluminium ions”. In: *Journal of Soil Science* 26.2, pp. 100–111. ISSN: 00224588. DOI: 10.1111/j.1365-2389.1975.tb01935.x. URL: <https://onlinelibrary.wiley.com/doi/pdf/10.1111/j.1365-2389.1975.tb01935.x>.
- Walker, D.A et al. (2001). “Calcium-rich tundra, wildlife, and the “Mammoth Steppe””. In: *Quaternary Science Reviews* 20.1-3, pp. 149–163. ISSN: 02773791. DOI: 10.1016/S0277-3791(00)00126-8.
- Walker, Donald A. et al. (2005). “The Circumpolar Arctic vegetation map”. In: *Journal of Vegetation Science* 16, pp. 267–282. ISSN: 1654-1103.
- Wang, J.. A. and M. A. Friedl (2019). “The role of land cover change in Arctic-Boreal greening and browning trends”. In: *Environmental Research Letters* 14.12, p. 125007. ISSN: 1748-9326. DOI: 10.1088/1748-9326/ab5429.
- Warren, J. (2000). “Dolomite: occurrence, evolution and economically important associations”. In: *Earth-Science Reviews* 52.1-3, pp. 1–81. ISSN: 00128252. DOI: 10.1016/S0012-8252(00)00022-2.
- Weil, R. R. and N. C. Brady (2017). *The nature and properties of soils*. Fifteenth edition, global edition. Harlow, England et al.: Pearson. ISBN: 9781292162232.
- Whatmore, A. M. and R. H. Reed (1990). “Determination of turgor pressure in *Bacillus subtilis*: a possible role for K⁺ in turgor regulation”. In: *Journal of general microbiology* 136.12, pp. 2521–2526. ISSN: 0022-1287. DOI: 10.1099/00221287-136-12-2521.
- Whittinghill, K. A. and S.h E. Hobbie (2012). “Effects of pH and calcium on soil organic matter dynamics in Alaskan tundra”. In: *Biogeochemistry* 111.1-3, pp. 569–581. ISSN: 1573-515X. DOI: 10.1007/s10533-011-9688-6. URL: <https://link.springer.com/article/10.1007/s10533-011-9688-6>.
- Wild, B., S. Monteux, et al. (2023). “Circum-Arctic peat soils resist priming by plant-derived compounds”. In: *Soil biology & biochemistry* 180, p. 109012. ISSN: 0038-0717. DOI: 10.1016/j.soilbio.2023.109012. URL: <https://www.sciencedirect.com/science/article/pii/S0038071723000743>.
- Wild, B., J. Schneckner, et al. (2014). “Input of easily available organic C and N sT.ulates microbial decomposition of soil organic matter in arctic permafrost soil”. In: *Soil biology & biochemistry* 75.100, pp. 143–151. ISSN: 0038-0717. DOI: 10.1016/j.soilbio.2014.04.014.
- Yi, Y. et al. (2015). “The role of snow cover and soil freeze/thaw cycles affecting boreal-arctic soil carbon dynamics”. In: *Biogeosciences Discussions* 12.14, pp. 11113–11157. DOI: 10.5194/bgd-12-11113-2015.

- Yokoyama, Takushi et al. (2002). “A study of the alumina-silica gel adsorbent for the removal of silicic acid from geothermal water: increase in adsorption capacity of the adsorbent due to formation of amorphous aluminosilicate by adsorption of silicic acid”. In: *Journal of colloid and interface science* 252.1, pp. 1–5. DOI: 10.1006/jcis.2002.8382.
- Yu, Yongxiang et al. (2020). “Soil salinity changes the temperature sensitivity of soil carbon dioxide and nitrous oxide emissions”. In: *CATENA* 195, p. 104912. ISSN: 03418162. DOI: 10.1016/j.catena.2020.104912. URL: <https://www.sciencedirect.com/science/article/pii/S0341816220304628>.
- Zamanian, Kazem, Konstantin Pustovoytov, and Yakov Kuzyakov (2016). “Pedogenic carbonates: Forms and formation processes”. In: *Earth-Science Reviews* 157, pp. 1–17. ISSN: 00128252. DOI: 10.1016/j.earscirev.2016.03.003.
- Zhang, Jianxin et al. (2022). “Severe freezing increases soil respiration during the thawing period: A meta-analysis”. In: *European Journal of Soil Science* 73.1, e13161. ISSN: 13510754. DOI: 10.1111/ejss.13161.
- Zheng, Jianqiu et al. (2022). “Quantifying pH buffering capacity in acidic, organic-rich Arctic soils: Measurable proxies and implications for soil carbon degradation”. In: *Geoderma* 424, p. 116003. ISSN: 00167061. DOI: 10.1016/j.geoderma.2022.116003.

4.4 List of figures

1	Fridtjof Nansen (1861-1930)	3
1.1	Map of the Arctic	8
1.2	Arctic landscape type	9
1.3	Permafrost structure and distribution	10
1.4	Permafrost temperature regime	11
1.5	Permafrost warming	12
1.6	GHG flux dynamics in a permafrost affected landscape	14
1.7	Vegetation in MAT and MNT	16
1.8	Ca-C-Fe aggregates	17
1.9	Microbial community structures int the Arctic	18
1.10	Fluvial Ca fluxes in Siberian river	22
1.11	Calcium iron cation-bridging	23
1.12	Illustrative structure of ASi	24
1.13	ASi pools in tundra systems	25
1.14	Interatction of silicate with the surface of Fe minerals.	26
2.1	Top-Down approach of the dissertation	31
2.2	Maps of element availability	35
2.3	Effect of Si and Ca on GHG release	38
2.4	Temperature regime of freeze-thaw cycles	40
2.5	GHG release during freeze-thaw cycles	41
2.6	SEM of MCS and GHG	43
2.7	Si effect on share of iron phases	46
2.8	Diagram of Si, Ca, Fe Al interactions	47

Index

- active layer, 10
 - annual freezing days, 39
 - cryoturbation, 11
 - freeze-thaw cycles, 11, 39, 40
 - freezing, 10, 40
 - thawing, 10
 - thickness, 10, 13
- Alaska, 36
- aluminium
 - Al(OH)₃, 46, 47
 - availability, 46
 - mobilization, 39, 45
 - short-range order aluminosilicates, 46
- amorphous silicon
 - extraction, 34
 - map, 33, 34
 - substitution, 38
- Arctic circle, 8
- Arctic Ocean
 - run-off, 33
- Arctic ocean
 - coccolithophores, 21
- Arctic warming, 12
- bedrock, 15
 - basalt, 42
 - weathering, 20, 21, 42
- Ca-Fe-SOM complexes, 22
- calcium
 - aragonite, 20
 - calcite, 20
 - carbonate, 20
 - carbonate lysis, 20
 - cation bridging, 22
 - gypsum, 20
 - macronutrient, 19
 - solubility, 20
- Canadian Shield, 36
- carbon dioxide (CO₂)
 - Ca effect, 37, 42
 - fixation, 16
 - Si effect, 37
- cation
 - bridging, 23, 47
 - exchange capacity, 20
- cryosphere, 12
- cryoturbation, 11, 38
- dry bulk density, 15
- earth system models, 36
 - QUINCY, 33
- ESM, *see* earth system models
- extraction methods
 - alkaline extraction, 34
 - Mehlich III, 34, 45
- Fe, 23
- GHG , *see* greenhouse gases¹³
- greenhouse gases
 - carbon dioxide (CO₂), 14
 - GC-FID, 37
 - methane (CH₄), 14

- nitrous gas (N₂O), 14
 PICARRO, 39
- Greenland, 42
 Disko Island, 42, 44
 Disko island, 42
 inland ice, 9
 Peary Land, 42
- hydraulic conductivity, 45
- ice
 freezing point, 41
 glaciers, 9, 12
 ice age, 9
 ice wedges, 11
 Iceland, 34
 inland ice, 9
- incubation, 36
 C1, 36
 C2, 36
 Ca1, 36
 MAT, 36
 MNT, 36
- iron
 e⁻ acceptors, 45
 availability, 45
 Ca-Fe-SOM aggregates, 47
 crystallinity, 46
 ferrihydrite, 45
 mobilization, 39, 45
 vivianite, 45
- lithology
 basalt, 34
 Geological Map, 33
 mineralogy, 40
 sediments, 36
- map
 circumpolar Arctic vegetation map, 33
- maps
 Geological Map Of The Arctic, 33
- MAT
 Ca concentrations, 39
 vegetation, 15
- methane (CH₄)
 sedges, 16
 waterlogged, 13
- microbes, 15
 abundance, 44
 activity, 41, 42
 bacteria, 19
 community structure, 17, 43
 Eutectophiles, 19
 fungi, 19, 44
 gram(+), 19, 43
 gram(-), 19, 43
 nutrient availability, 17
 spores, 19, 44
- mineral
 soils, 37
 layer, 10
- mineral binding sites
 substitution, 41
- MNT
 vegetation, 15
- models
 metric multi-dimensional scaling, 45
 structure equation model (SEM), 43
- nutrients
 nitrogen, 39
- organic carbon
 pool, 12
 organic layer, 10

-
- permafrost, 9
 - carbon feedback, 15
 - definition, 9
 - distribution, 10
 - temperature, 12
 - phosphorous
 - apatite, 21
 - co-precipitation, 21
 - mineral binding sites, 38, 45
 - phosphate, 21
 - pleistocene, 12
 - polar desert, 42
 - polar desserts, 9
 - potential toxic elements (PTE), *see* aluminium
 - precipitation
 - water availability, 36
 - Rivers, 36
 - rRNA, 42
 - salinity, 15, 21, 42
 - short-range order ironsilicates, 46
 - shrubs, 19
 - Si, 26
 - Siberia, 36, 39
 - silicon
 - silicic acid, 45, 46
 - substitution, 38
 - soil C3
 - incubation, 39
 - soil organic matter, *see* SOM
 - solubility, 47
 - SOM
 - decomposition, 13, 14, 16
 - mineral binding sites, 12
 - temperature
 - temperature regime, 39
 - thermokarst, 13
 - vegetation
 - browning, 12
 - cover, 16
 - greening, 12
 - period, 12
 - taiga, 8
 - tree line, 8
 - tundra, 9, 12
 - water
 - hydraulic conductivity, 38
 - precipitation rates, 13
 - snow, 13
 - supercooled, 41
 - water holding capacity, 38, 42
 - water availability, 41
 - X-Ray, 23
 - Yedoma
 - Ca pool, 19
 - cryoturbation, 11, 20
 - thermokarst, 20
 - Yedoma soils, 36

4.5 Danksagung

Diese Arbeit ist das Ergebnis von Durchhaltevermögen, Frustrationstoleranz, Kreativität und dem Willen immer wieder aufzustehen und weiterzumachen. Unsere individuelle Gesellschaft neigt dazu all diese Qualitäten immer auf sich selbst zu beziehen und vergisst, dass wir Menschen ohne unser soziales Gefüge nicht handlungsfähig sind.

Mein Dank gilt deswegen all den Menschen in meinem Leben, die mich unterstützt, aufgebaut, abgelenkt, inspiriert, motiviert, getröstet und aufgenommen haben. Die Liste kann hier nicht vollständig sein, aber ich möchte die wichtigsten Personen nennen:

Meinen Eltern und Großeltern, die mir diesen Bildungsweg ermöglicht haben und mir immer eine offene Tür und ein offenes Ohr geschenkt haben. Mein besonderer Dank gilt meinem Sohn Nemo und seiner Mutter, die mir in den schwersten Zeiten ein wunderbares Geschenk gemacht haben und mir den Rücken frei gehalten haben. Entschuldigung, dass ich nicht mehr für euch da sein konnte. Weiterhin möchte ich mich bei der LBV Hochschulgruppe bedanken, für all die schönen Exkursionen, Abende und die Selbstwirksamkeit. In den entscheidenden Momenten haben Urte, Anna und Nici mir die Gruppe abgenommen und sie noch besser weitergeführt.

Ein besonderer Dank gilt Carola, die mich zurück zu mir gebracht hat und immer Trost und Zuversicht gegeben hat. Amelie hat mir ein Zufluchtsort gegeben und mir so viel schöne Zeit in den Bergen ermöglicht. Ihr danke ich auch für die Korrektur. Meiner Partnerin Anna danke ich für die Unterstützung, Unterkunft, den inspirierenden Input und all die menschliche Wärme in einer zu kalten Wissenschaft. Ein besonderer Dank geht an Sarah, die mir immer wieder Mut gemacht hat und mit mir einen sehr schweren Weg gegangen ist. Weiterhin bedanke ich mich bei Tessa für all die schöne Zeit und die Träume, Stabilität und Pizza.

Mein fachlicher Dank geht an meinen Betreuer Jörg, für seine menschliche Art und fachliche Betreuung. Danke für die Freiheit, das Vertrauen in mich und meine wissenschaftlichen Fähigkeiten und in meine Kreativität. Danke für die Möglichkeit all diese tollen Erfahrungen zu machen und für deine Erreichbarkeit und Unterstützung. Johanna danke ich, dass Sie mich in Ihrer Gruppe aufgenommen hat und mir ein schönes Arbeitsumfeld und ein Büro in Bayreuth ermöglicht hat. Ein besonderer Dank geht an Martin für die Einarbeitung in die Röntgen-Daten. Weiterhin möchte ich mich bei Anders und Bo für die tolle Forschung und die Zeit in Kopenhagen bedanken. Ein besonderer Dank geht an Jens vom AWI für den Ansporn in der Endphase und den wunderbaren Austausch mit dem Fachkollegium. Weiterer Dank geht an all die tollen Arbeitskollegen von der Uni Bayreuth und dem ZALF, die mir immer eine schöne Zeit ermöglicht haben. Ein großes Danke geht an Jaquci und Vera für die praktische Bearbeitung von tausenden Proben. Danke auch an all die Co-Autoren und Reviewer, denen ich die fünf Publikationen zu verdanken habe.

Ein letzter Dank geht an all die Idole und Wegbereiter, denen wir die Kenntnisse über die Arktis erst zu verdanken haben. Menschen dieses Schlages gibt es heutzutage fast nicht mehr und Sie waren mir Vorbilder für Werte, Durchhaltevermögen und Menschlichkeit: Fridtjof Nansen, Roald Amundsen, Robert Falcon Scott, Alfred-Wegener, Umberto Nobile, Salomon August Andrée, Arved Fuchs und all die vielen weiteren Entdecker, die Ihre Forschung zu häufig mit dem Leben bezahlt haben. Ihr werdet immer einen Platz in meiner Bibliothek haben.

Macht´s gut, und Danke für den Fisch,

Peter Stimmler, Dezember 2023

4.6 (Eidesstattliche) Versicherungen und Erklärungen

(§ 8 Satz 2 Nr. 3 PromO Fakultät) *Hiermit versichere ich eidesstattlich, dass ich die Arbeit selbstständig verfasst und keine andere als die von mir angegebenen Quellen und Hilfsmittel benutzt habe (vgl. Art. 97 Abs. 1 Satz 8 BayHIG).*

(§ 8 Satz 2 Nr. 3 PromO Fakultät) *Hiermit erkläre ich, dass ich die Disseration nicht bereits zur Erlangung eines akademischen Grades eingereicht habe und nicht bereits diese oder eine gleichartige Doktorprüfung endgültig nicht bestanden habe.*

(§ 8 Satz 2 Nr. 4 PromO Fakultät) *Hiermit erkläre ich, dass ich Hilfe von gewerblichen Promotionsberatern bzw. -vermittlern oder ähnlichen Dienstleistern weder bisher in Anspruch genommen habe noch künftig in Anspruch nehmen werde.*

(§ 8 Satz 2 Nr. 7 PromO Fakultät) *Hiermit erkläre ich mein Einverständnis, dass die elektronische Fassung der Dissertation unter Wahrung meiner Urheberrechte und des Datenschutzes einer gesonderten Überprüfung unterzogen werden kann.*

(§ 8 Satz 2 Nr. 8 PromO Fakultät) *Hiermit erkläre ich mein Einverständnis, dass bei Verdacht wissenschaftlichen Fehlverhaltens Ermittlungen durch universitätsinterne Organe der wissenschaftlichen Selbstkontrolle stattfinden können.*

Ort, Datum, Unterschrift